UNIVERSITÉ DE LORRAINE | BIBLIOTHÈQUES UNIVERSITAIRES

AVERTISSEMENT

Ce document est le fruit d'un long travail approuvé par le jury de soutenance et mis à disposition de l'ensemble de la communauté universitaire élargie.

Il est soumis à la propriété intellectuelle de l'auteur. Ceci implique une obligation de citation et de référencement lors de l'utilisation de ce document.

D'autre part, toute contrefaçon, plagiat, reproduction illicite encourt une poursuite pénale.

Contact bibliothèque : ddoc-theses-contact@univ-lorraine.fr
(Cette adresse ne permet pas de contacter les auteurs)

LIENS

Code de la Propriété Intellectuelle. articles L 122. 4
Code de la Propriété Intellectuelle. articles L 335.2- L 335.10
http://www.cfcopies.com/V2/leg/leg_droi.php
http://www.culture.gouv.fr/culture/infos-pratiques/droits/protection.htm

Université de Lorraine

École doctorale C2MP

Laboratoire de Physique et Chimie Théoriques (LPCT)

Correlations in One-Dimensional Quantum Gases

Par Attila Takács

Thèse de doctorat de Physique

Dirigée par Jérôme Dubail

Et par Pasquale Calabrese

Présentée et soutenue publiquement le 10/10/2025

Devant un jury composé de :

Marco Schiro	Collège de France	Rapporteur
Benoit Estienne	Sorbonne Université	Rapporteur
Paola Ruggiero	King's College London, Angleterre	Rapportrice
Sara Murciano	Université Paris Saclay	Examinatrice
Christophe Chatelain	Université de Lorraine	Examinateur, Présidente du jury
Jérôme Dubail	Université de Strasbourg	Directeur de thèse
Pasquale Calabrese	SISSA, Italie	Co-directeur de thèse

Abstract

Describing the collective behavior of many body interacting systems is a central challenge in cold atom physics. Systems confined in one dimension are particularly interesting due to the fact that in many cases they are integrable. In this work, we focus on such systems—specifically, Bose gases solvable via the Bethe Ansatz. We begin the thesis by preparing the background, the tools and the motivation needed in the following, inlcuding a review of the Lieb-Liniger gas, it's Bethe Ansatz and the recent advancements in the experimental realization of it. We include a brief introduction of the theory of Generalized Hydrodynamics as well as effective field theoretical methods, such as the Luttinger liquid theory, used to compute correlation functions in ground states of low dimensional systems.

We then turn to the study of lattice hard core bosons out- of equilibrium. By computing analytical results for the one particle density matrix of a freely expanding system of hard-core bosons from an initial double domain wall potential we provide a fully analytical treatment of the phenomenon of dynamical quasicondensation and discuss the emergence of off-diagonal long range order.

Next, we investigate the dynamics of hard-core bosons released from a domain wall initial state in the presence of two conformal defects. The observed density profile differs from the Euler-scale hydrodynamic description due to quantum interference effects. By analyzing boson propagators, we show that repeated scattering on the defects leads to interference patterns that cannot be captured by the hydrodynamic approach. We derive an analytic expression for the density profile during free expansion and demonstrate that a modified semi-classical scattering framework is required for the description of systems with such conformal defects.

The final part of thesis deals with the calculation of the one particle density matrix of Lieb-Linger gas in smooth trapping potentials at finite temperature and interaction strengths. We introduce a method to obtain such correlation functions by combining long-distance asymptotics with known short distance expansions. For the limits of weak and strong interactions we derive analytical results, as well as a general protocol for computing one-particle correlations at any arbitrary repulsive interaction strengths. We include a detailed explanation of the numerical method used to compute Green's functions of field of the effective theory needed as an input to our procedure. We benchmark our results by comparing them to exact numerical calculations and to recent experimental findings.

"It's a dangerous business, Frodo, going out your door. You step onto the road, and if you don't keep your feet, there's no knowing where you might be swept off to."

J.R.R. Tolkien, The Lord of the Rings

Acknowledgments

I would like to sincerely thank Jérôme and Pasquale for guiding me during the development of this PhD thesis. Their supervision and guidance during these last three years have been very fruitful for my development and growth as a physicist and I will always be grateful for that. I am also grateful for their invaluable advice, be it in- or outside of scientific research.

I would like to thank Marco Schiro, Paola Ruggiero, Benoit Estienne, Sara Murciano and Christophe Chatelain for being part of the defence jury.

I would also like to thank my collaborators Marcos Rigol, Yicheng Zhang, Lev Vidmar, András Grabarits, Ion Cosma Fulga and János Asbóth who greatly contributed to my progress in becoming a researcher. Special thanks go to Stefano Scopa, who, in addition to being a great person to work with, helped me out in various instances, including finding flats to rent, understanding and managing bureaucracy among many other things. He also spent a lot of time discussing various projects with me giving his own perspective and understanding, widening mine in the process. For these I will be forever grateful to him, and I am very much looking forward to working with him in the future.

During my studies I had the chance to spend six months in SISSA working closely with the Statistical Physics group and to this day I think back fondly on the discussions and chats I had with the group members. I owe many thanks to Filiberto, Arthur, Colin, Federico, Michele F., Andrei, Konstantinos, Lata and Pasquale for their hospitality and kindness.

These years would not have been the same without the permanents, post-docs and doctoral students of LPCT. Many thanks to Séverine for always knowing how to fix everything I ever had an issue with. On the same note I also thank Vishal for helping me and giving me advice regarding bureaucracy and other matters. I am grateful to Alexandre, Raphaël, Jeremy and Yash for the after-lunch chess games and chess related discussions. I really appreciated the random occurrences when Andy showed up in my office every few weeks to give me a perfect synopsis on the current state of videogames beloved by both of us. I am grateful to Leïla and Mohamed for their help with anything related to french language and customs, especially french slang. Many thanks to Daniel for always keeping me updated on global politics and technology whether I wanted it or not. I thank Yulia for the Sunday gym sessions and for being a true friend during these years. I am grateful to Rita for the relatable conversations and the countless pieces of advice she gave me over these years. I really appreciated discussions with Michele C. and I hope we continue to do them in Ljubljana. I also am really happy to have the chance to work with Ali. I thank the entire lab for the welcoming atmosphere and working environment they created throughout these years.

While in Nancy, I spent nearly all the free time available to me in the rowing club, including evenings and weekends. I am grateful to the coaches and teammates for the experience, especially Thierry and Pauline, with whom I survived many late night training sessions, and discussed various topics all the way from physics and philosophy to rowing.

Finally I would like to thank my family, my parents and my siblings, who supported and encouraged me throughout these years, as well as Stefhany who made even the hardest days easy with her endless love and support.

Contents

Abstract i

Acknowledgments iii

List of Abbreviations vii

List of Publications viii

Introduction 1

1 Background & Tools 3

1.1 Thermalization of Quantum Systems . . . 3

1.1.1 Quantum Quenches and Local Observables . . . 3

1.1.2 Local Conservation Laws . . . 4

1.1.3 Non-equilibrium steady states . . . 5

1.2 Bosons in One Dimension . . . 5

1.2.1 The Lieb-Liniger gas . . . 6

1.2.2 Cold Atom Experiments in One Dimension . . . 6

1.2.3 Coordinate Bethe Ansatz . . . 9

1.2.4 Thermodynamic Bethe Ansatz . . . 12

1.2.5 The Tonks - Girardeau Limit . . . 15

1.2.6 The super Tonks - Girardeau (sTG) Gas . . . 16

1.2.7 Quasicondensation . . . 17

1.3 Generalized Hydrodynamics . . . 18

1.3.1 Separation of Scales . . . 20

1.3.2 The GHD Equations . . . 21

1.3.3 Zero Entropy GHD . . . 22

1.4 Low-Energy Effective Description of 1D Quantum Systems . . . 24

1.4.1 Bosonization and Effective Hamiltonian . . . 24

1.4.2 The Luttinger Parameter and The Sound Velocity . . . 26

1.4.3 Green's Functions of the Luttinger Liquid . . . 27

1.4.4 Long Range Asymptotics of Correlations in Trapped Gases . . . 30

1.4.5 Notions of Conformal Invariance . . . 32

1.4.6 Conformal Field Theories In the Complex Plane . . . 34

1.4.7 Boundary Conformal Field Theory . . . 35

1.5 Quantum Generalized Hydrodynamics . . . 40

1.5.1 Quantum fluctuations around Generalized Hydrodynamics . . . 40

1.5.2 Time evolution and Effective Hamiltonian of density fluctuations . . . 41

2 Non-equilibrium Dynamics of Bose gases **43**
2.1 Correlations of Hard Core Lattice Bosons . . . 43
2.1.1 Initial Conditions and the Hamiltonian . . . 45
2.1.2 Results for the One Particle Density Matrix . . . 47
2.1.3 The OPDM from Quantum Generalized Hydrodynamics . . . 50
2.1.4 Evaluation of The Correlation Functions . . . 59
2.1.5 Quasicondensation and Off-Diagonal Long-Range Order . . . 63
2.1.6 Discussion . . . 68
2.2 Double-Defect Interferometer for Hard-Core Bosons . . . 70
2.2.1 Hard Core Bosons on a Line With a Conformal Defect . . . 70
2.2.2 The Case of Two Conformal Defects . . . 75
2.2.3 The Propagator and the Density . . . 81
2.2.4 Discussion . . . 83

3 Correlations of Trapped Bose Gases at Finite Temperature **85**
3.1 Asymptotics of the OPDM . . . 86
3.2 Trapped bosons at finite temperature . . . 87
3.2.1 Weakly Interacting Bosons in a Harmonic trap, at Finite Temperature . . . 89
3.2.2 Hard-Core Bosons in a Trap, at Finite Temperature . . . 91
3.3 Finite Temperature Green's Function of the Inhomogeneous Luttinger Liquid . . . 93
3.4 OPDM and momentum distribution of trapped bosons at finite temperature . . . 97
3.4.1 Hard-Core Bosons . . . 98
3.4.2 Soft-Core Bosons . . . 100
3.5 Discussion . . . 101

4 Some Preliminary Results **105**
4.1 Quantum Newton's Cradle of Bose gas . . . 105
4.1.1 GHD of trapped Bose gas . . . 106
4.1.2 The quench and dynamics . . . 106
4.1.3 Quantum GHD approach . . . 107
4.1.4 Green's function of time evolution . . . 109
4.2 Correlations of the trapped sTG gas at finite temperature . . . 110
4.2.1 Density profile at zero temperature . . . 110
4.2.2 OPDM at finite temperature . . . 111

5 Conclusion **113**

A The numerical factor $B_\eta(\{k_a\})$ for Hard core bosons in a free expansion **115**
A.1 The numerical factor $B_\eta(\{k_a\})$ . . . 115
A.2 Two conjectures about asymptotic limits of products used . . . 117
A.2.1 Conjecture 1. . . . 118
A.2.2 Conjecture 2. . . . 118
A.2.3 Physical argument supporting the two conjectures. . . . 118
A.2.4 Fixing the constants D_0, $D_{1/2}$, $D_{-1/2}$. . . . 120

B Calculation of the nonuniversal amplitudes $B_m(\gamma)$ in Chapter 3 **121**

C Estimating the Error of the Momentum Distribution Obtained by *our approach* in Chapter 3 **123**

Bibliography **125**

List of Abbreviations

BEC Bose-Einstein Condensate. 5, 6, 26, 85

CFT Conformal Field Theory. 32, 35, 41, 42

GGE Generalized Gibbs Ensemble. 3, 5, 43

GHD Generalized Hydrodynamics. 5, 19–24, 27, 40, 41, 52, 70, 83, 107, 109, 113

HCB Hard Core Bosons. 4, 5, 7, 44, 46, 47, 68, 70, 85, 86, 105, 107, 113

LDA Local Density Approximation. 21, 22, 27, 32, 89, 90, 113

ODLRO Off-Diagonal Long Range Order. 17, 18

OPDM One Particle Density Matrix. vi, 4–7, 9, 15, 17, 18, 30–33, 36, 37, 44, 47, 50, 56, 57, 59, 68–70, 83, 85–87, 89, 91, 93, 96–103, 105, 107, 110, 111, 113, 114, 121, 122

PBC Periodic Boundary Condition. 10, 11, 71

QGHD Quantum Generalized Hydrodynamics. 2, 3, 5, 40, 43, 52, 70, 105, 107

sTG super Tonks - Girardeau. 1, 2, 16, 114

TG Tonks - Girardeau. 1, 2, 7, 15, 35, 41, 85, 86, 98, 105, 107

List of Publications

Parts of this thesis are based on the following publications:

- Attila Takács, Stefano Scopa, Pasquale Calabrese, Lev Vidmar and Jerôme Dubail
  Quasicondensation and off-diagonal long-range order of hard-core bosons during a free expansion, *Journal of Physics A: Mathematical and Theoretical* **57**, 49 (Nov. 2024), p. 495003. DOI link

- Attila Takács, Yicheng Zhang, Pasquale Calabrese, Jerôme Dubail, Marcos Rigol and Stefano Scopa
  One-body correlations and momentum distributions of trapped one-dimensional Bose gases at finite temperature, *Phys. Rev. A* **111**, (Mar. 2025), p. 033317. DOI link

- Attila Takács, Pasquale Calabrese and Jerôme Dubail
  Double-Defect Interferometer for Hard-Core Bosons, article in preparation

Other works:

- András Grabarits, Attila Takács, Ion Cosma Fulga and János K. Asbóth
  Floquet-Anderson localization in the Thouless pump and how to avoid it, *Phys. Rev. B* **109**, 18 (May 2024), p. L180202. DOI link

Introduction

In recent years, the study of one-dimensional (1D) quantum systems has become a remarkably rich field for both theoretical and experimental physics. Enabled by the recent advancements in cold atom experiments, it is now possible to realize and manipulate isolated quantum gases confined to effectively one-dimensional geometries, with great control over interactions, temperature, and trapping potentials. These technological advancements allowed experimentalists to have direct access to regimes where conventional thermodynamic descriptions break down, and where the effects of quantum statistics, interactions, and dimensional constraints become dominant. In particular we will focus on a specific kind of low-dimensional bosonic systems that belong to the group of integrable systems. While the exact definition of integrability in the context of quantum systems is a topic of hot debate, when we say integrable we refer to systems whose spectrum can be exactly solved using the Bethe Ansatz technology.

The work presented in this thesis focuses on describing the correlation properties of cold atomic gases confined in one dimension, with particular emphasis on both out-of-equilibrium dynamics and finite-temperature equilibrium behavior. Throughout, the aim is to understand how quantities like interaction strength and temperature influence observable quantities such as momentum distributions and one-particle density matrices, which encode fundamental information about coherence, condensation, and dynamical evolution in these low-dimensional quantum systems.

The thesis is organized into three main chapters: Chapter 1 introduces the general background and the theoretical tools used in this work, while also providing some necessary context. Namely, our goal here is to provide prologue and to arm the reader with the knowledge required to fully understand and appreciate the results that follow. Chapter 2 of the thesis is devoted to hard-core bosons—a limit of the Lieb-Liniger model where strong repulsion leads to effective fermionization. We study this system in out-of-equilibrium settings, focusing in particular on equal time correlations, dynamical fermionization, quasi-condensation and the effect of defects in the system. In Chapter 3 we investigate the finite-temperature equilibrium properties of a trapped Lieb-Liniger gas.

In **Chapter 1** we introduce the various methods and established theories used in the field of low dimensional cold atoms to set the stage for our results, as well as define some important quantities, methods and concepts. We start with a brief review of the thermalization of quantum systems, focusing on systems with conserved charges to set the stage for the coming section. We then turn to the discussion of Bose gases in 1 dimension, especially the Lieb-Liniger gas, discussing their basic properties and introducing some of the experimental advancements in observing and measuring such systems, that serve as very strong motivation for the results we later present. We review the exact diagonalization of its Hamiltonian by the Bethe Ansatz and its extension to the thermodynamic limit. We highlight some important and interesting limits in the interaction strength, namely the infinitely strong repulsive limit, called Tonk-Girardeau- (TG) and the attractive case referred to as the super Tonk-Girardeau (sTG) gases. The following section is used to review the theory of Generalized Hydrodynamics, a theoretical framework reported in 2016 in Castro-Alvaredo et al. [1]

and Bertini et al. [2] that provides a description of Euler scale hydrodynamics of integrable quantum systems. We especially focus on describing the evolution of so-called zero-entropy states, that we extensively use later in this work. We conclude this chapter with the discussion of the Tomonaga-Luttinger liquid theory in the context of its use in obtaining ground state correlation functions of low dimensional cold atomic systems, and the introduction to Quantum Generalized Hydrodynamics [3, 4].

The focus of **Chapter 2** is the out-of-equilibrium behavior of a particularly interesting class of quantum many-body systems consisting of bosons with strong repulsive interactions, commonly referred to as hard-core bosons (HCBs). In one spatial dimension, such systems can be mapped onto non-interacting spinless fermions via the Jordan-Wigner transformations [5]. This correspondence allows for the development of efficient numerical techniques for exploring their non-equilibrium dynamics. Despite this simplification, deriving analytical results for non-equilibrium quantities still proves to be a challenging task. As a result, much of the progress in this area has relied on numerical approaches [6–8]. Instead, we report analytical expressions for out-of-equilibrium correlation functions by building upon the framework of quantum generalized hydrodynamics (QGHD). These correlations provide insight into phenomena such as quasicondensation and dynamical fermionization. In addition, we explore a particular system of hard-core bosons out of equilibrium in the presence of so-called conformal defects. These defects give rise to quantum interference effects, leading to deviations from the density profiles predicted by the hydrodynamic description.

We report a method for computing the one-body correlations and the momentum distribution of one-dimensional Bose gases in smooth trapping potentials for finite interaction strengths and temperatures in **Chapter 3**. This method involves combining known short-distance expansions of the one particle density matrix with a long-distance behavior of the gas that we compute similarly to the framework of Luttinger liquid theory. In the case of the quasicondensate regime (weak repulsive interaction strength) and in the Tonks-Girardeau limit (strong interaction) we derive analytical results for the correlation functions. We also provide a general procedure for obtaining the one-body correlations at any interaction strength, along with a detailed explanation of the numerical method used to compute Green's functions that we need as input to our theory. Finally we benchmark the validity of our method against exact numerical calculations and recent experimental results.

With these results we aim to contribute to the broader understanding of low-dimensional quantum systems by bridging the gap between exact solutions, effective hydrodynamic descriptions, and experimentally relevant observables. We briefly discuss and motivate ongoing projects that build on the results we report in this work in **Chapter 4**. The thesis is partly based on published articles listed above as well as some work that is in the process of being published.

Chapter 1

Background & Tools

1.1 Thermalization of Quantum Systems

1.1.1 Quantum Quenches and Local Observables

A relevant and important problem in many body quantum physics is the description of their dynamics far from equilibrium. A standard method used both in analytical and experimental studies is the quantum quench. The protocol consists of preparing the many-particle system in a large, finite volume L in the eigenstate of a time-independent Hamiltonian (generally the ground state), after which the dynamics are studied with respect to a different time-independent Hamiltonian $\hat{H}$. This can be thought of as changing instantaneously the parameters of the initial Hamiltonian, hence the name quench. Thus, a system initially in the state $|\psi_0\rangle$ evolves in time according to the time-dependent Schrödinger equation

$$|\psi(t)\rangle = e^{-i\hat{H}t}\,|\psi_0\rangle = \sum_n e^{-iE_nt}\,|n\rangle\,\langle n|\psi_0\rangle = \sum_n e^{-iE_nt}c_n\,|n\rangle\,, \tag{1.1}$$

where $\{|n\rangle\}$ is the complete eigenbasis of $\hat{H}$ with the their corresponding set of eigenenergies $\{E_n\}$, and $c_n = \langle n|\psi_0\rangle$ is the overlap of the initial state with the eigenstates (we set $\hbar = 1$ throughout this chapter). Instead of looking at the evolution of the state, we focus on the evolution of local observables $\hat{O}_A$ at the thermodynamic limit during time evolution.

$$O_A(t) = \lim_{L\to\infty} \langle\psi(t)|\,\hat{O}_A\,|\psi(t)\rangle\,. \tag{1.2}$$

Here we defined local observables as operators that act as identity outside of a connected finite region A of the volume in the thermodynamic limit. An example of such operators in quantum spin chains are terms given as multiples of the Pauli matrices $\sigma^{\alpha_1}_{k_1}...\sigma^{\alpha_l}_{k_l}$ with $k_i \in [a,b]$ with a,b fixed. This strong constraint of locality can be relaxed to include *quasi-local* observables as discussed in [9].

Thermalization

Restricting ourselves first to homogeneous cases where both the initial state $|\psi(0)\rangle$ and the post quench Hamiltonian $\hat{H}$ are translationally invariant (in lattice systems this can be relaxed to periodicity over a finite number of sites n). In the following we will also assume that $\hat{H}$ consists of

local terms $\hat{h}_j$ that describe the energy of a subsystem. The first question one can ask is whether the system equilibrates, in other words the expectation values of local observables become time independent. This is equivalent to asking whether the limit

$$O_A = \lim_{t\to\infty} \lim_{L\to\infty} \langle\psi(t)|\, \hat{O}_A\, |\psi(t)\rangle \tag{1.3}$$

exists and is independent of time. Note that the density matrix of the system $\hat{\rho}(t) = |\psi(t)\rangle \langle\psi(t)|$ isn't necessarily independent of time as it describes a closed system in a pure state. Restricting ourselves to the density matrix of the subspace A, where our local observable acts non-trivially, the reduced density matrix

$$\hat{\rho}_A(t) = \mathrm{Tr}_{\overline{A}}[\hat{\rho}(t)] \tag{1.4}$$

describes a mixed state and can become time independent at late enough times. Thus we are looking for a time independent density matrix $\hat{\rho}_{SE}$ that describes the expectation values of local operators $\hat{O}_A$ at late times in terms of a statistical ensemble

$$\lim_{t\to\infty} \lim_{L\to\infty} \langle\psi(t)|\, \hat{O}_A\, |\psi(t)\rangle = \lim_{L\to\infty} \mathrm{Tr}[\hat{\rho}_{SE}\hat{O}_A] \tag{1.5}$$

As we are dealing with a closed quantum system, the energy is conserved during time evolution:

$$e_0 = \lim_{L\to\infty} \frac{\langle\psi_0|\, \hat{H}\, |\psi_0\rangle}{L} = \lim_{L\to\infty} \frac{\langle\psi(t)|\, \hat{H}\, |\psi(t)\rangle}{L} = \lim_{L\to\infty} \langle\psi(t)|\, \hat{h}(x)\, |\psi(t)\rangle\,, \tag{1.6}$$

with $\hat{h}(x)$ being the local energy density. In an isolated quantum system this is the minimal amount of information on the initial state $|\psi_0\rangle$ that is preserved under time evolution. In the case where the system has no other preserved quantities, the state $|\psi(t)\rangle$ approaches a thermal state in the late time dynamics. The Gibbs density matrix of this thermal state is defined as

$$\hat{\rho}_{GE} = \frac{e^{-\beta\hat{H}}}{Z_{GE}}, \tag{1.7}$$

where the effective equilibrium temperature β is given by condition on the energy density (1.6) prescribed by the initial state $|\psi_0\rangle$

$$e_0 = \lim_{L\to\infty} \frac{\mathrm{Tr}[\rho_{\mathrm{GE}}\hat{H}]}{L}, \tag{1.8}$$

thus the expectation values of local observables are

$$O_A = \lim_{L\to\infty} \mathrm{Tr}[\rho_{GE}\hat{O}_A]. \tag{1.9}$$

1.1.2 Local Conservation Laws

A Hermitian operator $\hat{Q}$ that has local density $\hat{q}(x)$ and commutes with the Hamiltonian $\hat{H}$

$$\hat{Q} = \int \mathrm{d}x\, \hat{q}(x), \quad \text{and} \quad [\hat{H}, \hat{Q}] = 0, \tag{1.10}$$

imposes the conservation law that the expectation value $\langle\psi(t)|\, \hat{Q}\, |\psi(t)\rangle$ is independent of time. Using translational invariance and rewriting this for the density $\hat{q}(x)$

$$\lim_{L\to\infty} \frac{1}{L} \int \mathrm{d}x\ \langle\psi(0)|\, \hat{q}(x)\, |\psi(0)\rangle = \lim_{t\to\infty} \lim_{L\to\infty} \langle\psi(t)|\, \hat{q}(x)\, |\psi(t)\rangle\,, \tag{1.11}$$

we see that having the conservation law (1.10) implies additional contraints on the steady state density $\hat{\rho}_{SE}$. More generally we will be looking at systems that contain multiple (infinite) such local conservation laws that are mutually compatible, meaning

$$[\hat{Q}^{(n)}, \hat{Q}^{(m)}] = 0, \tag{1.12}$$

for any operator $\hat{Q}^{(n)}$ with the attributes (1.10).

1.1.3 Non-equilibrium steady states

As discussed above, having one or multiple local conservation laws means that the system retains additional information about the initial state, that corresponds to equation (1.11). The ensemble describing the steady state of the system [10] is called a Generalized Gibbs Ensemble (GGE) and is given by

$$\hat{\rho}_{GGE} = \frac{1}{Z_{GGE}} e^{-\sum_n \beta_n \hat{Q}^{(n)}}, \tag{1.13}$$

where the Lagrange multipliers β_n are fixed by the condition

$$\mathbf{q}^{(n)} = \lim_{L\to\infty} \langle\psi_0|\, \hat{q}^{(n)}(x)\, |\psi_0\rangle = \mathrm{Tr}[\hat{\rho}_{GGE}\hat{q}^{(n)}(x)], \tag{1.14}$$

imposed by the conserved quantities. This description of systems with conservation laws in the steady state limit is ubiquitous in the field of integrability, as we will discuss later.

Integrable models with local interactions prepared in homogenous initial states relax locally to non-equilibrium steady states given by a Generalized Gibbs Ensemble, the parameters of which are defined by the expectation values if the conserved quantities in the initial state. According to this, the reduced density matrix of an arbitrary finite subsystem A is given by

$$\lim_{t\to\infty}\lim_{L\to\infty} \mathrm{Tr}_{\overline{A}}[\hat{\rho}(t)] = \lim_{L\to\infty} \mathrm{Tr}_{\overline{A}}[\hat{\rho}_{GGE}]. \tag{1.15}$$

The relaxation time in such cases depends on the size of the volume A for the given operator as well as the maximal propagation velocity of the elementary excitation of the theory.

1.2 Bosons in One Dimension

In three dimensions, interacting bosons at low temperatures undergo Bose-Einstein Condensation (BEC), a phenomenon, where below a critical temperature, a macroscopic fraction of the particles occupy the ground state, leading to long-range phase coherence. This condensate can be described within the framework of mean-field theories such as the Gross-Pitaevskii equation, which highlights the interplay between interactions and quantum statistics in many-body physics. In lower dimensions however, the behavior of bosonic systems deviates significantly from the three-dimensional case due to enhanced role of quantum fluctuations.

One-dimensional (1D) bosons, in particular, present a stark contrast to three-dimensional BECs. The restriction to a single spatial dimension amplifies the effects of interactions, preventing conventional Bose-Einstein condensation in the usual sense and leading to new quantum phases of matter. Depending on the interaction strength, 1D bosons can exhibit behaviors ranging from a weakly interacting regime to a strongly correlated Tonks-Girardeau gas, where fermionisation occurs due to

the suppression of multiple occupancy at short distances. Understanding these regimes is crucial not only for fundamental many-body physics but also for experimental realisations in ultracold atomic systems, where optical lattices and tight waveguides allow precise control over dimensionality and interactions.

A key feature of 1D bosonic systems is their integrability in specific cases, such as in the Lieb-Liniger model, where interactions are described by a delta-function potential. The exact solvability of this model via the Bethe Ansatz provides deep insight into the effects of interactions on the system's spectral properties, correlation functions, and dynamics. Unlike in three dimensions, where interactions are often treated perturbatively, the exact solutions of the Lieb-Liniger model reveal a rich structure even in the presence of strong interactions.

1.2.1 The Lieb-Liniger gas

Considering a system of N bosons confined in a volume of size L in 1D, interacting through 'density-density' interactions, its Hamiltonian in the 1st quantized form is

$$\hat{H} = \sum_{j=1}^{N} \frac{-\hbar^2}{2m} \frac{\partial^2}{\partial x_j^2} + \sum_{1 \le l < m \le N} V(x_l - x_m). \tag{1.16}$$

Introducing the canonical field operators $\hat{\Psi}(x,t)$, $\hat{\Psi}^\dagger(x,t)$ corresponding to the annihilation/creation of a particle at position x at time t. The standard bosonic equal-time commutation relations are

$$\left[\hat{\Psi}(x,t), \hat{\Psi}^\dagger(y,t)\right] = \delta(x-y), \quad \text{and} \quad \left[\hat{\Psi}(x,t), \hat{\Psi}(y,t)\right] = 0. \tag{1.17}$$

Thus, the Hamiltonian can be rewritten in the 2nd quantized form

$$\hat{H} = \int \mathrm{d}x \hat{\Psi}^\dagger(x) \left(-\frac{\hbar^2}{2m}\partial_x^2\right) \hat{\Psi}(x) + \frac{1}{2}\int \mathrm{d}x_1 \mathrm{d}x_2 V(x_1 - x_2) \hat{\Psi}^\dagger(x_1)\hat{\Psi}^\dagger(x_2)\hat{\Psi}(x_2)\hat{\Psi}(x_1). \tag{1.18}$$

We consider the interaction $V(x) = c\delta(x)$, and use $\hbar = 1$ and $m = 1$ in this section to keep the notation concise. The resulting first quantized Hamiltonian

$$\hat{\mathcal{H}} = -\frac{\infty}{\in} \sum_{|=\infty}^{\mathcal{N}} \frac{\partial^{\in}}{\partial \S_|^{\in}} + \rfloor \sum_{\infty \le | < \ell \le \mathcal{N}} \delta(\S_| - \S_\ell), \tag{1.19}$$

is known as the Lieb- Liniger model describing bosons interacting through a 'zero - range' potential of strength c. The corresponding second quantized Hamiltonian is then written as

$$\hat{H}_0 = \frac{1}{2}\int_0^L dx\ \hat{\Psi}^\dagger(x) \left[-\partial_x^2 + c\hat{\Psi}^\dagger(x)\hat{\Psi}(x)\right] \hat{\Psi}(x). \tag{1.20}$$

This system of interacting bosons belongs to a special class of low-dimensional systems that are integrable. To solve the model exactly, one can use the coordinate Bethe Ansatz, which constructs eigenstates of the Hamiltonian in terms of interacting plane waves with specific boundary conditions.

1.2.2 Cold Atom Experiments in One Dimension

Cold atomic setups are ideal for studying many-body physics. Due to the small energy scales and large distances between particles the interaction between particle can be modeled by simple terms.

In many cases they are well-represented by two-body contact interactions. These systems are also well isolated from the environment and the parameters controlling the physics, such as the interaction strength or the trapping potential are easily tunable. For these reasons cold atom setups are ideal to investigate the physics of 1D Bose gases with contact interactions. The main goal of this Section is to provide a brief review in the field of cold atomic experiments involving cold bosonic gases confined in low dimensions. This review is mostly based on the work [11], which we recommend for a more detailed discussion, along with [12].

Having tunable trapping potentials in cold atomic experiments is a powerful tool, as it allows the possibility to "freeze-out" dynamics in certain spatial dimensions, thus creating effectively low-dimensional system. One of the main drivers of the early pursuits of creating such low dimensional cold systems was the finding of Girardeau in 1960 [13]; who found that strongly interacting bosonic systems in one dimension display fermionic behavior in some aspects. This limit known today as the Tonks-Girardeau (TG) regime became a topic of great interest in the early 2000s as it allowed experimentalists to produce controllable samples of cold atoms in lower dimensional geometries (for a detailed review see [14]). For the theoretical treatment of such systems the key step was the work by Olshanii in 1998 [15] that provided a comprehensive description on modelling 1D physics, including very strong interactions, by tuning the confining geometry of the system. For quasi 1D-systems, pairwise interaction can be modelled via a δ-function interaction of the form

$$c = \frac{2\hbar^2 a_{3D}}{m a_\perp^2} \frac{1}{1 - C a_{3\mathrm{D}}/a_\perp}, \tag{1.21}$$

where a_{3D} is the three dimensional scattering length of the Bose gas, $a_\perp = \sqrt{\hbar/m\omega_\perp}$ is the characteristic harmonic oscillator length of the confining transverse potential with frequency $\omega_\perp$ and $C \approx 1.0326$ is a constant. The behaviour of the effective coupling constant varies as $a_{3\mathrm{D}}/a_\perp$ with a confinement-induced resonance (CIR) at the point $a_{3\mathrm{D}}/a_\perp = 1/C$, where one obtains $c \to \pm\infty$. Thus, in order to experimentally realize the Tonk-Girardeau regime one needs to get close to this value. One way to achieve it is to use the Feshbach resonance technique as it was utilized in one of the first experimental observation of CIR physics in 2005 [16].

Some of the first experiments used a combination of magnetic and optical traps to restrict the motion of atoms in weakly interacting Bose-Einstein condensates along the transverse directions [17, 18]. Alternatively, geometric confinement can be achieved using optical lattices to trap atoms on a grid, creating an array of effectively one dimensional "cigar-shaped" tubes of atoms [19–21]. It is done by creating a 2D optical lattice using laser fields with high intensity gradients resulting from interference. This optical lattice realizes a 2D array built up of 1D tubes of atoms where the effective 1D regime can be accessed [22–24], as shown on Fig 1.1. Such experimental setups have many advantages. It allows very strong transversal confinement as the light intensity can be modulated on distances as small as the laser wavelength. The atoms are loaded onto the optical lattice adiabatically from a 3D Bose-Einsten Condensate (BEC), allowing very low temperatures. Finally, the magnetic field is a free parameter which allows free tuning in order to approach Feshbach resonances and adjust the interaction strength of the atoms. These optical lattice realizations of 1D atomic systems have their own challenges and limitations. The most important being that all measurements conducted in such setups are ensemble measurements on the different tubes of the 2D array, since parameters like the particle number, interaction strength and even temperature vary between tubes, complicating the data analysis. This nature of the setup also prevents the measurement of correlations and fluctuations. The length of the tubes is also limited due to the nature of the trapping, this however does not prevent Time of Flight measurements (TOF) for obtaining rapidity and momentum distributions.

Another method to simulate low-dimensional systems is through the use of atom chips. These are carefully crafted surfaces with nano-wires that can trap atoms close to the surface [25, 26] (for

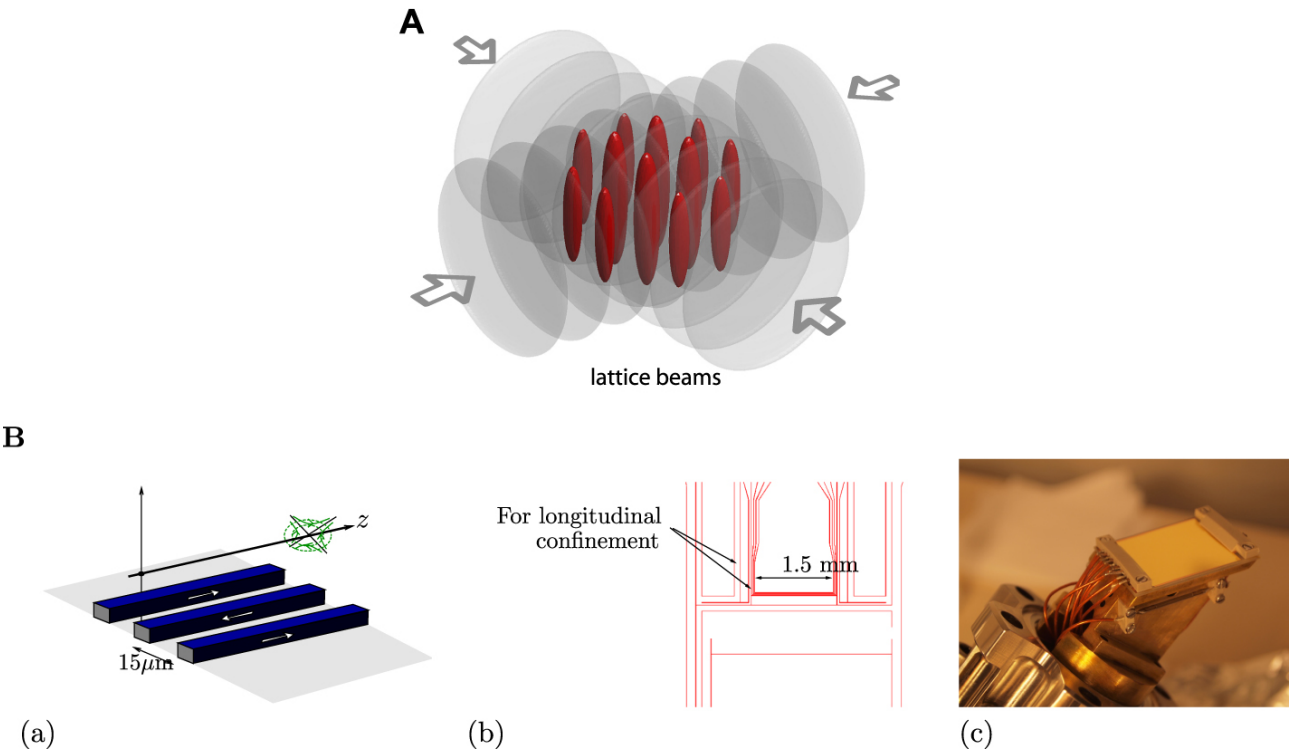


Figure 1.1: **A**. Schematic drawing of the typical realization of cigar shaped tubes from a 2D optical lattice (original figure published in [23], reused in the review [11]). **B**. From the review article [11]: Guiding atoms along a 3-wire guide on an atom chip. Pictures of the experimental atom-chip setup in Palaiseau, France. (a) The three wire guides with alternating current directions guide the atoms along the central wire. (b) Various other wires used for longitudinal confinement and preparation (c) Picture of the atom-chip covered with a gold mirror used in the experiment.

a detailed review see [12]). The idea of the atom chip setup is as follows. Consider a wire with a current running through it in an environment with a homogeneous magnetic field perpendicular to it. Atoms can be guided through the line (parallel to the wire guide, close to the surface of the atom chip) along which the magnetic field disappears. Now, replacing the homogeneous magnetic field with two wires on each side of the guiding wire with currents in the opposite direction, one obtains the configuration depicted on Figure 1.1. The main advantage of such experimental setups is that a single cloud of 1D gas can be obtained and studied (in contrast to the optical lattices), allowing direct comparison with theoretical predictions, as well as allowing the study of fluctuations and correlations. The nature of the trapping -namely that the transverse confinement is invariant along the whole microwire- allows a realization of 1D atoms on relatively long distances. One drawback of this method however is that -since the atoms are prepared and cooled directly in the atom chip- the temperatures that can be obtained are considerably higher than in the case of optical lattices [11, 27–29].

Through the experimental setups one gains access to many relevant quantities of low dimensional cold atoms. Some relevant quantities accessible are related to the density operator $\hat{\rho}(x)$, such as the zero-distance two-body correlation function [24]

$$g_2 = \langle (\hat{\Psi}^\dagger(0)^2 (\hat{\Psi}(0))^2 \rangle. \tag{1.22}$$

Other quantities include the measurement of the density fluctuations of the gas which are predicted by the Yang-Yang thermodynamics of the system [26] predicted by the theory of Yang and Yang in 1969 [30]. While these quantities involve only the real space momentum, information is contained

also in other observables such as the momentum distribution. One way of obtaining it is by the Bragg-technique which involves shining two laser fields with a well defined wavevector difference and frequency difference on the cold atoms, resulting in the absorption of a photon in one beam and a stimulated emission in the other, called the Bragg process. The atom absorbing the photon is effectively removed from the system. Measuring the loss-rate of the atomic cloud under the Bragg process gives access to the momentum distribution of the atoms, however it suffers from the drawback that it does not allow to record the whole momentum distribution in a single measurement [11, 31]. Another technique -referred to as the time-of-flight technique (TOF)- is based on the ability to switch off the interaction of the gas almost instantaneously with respect to the longitudinal motion. In the case of 1D gases this can be achieved by a sudden switching off of the transversal confinement, after which the remaining task is measuring the momentum distribution of an ideal gas. After sufficient time, when the size of the atomic cloud is much larger than its initial size, the density distribution and the momentum distribution are homothetic. Such methods were used in [31] and recently in [32, 33]. Theoretically, one way of obtaining the momentum distribution $f(\mathbf{p})$ is through the Fourier transform

$$f(\mathbf{p}) = \int d\mathbf{x} \int d\mathbf{y}\ e^{i\mathbf{p}(\mathbf{x}-\mathbf{y})} g_1(\mathbf{x}, \mathbf{y}), \tag{1.23}$$

of the equal-time correlation function

$$g_1(\mathbf{x}, \mathbf{y}) = \langle \hat{\Psi}^\dagger(\mathbf{x}) \hat{\Psi}(\mathbf{y}) \rangle, \tag{1.24}$$

which is known as the One-Particle Density Matrix (OPDM). During this thesis one of our main focus is obtaining these quantities in various setups and temperatures, focusing on equilibrium and dynamical cases, using the methods discussed in the coming parts of this Chapter.

1.2.3 Coordinate Bethe Ansatz

In this subsection, we present the coordinate Bethe Ansatz solution of the translationally invariant (no external potential $V(x_i)$ present in the Hamiltonian (1.19)) Lieb-Liniger model in the case of repulsive interactions ($c > 0$). This approach allows for the exact construction of many-body eigenstates of the Hamiltonian by expressing the wavefunction as a superposition of plane waves, constrained by interaction-dependent phase shifts. Then we detail the structure and implications of the Bethe equations that emerge in the thermodynamic limit, which we will be using extensively in the following parts of this work.

The Bethe Wavefunction

Let us consider N bosons with the Hamiltonian (1.19), with interaction strength $c > 0$. We write the ansatz for the eigenstates

$$\psi(x_1, ..., x_N, \mathcal{Q}) = \sum_{\mathcal{P}} A_{\mathcal{P}}(\mathcal{Q}) e^{i(\lambda_{\mathcal{P}_1} x_1 + \lambda_{\mathcal{P}_2} x_2 + ... + \lambda_{\mathcal{P}_N} x_N)}, \tag{1.25}$$

with energy

$$E = \sum_{j=1}^{N} \frac{\lambda_j^2}{2}; \tag{1.26}$$

It is also an eigenstate of the momentum operator

$$\hat{K} = -i \sum_{j=1}^{N} \frac{\partial}{\partial x_j}, \tag{1.27}$$

with eigenvalue $K = \sum_{j=1} \lambda_j$. Here λ_i is a set of quasi-momenta (also often called rapidities) given by a permutation $\mathcal{P}$ and $\mathcal{Q}$ is the permutation of the particles. Since we are writing the eigenstates of a system of bosons the wavefunction should remain invariant under different permutations of the particles $\mathcal{Q}$ and $\mathcal{Q}'$. This implies that $A_{\mathcal{P}'}(\mathcal{Q}) = A_{\mathcal{P}}(\mathcal{Q}')$, where the permutation $\mathcal{P}$ differs from $\mathcal{P}'$ in the same indices where $\mathcal{Q}'$ differs from $\mathcal{Q}$. Thus solving the spectrum for a choice of permutation $\mathcal{Q}$ is sufficient to solve the whole spectrum, as any other permutation $\mathcal{Q}'$ can be straightforwardly generated by permuting the momenta accordingly. In the following we suppress the explicit dependence on $\mathcal{Q}$ and focus on a subspace where $x_1 < x_2 < ... < x_N$ and solve the system in this sector.

Taking first $N = 2$, the complete wave function is written as

$$\psi(x_1, x_2) = f(x_1, x_2)\Theta(x_2 - x_1) + f(x_2, x_1)\Theta(x_1 - x_2), \tag{1.28}$$

with $\Theta(x)$ being the Heaviside step-function and

$$f(x_1, x_2) = A_{12} e^{i(\lambda_1 x_1 + \lambda_2 x_2)} + A_{21} e^{i(\lambda_2 x_1 + \lambda_1 x_2)}. \tag{1.29}$$

It is now easy to see that the eigenvalue equation for (1.28) with eigenenergy $\varepsilon = \frac{k_1^2 + k_2^2}{2}$ is satisfied if

$$\frac{A_{12}}{A_{21}} = \frac{i(\lambda_1 - \lambda_2) + c}{i(\lambda_1 - \lambda_2) - c} = e^{i\tilde{\theta}(\lambda_1 - \lambda_2)}, \tag{1.30}$$

with

$$\tilde{\theta}(\lambda) = 2 \arctan \frac{\lambda}{c} + \pi, \tag{1.31}$$

which is the phase shift resulting from the interaction present in the model. It is an important sidenote that in the limit of infinite interaction strength $c \to \infty$ it becomes the scattering phase of the free fermions. This is a result that has important consequences in describing the gas at strong interaction strengths, and one that we will extensively make use of throughout this thesis. Since the interaction is local and arises from the discontinuity of the derivative of the wave functions across sectors with different particle orderings (each corresponding to a two-particle permutation), there is no three-particle scattering (diffraction).

Coming back to the system of N bosons, we see that all permutations can be generated by exchanging two indices at a time, and the ratio of amplitudes of permutations $\mathcal{P}$ and $\mathcal{P}'$ that differ only in one permutation

$$\frac{A_{\mathcal{P}}}{A_{\mathcal{P}'}} = e^{i\tilde{\theta}(\lambda - \lambda')}, \tag{1.32}$$

is equivalent to the two particle scattering for the case of two particles. Thus for the amplitudes we obtain

$$A_{\mathcal{P}} \propto (-1)^{\mathcal{P}} \prod_{j<l} (\lambda_{\mathcal{P}_j} - \lambda_{\mathcal{P}_l} + ic) \tag{1.33}$$

The system can be quantized by imposing suitable boundary conditions. A straightforward choice is to impose periodic boundary conditions (PBC) on a system of size L and later take it to infinity.

The Bethe equations

Putting the system on a circle of length L by imposing PBC results in the equality

$$\psi(x_1, x_2, ..., x_j + L, ..., x_N) = \psi(x_1, x_2, ..., x_j, ..., x_N), \quad \text{for} j = 1, ..., N. \tag{1.34}$$

By taking a particle around the system it scatters across all other particles, acquiring the sum of all two particle scattering during that. It can also be understood as moving between sectors of particle orderings that can be expressed as different $\mathcal{P}$ permutations of momenta. This gives rise to the Bethe equations

$$e^{i\lambda_j L} = \prod_{\ell \neq j} \frac{\lambda_j - \lambda_\ell + ic}{\lambda_j - \lambda_\ell - ic}, \quad j = 1, \ldots, N, \tag{1.35}$$

or, equivalently, in logarithmic form

$$\lambda_j + \frac{1}{L} \sum_{\ell=1}^{N} 2 \arctan \frac{\lambda_j - \lambda_\ell}{c} = \frac{2\pi}{L} I_j \tag{1.36}$$

Equation (1.36) uniquely specifies a rapidity set $\boldsymbol{\lambda}$ [hence, an eigenstate of the Hamiltonian (1.110)] for a set of distinct integers (half-integers) $I_1, \ldots, I_N$ for N even (odd). In fact, the right-hand side of Eq. (1.36) can be interpreted as the set of momenta of a noninteracting Fermi gas. From this perspective, the Bethe Ansatz equations impose a nontrivial quantisation condition on the rapidities that encodes the effects of the contact interactions. For example, the ground-state configuration $\boldsymbol{\lambda}_{\text{GS}}$ corresponds to choosing the quantum numbers as $I_j = -\frac{N+1}{2} + j$, which amounts to filling a Fermi sea, as one would do for a free fermionic system. Another important consequence of the Bethe equations is that, due to the nature of $\arctan(\lambda_j - \lambda_k) = -\arctan(\lambda_k - \lambda_j)$ the full momenta of the system is quantized and is given by

$$K = \frac{2\pi}{L} \sum_{j=1}^{N} I_j, \tag{1.37}$$

independent of the coupling constant.

Elementary excitations

As stated before, since all the numbers must be distinct, the ground state that minimizes the energy and momentum is a symmetric configuration of the form

$$\{I_j\} = -\frac{N-1}{2}, -\frac{N-3}{2}, \ldots, \frac{N-1}{2}, \tag{1.38}$$

for which the total momentum is zero, $K = 0$. Making use of observation of the previous section we can interpret the excited states in terms of individual excitations, which are essentially of two types.

The first type of excitations consist of adding a particle to the N-particle ground state (1.38). The new particle must necessarily have a rapidity $|\lambda_p| > \lambda_N$. In the case of $\lambda_p > 0$, the excited state with a particle number $N + 1$ corresponds to the configuration

$$\{I'_j\} = -\frac{N}{2}, -\frac{N}{2} + 1, \ldots, \frac{N}{2} - 1, \frac{N}{2} + p \quad \text{with } p \in \mathbb{Z}, \tag{1.39}$$

with the total momentum $K = \frac{2\pi}{L}p$. The configuration of rapidities is therefore entirely modified by the addition of a particle,

$$\{\lambda_j\} = \frac{2\pi}{L}\{I_j\} \to \{\lambda'_j\} = \frac{2\pi}{L}\{I'_j\}, \tag{1.40}$$

as it can be seen by the form of the Bethe equations (1.36), meaning that the total momentum $K = \frac{2\pi}{L}p$ gained by the system is not simply equal to the rapidity λ_p of the new particle. Regardless of the interaction strength, the system is thus always strongly correlated, or in other words, excitations are always collective.

The other type of excitations are the opposite of the first, as they consist of removing a particle from the N-particle ground state (1.38), i.e., they create a hole. For excitations of this kind, the configuration of Bethe numbers $\{I''_j\}$ is constructed starting from the ground state with $N-1$ particles, from which a particle with rapidity $|\lambda_r| < \lambda_{\text{max}}$ is moved to the first unoccupied number in the configuration, with either positive or negative momentum. Such a configuration is, for example,

$$\{I''_j\} = -\frac{N}{2}+1, -\frac{N}{2}+2, \ldots, \frac{N}{2}-r-1, \frac{N}{2}-r+1, \ldots, \frac{N}{2} \quad \text{with } p \in \mathbb{Z}, \tag{1.41}$$

with the total momentum of $K = \frac{2\pi}{L}r$.

In the thermodynamic limit, it can be shown that these two types of excitations are sufficient to generate all low-energy excited states. For example, density fluctuations are particle-hole excitations and are therefore given by a combination of the two excitations.

In the form (1.36), the Bethe equations can be solved numerically for systems with thousands of particles. One can go further by considering the thermodynamic limit, in which the Bethe Ansatz simplifies.

1.2.4 Thermodynamic Bethe Ansatz

In the thermodynamic limit, $N \to \infty$ and $L \to \infty$ at fixed density $n = N/L$, it is convenient to replace the rapidity set $\boldsymbol{\lambda}$ with a smooth density distribution. In order to do this it is useful to introduce a counting function $y(\lambda)$

$$\lambda_j + \frac{1}{L}\sum_{l=1}^{N}\theta(\lambda_j - \lambda_l) = y(\lambda_j), \tag{1.42}$$

with $\theta(\lambda) = 2\arctan\frac{\lambda}{c}$ being the two-particle scattering phase, so that by definition $y(\lambda_j) = \frac{2\pi I_j}{L}$, which is a monotonically increasing function that counts the integers as a function of the rapidities. Taking now the thermodynamic limit we introduce the rapidity density as

$$\rho(\lambda_j) = \lim_{N,L\to\infty}\frac{1}{L(\lambda_{j+1}-\lambda_j)}. \tag{1.43}$$

Now we can replace the summations with integrals as

$$\sum_{j=1}^{N} \to L\int \rho(\lambda')\mathrm{d}\lambda'. \tag{1.44}$$

Furthermore, using Equations (1.43) and (1.42) we can prove the equality

$$y'(\lambda_j) = \lim_{N,L\to\infty}\frac{y(\lambda_j)-y(\lambda_{j-1})}{\lambda_j-\lambda_{j-1}} = \lim_{N,L\to\infty}\frac{2\pi}{L(\lambda_j-\lambda_{j-1})} = 2\pi\rho(\lambda_j), \tag{1.45}$$

leading to

$$\frac{1}{2\pi}y(\lambda) = \int_{-\infty}^{\lambda} \rho(\lambda')\mathrm{d}\lambda', \tag{1.46}$$

giving the distribution of integers as a function of rapidity density (or root density, as often referred to in litwerature). Using these definitions, the system of algebraic equations can be rewritten as an integral equation for the counting function and rapidity density in the thermodynamic limit as

$$y(\lambda) = \lambda + \int_{-\infty}^{\infty} \theta(\lambda - \lambda')\rho(\lambda')\mathrm{d}\lambda'. \tag{1.47a}$$

Taking the derivative with respect to λ we obtain

$$2\pi\rho(\lambda) = 1 + \int_{-\infty}^{\infty} \mathcal{K}(\lambda - \lambda')\rho(\lambda')\mathrm{d}\lambda', \tag{1.47b}$$

where we introduced the Kernel of the Lieb-Liniger model $\mathcal{K}(\lambda)$ as the derivative of the scattering phase:

$$\mathcal{K}(\lambda) = \frac{\mathrm{d}}{\mathrm{d}\lambda}\theta(\lambda) = \frac{2c}{c^2 + \lambda^2}. \tag{1.48}$$

The integral equation with this kernel is known as the Lieb-Liniger equation [34, 35], it allows us to determine the distribution of the rapidities. This distribution depends on the support of the kernel, that is determined by the choice of the integers in the original Eqs. (1.36). Through this equation, we find that the densities of physical quantities such as particle density and energy density are given by the root density as

$$n = \frac{N}{L} = \int_{-\infty}^{\infty} \rho(\lambda')\mathrm{d}\lambda', \quad p = \frac{K}{L} = \int_{-\infty}^{\infty} \lambda'\rho(\lambda')\mathrm{d}\lambda' \quad \text{and} \quad \varepsilon = \frac{E}{L} = \int_{-\infty}^{\infty} \rho(\lambda')\frac{\lambda'^2}{2}\mathrm{d}\lambda'. \tag{1.49}$$

Through these equations one can gain access to thermodynamic quantities such as the chemical potential:

$$\mu = \frac{\partial\varepsilon}{\partial\rho}. \tag{1.50}$$

In many cases throughout this work we will introduce a chemical potential μ to fix the number of particles N through the support of the Lieb-Liniger kernel.

In the example of the N particle ground state, the Bethe integers that define the state are given by (1.38), thus in the thermodynamic limit the support of $\rho(\lambda)$ is symmetric so that the energy and the momentum are minimized $\lambda \in [-\lambda_F, \lambda_F]$, with a Fermi rapidity λ_F fixed by the condition

$$n = \frac{N}{L}\int_{-\lambda_F}^{\lambda_F} \rho(\lambda')d\lambda', \tag{1.51}$$

and with sound velocity

$$v = \sqrt{\rho\frac{\partial^2\varepsilon}{\partial\rho^2}}. \tag{1.52}$$

From the equations written in (1.59), the root density written in terms of the counting function is

$$\rho(\lambda)\mathrm{d}\lambda = \vartheta(\lambda)\frac{\mathrm{d}y}{\mathrm{d}\lambda}\mathrm{d}\lambda, \tag{1.53}$$

where we defined the *occupation function* $\vartheta(\lambda)$. It is also customary to define the hole density $\rho_h(\lambda)$ as

$$\frac{\rho(\lambda)}{\vartheta(\lambda)} = \rho(\lambda) + \rho_h(\lambda), \tag{1.54}$$

establishing that, instead of the counting function $y(\lambda)$ the root density can be used to characterize the thermodynamic limit of the system, that we call macro-state. Another important implication of this is that different micro-states given by $\{I_j\}$, $\{\tilde{I}_j\}$ can lead to the same macro-state characterized by $\rho(\lambda)$ in the thermodynamic limit.

The Dressing Operation

To make notations and calculations clearer in the following, we introduce the 'dressing operation' on a generic function of rapidities $h(\lambda)$ as

$$h^{\mathrm{dr}}(\lambda) = h(\lambda) + \int_{-\infty}^{\infty} \frac{d\lambda'}{2\pi} \frac{2c}{c^2 + (\lambda - \lambda')^2} h^{\mathrm{dr}}(\lambda')\vartheta(\lambda'), \tag{1.55}$$

in terms of which $\rho(\lambda) \equiv [1/(2\pi)]^{\mathrm{dr}}$ following Eq. (1.59).

Expectation Values of Conserved Quantities

The Lieb-Liniger gas has infinitely many conserved charges given by densities $Q^{(n)}(x)$. Taking a micro-state $|\lambda_1, ..., \lambda_N\rangle$ the expectation value of these charges, due to translational invariance fulfills

$$\langle \lambda_1, ..., \lambda_N | \, Q^{(n)}(x) \, | \lambda_1, ..., \lambda_N \rangle = \int_{-\infty}^{\infty} q_n(\lambda)\rho(\lambda)\mathrm{d}\lambda, \tag{1.56}$$

where the micro-state $|\lambda_1, ..., \lambda_N\rangle$ with particle number N and system size L corresponds to a macro-state $\rho(\lambda)$ with $N, L \to \infty$ and particle density $n = \frac{N}{L} = const.$, with

$$q_n = \lambda^n, \quad n = 0, 1, ..., \tag{1.57}$$

with $n = 0, 1, 2$ corresponding to particle number, momentum and energy respectively. Thus in the thermodynamic limit these expectation values don't depend on the choice of the micro-state and the expectation value is fixed by the root density $\rho(\lambda)$:

$$\langle \rho | \, Q^{(n)}(x) \, | \rho \rangle = \lim_{N,L\to\infty} \langle \lambda_1, ..., \lambda_N | \, Q^{(n)}(x) \, | \lambda_1, ..., \lambda_N \rangle \, . \tag{1.58}$$

The Ground State

The ground in the thermodynamic limit that minimizes momentum and energy at a given density $n = N/L$ is characterized by the root density defined by

$$2\pi\rho(\lambda) = 1 + \int_{-\lambda_{\mathrm{F}}}^{\lambda_{\mathrm{F}}} \mathcal{K}(\lambda - \lambda')\rho(\lambda')\mathrm{d}\lambda', \tag{1.59}$$

where λ_F is the Fermi rapidity which determines the support of the density. Physically, λ_{F} plays the role of a Fermi momentum in this interacting system: all rapidities λ with $|\lambda| < \lambda_{\mathrm{F}}$ are occupied,

while those with $|\lambda| > \lambda_{\mathrm{F}}$ are empty at zero temperature. The value of λ_{F} is fixed by the total density n through the normalization condition

$$n = \int_{-\lambda_{\mathrm{F}}}^{\lambda_{\mathrm{F}}} \rho(\lambda)\mathrm{d}\lambda. \tag{1.60}$$

For a fixed interaction strength c and density n the Fermi rapidity λ_{F} is uniquely determined, and the ground state is fully characterized.

1.2.5 The Tonks - Girardeau Limit

In the limit of strong interactions $c \to \infty$ the Bethe equations (1.36) derived for the Lieb- Liniger gas simplify, giving

$$\lambda_j = 2\pi \frac{I_j}{L}, \tag{1.61}$$

which correspond to the momenta N of non-interacting fermions. Looking at the thermodynamic limit we can also see that in the limit $c \to \infty$ the ground-state rapidity distribution reduces to the momentum distribution of spinless free fermions:

$$\rho(\lambda) = \begin{cases} \frac{1}{2\pi}, & \text{if} \quad \lambda < \lambda_F \\ 0, & \text{otherwise.} \end{cases} \tag{1.62}$$

While for finite interaction strength there is an effective Pauli principle at the level of rapidities, it is straighforward to see that the infinite interaction limit corresponds to a gas of hard-core, impenetrable particles also known as the Tonks - Girardeau (TG) gas studied by M. Girardeau in 1960 [36], leading to a Pauli principle in real space as well, as the eigenstate of such a gas must vanish if two particles are in the same position. It was shown by Girardeau that the bosonic eigenstate obtained from the Bethe Ansatz is related to an eigenstate of fermions under the constraint

$$\psi(x_1, ..., x_N) = \prod_{j>k} \mathrm{sign}(x_j - x_k)\psi_F(x_1, ..., x_N), \tag{1.63}$$

where the product symmetrizes the fermionic state $\psi_F(x_1, ..., x_N)$. The transformation can be formulated at the level of the Hamiltonian (1.20) and the bosonic creation/annihilation operators $\hat{\Psi}^\dagger(x)/\hat{\Psi}(x)$. Defining fermionic ladder operators $\hat{\Psi}_F^\dagger(x)/\hat{\Psi}_F(x)$ with fermionic anti-commutation relations

$$\{\hat{\Psi}_F^\dagger(x), \hat{\Psi}_F(y)\} = \delta(x-y), \quad \text{and} \quad \{\hat{\Psi}_F(x), \hat{\Psi}_F(y)\} = 0, \tag{1.64}$$

they are related to their hard-core bosonic counterparts by the transformation

$$\hat{\Psi}_F^\dagger(x) = e^{i\pi \int_{y<x} \hat{\Psi}^\dagger(y)\hat{\Psi}(y)\mathrm{d}y} \hat{\Psi}^\dagger(x), \tag{1.65}$$

which makes the Hamiltonian

$$\hat{H}_0 = -\frac{1}{2}\int_0^L dx\ \hat{\Psi}_F^\dagger(x)\partial_x^2\hat{\Psi}_F(x), \tag{1.66}$$

quadratic in the fermions. This fermion-boson correspondence [37] can be understood as the continuous analogue of the Jordan-Wigner transformation [38, 39]. Despite the mapping discussed, the out-of-equilibrium dynamics and equal time correlation functions of hard-core bosons can differ significantly from that of free fermions. An example of such a striking difference is the evolution of the momentum distribution and the One Particle Density Matrix (OPDM), as we discuss later in detail. Nevertheless this correspondence provides us with a powerful tool, which in many cases simplifies calculations and allows us to obtain analytical results for correlations in the hydrodynamic regime.

1.2.6 The super Tonks - Girardeau (sTG) Gas

Bound states and string solutions

In the Coordinate Bethe Ansatz detailed so far, we assumed repulsive ($c > 0$) interactions. For the attractive case, additional solutions can be constructed, corresponding to bound states, with rapidities that are complex valued. General solutions with complex momenta for a three particle problem with an attractive $c < 0$ interaction strength can be written in two different ways:

$$\lambda_1 = q - ic, \quad \lambda_2 = q + ic, \quad \lambda_3 = k, \tag{1.67a}$$

or

$$\lambda_1 = q - ic, \quad \lambda_2 = q + ic, \quad \lambda_3 = q; \tag{1.67b}$$

While the first case is a bound state of two particles scattering on an independent particle, the second case is a three-particle bound state. Bounds states with n particles appear in strings of particles with the same real part of the rapidity. A string of length n has the rapidities equispaced symmetrically along the imaginary axis. Thus an n-string in the attracive Lieb-Liniger gas is characterised by the rapidities

$$\lambda_j = \frac{Q}{n} - i\frac{n+1-2j}{2}c, \quad \text{with} \quad j = 1, ..., n, \tag{1.68}$$

with total momentum Q and energy

$$E = \frac{Q^2}{n} - \frac{n(n^2-1)}{12}c^2. \tag{1.69}$$

A state of a gas of N particles for an attractive interaction can be characterised by the full rapidity of each given string Q_{L_n} where index L_n counts the number of strings of size n present with

$$N = \sum_{n=1}^{N} L_n n, \tag{1.70}$$

where $n = 1$ denotes the unbound states, and L_n is the number of strings of size n. The energy of an n-string monotonously decreases with the number n. Therefore the ground state of a system containing N particles is characterized by a zero total momentum string of length N, whose energy diverges negatively like N^3. For the thermodynamic limit to exist, the ground state energy should scale linearly with N, leading to the conclusion that the attractive Lieb-Liniger is unstable in the thermodynamic limit.

Despite the collapse of the thermodynamic limit of the attractive Bose gas, the strongly attractive regime, known as the super-Tonks-Girardeau gas (sTG gas for short) can be experimentally observed. The reason for this lies in the preparation of the state by abruptly changing the effective coupling c from large positive to large negative values, through Feshbach resonances of a trapped three dimensional bosonic gas [40–42] .

The sTG gas

The coupling c of the δ interaction can be expressed with the parameters of a trapped three dimensional Bose gas as

$$c = \frac{2\hbar^2 a_{3D}}{m a_\perp^2} \frac{1}{1 - C a_{3D}/a_\perp}, \tag{1.71}$$

where a_{3D} is the three dimensional scattering length of the Bose gas, $a_\perp = \sqrt{\hbar/m\omega_\perp}$ is the characteristic harmonic oscillator length of the confining transverse potential with frequency $\omega_\perp$ and $C \approx 1.0326$ is a constant. The dimensionless coupling can be defined as

$$\gamma = \frac{mc}{\hbar^2 n}, \tag{1.72}$$

where $n = N/L$ is the particle density (with the length of the system being L). In the repulsive ($\gamma > 0$) weakly interacting regime $\gamma \ll 1$ the Bogoliubov approximation gives a good estimate of the ground–state energy of the system. Whereas in the strongly interacting limit of $\gamma \gg 1$ one approaches the Tonks-Girardeau limit, where the effect of being confined in one dimension and the strong repulsion leads to an effective Pauli exclusion and the system can be mapped into free fermions. It was predicted several years ago that if γ is large and negative there exists a highly excited gaseous state called the super Tonks-Girardeau gas [43], which is metastable against collapsing into the ground state (which consists of an N particle bound state). This state was recreated by suddenly switching the interaction from strongly repulsive to strongly attractive [40–42]. By tuning $a_\perp$ with the help of magnetic fields, the dimensionless coupling can change sign. The critical value for $a_\perp$, as can be seen from (1.71), is at $a_\perp = Ca_{3D}$. Changing the parameter $a_\perp$ so that it crosses this value corresponds to abruptly changing from large positive values of γ to large negative values.

For $\gamma < 0$ the solutions for the set $\{\lambda_j\}$ in the Bethe equations can be complex, which allows for bound states or string solutions. The ground state of such an attractive model is an N-string consisting of all the particles in the system. The lowest lying gas like state however is highly excited state of the system which can be realized in tight waveguides by crossing adiabatically the critical $a_\perp$ value. The resulting state closely resembles the ground state of a repulsive system with $I_j \in \left[-\frac{N-1}{2}, -\frac{N-2}{2}, ..., \frac{N-1}{2}\right]$. This is the super Tonks-Girardeau gas from the Bethe Ansatz description.

The structure of excitations around this state is similar to the repulsive case (particle-hole excitations) with the addition of the formation of bound states. It was shown however [43–45] that local fluctuations are not efficient at bringing particles together. This makes the formation of bound states very slow, which allows the system to be sufficiently long-lived to be experimentally observable. This stability can be seen from the fact that the rate of formation of bound states is approximately only one order of magnitude larger than the rate of 3-body collisions, and that the compressibility of the gas is positive for large attractive interactions.

1.2.7 Quasicondensation

In three dimensions the Bose-Einstein condensate is charaterised by a macroscopic occupation of a single eigenstate that leads to the phenomenon of off-diagonal long range order (ODLRO) in the One Particle Density Matrix (1.24) that decays to a constant value over large distances indicating a coherent phase. In the case of one dimension however, this description breaks down due to the enhanced effect of quantum fluctuations in low-dimensional systems, even at zero temperature. Instead, zero temperature Bose gases exhibit a quasi-condensate regime, characterized by a power law decay of (1.24). The theoretical framework to describe this regime combines mean-field approaches (e.g., modified Gross-Pitaevskii equations), stochastic classical field methods, and low-energy effective theories such as the Luttinger liquid and Bogoliubov theory in one dimension. For example, as discussed in more detail later, Luttinger liquid theory provides well-known asymptotic results for the OPDM of one-dimensional bosonic gases. In homogeneous (i.e., translationally invariant) ground states, the long-distance behavior of $g_1(x, y)$ is predicted to follow a universal form derived

from Luttinger liquid theory [46–49]:

$$\frac{g_1(x,y)}{n} \underset{|x-y|\gg d(n)}{\simeq} \sum_{m\geq 0} \frac{B_m 2\cos(2mk_F|x-y|)}{(n|x-y|)^{2m^2K+\frac{1}{2K}}}. \tag{1.73}$$

Here, n denotes the one-dimensional atomic density, k_F is the Fermi momentum, and K is the Luttinger parameter, which depends on the strength of interactions between the bosons. The parameter $d(n)$ is the characteristic length scale of the microscopic problem, generally taken to be the maximum between the interparticle distance n^{-1} and the healing length $\xi_{\text{heal}} \propto 1/\sqrt{n}$.

Another quantity used to determine the existence of a quasicondensate is the occupation of the natural orbitals (NO) given by the eigenspectrum of the OPDM:

$$\int_L g_1(x,y;t)\ \xi_i(y)\mathrm{d}x = \Lambda_i\ \xi_i(y). \tag{1.74}$$

The scaling of the largest eigenvalue Λ_0 of the one-particle density matrix $g_1(x,y)$ with the number of particles defines an exponent $\mathcal{C}$ via the relation

$$\Lambda_0 \propto N^{\mathcal{C}}. \tag{1.75}$$

This exponent $\mathcal{C}$ characterizes the occupation of the most populated natural orbital. According to the Penrose–Onsager criterion [50], $\mathcal{C} = 1$—that is, $\Lambda_0 \propto N$—indicates the presence of a true Bose–Einstein condensate, as a macroscopical part of the particles occupies a single natural orbital.

In one-dimensional systems with particle-number conservation, however, $\mathcal{C}$ is strictly less than one due to the Mermin–Wagner theorem, which forbids spontaneous breaking of continuous symmetries at finite temperature in low-dimensional systems with short-range interactions. Nonetheless, when $\mathcal{C}$ remains close to one, the system is typically referred to as a quasicondensate, since the leading natural orbital still hosts a macroscopically large number of particles [51–55].

In the quasi-condensate many thermodynamic properties (such as ODLRO and macroscopic occupancy of natural orbitals) resemble those of a true condensate. The momentum distribution instead of being a true delta-function peak at $k = 0$, shows a broadened central feature. These features have been observed experimentally through measurements of coherence functions and momentum distributions in cold atoms trapped in optical waveguides [56–58].

1.3 Generalized Hydrodynamics

In classical 1+1 dimensional (1 spatial and 1 temporal dimension) systems hydrodynamics is used to describe the non-equilibrium dynamics of systems on an intermediate time and length scale, assuming that the fluid is locally equilibrated at all times, meaning that it relaxes to a local equilibrium state characterized by the conserved quantities of the system. The time evolution of these conserved quantities is governed by continuity equations. A notable example is the Galilean fluid [11], which conserves particle number, momentum, and energy. At the Euler scale, the hydrodynamic description is then given by the continuity equations for the particle density, momentum density, and energy density:

$$\begin{aligned}
&\frac{\partial}{\partial t}\rho_n(x,t) + \frac{\partial}{\partial x} j_n(x,t) = 0 \\
&\frac{\partial}{\partial t}\rho_P(x,t) + \frac{\partial}{\partial x} j_P(x,t) = -\frac{1}{m}\frac{\partial V(x)}{\partial x} q_n(x,t) \\
&\frac{\partial}{\partial t}\rho_E(x,t) + \frac{\partial}{\partial x} j_E(x,t) = 0.
\end{aligned} \tag{1.76}$$

It has to be noted that the second equation is only a continuity equation if there are no forces acting on the fluid i.e. $\frac{\partial V(x)}{\partial x} = 0$. Because of local equilibration, the currents depend on x and t implicitly through the charge densities. In general, the currents $j_i(x,t)$ are functions of all densities as well as their first and second derivatives $\rho_j(x,t), \partial_x\rho_j(x,t), \partial_x^2\rho_j(x,t)$. However, for smoothly varying density (very long wavelengths), the dependence on spatial derivatives can be neglected, and the currents become functions of the local densities only. The resulting zeroth-order hydrodynamic equations are commonly referred to as *Euler-scale* hydrodynamics.

In integrable quantum systems such as the Lieb-Liniger gas the number of conserved quantities is infinite (1.57), and the time evolution is governed by the time dependent Schrödinger equation. The framework of Generalized Hydrodynamics (GHD) constructed in 2016 [1, 2] provides a description of Euler scale hydrodynamics of integrable quantum systems. The basic idea [59, 60] is given by assuming that the system with local time-independent Hamiltonian $\hat{H}$ at time $t = 0$ is described by the density matrix $\hat{\rho}(0)$. According to the Scrhödinger equation the system evolves as

$$\hat{\rho}(t) = e^{-i\hat{H}t}\hat{\rho}(0)e^{i\hat{H}t}. \tag{1.77}$$

Assuming now that the system has other local conservation laws $[\hat{Q}^{(n)}, \hat{H}] = [\hat{Q}^{(n)}, \hat{Q}^{(m)}]$ in addition to the energy (it is conserved as the time evolution is unitary) given by local operators

$$\hat{Q}^{(n)} = \int \hat{Q}^{(n)}(x)\mathrm{d}x, \tag{1.78}$$

We write the time evolution of the local operators as a continuity equation

$$\partial_t\hat{Q}^{(n)}(x,t) + \partial_x\hat{J}^{(n)}(x,t) = 0, \tag{1.79}$$

with $\hat{J}^{(n)}(x,t)$ being the current associated to the local observable $\hat{Q}^{(n)}(x,t)$. Taking the expectation values

$$\mathbf{q}_n(x,t) = \mathrm{Tr}\left[\hat{\rho}(t)\hat{Q}^{(n)}(x,t)\right], \tag{1.80}$$

$$\mathbf{j}_n(x,t) = \mathrm{Tr}\left[\hat{\rho}(t)\hat{J}^{(n)}(x,t)\right], \tag{1.81}$$

we choose to look at the system at length and time scales that are large compared to the *mesoscopic* Euler scale. Now, we assume that at these time scales the system has relaxed locally to a state that is fully characterize by the conserved quantities. This implies

$$\mathbf{j}_n(x,t) = \mathbf{j}_n[\{\mathbf{q}_m(x,t)\}], \tag{1.82}$$

which leads to

$$\partial_x\mathbf{j}_n(x,t) \equiv \sum_m A_{n,m}[\{\mathbf{q}_m(x,t)\}]\partial_x\mathbf{q}_m(x,t) \tag{1.83}$$

Assuming that $A_{n,m}[\{\mathbf{q}_m(x,t)\}]$ can be diagonalized with eigenvectors $v_\alpha[\{\mathbf{q}_m(x,t)\}]$, it leads to the equation

$$\partial_t\xi_n(x,t) + v_n(x,t)\partial_x\xi_n(x,t) = 0, \tag{1.84}$$

where $\xi_n(x,t)$ are the "hydrodynamic normal modes" defined by the transformation $R_{n,m} = \frac{\partial\mathbf{q}_n}{\partial\xi_m}$. The difficulty in this formalism lies in the fact that the velocities $v_n(x,t)$ depend on the consevation laws in an unknown way. In integrable models, such as the Lieb-Liniger gas, this dependence can be worked out, which then allows the calculation of the modes $\xi_n(x,t)$, that fixes the expectation values of observables.

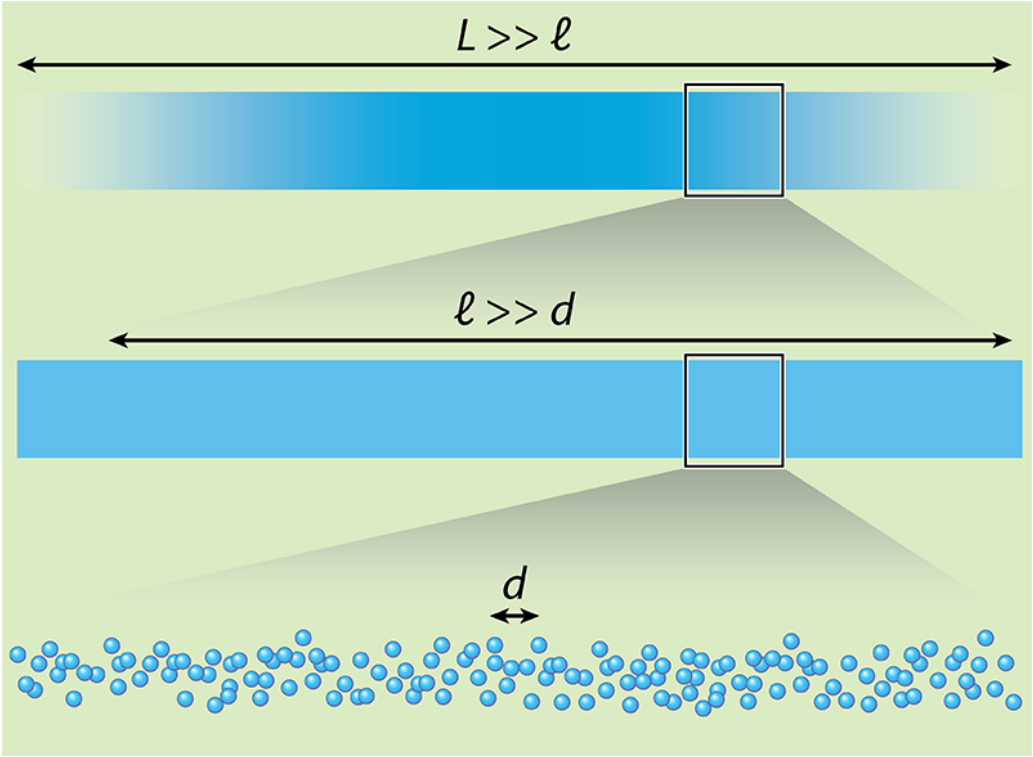


Figure 1.2: Sketch of the assumption of *separation of scales*, from [61]. Hydrodynamic models apply in the limit where we have separations of distance and time scales. When the densities and potentials vary on scales characterised by a distance L that is much larger than the microscopic length scale d (generally comparable to the distance of individual particles) the system can be viewed as a continuum of homogeneous fluid cells of size l(such that $d \ll l \ll L$) which are large enough to contain a thermodynamically large number of particles, while being small enough so that the quantities varying on the scale L can be considered as constants in each fluid cell, each fluid cell is relaxed into a local stationary state

1.3.1 Separation of Scales

Before moving on to the application of GHD in the Lieb-Liniger model (and similarly in integrable quantum systems), we clarify what the *Euler scale* means.

Let's consider some initial state $\hat{\rho}(0)$, which is generally a non-stationary dynamic state evolving in time. We denote the average of a local observable $\hat{O}(x,t)$ by $\langle\hat{O}(x,t)\rangle$ in position x evolved up to time t according to the time-dependent Schrödinger equation. The assumption of (generalized) hydrodynamics is local entropy maximization. This means that with good approximation the average can be evaluated as

$$\langle\hat{O}(x,t)\rangle = \langle\hat{O}(0,0)\rangle_{\vec{\beta}(x,t)}, \tag{1.85}$$

where by stationarity and homogeneity of the stationary state, we could have chosen any time and place for the observable. The average of the observable now depends on the effective temperatures of the (Lagrangian parameters) $\vec{\beta}(x,t)$ correspondong to the approriate ensemble, which in the case of the Lieb-Liniger gas is a GGE characterized by the Lagrangian parameters corresponding to its conserved quantities. These parameters are not dependent on the observable $\hat{O}$ and the same state describes any local or quasi-local observable at space and time x,t. This means that generalized hydrodynamics is a valid description of the dynamics in the *Euler scale* if the corresponding *separation of scales* can be assumed. The hydrodynamic equations describe the time evolution of the system on length scales that are comparable with the size of the system L. When the charge densities in

the system vary sufficiently slowly in space and time, the gas can be regarded as a continuum of locally equilibrated fluid cells with characteristic size l (such that $1/\rho(x) \ll l \ll L$, where $1/\rho(x)$ is the characteristic distance between particles. The first inequality ensures that each fluid cells contains a thermodynamically large amount of particles, while the second one ensures that the densities in the gas vary sufficiently slowly), fully characterized by the space and time dependent Lagrange parameters of the GGE ($\vec{\beta}(x,t)$, where x,t now refer to coarse grained values at the mesoscopic scale).

1.3.2 The GHD Equations

Assuming separation of scales (see Fig.1.2), the Lieb- Liniger gas is described by the rapidity distribution $\rho(\lambda)$ (or equivalently the occupation function $\vartheta(\lambda)$) within each fluid cell in $[x, x+\mathrm{d}x]$ at time t. Then this position dependent rapidity distribution will evolve in time according to the GHD equations

$$\begin{cases} \partial_t \rho(x,t,\lambda) + \partial_x (v^{\mathrm{eff}}[\rho]\rho(x,t,\lambda)) = 0 \\ \\ v^{\mathrm{eff}}[\rho](\lambda) = \lambda - \int_{-\infty}^{\infty} \mathcal{K}(\lambda-\lambda')(v^{\mathrm{eff}}[\rho](\lambda) - v^{\mathrm{eff}}[\rho](\lambda'))\rho(\lambda')\mathrm{d}\lambda'. \end{cases} \tag{1.86}$$

These equations for quantum integrable systems were first written down in [1, 2]. Here $v^{\mathrm{eff}}[\rho]$, a functional of the rapidity distribution $\rho(x,t,\lambda)$ is called the effective velocity due to the fact the, in addition to the 'bare' velocity of the particles it encompasses the additional terms coming from the interaction. In free theories such as the free fermions (or the Tonks-Girardeau/hardcore boson gas) this velocity reduces to the 'bare velocity' and greatly simplifies the GHD equations. Another form of writing the second equation in (1.86) is

$$v^{\mathrm{eff}}[\rho](\lambda) = \frac{\mathrm{id}^{\mathrm{dr}}(\lambda)}{1^{\mathrm{dr}}(\lambda)}, \tag{1.87}$$

with $\mathrm{id}(\lambda) = \lambda$, $1(\lambda) = 1$ with the definition of the dressing given in (1.55).

Breaking of integrability by a confining potential

An important aspect of modeling cold atom experiments is accounting for the presence of a confining potential $V(x)$, which breaks translational invariance and, in general, destroys the integrability of the system. However, if a separation of scales holds and the potential $V(x)$ varies slowly in space—consistent with the assumptions made for the density profiles (see Fig. 1.2)—then integrability can be approximately restored through the Local Density Approximation (LDA) [5, 14]. Under these conditions, the Lieb-Liniger Hamiltonian in the presence of a confining potential takes the form:

$$H = \int dx \left[\hat{\Psi}^\dagger(x) \left(-\partial_x^2 - \mu + V(x) \right) \hat{\Psi}(x) + \frac{c}{2} \hat{\Psi}^{\dagger 2}(x) \hat{\Psi}^2(x) \right], \tag{1.88}$$

with a constant μ chemical potential added. In the framework of the coordinate Bethe Ansatz, LDA is given by obtaining a position-dependent Fermi rapidity $\lambda_F(x)$ in Eqs. (1.59) and (1.55), fixed such that

$$n_{\mathrm{LDA}}(x) = \int_{-\lambda_F(x)}^{\lambda_F(x)} d\lambda\, \rho(\lambda). \tag{1.89}$$

In the grand canonical ensemble, $\lambda_F(x)$ is directly obtained from $V(x)$ through the self-consistent equation $e^{\rm dr}[\pm\lambda_F(x)] = 0$ with the dressed energy $e^{\rm dr}(\lambda)$ satisfying

$$e^{\rm dr}(\lambda) = \frac{\lambda^2}{2} - \mu + V(x) + \int_{-\lambda_F(x)}^{\lambda_F(x)} \frac{d\lambda'}{2\pi} \frac{2c\, e^{\rm dr}(\lambda')}{c^2 + (\lambda - \lambda')^2}. \tag{1.90}$$

The presence of the external potential $V(x)$ also modifies the Generalized Hydrodynamics (GHD) equations given in (1.86). The evolution equation for the root density becomes:

$$\partial_t \rho(x,t,\lambda) + \partial_x(v^{\rm eff}[\rho]\rho(x,t,\lambda)) = (\partial_x V(x))\partial_\lambda \rho(x,t,\lambda), \tag{1.91}$$

while the second GHD equation remains unchanged. The additional term on the right-hand side accounts for the effect of the external force and reflects Newton's second law, as introduced in [62]. Instead of the root density $\rho(x,t,\lambda)$, one may equivalently describe the macrostate of the gas using the occupation function $\vartheta(x,t,\lambda)$ defined in(1.53). This function serves as an alternative fluid variable. In terms of $\vartheta(x,t,\lambda)$ the GHD equation (1.91) takes the form:

$$\partial_t \vartheta(x,t,\lambda) + v^{\rm eff}[\vartheta]\partial_x \vartheta(x,t,\lambda) = (\partial_x V(x))\partial_\lambda \vartheta(x,t,\lambda). \tag{1.92}$$

Both in theoretical and experimental works, ground states of systems with inhomogeneous potentials (see Eq. (1.88)) are natural initial conditions, where local average are well described by the local density approximation (LDA), which provides the initial condition for the GHD equations (1.86).

1.3.3 Zero Entropy GHD

When one restricts the dynamics to the subspace of fluid states with zero entropy, the GHD equations (1.86) simplify significantly. In the context of integrable systems zero entropy states refer to quantum states that have no thermal fluctuation and all information about the systems is contained in a single well defined configuration. This typically corresponds to a pure state with zero entropy, in contrast to thermal states, which are characterized by a macro-state that is accessible through many different micro-states. In integrable systems, zero-entropy states are often associated with situations such as low-temperature limits, where only a single quasiparticle configuration (or a sharp Fermi surface) is populated, and the system exhibits no disorder or randomness.

The occupation function at zero temperature is characterized by steep cutoffs at the Fermi rapidities and is given by

$$\vartheta_{T=0}(\lambda) = \chi(\lambda \in [-\lambda_F, \lambda_F]), \tag{1.93}$$

where $\chi(\lambda)$ is the indicator function and λ_F is the Fermi rapidity, representing the Fermi surface, that depends on the potential $V(x)$. Considering the full space of zero entropy occupation functions, they can be written in the most general way as

$$\vartheta(\lambda) = \chi(\lambda \in \cup_{j=1}^{k}[-\lambda_F^j, \lambda_F^j]) \tag{1.94}$$

where k is the number of separate Fermi seas, characterized by $2k$ rapidities

$$\lambda_1^- < \lambda_1^+ < \ldots < \lambda_k^- < \lambda_k^+. \tag{1.95}$$

A fluid in a zero entropy state stays in a zero entropy state throughout the time evolution [64], thus at zero entropy GHD is reduced to hydrodynamics with a finite number of fluid variables (as shown on Fig. 1.3), meaning that in every point x the Euler scale dynamics of the fluid are completely characterized by a set of Fermi rapidities $\{\lambda_j^\pm\}_{j=1}^k$ where k denotes the number of disjoint Fermi

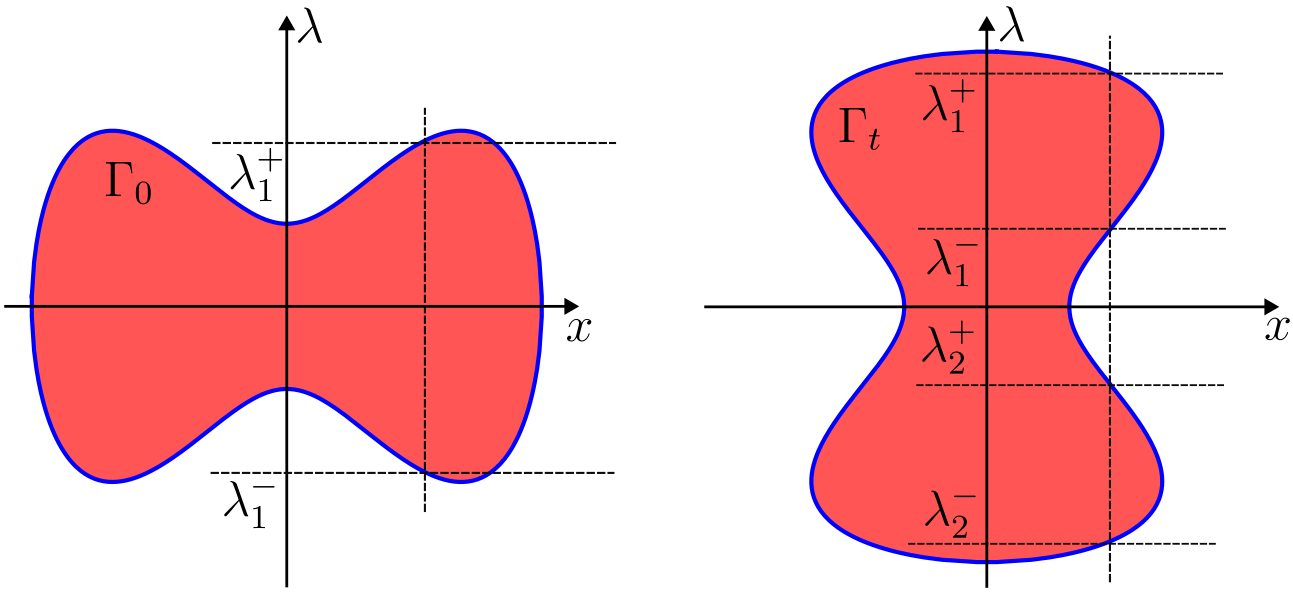


Figure 1.3: Sketch of the time evolution of the occupation function $\vartheta(x,t,\lambda)$, inspired by [63]. A Tonks-Girardeau gas is initially prepared in the ground state of a double-well potential. At time $t=0$, the potential is suddenly quenched to a harmonic trap. At later times $t>0$, the occupation function—characterized by the Fermi contour Γ_t in phase space—develops regions where split Fermi seas emerge at certain positions x, reflecting the complex structure of the post-quench state.

seas (called 'split Fermi seas') at position x. Then, the state of the gas at any time t is parameterized by a contour Γ_t in phase space, that separates the region where the occupation function is 1 from where it is 0:

$$\vartheta(x,t,\lambda)=\begin{cases}1, & \text{if} \quad (x,\lambda) \quad \text{inside} \quad \Gamma_t \\ 0, & \text{if} \quad (x,\lambda) \quad \text{outside} \quad \Gamma_t.\end{cases} \tag{1.96}$$

Parameterizing the contour $\Gamma_t=\{(x_t(s),\lambda_t(s));s\in(0,2\pi]\}$ the GHD equation (1.92) can be rewritten in terms of the evolution of contour Γ_t to give

$$\frac{\mathrm{d}}{\mathrm{d}t}\begin{pmatrix}x_t(s)\\ \lambda_t(s)\end{pmatrix}=\begin{pmatrix}v^{\mathrm{eff}}(\lambda_t(s))\\ -\partial_x V(x_t(s)).\end{pmatrix} \tag{1.97}$$

This formulation of the GHD equation in cases where the initial state is the ground state of the system in the *local density approximation* -although identical to equation (1.92)- is a very useful numerical tool, as it allows the simplification of solving the hydrodynamics, because instead of simulating the complete $\rho(x,t,\lambda)$ or $\vartheta(x,t,\lambda)$, it is enough to simulate the contour Γ_t.

GHD of hard-core bosons

In the case of effectively non-interacting systems—such as hard-core bosons (or, in the continuum limit, the Tonks-Girardeau gas)—the Bose-Fermi mapping allows us to simplify the GHD equations (1.86). Specifically, the effective velocity v^{eff} reduces to the group velocity of free fermions. In certain situations, this simplification enables full analytical solutions of the GHD equations. A prominent example is the free expansion of particles initially confined by a potential, a scenario we will explore in more detail later. Such setups have been studied extensively in the literature, see for instance Refs. [6, 10, 65–68], and have also been realized experimentally with ultracold atoms in optical lattices [69–71].

Consider a system of hard-core bosons initially described by an occupation function $\vartheta_0(x,\lambda)$. Under free expansion, the GHD equation takes the form

$$\partial_t\vartheta(x,k,t)+\sin(k)\partial_x\vartheta(x,k,t)=0, \tag{1.98}$$

where $k\in[0,2\pi)$ is now the quasimomentum free fermions on a lattice with dispersion relation $\varepsilon(k)=-\cos(k)$ and group velocity $v_g=\sin(k)$. In this case the general solution to Eq. (1.98) is straightforward and reads

$$\vartheta(x,t,k)=\vartheta_0(x-t\sin(k),k). \tag{1.99}$$

The dynamics become even more transparent in the zero-entropy regime, where the initial occupation satisfies $\vartheta_0(x,k)\in\{0,1\}$. As discussed earlier, in this regime the evolution is most effectively captured by tracking the deformation of the Fermi contour Γ_t, which fully characterizes the time-evolving state.

1.4 Low-Energy Effective Description of 1D Quantum Systems

Bosonic gases confined to one dimension, propagating in a translationally invariant line exhibit a liquid phase at low temperatures which has two distinct features: i) The low-energy excitations around the ground state are collective modes with linear dispersion. This can be understood by a close inspection of Bethe Ansatz solution detailed earlier. In the presence of interactions, a particle interacts with its neighbors in order to propagate. Thus, when particles are confined to move on a line, any individual motion becomes a collective one. ii) At zero temperature the correlations of the system are described by an algebraic decay characterized by exponents that depend on the model parameters. It was realised by Haldane [47] in the 1980s that one dimensional bosons at low temperatures form a universality class that encompasses a large number of models of interacting bosons. This universality class, called the Tomonaga-Luttinger liquids is characterized by a single parameter called the Luttinger parameter, that depends on the underlying microscopic theory [48].

The collective behavior that results from the confined and interacting nature of these systems motivates an effective field-theoretical description. In this section we present the main ideas of this theory and it's applicability to the Lieb-Liniger gas, where the procedure is to describe low-energy quantum fluctuations around the ground state with fluctuating bosons around the Fermi sea $\lambda\in[-\lambda_F,\lambda_F]$ obtained through the thermodynamic Bethe Ansatz.

1.4.1 Bosonization and Effective Hamiltonian

Let's consider a homogeneous system of size $L\gg 1$ containing $N\gg 1$ particles with density $n=N/L$. The density operator $\hat\rho(x)$ describing the system is given by

$$\hat\rho(x)=\sum_{l=1}^{N}\delta(x-x_l), \tag{1.100}$$

where x_l is the position operator of the lth particle. Using this operator is not practical, so it is customary to rewrite it in a different form by introducing a height field $\hat\phi_h(x)$ [47, 48]. It is defined such that it is a continuous function of the coordinate and takes the value $2\pi l$ at the position of the lth particle. This field is always well defined, as in one dimension one can always number the particles in a unique way. The density operator is then given in the form

$$\hat\rho(x)=\sum_{l=1}^{N}|\partial_x\hat\phi_h(x)|\delta(\hat\phi_h(x)-2\pi l)=\frac{\partial_x\hat\phi_h(x)}{2\pi}\sum_{p\in\mathbb{Z}}e^{ip\hat\phi_h(x)}, \tag{1.101}$$

where p is an integer, and in the second equation the thermodynamic limit ($N, L \to \infty$ and $n = \text{const.}$) was taken. Separating the the expectation value $\langle\hat{\phi}_h(x)\rangle = 2\pi\rho x$ from the fluctuations: $\hat{\phi}_h(x) \to \langle\hat{\phi}_h(x)\rangle + \hat{\phi}(x)$ the density operator becomes

$$\hat{\rho}(x) = \left(n + \frac{1}{2\pi}\partial_x\hat{\phi}(x)\right)\sum_{p\in\mathbb{Z}} e^{ip(2\pi n + \hat{\phi}(x))}. \tag{1.102}$$

On short distances one can assume that the field $\hat{\phi}(x)$ is constant and the density is dominated by the term

$$\hat{\rho}(x) \sim n\cos(2\pi n x + \hat{\phi}(x)), \tag{1.103}$$

on long distances ($x \gg 1/n$) the oscillating terms vanish and Eq. (1.103) is dominated by the term

$$\hat{\rho}(x) \simeq n + \frac{1}{2\pi}\partial_x\hat{\phi}(x), \tag{1.104}$$

thus the addition of a particle in position x corresponds to a jump of 2π in the field $\hat{\phi}(x)$

Effective Hamiltonian

The next step in the formalism is to identify the bosonic creation/annihilation operators $\hat{\psi}^\dagger(x)/\hat{\psi}(x)$, with commutation relation $\left[\hat{\psi}(x), \hat{\psi}^\dagger(x')\right] = \delta(x - x')$. This can be done by writing

$$\hat{\psi}^\dagger(x) = [\hat{\rho}(x)]^{1/2}\, e^{-i\hat{\theta}(x)}, \tag{1.105}$$

with some operator $\hat{\theta}(x)$ that can be fixed by requiring Eq. (1.105) to fulfill the bosonic commutation relations. Putting Eq. (1.105), the commutation $\hat{\theta}(x)$ has to satisfy is

$$\left[\hat{\rho}(x), e^{-i\hat{\theta}(x')}\right] = \delta(x - x')e^{-i\hat{\theta}(x')}, \tag{1.106}$$

which rewritten in terms of the field $\hat{\phi}(x)$ gives

$$\left[\frac{1}{2\pi}\partial_x\hat{\phi}(x), \hat{\theta}(x')\right] = i\delta(x - x'), \tag{1.107}$$

thus the field $\frac{1}{2\pi}\partial_x\hat{\theta}(x)$ can be interpreted as the canonical conjugate momentum to the field $\hat{\phi}(x)$.

Obtaining the formula for the Hamiltonian of this system is done by identifying the interaction term to be of the form

$$\sim \int \mathrm{d}x\hat{\rho}^2(x), \tag{1.108}$$

and the kinetic energy term coming from

$$\sim \int \mathrm{d}x(\partial_x\hat{\psi}^\dagger(x))(\partial_x\hat{\psi}(x)). \tag{1.109}$$

Using this the most general effective Hamiltonian written in terms of fields $\hat{\phi}(x)$ and $\hat{\theta}(x)$ is

$$\hat{\mathcal{H}} = \frac{1}{2\pi}\int_0^L dx\left(vK\left[\partial_x\hat{\theta}(x)\right]^2 + \frac{v}{K}\left[\partial_x\hat{\phi}(x)\right]^2\right), \tag{1.110}$$

where v is the sound velocity of excitations and K is the dimensionless Luttinger parameter that can be understood as the stiffness of the gas. These coefficients are phenomenological and model dependent. They characterize the low energy properties of the underlying microscopic one dimensional system. The field $\hat{\phi}(x)$ has Dirichlet boundary conditions,

$$\hat{\phi}(0) = \hat{\phi}(L) = 0, \tag{1.111}$$

due to the conservation of particles, while the field $\hat{\theta}(x)$ has Neumann boundary conditions (which are dual to the Dirichlet boundary conditions). Additionally the fields $\hat{\phi}$ and $\hat{\theta}$ are compactified: $\hat{\theta} \equiv \hat{\theta} + 2\pi$ and $\hat{\phi} \equiv \hat{\phi} + 2\pi$. This can be understood by looking at the connection between the fields in the Luttinger liquid and the quantities of the microscopic theory. From the formula for the particle density $\hat{\rho}(x)$ in Eq. (1.104) we see that the jump of the field $\hat{\phi}$ by $\pm 2\pi$ corresponds to adding or removing a particle. The field $\hat{\theta}$ -according to Eq. (1.105)- is interpreted as a phase and therefore takes values in $[0, 2\pi]$.

Qualitatively, two limiting regimes are expected. At large values of K density fluctuations are enhanced while phase fluctuations are suppressed leading to a regime similar to Bose-Einstein condensates (BECs) in higher dimensions. If K is small the system is similar to a crystal to some extent. The invariance of the Hamiltonian under the transformation $K \to 1/K$ and $\hat{\phi} \to \hat{\theta}$ suggests that $K = 1$ is a special point. Indeed as we see later it corresponds to the case of free fermions.

For a time dependent system, the time evolution of operators is introduced through the Heisenberg reperesentation in real time

$$\hat{O}(t) = e^{i\hat{\mathcal{H}}t}\hat{O}e^{-i\hat{\mathcal{H}}t} \tag{1.112}$$

or in imaginary time with the Wick rotation $t \to i\tau$.

1.4.2 The Luttinger Parameter and The Sound Velocity

By introducing bosonic creation and annihilation operators $[\hat{b}_q, \hat{b}^\dagger_{q'}] = \delta_{q,q'}$ the Luttinger liquid Hamiltonian (1.110) is diagonalizable and takes the form

$$\mathcal{H} = \sum_{q \neq 0} \omega(q)\hat{b}^\dagger_q \hat{b}_q, \tag{1.113}$$

with

$$\omega(q) = v|q|, \tag{1.114}$$

that is a sound-like spectrum associated to density waves. It describes gapless linear-dispersion excitations (phonon-like), that one expects from one dimensional interacting bosons. Another important point is that the dispersion relation (1.114) doesn't explicitly depend on the parameter K, suggesting that K and v are not independent. Indeed, by taking the form of the bosonic creation operator in Eq. (1.105) and substituting it into the kinetic part of the Lieb-Liniger Hamiltonian in Eq. (1.88) one finds

$$v = \frac{\pi\rho}{K}. \tag{1.115}$$

The sound velocity is given by the dressed velocity of the excitations at the edge of the Fermi sea in the ground state of the Lieb-Liniger gas and, thus can be written in terms of quantities in the Bethe-Ansatz as

$$v = \frac{\mathrm{id}^{\mathrm{dr}}(\lambda_F)}{1^{\mathrm{dr}}(\lambda_F)}. \tag{1.116}$$

The Luttinger paramter K then can be obtained as

$$K = \left[1^{\mathrm{dr}}(\lambda)\right]^2, \tag{1.117}$$

in terms of dressed quantities.

The Inhomogeneous Case

In the presence of a slowly varying external potential $V(x)$ -that is often the case for experiments with cold atomic gases- the local properties of a one-dimensional quantum gas at low energies can be effectively captured by an extension of the upper introduced theory, called the inhomogeneous Luttinger liquid. Within this framework, the Local Density Approximation (LDA) is employed, justified by a separation of scales between the variation of the external potential and the intrinsic correlation length of the system, as it was done in the case of the thermodynamic Bethe Ansatz earlier. Thus the system consists of locally homogeneous Luttinger liquids, each characterized by spatially dependent Luttinger parameters $K(x)$ and $v(x)$. These quantities are determined from the local Fermi sea structure of the thermodynamic Bethe Ansatz. The Hamiltonian of the inhomogeneous Luttigner liquid is written as

$$\hat{\mathcal{H}}_{\mathrm{inh}} = \int_0^L \frac{dx\, v_{\mathrm{LDA}}(x)}{2\pi} \left(K(x) \left[\partial_x \hat{\theta}(x)\right]^2 + \frac{\left[\partial_x \hat{\phi}(x)\right]^2}{K(x)} \right), \tag{1.118}$$

where

$$K(x) = [1^{\mathrm{dr}}(\lambda_F(x))]^2 \tag{1.119}$$

is the local Luttinger parameter and

$$v_{\mathrm{LDA}}(x) = \pi n_{\mathrm{LDA}}(x)/K(x) \tag{1.120}$$

is the local sound velocity in terms of the LDA density profile $n_{\mathrm{LDA}}(x)$ and Luttinger parameter $K(x)$. The quantities of the local Thermodynamic Bethe Ansatz are obtained the same way as in the case of the GHD equations detailed in Equations (1.89) and (1.90). It is important to note here that, the Luttinger parameter K (and consequently the sound velocity v) depends on the interaction parameter c, or more importantly on the dimensionless effective interaction strength $\gamma(x) = c/n_{\mathrm{LDA}}(x)$.

1.4.3 Green's Functions of the Luttinger Liquid

To obtain the correlation functions of fields $\hat{\phi}(x)$ and $\hat{\theta}(x)$ it is a good idea to write the action corresponding to the Hamiltonian (1.118); which is given in the form

$$\mathcal{S} = \frac{1}{2\pi} \int d^2\mathbf{x} \frac{\sqrt{g}}{K(x)} g^{ab} (\partial_a \phi)(\partial_b \phi), \tag{1.121}$$

where $\mathbf{x} = (x, \tau)$ with τ being the imaginary time and g^{ab} is the metric

$$g^{ab} d^a\mathbf{x} d^b\mathbf{x} = dx^2 + v_{\mathrm{LDA}}^2 d\tau^2, \tag{1.122}$$

The coordinates can be transformed to give an isothermal coordinate system, to make the calculation of correlation functions easier. The stretched coordinate in the new system can be written:

$$x \to \tilde{x} = \frac{1}{\mathcal{T}} \int_0^x dx' \frac{1}{v_{\mathrm{LDA}}(x')}, \tag{1.123}$$

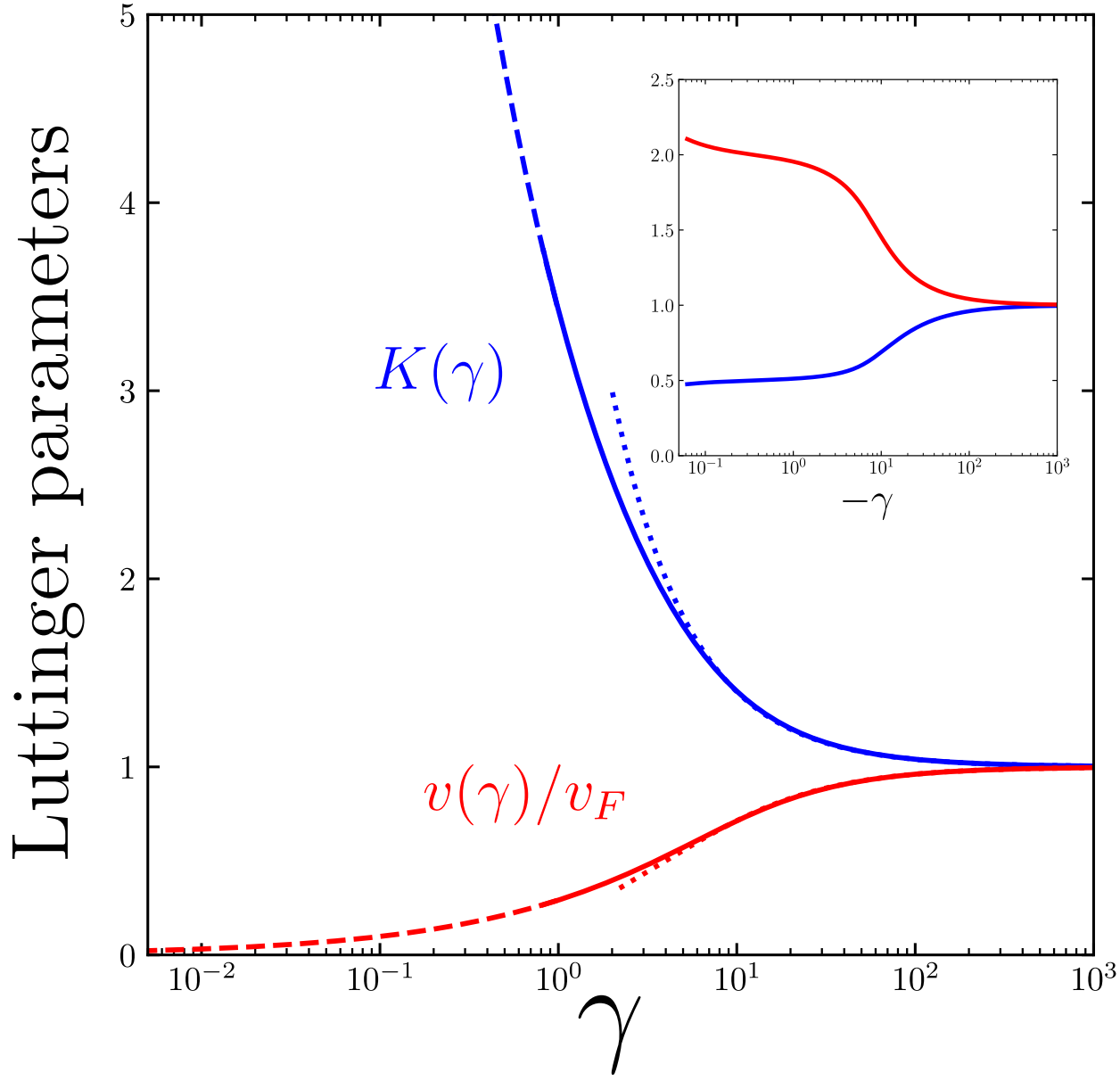


Figure 1.4: The Luttinger parameter K (solid blue) and the sound velocity v divided by the Fermi velocity v_F (solid red) as a function of the dimensionless coupling γ of the Lieb-Liniger gas, with $\gamma \to \infty$ corresponding to the case of free fermions (or the Tonks-Girardeau gas). The known asymptotic limits for $K(\gamma \gg 1) = 1 + \frac{4}{\gamma} + \mathcal{O}(\gamma^{-1})$ [72] and $K(\gamma \ll 1) \simeq \frac{\pi}{\sqrt{\gamma}} \left(1 - \frac{\sqrt{\gamma}}{2\pi}\right)^{-1/2}$ [49] are plotted with dotted and staggered lines respectively. The values for attractive interactions ($\gamma < 0$) are shown in the **inset** as a function of $-\gamma$.

where we defined the time scale

$$\mathcal{T} = \int_0^L \frac{dx}{v_{\mathrm{LDA}}(x)}, \tag{1.124}$$

associated to the inhomogeneous Luttinger liquid model (1.118), which is the time needed by an excitation with velocity $v_{\mathrm{LDA}}(x)$ to go from one boundary of the atomic cloud to the other.

The ground state correlation function of fields $\hat{\phi}(x)$ and $\hat{\theta}(x)$can be written as the Green's functions of the generalized Poisson equations [73]. For the two-point function $\langle\hat{\phi}(\mathbf{x})\hat{\phi}(\mathbf{y})\rangle = -\frac{1}{4}G^D_{[K]}(\mathbf{x},\mathbf{y})$ one gets:

$$\nabla_{\mathbf{x}}\frac{1}{K(\mathbf{x})}\nabla_{\mathbf{x}}G^D_{[K]}(\mathbf{x},\mathbf{y}) = 4\pi\delta^2(\mathbf{x}-\mathbf{y}), \tag{1.125}$$

where the subscript D denotes the Dirichlet boundary conditions. Similarly, for $\langle\hat{\theta}(\mathbf{x})\hat{\theta}(\mathbf{y})\rangle$ the generalized Poisson equation is

$$\nabla_{\mathbf{x}}4K(\mathbf{x})\nabla_{\mathbf{x}}G^N_{[1/4K]}(\mathbf{x},\mathbf{y}) = 4\pi\delta^2(\mathbf{x}-\mathbf{y}) - \frac{4\pi}{\mathrm{Vol}(\Omega)}, \tag{1.126}$$

with the N subscript denoting the Neumann boundary conditions, with Ω denoting the subset of 2D spacetime over which the action is integrated.

Additionally, as usual in field theory, one also has to introduce a regularization procedure to make sense of having multiple $\phi(\mathbf{x})$ operator insertions at the same points. This can be done by normal ordering. The definition is the following for $:\phi^n(x):$, where :: denotes normal ordering. For $n = 0 : 1 := 1$ and $n = 1 : \hat{\phi}(\mathbf{x}) := \hat{\phi}(x)$. For $n > 1$ it is defined as

$$\begin{aligned} :\hat{\phi}^n(\mathbf{x}): = \lim_{\mathbf{x}'\to\mathbf{x}}[:\hat{\phi}^{n-1}(\mathbf{x}):\hat{\phi}(\mathbf{x}')+ \\ + (n-1)K(\mathbf{x})\log|\mathbf{x}-\mathbf{x}'|^2 :\hat{\phi}^{n-2}(\mathbf{x}):], \end{aligned} \tag{1.127}$$

with the second term being introduced in order cancel the divergence of the Green's function in the limit $x \to x'$. It is important to note here that equation (1.127) is the recursive form of Wick's theorem. This scheme can then be applied to all the local operators in the theory. The regularised Green's function can be written as

$$G^D_{[K]}(\mathbf{x}) = \lim_{\mathbf{x}'\to\mathbf{x}}[G^D_{[K]}(\mathbf{x},\mathbf{x}') - K(\mathbf{x})\log|\mathbf{x}-\mathbf{x}'|^2], \tag{1.128}$$

by using the known result for the homogeneous gas to cancel the ultraviolet divergences (similarly for $G^N_{[1/4K]}(\mathbf{x})$) [48].

In contrast to translationally invariant systems -where conformal invariance allows for analytical results- obtaining results for these correlations generally poses a challenge. However, they can be obtained through numerics efficiently, such as in [73, 74]. An example case where analytical formulas can be obtained is the limit of a Tonks-Girardeau gas ($\gamma \to \infty$) in a harmonic potential trap, where after a change of coordinates (1.123) one recovers conformal invariance [73].

The weakly interacting regime

In the quasicondensate regime $\gamma(x) \to 0^+$, namely, at weak repulsive interactions $c \to 0^+$ and high density $n_{\mathrm{LDA}}(x) \to \infty$ such that the quantity $n_{\mathrm{LDA}}(x)c$ is kept constant Bogoliubov theory predicts a divergent Luttinger parameter (see Figure 1.4) given by [49]

$$K(x) \overset{\gamma\to 0^+}{\simeq} \frac{\pi}{\sqrt{\gamma(x)}} = \pi\sqrt{\frac{n_{\mathrm{LDA}}(x)}{c}}, \tag{1.129}$$

while the sound velocity is

$$v_{\mathrm{LDA}}(x) \overset{\gamma\to 0^+}{\simeq} \sqrt{c\, n_{\mathrm{LDA}}(x)}. \tag{1.130}$$

It is also known that in this limit of interaction strength the equation of state for the gas is given by (see for example the book by Pitaevskii and Stringari [75] for a detailed review)

$$\mu(x) = c n_{LDA}(x). \tag{1.131}$$

For a harmonic trapping potential

$$V(x) = \frac{1}{2}\omega^2 x^2, \tag{1.132}$$

with edges $R = \frac{\sqrt{2\mu}}{\omega}$, one finds the local density to be

$$n_{\mathrm{LDA}}(x) = \frac{\omega^2 R^2}{2c}\left(1 - \frac{x^2}{R^2}\right). \tag{1.133}$$

Equivalently, R can be related to the number of particles through

$$N = \frac{2\omega^2 R^3}{6c}. \tag{1.134}$$

Thus one can obtain an analytical formula for the Luttinger parameters $K(x)$ and $v_{\mathrm{LDA}}(x)$. As we show later, in the special case of a harmonic potential, the Luttinger liquid Hamiltonian (1.118) can be diagonalized using a mode expansion [76–78], allowing the analytical calculation of correlation functions.

1.4.4 Long Range Asymptotics of Correlations in Trapped Gases

Although the Bethe Ansatz provides an exact solution for the spectrum of the Lieb-Liniger model (1.20), computing correlation functions within this framework remains a significant challenge. With the derivation of determinant formulae for the field form factors $\langle \boldsymbol{\lambda}|\hat{\Psi}^\dagger(0)|\boldsymbol{\mu}\rangle$ between generic Bethe eigenstates [79], it is possible to express the OPDM (1.24) as

$$g_1(x,0) = \sum_{\{\mu\}} \frac{\langle \boldsymbol{\lambda}|\hat{\Psi}^\dagger(x)|\boldsymbol{\mu}\rangle\langle \boldsymbol{\mu}|\hat{\Psi}(0)|\boldsymbol{\lambda}\rangle}{\langle \boldsymbol{\lambda}|\boldsymbol{\lambda}\rangle\langle \boldsymbol{\mu}|\boldsymbol{\mu}\rangle}, \tag{1.135}$$

where $\boldsymbol{\lambda}$ is the rapidity set of the reference state (e.g., the ground state), and $\hat{\Psi}^\dagger(x)$, $\hat{\Psi}(x)$ are bosonic creation and annihilation operators. In practice, however, the summation over intermediate states $|\boldsymbol{\mu}\rangle$ becomes computationally demanding for large systems, and must be tackled with advanced numerical techniques, such as those used in Ref.[80]. As an alternative, the low-energy, long-distance behavior of the system can be described effectively using Luttinger liquid theory[47, 48], which captures universal features of 1D quantum fluids.

In general, observables of the underlying microscopic theory $\hat{O}(x)$ are related to the operators of the effective field theory through non-universal coefficients C. In homogeneous systems these coefficients contribute as global prefactors to the correlation functions (a detailed discussion of said coefficients can be found in the works [81–84]). In inhomogeneous cases however, these coefficients themselves depend on the coordinate [85]. Thus expansions of an observable $\hat{O}(x)$ are generally given in the form

$$\hat{O}(x) = \sum_j C_j^{(\hat{O})}(x)\hat{\phi}_j(x), \tag{1.136}$$

where the summation j runs over all possible local operators $\hat{\phi}_j$ of the field theory and the non-universal coefficinets $C_j^{(\hat{O})}(x)$ are dimensionful numbers. As mentioned in the previous section, observables of the microscopic theory (in our case the Lieb-Liniger gas) now have to be invariant under $\hat{\phi}(\mathbf{x}) \to \hat{\phi}(\mathbf{x}) + 2\pi$ and $\hat{\theta}(\mathbf{x}) \to \hat{\theta}(\mathbf{x}) + 2\pi$ -due to the compactification of the Luttinger liquid. The local fields that are left to construct the observables are the derivative fields $\partial_a\hat{\phi}(\mathbf{x})$, $\partial_a\partial_b\hat{\phi}(\mathbf{x})$,... and the vertex operators $\hat{\mathcal{V}}_{p,q}$, which can be written as

$$\hat{\mathcal{V}}_{p,q} = e^{ip\hat{\phi}(\mathbf{x})}e^{iq\hat{\theta}(\mathbf{x})}. \tag{1.137}$$

Knowing the operator content of the sum in Eq. (1.136) allows the calculation of correlation functions of observables. Moreover, exploiting the fact that the Luttinger liquid Hamiltonian is quadratic in the field $\hat{\phi}(x)$ and $\hat{\theta}(x)$, one can obtain a general expression for the long-distance asymptotics of correlation functions. Such an example is the OPDM (1.24), which at leading order, in the presence of confining potentials takes the form

$$g_1(x,y) = e^{G^N_{[1/4K]}(x,y)} \prod_{z=x,y} \frac{\sqrt{B(z)}n_{\mathrm{LDA}}(z)^{\frac{2K(z)-1}{4K(z)}}}{[\mathcal{T}v_{\mathrm{LDA}}(z)]^{\frac{1}{4K(z)}}} e^{-\frac{1}{2}G^N_{[1/4K]}(z)}, \tag{1.138}$$

valid for large distances. Here, $B(x) = B(c/n_{\mathrm{LDA}}(x))$ is the local nonuniversal amplitude (see Fig. 1.6), and $G^N_{[1/4K]}(x)$ and $G^N_{[1/4K]}(x,y)$ are the Green's functions $G^N_{[1/4K]}(\mathbf{x},\mathbf{y})$ and its regularized version evaluated at zero imaginary time. Similarly for the density profile, one can obtain a general formula in leading order, valid for any confining potential [73]:

$$\langle\hat{n}(x)\rangle = n_{LDA}(x) + 2\cos(2\vartheta(x)) \cdot \frac{n_{LDA}(x)^{1-K(x)}}{v(x)^{K(x)}} A(x) e^{\frac{1}{2}G^{[D]}_K(x)}, \tag{1.139}$$

where $G^{[D]}_K(x)$ is the regularised Green's function evaluated at zero imaginary time (1.128), $v_{\mathrm{LDA}}(x)$ and $K(x)$ are the sound velocity and the Luttinger parameter at point x respectively, $A(x)$ is the corresponding local non-universal amplitude shown on Fig. 1.6 and $\vartheta(x)$ is defined as

$$\vartheta(x) = \pi \int_0^x n_{LDA}(u)du. \tag{1.140}$$

Non-Universal Amplitudes

The dimensionful coefficients $C_j^{(\hat{O})}$ appearing in the operator correspondence in Eq. (1.136) in infinite homogeneous, translationally invariant cases can be evaluated numerically through considering conformal transformations and operator-state correspondence. They are obtained through the formula

$$C_j^{(\hat{O})} = \lim_{L\to\infty} \left[\left(\frac{L}{2\pi}\right)^{\Delta_{\hat{\phi}}} \frac{{}_L\langle\hat{\phi}|\,\hat{O}(0)\,|0\rangle_L}{\sqrt{{}_L\langle 0|0\rangle_L\,{}_L\langle\hat{\phi}|\hat{\phi}_j\rangle_L}} \right], \tag{1.141}$$

where $\Delta_{\hat{\phi}}$ is the scaling dimension of the operator ϕ_j in the conformal field theory, $|0\rangle_L$ corresponds to a microscopic equivalent of the conformal vacuum $|0\rangle$ and $|\hat{\phi}_j\rangle_L$ -similarly- to the conformal state $|\hat{\phi}_j\rangle$.

Numerically these coefficients are evaluated by solving the Bethe equations (1.36) for varying particle numbers N, L such that the density $n = N/L$ is kept constant. The states $|\hat{\phi}_j\rangle_N$ correspond

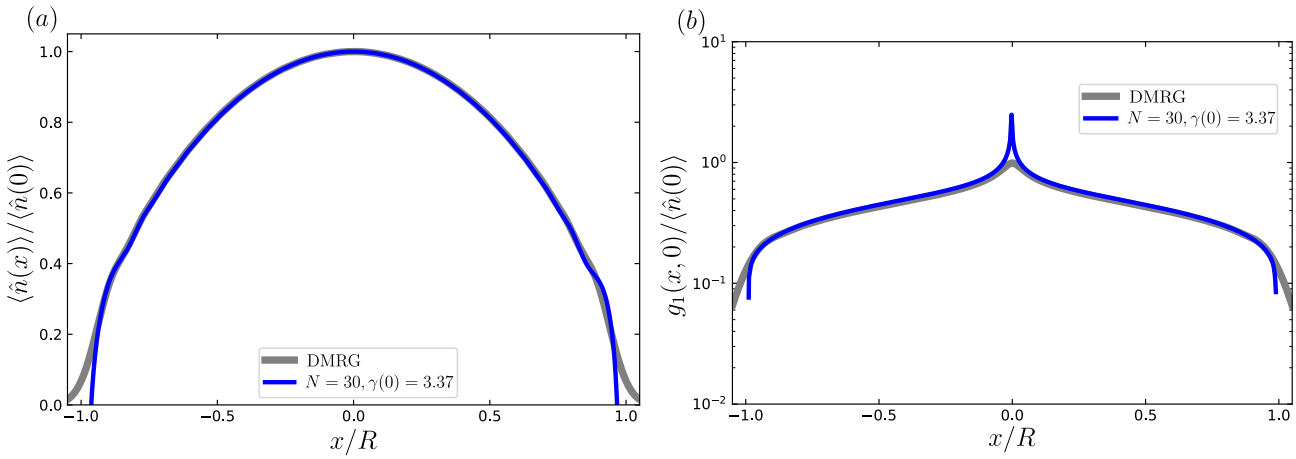


Figure 1.5: Reproduction of results from [73] where corrections to the LDA density profile and real space correlation functions such as $g_1(x, y)$ were obtained for a trapped Lieb-Liniger gas. Results for the (a) Density profile, (b) OPDM of a Lieb-Liniger gas consisting of $N = 30$ particles in a harmonic trap (the parameter R is the size of the gas packet from its center) with dimensionless interaction strength $\gamma(0) = 3.37$ in the center of the trap. Results from inhomogenous Luttinger liquid (solid blue) are compared to DMRG results (solid grey).

to Bethe states characterized by the Bethe Integers $\{I_j\}_{j=1}^N$ (1.36), with $|0\rangle_N$ being the N-particle ground state (1.38). The matrix elements in (1.141) are then evaluated according to the formulas detailed in the works [79, 86, 87].

The case of inhomogeneous systems where translational invariance (and conformal) is broken are then generalized according to [73], by making the nonuniversal coefficients $C_j^{(\hat{O})}$ coordinate dependent (the coefficients depend on the dimensionless coupling $\gamma = c/n_{LDA}(x)$, that depends on the coordinate through the LDA density).

1.4.5 Notions of Conformal Invariance

The universality of the Luttinger liquid theory for describing low energy excitations of one dimensional bosonic systems can be understood more by its connection to conformal field theories (CFTs). The idea of using conformal invariance to study critical systems dates back to the 1970s [88], and it's potential was revealed in the 1980's when it's ability to effectively describe two-dimensional critical systems was demonstrated [89] . Other works also found its connection to the idea of bosonization underlying the theory of Luttinger liquids [90, 91]. The aim of this section is to provide a practical overview of conformal field theories in the context of Luttinger liquid theory, for a more complete introduction we refer the reader to the notes by Cardy [92] or Ginsparg [93], and for a more in-depth discussion to the book by Di Francesco, Mathieu and Sénéchal [94].

At critical points, a classical system is scale invariant, meaning that the coordinates of the system transform simply under a renormalization $\mathbf{x} \to b^{-1}\mathbf{x}$, where $\mathbf{x} = (x^1, x^2)$ and b is a constant scaling factor. In addition to this the system generally also exhibits translational and rotational invariance. These three transformations generate a conformal group under which the correlation functions of operators in the effective theory transform in a simple way:

$$\langle\hat{\phi}_1(\mathbf{x}_1)...\hat{\phi}_n(\mathbf{x}_n)\rangle \to b^{-\Delta_{\hat{\phi}_1}}...b^{-\Delta_{\hat{\phi}_n}}\langle\hat{\phi}_1(\mathbf{x}_1)...\hat{\phi}_n(\mathbf{x}_n)\rangle, \tag{1.142}$$

where $\Delta_{\hat{\phi}_1}$ is called the scaling dimension of field $\hat{\phi}_1$. A system in two dimensions with local interactions has a larger symmetry group. Transformations that locally combine translations, rotations,

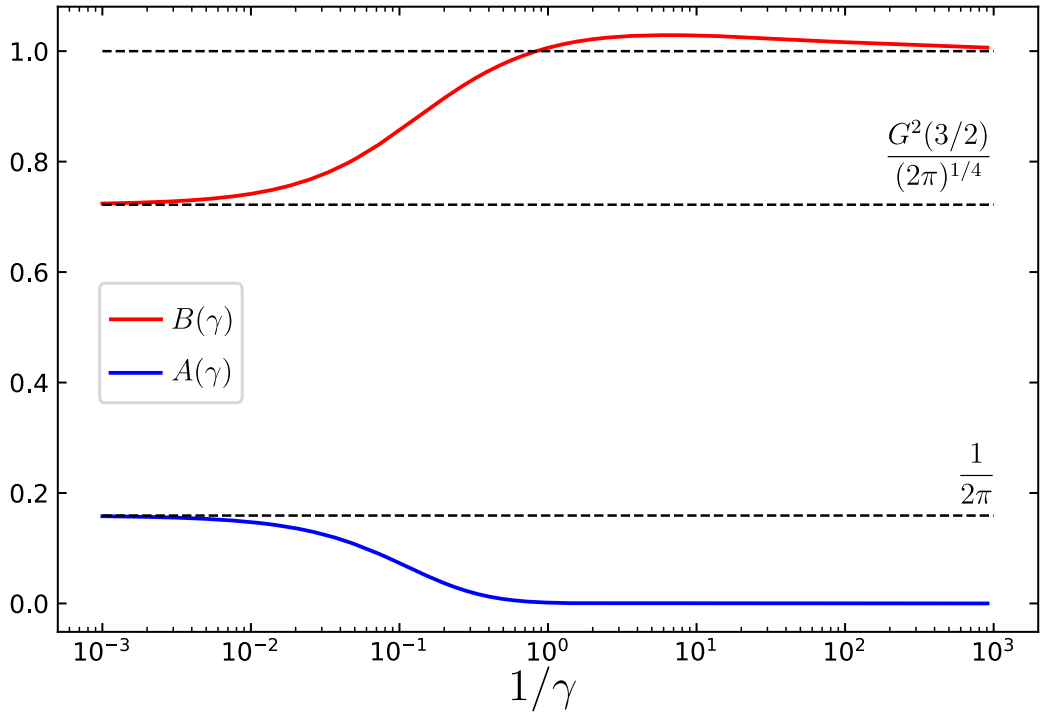


Figure 1.6: The form factor $A(\gamma)$ entering the expression of the density (solid blue) and the form factor $B(\gamma)$ entering the expression of the OPDM (solid red), as a function of the dimensionless coupling γ for repulsive interactions ($0 < \gamma$), with the corresponding limits for large and small values of γ. The results are obtained by evaluating the form factors given in (1.141) for varying particle numbers N (or system sizes $L = N/n$, for fixed density n) according to [79, 86, 87] and performing a polymnomial fit in $1/N$ in order to obtain the $N \to \infty$ limit. Reproduction of [73].

and dilations define the conformal symmetry group. To be precise, the transformations of the conformal symmetry group are those that preserve the metric of the field theory up to a Weyl factor [95]:

$$\mathrm{d}s^2 = g_{ab}\mathrm{d}x^a\mathrm{d}x^b \quad \text{and} \quad g'_{ab}(x) = e^{2\sigma(x)}g_{ab}(x). \tag{1.143}$$

Under such local conformal transformations, the operators are renormalized by a local coordinate dependent factor $b(x)$. This has important consequences for the correlation functions of the operators. Taking for example a two-point function; looking for a formula similar to (1.142) results in the

$$\langle\hat{\phi}_i(\mathbf{x_1})\hat{\phi}_j(\mathbf{x_2})\rangle \propto \frac{\delta_{\Delta_{\hat{\phi}_i},\Delta_{\hat{\phi}_j}}}{(\mathbf{x}_1-\mathbf{x}_2)^{2\Delta}}, \tag{1.144}$$

orthogonality relation of the operators in the theory, with $\Delta = \Delta_{\hat{\phi}_i} = \Delta_{\hat{\phi}_j}$.

1.4.6 Conformal Field Theories In the Complex Plane

By introducing complex coordinates $z = x + iv\tau$ and $\bar{z} = x - iv\tau$ the subgroup of dilations, translations and rotation are generated by the Möbius transformations defined as

$$z' = \frac{az+b}{cz+d}, \tag{1.145}$$

where the complex coefficients satisfy $ad - bc \neq 0$. Under such transformations the Riemann sphere $\mathbb{C}$ is mapped into itself and one often talks about special conformal transformation. If one only considers the local constraint (1.143), we find that it is satisfied by any holomorphic function $z' = w(z)$:

$$\mathrm{d}z'\mathrm{d}\bar{z}' = \left|\frac{\mathrm{d}w(z)}{\mathrm{d}z}\right|^2 \mathrm{d}z\mathrm{d}\bar{z}, \tag{1.146}$$

where the derivative is identified as the local Weyl factor. The conformal group is thus generated by an infinite number of conformal transformations. There always exists a set of isothermal coordinates $(z, \bar{z})$ such that the metric is flat, up to a Weyl factor. If this coordinate system is known explicitly, one can always perform a conformal transformation and map the problem to a geometry where the correlation functions are already known.

A relevant example when such a methodology can be applied for cold atomic systems is the effective description of a trapped Tonks-Girardeaus gas. In the infinite interaction limit $\gamma \to \infty$ the action of the effective theory describing small fluctuations around the ground state written in (1.121) is simplified due to

$$\lim_{\gamma\to\infty} K(\gamma) = 1, \tag{1.147}$$

as shown in Fig (1.4). The only coordinate dependence now is hidden in the metric g^{ab} (1.122). The transformation detailed in Eq. (1.123) introduces isothermal coordinates with the Weyl factor

$$\left|\frac{\mathrm{d}x'}{\mathrm{d}x}\right| = \frac{1}{\mathcal{T}v_{LDA}(x)}. \tag{1.148}$$

In this new coordinate system the correlation functions are known to be the solutions of the Poisson equations (as seen for example in [63, 73]), and can be easily evaluated, giving access to the correlation functions. The resulting field theory is called the Gaussian Free Field (GFF) and is ubiquitous in the description of cold atoms and the theory of Luttinger liquids [48].

1.4.7 Boundary Conformal Field Theory

Boundary conformal field theories are instrumental in describing systems with conformal invariance that are defined on portions of the complex plane restricted by one or more boundaries, with various kinds of boundary conditions. Studying these models is relevant for multiple reasons. For instance, the numerical study of 2d statistical and one-dimensional quantum systems is restricted to finite system sizes L, and properties in the thermodynamic limit (i.e. $L \to \infty$) of the systems are then inferred from results obtained in finite sizes. Using a boundary conformal field theory to describe such models provides -in many cases- the size dependence naturally, allowing a more precise study of the limit $L \to \infty$. As we see in Chapter 3 in quantum systems the plane may be restricted in the complex plane corresponding to finite temperature, allowing the study of the finite temperature behavior of a quantum system. In this section we illustrate the effectiveness of the boundary conformal field theories through the example of deriving correlation functions of the inhomogeneous Gaussian Free Field on an infinite strip of size L. Then we derive correlation functions of the same theory at finite temperature, the result of which explicitly use in Chapter 3.

OPDM of trapped hard core bosons at zero temperature

We take a cloud of Lieb-Liniger gas in a smooth trapping potential, such that the size of the cloud is L. As discussed in this Section the effective theory describing small fluctuations around the LDA ground state is given by the inhomogeneous Luttinger liquid. By taking the Tonks-Girardeau limit of strong interaction strength $\gamma \gg 1$ the action of the effective field theory is

$$\mathcal{S} = \frac{1}{2\pi} \int d^2\mathbf{x} \sqrt{g} g^{ab} (\partial_a \phi)(\partial_b \phi), \tag{1.149}$$

with $K(x) = 1$ at any point in space according to the TG limit. The metric (1.122) can be transformed into a flat one through transforming the real space according to (1.123), resulting in the coordinates

$$z(x,\tau) = \frac{1}{\mathcal{T}} \int_0^x dx' \frac{1}{v_{\mathrm{LDA}}(x')} + i\tau = \tilde{x} + i\tau, \quad \text{with} \quad e^{\sigma(x)} = \mathcal{T} v_{\mathrm{LDA}}(x), \tag{1.150}$$

corresponding to a local conformal transformation according to Eqn. (1.143). The theory is thus defined on an infinite strip parametrized by the coordinates

$$\mathcal{L}_{flat} = (\tilde{x}, \tau) \in [0,1] \times \mathbb{R}. \tag{1.151}$$

Under this transformation a primary field of the CFT transforms as $\hat{\Phi}(z,\bar{z}) \to e^{-\Delta\sigma(z,\bar{z})}\hat{\Phi}(z,\bar{z})$, with Δ being the scaling dimension of field $\hat{\Phi}$ and $\bar{z}$ is the complex conjugate of z. The two-point correlation function of field $\hat{\Phi}$ on the flat metric is related to the curved one through

$$\langle \hat{\Phi}(z,\bar{z}) \hat{\Phi}(z',\bar{z}') \rangle_{\mathcal{L}_{\mathrm{curved}}} = \left(\frac{1}{v_{\mathrm{LDA}}(x)\mathcal{T}} \right)^{\Delta} \left(\frac{1}{v_{\mathrm{LDA}}(x')\mathcal{T}} \right)^{\Delta} \langle \hat{\Phi}(z,\bar{z}) \hat{\Phi}(z',\bar{z}') \rangle_{\mathcal{L}_{\mathrm{flat}}}. \tag{1.152}$$

All we are left with is evaluating the correlation function $\langle \hat{\Phi}(z,\bar{z}) \hat{\Phi}(z',\bar{z}') \rangle_{\mathcal{L}_{flat}}$ defined on the infinite strip (1.151). One two-point function we are particularly interested in in this work is the One Particle Density Matrix of the Lieb-Liniger bosons (1.4.4). Through bosonization arguments one finds that up to leading order in scaling dimension the bosonic annihilation operator is given as

$$\hat{\Psi}(x,\tau) = n_{\mathrm{LDA}}(x)^{\frac{1}{4}} B(x) \hat{\mathcal{V}}_{0,1}(x,\tau) \quad + \text{less relevant operators}, \tag{1.153}$$

where we used that the dimension of $\hat{\Psi}(x,\tau)$ is $\frac{1}{2}$ while the scaling dimension of vertex operator $\mathcal{V}_{0,1}(x,\tau)$ is $\frac{1}{4}$. Indeed the correlation function (1.152) for the OPDM is written as [85]

$$\begin{aligned}\langle\hat{\Psi}^\dagger(z,\bar{z})\hat{\Psi}(z',\bar{z}')\rangle_{\mathcal{L}_{\text{curved}}} &= |B(\gamma\to\infty)|^2\frac{n_{\text{LDA}}(x)^{\frac{1}{4}}}{(\mathcal{T}v_{\text{LDA}}(x))^{\frac{1}{4}}}\frac{n_{\text{LDA}}(x')^{\frac{1}{4}}}{(\mathcal{T}v_{\text{LDA}}(x'))^{\frac{1}{4}}}\langle:\hat{\mathcal{V}}_{0,1}(x',\tau')::\hat{\mathcal{V}}_{0,-1}(x,\tau):\rangle_{\mathcal{L}_{\text{flat}}}\\ &= |B(\gamma\to\infty)|^2\sqrt{\frac{1}{\pi\mathcal{T}}}\langle:\hat{\mathcal{V}}_{0,1}(x,\tau)::\hat{\mathcal{V}}_{0,-1}(x,\tau):\rangle_{\mathcal{L}_{\text{flat}}}\end{aligned} \tag{1.154}$$

In order to obtain the two-point function $\langle:\hat{\mathcal{V}}_{0,1}(x',\tau')::\hat{\mathcal{V}}_{0,-1}(x,\tau):\rangle_{\mathcal{L}_{\text{flat}}}$ we use a conformal mapping, that maps the infinite strip to the upper-half-plane $\mathbb{H}$. However we need to give special attention to the boundary. To deal with boundary conditions in conformal field theories a common method to use is the method of image charges, taken directly from electrostatics. This trick consists of writing an n-point correlation function in a domain with a boundary as a 2n-point correlation function without the boundary, such that the boundary condition is automatically satisfied.

The mapping $\mathcal{L}_{\text{flat}}\to\mathbb{H}$ is given by the transformation

$$z\to w(z)=e^{i\pi z}, \tag{1.155}$$

resulting in

$$\langle:\hat{\mathcal{V}}_{0,1}(z,\bar{z})::\hat{\mathcal{V}}_{0,-1}(z',\bar{z}'):\rangle_{\mathcal{L}_{\text{flat}}}=\left|\frac{\mathrm{d}w}{\mathrm{d}z}\right|^{\frac{1}{4}}\left|\frac{\mathrm{d}w'}{\mathrm{d}z'}\right|^{\frac{1}{4}}\langle:\hat{\mathcal{V}}_{0,1}(w,\bar{w})::\hat{\mathcal{V}}_{0,-1}(w',\bar{w}'):\rangle_{\mathbb{H}}. \tag{1.156}$$

To r.h.s. of (1.156) can be evaluated by using the method of images. On the boundary we have the boundary condition

$$\hat{\phi}(w,\bar{w})=0,\quad \text{if}\quad \text{Im}(w)=0, \tag{1.157}$$

corresponding to a Dirichlet boundary condition. Using the analogy that in electrostatics Dirichlet boundary conditions correspond to a fixed electric potential we can construct the image charges that satisfy Eqn. (1.157). We first define fields $\varphi(z)$ and $\bar{\varphi}(\bar{z})$ as the chiral and anti-chiral part of field $\hat{\phi}(z,\bar{z})$, with correlations (for a more detailed introduction see [96] or [48])

$$\begin{aligned}\hat{\phi}(z,\bar{z})=\varphi(z)+\bar{\varphi}(\bar{z}),\quad \langle\varphi(z)\varphi(z')\rangle_{\mathbb{C}}=-\log(z-z'),\quad \langle\bar{\varphi}(\bar{z})\bar{\varphi}(\bar{z}')\rangle_{\mathbb{C}}=-\log(\bar{z}-\bar{z}')\\ \text{and}\quad \langle\bar{\varphi}(\bar{z})\varphi(z')\rangle_{\mathbb{C}}=0.\end{aligned} \tag{1.158}$$

In terms of these operators the vertex operator can be expressed as

$$:\hat{\mathcal{V}}_{0,1}(z,\bar{z}):=:e^{-i\frac{1}{2}(\varphi(z)-\bar{\varphi}(\bar{z}))}:. \tag{1.159}$$

Using the definition of the chiral fields (1.158) we see that the boundary condition (1.157) means that fields φ and $\bar{\varphi}$ are not independent and $\bar{\varphi}$ can be understood at the analytic continuation of $-\varphi$ meaning that the operator $:e^{-i\frac{1}{2}\bar{\varphi}(\bar{w})}:$ on $\mathbb{H}$ can be replaced by $:e^{i\frac{1}{2}\varphi(\bar{w})}:$ in the full complex plane $\mathbb{C}$ as illustrated in Fig 1.7, leading to the formula [85]

$$\langle:e^{-i\frac{1}{2}(\varphi(w)-\bar{\varphi}(\bar{w}))}::e^{-i\frac{1}{2}(\varphi(w)-\bar{\varphi}(\bar{w}'))}:\rangle_{\mathbb{H}}=\langle:e^{-\frac{1}{2}\varphi(w)}::e^{-\frac{1}{2}\varphi(\bar{w})}::e^{\frac{1}{2}\varphi(w')}::e^{-\frac{1}{2}\varphi(w')}:\rangle_{\mathbb{C}}. \tag{1.160}$$

All that is left now is to evaluate the correlation function using the formula

$$\langle\prod_{i=1}^{l}:e^{i\alpha_j\varphi(z_i)}:\rangle_{\mathbb{C}}=\prod_{1\le j<k\le l}|z_j-z_k|^{\alpha_j\alpha_k}, \tag{1.161}$$

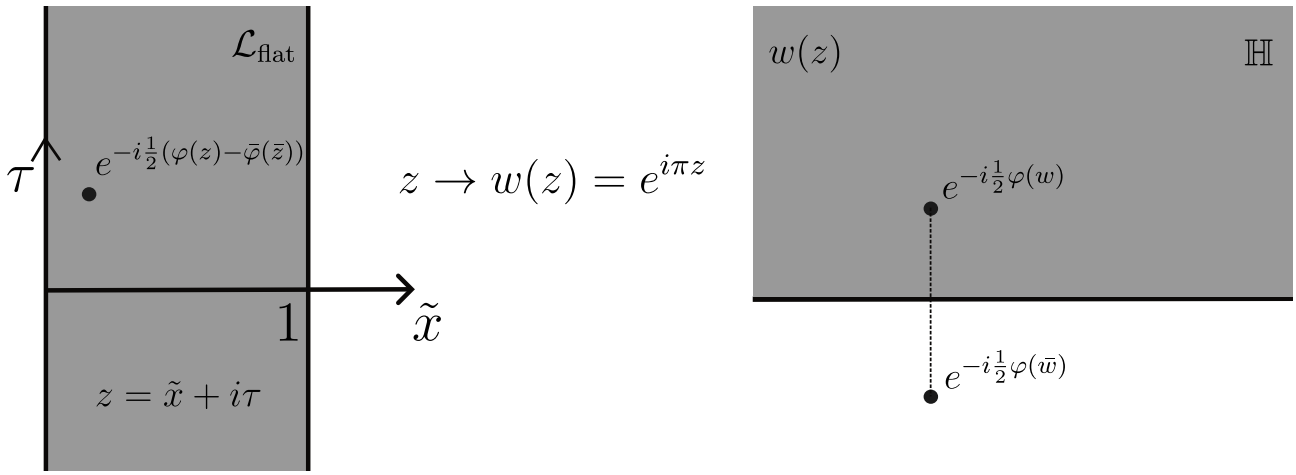


Figure 1.7: The infinite strip $\mathcal{L}_{\text{flat}} = [0,1] \times \mathbb{R}$ and the upper-half-plane $\mathbb{H}$ obtained from $\mathcal{L}_{\text{flat}}$ with the transformation (1.155), showing a vertex operator in terms of the chiral fields φ,$\bar{\varphi}$ defined in (1.158) and illustrating the method of images. Reproduction of Figure 2 of [85].

and rewrite the correlation function in terms of the original coordinates z and $\bar{z}$. Taking $\tau = \tau'$ then results in the equal time correlation function, giving the OPDM of a Tonk-Girardeau gas in a trapping potential to be [85]

$$g_1(x,y) = \frac{G^4(3/2)}{\sqrt{2\pi}} \sqrt{\frac{1}{2\mathcal{T}}} \frac{\left|\sin\left(\frac{\pi}{\mathcal{T}}\tilde{x}\right)\right|^{\frac{1}{4}} \left|\sin\left(\frac{\pi}{\mathcal{T}}\tilde{x}'\right)\right|^{\frac{1}{4}}}{\left|\sin\left(\frac{\pi}{\mathcal{T}}\frac{\tilde{x}-\tilde{x}'}{2}\right)\right|^{\frac{1}{2}} \left|\sin\left(\frac{\pi}{\mathcal{T}}\frac{\tilde{x}+\tilde{x}'}{2}\right)\right|^{\frac{1}{2}}}, \tag{1.162}$$

where we used $B(\gamma \to \infty) = \frac{G^2(3/2)}{(\sqrt{2\pi})^{1/4}}$ (see Fig. 1.6).

Green's function of trapped hard-core bosons at finite temperature

In the case of finite temperatures the infinite strip becomes an annulus by imposing periodic boundary conditions on the complex plane such that the circumference after transformation given in Eqn. (1.123) becomes $\frac{\beta}{\mathcal{T}}$, where $\beta = 1/T$ is the inverse temperature of the system.

Here we derive the analytical formula obtained for the Green's function of trapped hard-core bosons at finite temperature that we present in Eq. (3.35) of Chapter 3. There are multiple ways to derive the Green's functions of the Luttinger fields in this configuration, such as the method of images used before, or using the results for the infinite strip discussed in [85] and accounting for the periodic boundary conditions in the complex direction. Instead, we proceed by writing the Luttinger fields $\hat{\phi}$ and $\hat{\theta}$ in their mode decomposition. After applying the local conformal transformation (1.123) that we used in previous sections, the Luttinger liquid Hamiltonian with Dirichlet boundary conditions on both sides ($\hat{\phi}(s=0) = \hat{\phi}(s=1) = 0$) and with $K = 1$ becomes

$$\hat{H}_{\text{inh}} = \int_0^1 \frac{ds}{2\pi\mathcal{T}} \left[(\partial_s\hat{\theta})^2 + (\partial_s\hat{\phi})^2\right] = \frac{\pi}{\mathcal{T}} \sum_{n\geq 1} [\hat{a}_n^\dagger \hat{a}_n + \frac{1}{2}],$$

where the parameter $\mathcal{T}$ can be interpreted as the time needed for a gapless excitation to travel from the left to the right boundary. The mode expansion of the fields is written as

$$\hat{\phi}(s) = \sum_{n\geq 1} \frac{1}{n} \sin(\pi n s)(\hat{a}_n^\dagger + \hat{a}_n)\,, \tag{1.163}$$

$$\hat{\theta}(s) = \sum_{n\geq 1} \frac{1}{i\,n} \cos(\pi n s)(\hat{a}_n^\dagger - \hat{a}_n)\,, \tag{1.164}$$

with the canonical commutation relation

$$[\hat{a}_n, \hat{a}_m^\dagger] \;=\; n\,\delta_{n,m}\,, \tag{1.165}$$

such that

$$[\hat{\phi}(s), \frac{1}{\pi}\partial\hat{\theta}(s')] = [\hat{\phi}(s), \hat{\Pi}(s')] = i\delta(s-s') \quad \text{for} \quad s, s' \in (0,1). \tag{1.166}$$

Then, the Green's function at finite temperature can be written as

$$\begin{aligned}\left\langle \hat{\theta}(s)\hat{\theta}(s')\right\rangle_\beta &= -\sum_n \frac{\cos(\pi n s)\cos(\pi n s')}{n^2}\left\langle (\hat{a}_n^\dagger - \hat{a}_n)^2\right\rangle_\beta \\ &= 2\sum_n \frac{\cos(\pi n s)\cos(\pi n s')}{n^2}\left\langle \hat{a}_n^\dagger\hat{a}_n + \frac{n}{2}\right\rangle_\beta .\end{aligned}$$

This we can evaluate by using the finite temperature average

$$\left\langle \hat{a}_n^\dagger\hat{a}_n\right\rangle_\beta \;=\; \frac{\mathrm{tr}\left[e^{-\beta H}\hat{a}_n^\dagger\hat{a}_n\right]}{\mathrm{tr}\left[e^{-\beta H}\right]} \;=\; n\,\frac{\sum_{p\geq 0} p q^{np}}{\sum_{p\geq 0} q^{np}}\,, \tag{1.167}$$

where we introduced the parameter

$$q = \exp\left(-\pi\beta/\mathcal{T}\right), \tag{1.168}$$

and used the identity

$$\begin{aligned}\sum_{n\geq 1}\frac{1}{n}u^n\frac{\sum_{p\geq 0}(p+\frac{1}{2})q^{np}}{\sum_{p\geq 0}q^{np}} &= \frac{1}{2}\sum_{n\geq 1}\frac{1}{n}u^n\frac{1+q^n}{1-q^n} \\ &= \frac{1}{2}\sum_{p\geq 0}\sum_{n\geq 1}\frac{1}{n}u^n(1+q^n)q^{pn} \\ &= \frac{1}{2}\sum_{p\geq 0} -\log\left(1-uq^p\right) - \log\left(1-uq^{p+1}\right) \\ &= -\log\left[(u;q)_\infty\right] \;+\; \frac{1}{2}\log\left(1-u\right),\end{aligned}$$

where

$$(u;q)_\infty \;=\; \prod_{p\geq 0}(1-uq^p) \tag{1.169}$$

is the 'q-Pochhammer symbol'. After some further manipulation of the formula we obtain

$$\begin{aligned}\langle\hat{\theta}(s)\hat{\theta}(s')\rangle_\beta \;=\; &-\frac{1}{2}\log\left[\left(e^{i\pi(s-s')},q\right)_\infty\left(e^{-i\pi(s-s')},q\right)_\infty\right] \\ &-\frac{1}{2}\log\left[\left(e^{i\pi(s+s')},q\right)_\infty\left(e^{-i\pi(s+s')},q\right)_\infty\right] \\ &+\frac{1}{4}\log\left[\left(1-e^{i\pi(s-s')}\right)\left(1-e^{-i\pi(s-s')}\right)\right] \\ &+\frac{1}{4}\log\left[\left(1-e^{i\pi(s+s')}\right)\left(1-e^{-i\pi(s+s')}\right)\right],\end{aligned}$$

for the correlation function. This can be further simplified by reorganizing the terms in the equation. The correlation function then takes the form

$$\langle\hat{\theta}(s)\hat{\theta}(s')\rangle_\beta = \\ -\frac{1}{4}\log\left[\prod_{n\in\mathbb{Z}}\left|\frac{\sin\frac{\pi(s-s'-in\frac{\beta}{\mathcal{T}})}{2}\sin\frac{\pi(s+s'-in\frac{\beta}{\mathcal{T}})}{2}}{\left(\sin\frac{\pi(s-in\frac{\beta}{\mathcal{T}})}{2}\sin\frac{\pi(s'-in\frac{\beta}{\mathcal{T}})}{2}\right)^2}\right|^2\right]. \tag{1.170}$$

We see that the result is periodic under $s \to s + i\frac{\beta}{\mathcal{T}}$ (as expected), thus we can rewrite the solution in terms of the Jacobi's theta function $\vartheta_1(z|\tau)$ defined

$$\vartheta_1(z|\tau) = -i\sum_{r\in\mathbb{Z}+\frac{1}{2}}(-1)^{r-\frac{1}{2}}e^{2\pi riz}e^{2\pi\frac{r^2}{2}i\tau}. \tag{1.171}$$

The final form of the correlation function is then

$$\left\langle\hat{\theta}(s)\hat{\theta}(s')\right\rangle_\beta = -\frac{1}{2}\log\left|\frac{\vartheta_1\left(\frac{s-s'}{2}\middle|\frac{i\beta}{2\mathcal{T}}\right)\vartheta_1\left(\frac{s+s'}{2}\middle|\frac{i\beta}{2\mathcal{T}}\right)}{\left[\partial_s\vartheta_1\left(0\middle|\frac{i\beta}{2\mathcal{T}}\right)\right]^2}\right|, \tag{1.172}$$

which is also the correlation function we use in Eq. (3.35). One way to verify the last step in the calculation is check the coefficients of the expansions in parameter q of equations Eqs. (1.170) and (1.172) and see that they are equal at all orders. Following the same ideas in the calculation leads to the Green's function of the field $\hat{\phi}$

$$\begin{aligned}\left\langle\hat{\phi}(s)\hat{\phi}(s')\right\rangle_\beta &= -\frac{1}{4}\log\left(\prod_{n\in\mathbb{Z}}\left|\frac{\sin\frac{\pi(s-s'-in\frac{\beta}{\mathcal{T}})}{2}}{\sin\frac{\pi(s+s'-in\frac{\beta}{\mathcal{T}})}{2}}\right|^2\right) \\ &= -\frac{1}{2}\ln\left|\frac{\vartheta_1(\frac{x-x'}{2}|i\beta/2)}{\vartheta_1(\frac{x+x'}{2}|i\beta/2)}\right|.\end{aligned} \tag{1.173}$$

Interestingly, the Green's function in Equation (1.172) and (1.173) can be obtained by using the correlation function of the 2D massless free boson theory on a torus

$$\langle\phi(z,\bar{z})\phi(0,0)\rangle_{\text{torus}} = -\frac{1}{2}\log\left|\frac{\vartheta_1(z|i\tau)}{\partial_z\vartheta_1(0|i\tau)}e^{-\pi\frac{(\text{Im}\,z)^2}{\tau}}\right|. \tag{1.174}$$

taken from Eq. (12.142) in the of the book Di Francesco, Mathieu, and Senechal [97]), and using the method of images relying on the analogy between the free massless gaussian bosonic field and electromagnetism (detailed in the works [49, 85]) to construct the correlation function on an annulus with the corresponding Dirichlet/Neumann boundary conditions on both sides for $\hat{\phi}/\hat{\theta}$ respectively.

1.5 Quantum Generalized Hydrodynamics

The behavior of fluids at very low temperatures is very peculiar, as quantum effects dominate over thermal fluctuations. In order to give an effective description to collective quantum effects in such system it is customary to start from a classical hydrodynamics description and quantize the theory accordingly. This approach was taken by Landau when describing superfluid helium in 1941 [98]. Since then, various other similar approaches to describing quantum fluids have been developed, such as the description of Bose-Einstein condensates with Bogoliubov theory [75, 99, 100], quantum Hall liquids [101–103], or the previously discussed Luttinger liquid theory (see Section 1.4) used to describe one-dimensional quantum fluids. The theory called quantum generalized hydrodynamics (QGHD), introduced in [3, 4] is an extension of Generalized Hydrodynamics (see Section 1.3); a classical hydrodynamic description of one-dimensional integrable models. In this section, we give a brief review of the theory by discussing the main ideas behind it, following recent results in the field [3, 4, 63].

1.5.1 Quantum fluctuations around Generalized Hydrodynamics

The goal of quantum generalized hydrodynamics is to obtain equal time correlation functions between fluid cells, by describing small fluctuations around the solutions of generalized hydrodynamics. Let us consider a gas of interacting bosons in their ground state in a trapping potential (as it was done, for example, in the works [4, 63, 104]), then at $t = 0$ the trap is abruptly changed to a different potential following a global quench protocol. The resulting hydrodynamics of the gas are given by generalized hydrodynamics on the Euler scale. Restricting ourselves to zero-entropy dynamics the GHD equations for the time evolution are given by zero entropy GHD

$$\frac{\mathrm{d}}{\mathrm{d}t}\begin{pmatrix} x_t(s) \\ \lambda_t(s) \end{pmatrix} = \begin{pmatrix} v^{\mathrm{eff}}(\lambda_t(s)) \\ -\partial_x V(x_t(s)). \end{pmatrix}, \tag{1.175}$$

discussed previously in Section 1.3.3, where the contour $\Gamma_t = \{(x_t(s), \lambda_t(s)); s \in (0, 2\pi]\}$ describes the Fermi surface of the gas in this quasi phase space. Locally at a given fluid cell the time evolution is fully characterized by the Fermi rapidities $\{\lambda^j(x,t)\}_{j=1}^{2Q}$, with Q denoting the number of split Fermi seas of the fluid cell at coarse grained coordinate x. Small fluctuations can be expressed as deformations of the contour Γ_t [48, 49], meaning locally -in terms of rapidities- $\lambda^j \to \lambda^j + \delta\lambda^j$. These fluctuations then correspond to a fluctuation of the Fermi momenta, related to the rapidity through the equation

$$p(\lambda) = \lambda + \int \frac{\mathrm{d}\lambda'}{2\pi}\theta(\lambda - \lambda')\vartheta(\lambda')1^{\mathrm{dr}}(\lambda'), \tag{1.176}$$

where $\theta(\lambda - \lambda')$ denotes the two particle-scattering phase of the Lieb-Liniger model (1.42) and $\vartheta(\lambda)$ the occupation function (1.53). In terms of the Fermi momenta, the fluctuations are written as

$$p^j(x,t) \to p^j(x,t) + \delta p^j(x,t). \tag{1.177}$$

It was shown in the work by Ruggiero et. al. [3] that these small fluctuations, at first order, obey

$$\partial_t \delta p^j(x,t) + \sum_{l=1}^{2Q} \partial_x \left[A_j^l \partial p^l(x,t)\right] = 0, \tag{1.178}$$

where

$$A_j^l = \frac{\partial \epsilon_j}{\partial p^l}, \tag{1.179}$$

is the flux Jacobian and

$$\epsilon_j = E(x,\lambda) + \int \frac{\mathrm{d}\lambda'}{2\pi}\theta(\lambda-\lambda')\vartheta(\lambda')1^{\mathrm{dr}}(\lambda')v^{\mathrm{eff}}(\lambda'), \tag{1.180}$$

is the energy of an excitation with rapidity λ^j. These fluctuations are then quantized by viewing the small displacements of the contour as operators acting on a Hilbert space,

$$\delta p^j(x,t) \to \delta\hat{p}^j(x,t), \quad j = 1,..,2Q. \tag{1.181}$$

These small fluctuations around the contour are equivalent to a small excess of particles around the point $(x(t), p(t))$ in phase space, allowing the introduction of the excess density operator

$$\delta\hat{\rho}(x,t) = \sum_{j=1}^{2Q} \frac{1}{2\pi}\delta\hat{p}^j, \tag{1.182}$$

which -with a coordinate transform- can be written more conveniently as the excess density along the Fermi contour Γ_t

$$\delta\hat{\rho}(t,s) = \sum_{s=1}^{2Q} \left|\frac{\mathrm{d}x_t(s)}{\mathrm{d}s}\right| \delta\hat{\rho}(x_t(s),t), \tag{1.183}$$

where the sum over s is such that $p_t(s) = p_j(x,t)$.

1.5.2 Time evolution and Effective Hamiltonian of density fluctuations

The operator $\delta\hat{\rho}(s)$ has the commutation relation

$$[\delta\hat{\rho}(s), \delta\hat{\rho}(s')] = \frac{1}{2\pi i}\delta'(s-s'), \tag{1.184}$$

where the function $\delta'(.)$ is the derivative of the Dirac-delta function. The Hamiltonian corresponding to the system and reproducing the time evolution in Equation (1.178) can be taken as [3]

$$\hat{H}[\Gamma_t] = \frac{1}{4\pi}\int \mathrm{d}x \sum_{l,j=1}^{2Q} \delta\hat{p}^j(x)A^{jl}\delta\hat{p}^l(x). \tag{1.185}$$

The two-point correlations of the density fluctuations can be expressed in terms of the Green's function

$$G((s,t),(s',t')) = \langle\delta\hat{\rho}(s,t)\delta\hat{\rho}(s',t')\rangle \tag{1.186}$$

as

$$\langle\delta\hat{\rho}(x,t)\delta\hat{\rho}(x',t)\rangle = \sum_s\sum_{s'}\left|\frac{\mathrm{d}s}{\mathrm{d}x}\right|\left|\frac{\mathrm{d}s'}{\mathrm{d}x'}\right|\langle\delta\hat{\rho}(s,t)\delta\hat{\rho}(s',t)\rangle, \tag{1.187}$$

and at $t = t' = 0$ the correlation $\langle\delta\hat{\rho}(s,0)\delta\hat{\rho}(s',0)\rangle$ are the ground state correlations of the Hamiltonian $\hat{H}[\Gamma_0]$ in Equation (1.185).

For general interaction strengths and quench protocols, these correlation functions are difficult to evaluate due to the complicated form of the GHD equations (in Eq. (4.4)) describing the time evolution. In the special case of infinite interaction strength $c \to \infty$ (hard core bosons/ TG gas) the time evolution of the operator $\delta\hat{\rho}(s,t)$ (see Equation (1.178)) simplifies to a rotation of the field, as shown in [4], where correlation functions were calculated for a case of a quantum Newton's cradle setup for a trapped TG gas. The Hamiltonian (1.185) is that of a Gaussian boson CFT on the

contour Γ_t, parametrized by s, allowing the evaluation of the ground-state correlations following CFT arguments.

The interpretation of quantum generalized hydrodynamics [3, 4, 105] is as follows: The equal time quantum correlations between fluid cells are hidden in the initial state, while the fluid cells themselves evolve according to generalized hydrodynamics. The general recipe to calculating these correlations is the following:

- Obtain the initial state of the system using the Local Density Approximation.
- Identify the Fermi contour Γ_0 around which the fluctuation can be defined.
- Identify the effective Hamiltonian (1.185) corresponding to the fluctuations and evaluate their ground state correlations.
- The equal time correlations are then obtained by evolving the Green's function according to the time evolution (1.178).

We follow this idea of quantum generalized hydrodynamics in the calculation of the One Particle Density Matrix of hard-core lattice bosons during a free expansion in the following chapter. We also discuss a method to efficiently numerically evaluate the time evolution in the case of arbitrary interaction strengths.

Chapter 2

Non-equilibrium Dynamics of Bose gases

A particularly interesting class of quantum many-body systems consists of bosons with strong repulsive interactions, commonly referred to as hard-core bosons (HCBs). In one spatial dimension, such systems can be mapped onto non-interacting spinless fermions via the Jordan-Wigner transformations [5]. This correspondence allows for the development of efficient numerical techniques for exploring their non-equilibrium dynamics. However, despite this simplification, obtaining analytical results, especially closed-form expressions for the time evolution of specific observables remains a challenging task. As a result, much of the progress in this area has relied on numerical approaches [6–8].

In this chapter, we derive analytical expressions for out-of-equilibrium correlation functions by building upon the framework of quantum generalized hydrodynamics (QGHD). These correlations provide insight into phenomena such as quasicondensation and dynamical fermionization. In addition, we explore a particular system of hard-core bosons out of equilibrium in the presence of so-called conformal defects. These defects give rise to quantum interference effects, leading to deviations from the density profiles predicted by the hydrodynamic description.

2.1 Correlations of Hard Core Lattice Bosons

One of the most intriguing features of one-dimensional (1D) hard-core bosons (HCBs) is that, despite their mapping to non-interacting spinless fermions, their non-equilibrium dynamics can exhibit fundamentally different behavior. An example of this difference lies in the evolution of the momentum distribution: while translationally invariant fermionic systems either show no time evolution under periodic boundary conditions or display persistent oscillations under open boundaries [106], the momentum distribution of 1D HCBs relaxes toward a stationary value [10, 107], which is well described by the Generalized Gibbs Ensemble (GGE)[108]. Furthermore, in equilibrium, 1D HCBs are known to exhibit quasicondensation[6], a phenomenon that is not limited to the ground state. In far-from-equilibrium regimes, features reminiscent of quasicondensation—in particular, momentum peaks at finite values—can also emerge [55].

Theoretical insight into this behavior has been provided by the framework of the emergent eigenstate solution to quantum dynamics [109]. Within this approach, it is argued that for a suitable class of nonequilibrium initial states, the system evolves through a sequence of instantaneous eigenstates of an effective local Hamiltonian. This emergent description remains valid over timescales that grow linearly with the particle number [109–112].

A particularly suitable protocol for observing quasicondensation in HCBs involves initializing the system in a domain-wall product state, where regions of fully occupied and empty sites are sharply separated. Such configurations can be engineered experimentally by preparing HCBs in a central region flanked by empty sites, for example, using a box potential. The integrability of the 1D HCB model ensures that memory of the initial state persists well beyond the timescales on which quasicondensation signatures become visible. During the expansion from a box trap, the momentum distribution evolves and eventually approaches that of noninteracting spinless fermions, reflecting the underlying mapping. This process, known as dynamical fermionization, has also been observed in other integrable models [57, 113–116].

What makes HCBs particularly appealing from a practical standpoint is their experimental accessibility. Realizations exist in both continuous systems [117] and optical lattice setups [118, 119], enabling direct experimental observation of both quasicondensation [120] and dynamical fermionization [33]. These developments underscore the theoretical importance of constructing analytical frameworks that can capture the full nonequilibrium dynamics of such systems.

At equilibrium, theoretical insights into quasicondensation have largely stemmed from analyses of the one-particle density matrix (OPDM), whose Fourier transform yields the momentum distribution. In homogeneous systems, Luttinger liquid theory predicts a power-law decay of the OPDM, indicating off-diagonal long-range order. This can be interpreted as a form of quasicondensation through the scaling behavior of the OPDM's largest eigenvalue, in line with the Penrose-Onsager criterion [50], or via the emergence of peaks in the momentum distribution [6, 56]. Such analyses were first extended to harmonically trapped HCB ground states [53], and later generalized to arbitrary inhomogeneous setups using extensions of Luttinger liquid theory [54, 73, 85, 121, 122].

Only recently has it become possible to obtain fully analytical expressions for the equal-time OPDM in generic potentials out of equilibrium [63], made possible by the development of a novel quantum hydrodynamics (QHD) framework. The core idea is conceptually simple: large-scale correlation functions can be analytically approximated by constructing a spatially varying Luttinger liquid theory on top of the classical hydrodynamic profile of the evolving HCB system at zero temperature [3, 4, 123, 124]. This approach has yielded a variety of analytical results, especially for entanglement dynamics, and its validity has been corroborated in domain-wall melting scenarios [68, 123, 125–129].

In this Section we focus on the calculation of the equal-time OPDM for 1D HCBs initially confined in a box potential. Building upon recent analytical advancements, we derive exact expressions for the OPDM in this nonequilibrium setting. These results allow us to revisit the emergence of quasicondensation and analyze the development of off-diagonal correlations in the far-from-equilibrium dynamics of hard-core bosons. This Section is organized as follows. First we discuss the setup: we recall the hard-core boson (HCB) Hamiltonian and the mapping into that of spinless free fermions; we then specify the initial domain-wall state and the quench protocol that we have studied. We continue by presenting the main result for the equal-time OPDM of HCBs during the free expansion. The discussion that follows contains a detailed derivation of the main result. This consists of the revision of the classical hydrodynamics of free fermions, its requantization with bosonization arguments (see Section 2.1.3), and several non-trivial details about the derivation of the OPDM. We then turn to applications of our results. In particular, we demonstrate the emergence of quasicondensation and the phenomenon known as dynamical fermionization at different stages of the evolution. This is achieved by analyzing the behavior of the largest eigenvalue of the OPDM, using the Penrose–Onsager criterion, and by examining the time evolution of the momentum distribution obtained from our calculations. This Section is based on our article [130], where the findings presented here were originally published.

2.1.1 Initial Conditions and the Hamiltonian

The Bose-Fermi mapping

We write the Hamiltonian of a lattice gas of 1D bosons with nearest-neighbor hopping and repulsive on-site interaction U using the Bose-Hubbard Hamiltonian

$$\hat{H} = -\frac{1}{2}\sum_x (\hat{a}^\dagger_{x+1}\hat{a}_x + \text{h.c.}) + \frac{U}{2}\sum_x \hat{n}_x(\hat{n}_x - 1). \tag{2.1}$$

The operators $\hat{a}^\dagger_x$, $\hat{a}_x$ are standard bosonic creation and annihilation operator with $\hat{n}_x = \hat{a}^\dagger_x\hat{a}_x$ being the density operator acting on site x. The limit of strong repulsion is given by taking $U \gg 1$, where the Hamiltonian (2.1) becomes

$$\hat{H} = -\frac{1}{2}\sum_x (\hat{b}^\dagger_{x+1}\hat{b}_x + \text{h.c.}). \tag{2.2}$$

We consider hard-core bosonic operators $\hat{b}^\dagger_x$, $\hat{b}_x$ that satisfy on-site anticommutation relations, $\{\hat{b}_x, \hat{b}^\dagger_x\} = 1$, which enforce the constraint of single occupation of sites, while the operators commute on different sites. By identifying each filled (empty) site with a spin-↑ (spin-↓), the Hamiltonian of hard-core bosons (HCBs), Eq. (2.2), becomes equivalent to the XX spin chain:

$$\hat{H} = -\frac{1}{2}\sum_{x\in\mathbb{Z}+\frac{1}{2}} (\hat{\sigma}^+_x\hat{\sigma}^-_{x+1} + \hat{\sigma}^+_{x+1}\hat{\sigma}^-_x) = -\frac{1}{4}\sum_{x\in\mathbb{Z}+\frac{1}{2}} \left(\hat{\sigma}^x_x\hat{\sigma}^x_{x+1} + \hat{\sigma}^y_x\hat{\sigma}^y_{x+1}\right), \tag{2.3}$$

where $\hat{\sigma}^a_x$ are Pauli matrices acting on site x, and $\hat{\sigma}^\pm_x = (\hat{\sigma}^x_x \pm i\hat{\sigma}^y_x)/2$. For convenience, we label the sites of the lattice by half-integers $x = \ldots, -\frac{3}{2}, -\frac{1}{2}, \frac{1}{2}, \frac{3}{2}, \ldots$, a convention also adopted in Ref. [131], which simplifies some expressions appearing later. It is well known that this model maps to noninteracting fermions via the Jordan-Wigner transformation, the lattice analog of the Bose–Fermi mapping used for the Tonks–Girardeau gas (see Sec.1.2.5):

$$\hat{\sigma}^+_x = e^{i\pi\sum_{l=-\infty}^{x-1}\hat{c}^\dagger_l\hat{c}_l}\,\hat{c}^\dagger_x, \qquad \hat{\sigma}^-_x = e^{-i\pi\sum_{l=-\infty}^{x-1}\hat{c}^\dagger_l\hat{c}_l}\,\hat{c}_x, \tag{2.4}$$

where $\hat{c}^\dagger_x$, $\hat{c}_x$ are fermionic creation and annihilation operators, obeying the canonical anticommutation relations $\{\hat{c}_x, \hat{c}^\dagger_{x'}\} = \delta_{x,x'}$. Under this mapping, the Hamiltonian (2.3) becomes a simple hopping Hamiltonian:

$$\hat{H} = -\frac{1}{2}\sum_{x\in\mathbb{Z}+\frac{1}{2}} \left(\hat{c}^\dagger_x\hat{c}_{x+1} + \hat{c}^\dagger_{x+1}\hat{c}_x\right). \tag{2.5}$$

The Quench Protocol

The time evolution begins from a simple domain-wall product state $|\psi_0\rangle$, prepared at time $t = 0$:

$$|\psi_0\rangle = \bigotimes_{x<0} |{\downarrow_x}\rangle \otimes \bigotimes_{0<x<N} |{\uparrow_x}\rangle \otimes \bigotimes_{x>N} |{\downarrow_x}\rangle, \tag{2.6}$$

where $|{\uparrow_x}\rangle$ and $|{\downarrow_x}\rangle$ are eigenstates of $\hat{\sigma}^z_x$ with eigenvalues $+1$ and -1, respectively. In the language of hard-core bosons, this corresponds to a state with N particles initially localized on the sites $x = \frac{1}{2}, \frac{3}{2}, \ldots, N - \frac{1}{2}$, while all other sites are empty (see Fig. 2.1). One way to realize such an initial state (2.6) is to put the system in a box shaped potential, such that the initial Hamiltonian is

$$\hat{H}_0 = \hat{H} + \sum_{x\in\mathbb{Z}+\frac{1}{2}} V(x)\hat{c}^\dagger_x\hat{c}_x \tag{2.7}$$

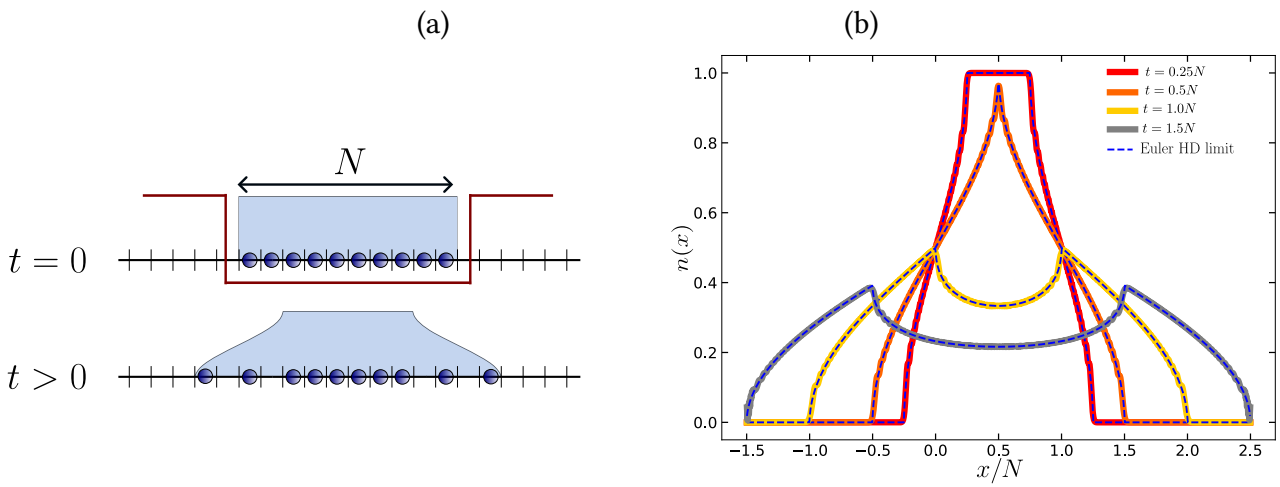


Figure 2.1: (a) – Schematic drawing of the quench protocol (figure from [130]). The initial state is a region of N bosons in a box potential (eq. (2.8)) in the region $0 < x < N$ of a 1D lattice. At $t > 0$, the box potential is switched off spontaneously and the bosons are allowed to freely expand. (b) – Density curves $n(x)$ at different times during time evolution. The results of the hydrodynamic equation Eq. (2.11) (dashed lines) are compared with exact free fermion numerics (solid lines), showing very good agreement.

with

$$V(x) = \begin{cases} -V_0 & \text{if} \quad 0 < x < N \\ +V_0 & \text{otherwise;} \end{cases} \tag{2.8}$$

setting $V_0 \gg 1$, so that the state $|\psi_0\rangle$ is to the ground state of $\hat{H}_0$. This setup has been considered in numerous earlier works [6, 10, 65–68]. It has also been experimentally realized with ultracold atoms in optical lattices in works [69–71].

At time $t > 0$, the box trap is switched off ($V(x) = 0$), and the HCBs are let to expand freely according to the Hamiltonian (2.3),

$$|\psi_t\rangle = e^{-i\hat{H}t} |\psi_0\rangle \,. \tag{2.9}$$

Since the dynamics maps to the one of free spinless fermions using the Jordan-Wigner mapping, the density profile can be computed in the Euler hydrodynamic limit [65, 128, 132–134]:

$$x, t, N \to \infty \quad \text{with} \quad x/t \quad \text{and} \quad N/t \quad \text{fixed}, \tag{2.10}$$

with the ratios x/t and y/t fixed. The result -derived e.g. in Refs. [68], see also Subsection 2.1.3- reads

$$n(x,t) = \langle\psi_t| \frac{1+\hat{\sigma}_x^z}{2} |\psi_t\rangle = \begin{cases} 0 & \text{if} \quad x < -t \\ \frac{1}{\pi}\arccos(\frac{-x}{t}) & \text{if} \quad -t < x < \min(N-t, t) \\ 1 & \text{if} \quad t < \frac{N}{2} \quad \text{and} \quad t < x < N-t \\ \frac{1}{\pi}\arccos(\frac{x-N}{t}) - \frac{1}{\pi}\arccos(\frac{x}{t}) & \text{if} \quad t > \frac{N}{2} \quad \text{and} \quad N-t < x < t \\ \frac{1}{\pi}\arccos(\frac{x-N}{t}) & \text{if} \quad \max(N-t, t) < x < N+t \\ 0 & \text{if} \quad x > N+t. \end{cases} \tag{2.11}$$

The density profile $n(x,t)$ computed using exact numerics for finite N is shown in Fig. 2.1; it matches the asymptotic result (2.11) perfectly.

2.1.2 Results for the One Particle Density Matrix

One of our main results of this Section is the analytic result for the equal-time OPDM in the Euler-limit (i.e., analogous to Eq. (2.11)). The equal-time OPDM of the hard-core bosons is defined as

$$g_1(x,y;t) \;:=\; \langle\psi_t|\,\hat{\sigma}_x^+\hat{\sigma}_y^-\,|\psi_t\rangle\,. \tag{2.12}$$

from which the the momentum distribution can be computed by a Fourier transform, which is a key quantity in cold atom experiments, see Refs. [58, 135, 136]. We will discuss the momentum distribution of the bosons in detail in Sec. 2.1.5 in the context of Off-Diagonal Long Range Order and quasicondenation, but first we focus on the calculation of the quantity (2.12). Obtaining analytically the OPDM for HCBs is an extremely challenging task, since it is non-local in terms of the fermion creation/annihilation operators as can be seen by writing $g_1(x,y;t)$ in terms of fermionic operators $\hat{c}_x^\dagger/\hat{c}^x$

$$g_1(x,y;t) = \langle\psi_t|\,\hat{c}_x^\dagger(-1)^{\sum_j \hat{c}_j^\dagger\hat{c}_j}\hat{c}_y\,|\psi_t\rangle\,, \tag{2.13}$$

where the sum extends over all sites j located between x and y. Since the state $|\psi_t\rangle$ describes a system of non-interacting fermions —expressible as a Slater determinant—Wick's theorem can be applied to compute (2.13). Nonetheless, the Jordan-Wigner string $(-1)^{\sum_j \hat{c}_j^\dagger\hat{c}_j}$ remains non-trivial and cannot be simplified further. As a result, the expression for $g_1(x,y;t)$ takes the form of a determinant of a matrix whose size scales as $O(N)$. In certain cases, these large determinants can be treated analytically using asymptotic methods, most notably through the theory of Toeplitz determinants [51, 137, 138]. Such analytical approaches, however, are generally limited to translationally invariant systems. In most scenarios—especially in the strongly out-of-equilibrium regime such as the box release considered in this chapter—no analytical solutions are available, and the determinants must instead be evaluated numerically. Numerous studies in the literature have utilized such numerical approaches to compute $g_1(x,y;t)$ for hard-core boson gases [6, 10].

In contrast, in this chapter we discuss a closed expression for the quantity $g_1(x,y;t)$ in the Euler limit (2.10), expressed entirely in terms of simple functions. This chapter discusses results and calculations that we previously published in the work [130].

As seen in formula (2.11) several different regions of the phase space need to be distinguished. For a given time t, the labels of the different spatial regions are summarized here:

Interval	**Name**
$x < -t$ or $x > N + t$	Empty (E)
$-t < x < \min(t, N-t)$	Left (L)
$N - t < x < t \quad (\text{if } t > \frac{N}{2})$	Central (C)
$\max(t, N-t) < x < N + t$	Right (R)
$t < x < N - t \quad (\text{if } t < \frac{N}{2})$	Filled (F)

(2.14)

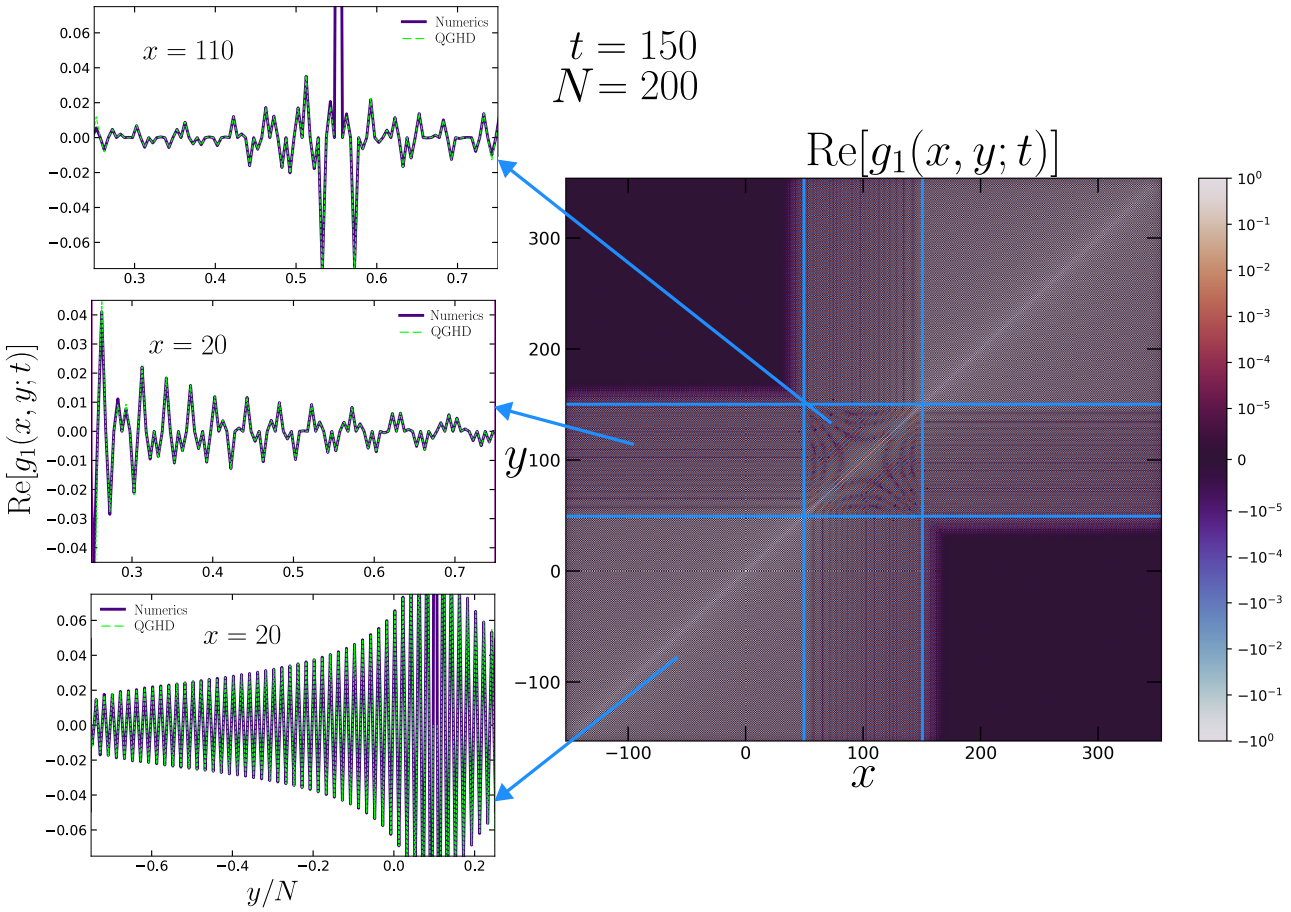


Figure 2.2: (Right) — Color map of $g_1(x, y; t)$ at fixed time $t = 150$ and particle number $N = 200$. Light-blue lines partition the x–y plane into nine distinct regions, three of which exhibit qualitatively different behaviors.(Left) — From top to bottom: (i) region where both x and y are characterized by split Fermi seas (see Sec. 2.1.3 for details); (ii) region where x corresponds to a split Fermi sea, while y corresponds to a connected one; (iii) region where both x and y correspond to connected Fermi seas. Analytical predictions (dashed lines) and exact numerical results (solid lines) show perfect agreement across all cases. Results and figure published in [130].

Then $g_1(x, y; t)$ is given as follows:

$g_1(x,y;t)$	$x \in E$	$x \in L$	$x \in C$	$x \in R$	$x \in F$
$y \in E$	0	0	0	0	0
$y \in L$	0	$f(x,y)$	$g(x,y)$	0	0
$y \in C$	0	$(g(y,x))^*$	$h(x,y)$	$(g(N-y,N-x))^*$	0
$y \in R$	0	0	$g(N-x,N-y)$	$f(N-x,N-y)$	0
$y \in F$	0	0	0	0	0

(2.15)

We remark that eq. (2.15) applies to any time (with region C enabled for $t > N/2$), as specified in

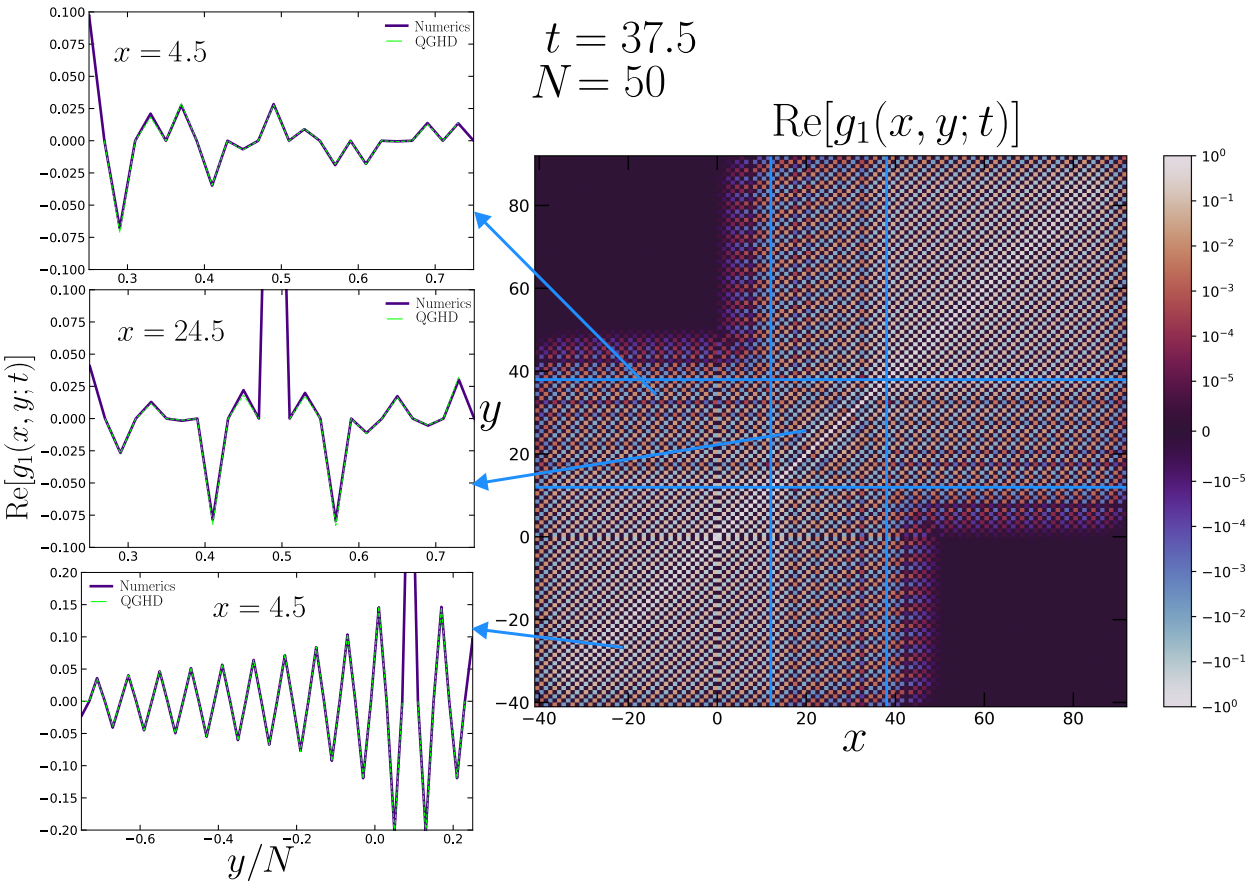


Figure 2.3: (Right) – Another Color map of $g_1(x, y; t)$ at time $t = 37.5$ for a smaller number of hard-core bosons in the initial state, $N = 50$. The time is chosen such that the ratio $\frac{N}{t}$ matches that of Fig. 2.2. (Left) – From top to bottom: i) region where in both positions x and y the local state of the gas is given by split Fermi seas (see discussion in Sec. 2.1.3); ii) region where x corresponds to a split Fermi sea while y corresponds to a connected one; (iii) region where both x and y correspond to connected Fermi seas. Analytical predictions (dashed lines) and exact numerical results (solid lines) are in excellent agreement. Results and figure published in our work [130].

eq. (2.14). The superscript $*$ denotes complex conjugation, and we define the functions f, g and h as

$$
\begin{aligned}
f(x,y) &:= \frac{G(3/2)^4}{\pi} e^{i\frac{\pi}{2}(x-y)} \frac{r(x)^{1/4} r(y)^{1/4}}{(2t)^{1/2}|x-y|^{1/2}} \\
g(x,y) &:= \frac{G(3/2)^6}{\pi^{3/2}} \cos\left[\varphi(N-x)\right] e^{i\frac{\pi}{2}(x-y)} \frac{r(x)^{1/4} r(y)^{1/4}}{r(N-x)^{3/4}|x-y|^{1/2}}, \\
h(x,y) &:= \frac{G(3/2)^8}{\pi^2} \left(\cos[\varphi(y)-\varphi(x)] D^{-1/2}(x,y) + \cos[\varphi(y)+\varphi(x)] D^{1/2}(x,y)\right) \\
&\quad \times e^{-i\frac{\pi}{2}(x-y)} \frac{(t/2)^{1/2} r(N-x)^{1/4} r(N-y)^{1/4}}{r(x)^{3/4} r(y)^{3/4}|x-y|^{1/2}} \\
&\quad + \quad \{x \to N-x, \quad y \to N-y\},
\end{aligned}
\tag{2.16}
$$

where $G(.)$ is the Barnes' G function with $G(3/2) \simeq 1.06922$. Here $\{x \to N-x, y \to N-y\}$ stands for the same term as in the two previous lines with x replaced by $N-x$ and y by $N-y$. We

have also defined the functions

$$r(x) := \sqrt{t^2 - x^2}, \qquad \varphi(x) := \sqrt{t^2 - x^2} - x \arccos\left(\frac{x}{t}\right),$$
$$D(x,y) := \frac{|x-y|}{t} \frac{1}{1 - \frac{xy}{t^2} + \sqrt{1 - \frac{x^2}{t^2}}\sqrt{1 - \frac{y^2}{t^2}}}. \tag{2.17}$$

We omit the explicit dependence on t to simplify notations. Furthermore, note that all expressions inside the roots are always positive, and all square roots are defined to be positive.

Fig. 2.2 shows a comparison between our asymptotic expression and the direct numerical evaluations of the OPDM (2.12), obtained by evaluating determinants of order $O(N)$ [6, 55]. We find that the agreement is excellent. Remarkably, although our formula is derived in the thermodynamic limit $N \to \infty$, it accurately captures the behavior of the OPDM even for relatively small systems, with N on the order of a few tens, as illustrated in Fig.2.3.

2.1.3 The OPDM from Quantum Generalized Hydrodynamics

In this Section we detail the derivation of the exact asymptotic formula (2.15) for the equal-time OPDM. We start with recalling the 'Generalized Hydrodynamics' (GHD) [1, 2] description of HCBs released from the infinite box trap, after Ref. [68] (see also e.g. Refs. [123, 125–128, 139–142]). We then incorporate quantum fluctuations in the initial state, following the ideas of bosonization (see 2.1.3). These correlation are then transported with the hydrodynamic equation to later times, following the prescriptions of 'inhomogeneous conformal field theory' [85, 124, 131, 143] or quantum generalized hydrodynamics (QGHD)) [3, 4].

Our approach is entirely based on propagating the quantum fluctuations present in the initial state to later times $t > 0$, on top of the hydrodynamic (GHD) background in the Euler limit. The corrections to the propagation equation from the expansion of the Moyal product [144–146] are not included in our analysis. These corrections are expected to be subleading, and a systematic method for incorporating them into the calculation of the OPDM is still lacking.

Hydrodynamics of free fermions

The Hamiltonian of free fermions (2.5) is diagonalized by the Fourier transform

$$\hat{c}(k) = \sum_{x \in \mathbb{Z}+\frac{1}{2}} e^{-ikx} \hat{c}_x, \qquad \hat{c}^\dagger(k) = \sum_{x \in \mathbb{Z}+\frac{1}{2}} e^{ikx} \hat{c}_x^\dagger, \tag{2.18}$$

with the operators $\hat{c}(k)$ ($\hat{c}^\dagger(k)$) annihilating (creating) a particle of momentum k, with $k \in \mathbb{R}/2\pi\mathbb{Z}$ (i.e. k is defined modulo 2π). The diagonalized Hamiltonian is

$$\hat{H} = \sum_k \varepsilon(k) \hat{c}^\dagger(k) \hat{c}(k), \tag{2.19}$$

with the dispersion relation $\varepsilon(k) = -\cos(k)$. Instead of using the Hamiltonian directly to describe the dynamics, we turn to a hydrodynamic description valid at large distances and large times. In this description the variable x becomes a continuous variable, as discussed previously in Section 1.3.3. The state of the gas at time t is then given by the phase-space occupation function of fermions:

$$\nu(x,k,t) \in [0,1], \tag{2.20}$$

where $(x, k) \in \mathbb{R} \times (\mathbb{R}/2\pi\mathbb{Z})$ are the coordinates in phase-space. It evolves in time according to the hydrodynamic equation

$$\partial_t \nu(x,k,t) + \sin(k)\partial_x \nu(x,k,t) = 0, \tag{2.21}$$

where $\sin(k)$ is the group velocity corresponding to the dispersion relation $-\cos(k)$ of free fermionic Hamiltonian (2.5). The function $\nu(x,k)$ can be interpreted as the Wigner function of the fermions, which becomes a classical (i.e., non-negative) probability distribution in the limit of smooth density variations [124, 147]. The definition of the Wigner function in lattice systems is subtle and requires a more careful treatment, as elaborated in Refs.[144, 145, 148]. In this work, following a common assumption in the literature (see, e.g.,[128, 132, 149]), we assume that, at large scales, the gas of hard-core bosons is described by the coarse-grained occupation function $\nu(x,k)$, defined in Eq.(2.20), which evolves according to the hydrodynamic equation (2.21).

The occupation function corresponding to the initial state (2.6) is

$$\nu(x,k,0) = \begin{cases} 1 & \text{if} \quad 0 < x < N, \\ 0 & \text{otherwise.} \end{cases} \tag{2.22}$$

As discussed earlier in Section 1.3.3, the cases where the initial occupation $\nu(x,k,0)$ is either 0 or 1, are special cases known as or 'zero-entropy GHD' [147]. In such cases, it is easy to see that the solution of the evolution equation (2.21) is

$$\nu(x,k,t) = \begin{cases} 1 & \text{if} \quad t\sin k < x < N + t\sin k \\ 0 & \text{otherwise.} \end{cases} \tag{2.23}$$

The particle density at position x is obtained by integrating the phase-space occupation over k,

$$n(x,t) = \int_{-\pi}^{\pi} \nu(x,k,t)\frac{dk}{2\pi}, \tag{2.24}$$

which reproduces the anticipated formula (2.11) for the density profile.

The two curves that separate the phase-space region where $\nu = 1$ from the ones where $\nu = 0$ play a central role in this work. We refer to them as the left and right 'Fermi contours'. At a fixed time t, they are defined as

$$\begin{aligned} \Gamma_{\rm L} &:= \{(x,k) = (N\sin s, s),\ s \in [-\pi,\pi]\}, \\ \Gamma_{\rm R} &:= \{(x,k) = (N + t\sin s, s),\ s \in [-\pi,\pi]\}. \end{aligned} \tag{2.25}$$

In the following, we sometimes use the parametrization (see Fig. 2.4):

$$\begin{aligned} k_{\rm L,1}(x) &:= \left(\pi - \arcsin\left(\frac{|x|}{t}\right)\right)\text{sign}(x) && \in[-\pi, -\frac{\pi}{2}] \cup [\frac{\pi}{2}, \pi] \\ k_{\rm L,2}(x) &:= \arcsin\left(\frac{x}{t}\right) && \in[-\frac{\pi}{2}, \frac{\pi}{2}] \\ k_{\rm R,1}(x) &:= \arcsin\left(\frac{x-N}{t}\right) && \in[-\frac{\pi}{2}, \frac{\pi}{2}] \\ k_{\rm R,2}(x) &:= \left(\pi - \arcsin\left(\frac{|x-N|}{t}\right)\right)\text{sign}(x-N) && \in[-\pi, -\frac{\pi}{2}] \cup [\frac{\pi}{2}, \pi], \end{aligned} \tag{2.26}$$

so that

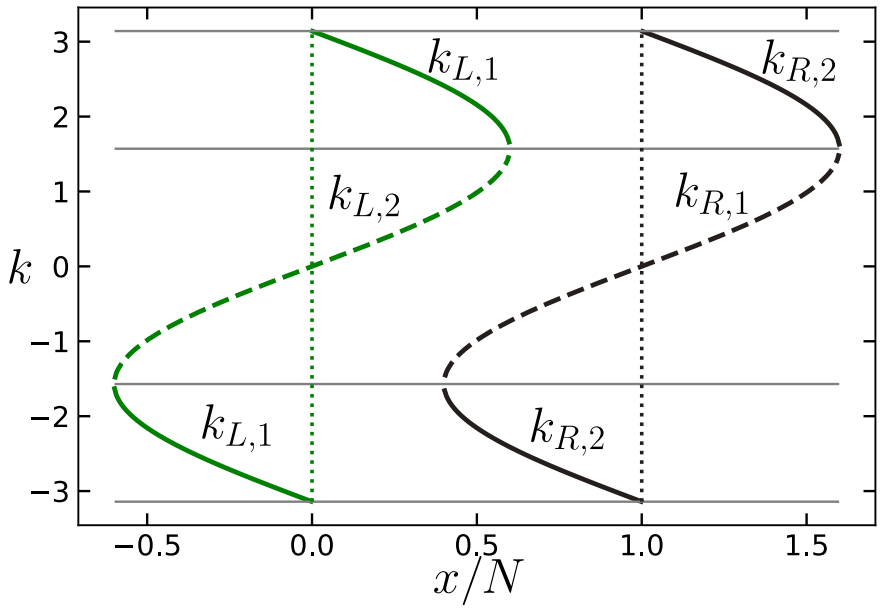


Figure 2.4: The conventions for parameterizing the left/right Fermi contours for a system containing $N = 200$ particles at $t = 120$. The green (resp. black) solid line shows $k_{L,1}(x)$ (resp. $k_{R,2}(x)$), while the green (resp. black) dashed line shows $k_{L,2}(x)$ (resp. $k_{R,1}(x)$). The dotted lines show the Fermi contours at $t = 0$ (green – left; black – right); horizontal gray lines indicate the momenta $k = \pi$, $\frac{\pi}{2}$, $-\frac{\pi}{2}$ and $-\pi$ from top to bottom respectively.

$$\begin{aligned}\Gamma_{\mathrm{L}} &= \{(x, k_{\mathrm{L},1}(x)),\ x \in [-t, t]\} \cup \{(x, k_{\mathrm{L},2}(x)),\ x \in [-t, t]\} \\ \Gamma_{\mathrm{R}} &= \{(x, k_{\mathrm{R},1}(x)),\ x \in [N-t, N+t]\} \cup \{(x, k_{\mathrm{R},2}(x)),\ x \in [N-t, N+t]\}\,. \end{aligned} \tag{2.27}$$

We emphasize here again, that the description of the dynamics of the gas in terms of the occupation ratio (2.20) and the evolution equation (2.21) introduced so far is entirely classical, (for more see the introduction to GHD in 1.3 and the review of QGHD in Sections 1.5). It does capture some quantities, such as the density profile (2.11), in the limit of large time and large distances. However, it does not give access to other quantities like the OPDM (1.24). To obtain such correlations, we follow the approach of Refs. [3, 4, 63, 68, 123–125, 143] and reintroduce some 'quantumness' into the description, which enables access to the OPDM, following the framework of Quantum Generalized Hydrodynamics (see Section 1.5). The 'quantumness' of the system resides in the initial state and is then propagated in time according to the classical equation (2.21).

In the following parts of this Section, we explain how this approach is implemented and how it leads to the time evolution of the One-Particle Density Matrix. We begin by analyzing the fermionic two-point function at time t, which can be computed exactly and expressed as a double integral that can be evaluated using the stationary phase approximation. Remarkably, the result coincides with that obtained in a quantum theory describing quantum fluctuations of the two Fermi contours Γ_{L} and Γ_{R}.

Fermionic two-point function.

The fermionic two-point function is defined

$$\langle\psi_t|\, \hat{c}_x^\dagger \hat{c}_y\, |\psi_t\rangle \tag{2.28}$$

for any two points x and y on the lattice. At time $t = 0$, according to the initial state we have (see Eq. (2.6))

$$\langle\psi_0|\,\hat{c}_x^\dagger\hat{c}_y\,|\psi_0\rangle = \begin{cases}\delta_{x,y} & \text{if} \quad 0 < x < N,\\ 0 & \text{otherwise.}\end{cases} \tag{2.29}$$

In momentum space, it takes the form

$$\begin{aligned}\langle\psi_0|\,\hat{c}^\dagger(k)\hat{c}(q)\,|\psi_0\rangle &= \sum_{x,y\in\mathbb{Z}+\frac{1}{2}} e^{i(kx-qy)}\,\langle\psi_0|\,\hat{c}_x^\dagger\hat{c}_y\,|\psi_0\rangle\\ &= \sum_{x=\frac{1}{2}}^{N-\frac{1}{2}} e^{i(k-q)x} = -2\pi\delta(k-q) + \sum_{x=\frac{1}{2}}^{+\infty} e^{i(k-q+i0^+)x} + \sum_{x=-\infty}^{N-\frac{1}{2}} e^{i(k-q-i0^+)x}\\ &= -2\pi\delta(k-q) + \frac{-1}{2i\sin\left(\frac{k-q}{2}+i0^+\right)} + \frac{e^{i(k-q)N}}{2i\sin\left(\frac{k-q}{2}-i0^-\right)}.\end{aligned} \tag{2.30}$$

At later times $t > 0$, we use the fact that the Hamiltonian (2.5) is diagonal in the fermionic Fourier modes $\hat{c}_k/\hat{c}_k^\dagger$,

$$e^{i\hat{H}t}\hat{c}^\dagger(k)e^{-i\hat{H}t} = e^{i\varepsilon(k)t}\hat{c}^\dagger(k), \tag{2.31}$$

so that

$$\langle\psi_t|\,\hat{c}^\dagger(k)\hat{c}(q)\,|\psi_t\rangle = e^{it[\varepsilon(k)-\varepsilon(q)]}\,\langle\psi_0|\,\hat{c}^\dagger(k)\hat{c}(q)\,|\psi_0\rangle\,. \tag{2.32}$$

This leads to the following double integral for the fermionic two point function:

$$\begin{aligned}\langle\psi_t|\,\hat{c}_x^\dagger\hat{c}_y\,|\psi_t\rangle &= \int_{-\pi}^{\pi}\frac{dk}{2\pi}\int_{-\pi}^{\pi}\frac{dq}{2\pi}e^{-i(kx-qy)}\,\langle\psi_t|\,\hat{c}^\dagger(k)\hat{c}(q)\,|\psi_t\rangle\\ &= -\delta_{x,y} + \int_{-\pi}^{\pi}\frac{dk}{2\pi}\int_{-\pi}^{\pi}\frac{dq}{2\pi}e^{-i(kx-\varepsilon(k)t)}e^{i(qy-\varepsilon(q)t)}\\ &\qquad\left(\frac{-1}{2i\sin\left(\frac{k-q}{2}+i0^+\right)} + \frac{e^{i(k-q)N}}{2i\sin\left(\frac{k-q}{2}-i0^+\right)}\right).\end{aligned} \tag{2.33}$$

In the limit of large time t, with the ratios x/t and y/t kept fixed, this double integral can be evaluated using the stationary phase approximation. For the first term in the parenthesis, the phase is stationary when

$$k = k_{\mathrm{L},1} \quad \text{or} \quad k = k_{\mathrm{L},2}, \tag{2.34}$$

so that

$$x - \varepsilon'(k)t = 0. \tag{2.35}$$

Expanding the phase around the stationary point $k_{\mathrm{L},a}(x)$ ($a = 1, 2$), we get

$$\begin{aligned}kx - \varepsilon(k)t &\simeq \Phi(k_{\mathrm{L},a}(x)) - \frac{1}{2}\varepsilon''(k_{\mathrm{L},a}(x))\,t\,(k-k_{\mathrm{L},a}(x))^2\\ &= \Phi(k_{\mathrm{L},a}(x)) - \frac{1}{2}\left(\frac{dk_{\mathrm{L},a}(x)}{dx}\right)^{-1}(k-k_{\mathrm{L},a}(x))^2,\end{aligned} \tag{2.36}$$

where we used that $dk_{\mathrm{L},a}/dx = 1/(\varepsilon''(k_{\mathrm{L},a})t)$, which follows from Eq. (2.35), and we defined the 'WKB phase' (Brioullin-Kramers-Wentzel) as

$$\Phi(k) := kt\sin k - \varepsilon(k)t. \tag{2.37}$$

We have a similar expansion for the second term in the parenthesis in Eq. (2.33), around the points $k = k_{\mathrm{R},1}(x)$ and $k = k_{\mathrm{R},2}(x)$, which solve the stationary phase condition $x - N - \varepsilon'(k)t = 0$. Around that point the expansion reads

$$k(x-N) - \varepsilon(k)t \approx \Phi(k_{\mathrm{R},a}(x)) - \frac{1}{2}\left(\frac{dk_{\mathrm{R},a}(x)}{dx}\right)^{-1}(k - k_{\mathrm{R},a}(x))^2, \tag{2.38}$$

with the same function $\Phi(k)$ as in Eq. (2.37). Notice that there may be no stationary points, depending on the region where the point x is, see the discussion in the table later in (2.14).

Let us first focus on the first term in the integral in Eq. (2.33), assuming that $-t < x, y < t$. Then there are two stationary points for both integrals, over k and over q. Evaluating the Gaussian integrals, we arrive at

$$\begin{aligned}
&\int_{-\pi}^{\pi}\frac{dk}{2\pi}\int_{-\pi}^{\pi}\frac{dq}{2\pi}e^{-i(kx-\varepsilon(k)t)}e^{i(qy-\varepsilon(q)t)}\frac{-1}{2i\sin\left(\frac{k-q}{2}+i0^+\right)}\\
&\simeq \sum_{a=1,2}\sum_{b=1,2}\int_{-\infty}^{\infty}\frac{dk}{2\pi}\int_{-\infty}^{\infty}\frac{dq}{2\pi}\frac{e^{-i\Phi(k_{\mathrm{L},a}(x))+\frac{i}{2}(k-k_{\mathrm{L},a}(x))^2\varepsilon''(k_{\mathrm{L},a})t}e^{i\Phi(k_{\mathrm{L},b}(y))-\frac{i}{2}(k-k_{\mathrm{L},b}(y))^2\varepsilon''(k_{\mathrm{L},b})t}}{-2i\sin\left(\frac{k_{\mathrm{L},a}(x)-k_{\mathrm{L},b}(y)}{2}\right)}\\
&= \sum_{a,b}\frac{1}{2\pi}\sqrt{\frac{dk_{\mathrm{L},a}(x)}{dx}}\sqrt{\frac{dk_{\mathrm{L},b}(y)}{dy}}\frac{i\,e^{-i[\Phi(k_{\mathrm{L},a}(x))-\Phi(k_{\mathrm{L},b}(y))]}}{2\sin\left(\frac{k_{\mathrm{L},a}(x)-k_{\mathrm{L},b}(y)}{2}\right)},
\end{aligned} \tag{2.39}$$

where if the expression inside the square roots is negative the branches are chosen in the following way:

$$\begin{aligned}
&\mathrm{Im}\left[\sqrt{\frac{dk_{\mathrm{L},a}(x)}{dx}}\right] < 0, \quad \text{if} \quad \frac{dk_{\mathrm{L},a}(x)}{dx} < 0 \qquad \text{i.e.} \quad \text{if } a = 1, \qquad \text{and}\\
&\mathrm{Im}\left[\sqrt{\frac{dk_{\mathrm{L},b}(y)}{dy}}\right] > 0, \quad \text{if} \quad \frac{dk_{\mathrm{L},b}(x)}{dx} < 0 \qquad \text{i.e.} \quad \text{if } b = 1.
\end{aligned} \tag{2.40}$$

Similarly, for the second term in the parenthesis in Eq. (2.33), we arrive at

$$\begin{aligned}
&\int_{-\pi}^{\pi}\frac{dk}{2\pi}\int_{-\pi}^{\pi}\frac{dq}{2\pi}e^{-i(kx-\varepsilon(k)t)}e^{i(qy-\varepsilon(q)t)}\frac{e^{i(k-q)N}}{2i\sin\left(\frac{k-q}{2}-i0^+\right)}\\
&\simeq \sum_{a=1,2}\sum_{b=1,2}\int_{-\infty}^{\infty}\frac{dk}{2\pi}\int_{-\infty}^{\infty}\frac{dq}{2\pi}\frac{e^{-i\Phi(k_{\mathrm{R},a}(x))+\frac{i}{2}(k-k_{\mathrm{R},a}(x))^2\varepsilon''(k_{\mathrm{R},a}(x))t}e^{i\Phi(k_{\mathrm{R},b}(y))-\frac{i}{2}(k-k_{\mathrm{R},b})^2\varepsilon''(k_{\mathrm{R},b})t}}{2i\sin\left(\frac{k_{\mathrm{R},a}(x)-k_{\mathrm{R},b}(y)}{2}\right)}\\
&= \sum_{a,b}\frac{1}{2\pi}\sqrt{\frac{dk_{\mathrm{R},a}(x)}{dx}}\sqrt{\frac{dk_{\mathrm{R},b}(y)}{dy}}\frac{-ie^{-i[\Phi(k_{\mathrm{R},a}(x))-\Phi(k_{\mathrm{R},b}(y))]}}{2\sin\left(\frac{k_{\mathrm{R},a}(x)-k_{\mathrm{R},b}(y)}{2}\right)},
\end{aligned} \tag{2.41}$$

where we choose the branches the same way as we did in Eq. (2.40).

Identification with field theory correlators

The key point is to observe that the above expressions for the different terms contributing to $\langle\psi_t|\,\hat{c}_x^\dagger\hat{c}_y\,|\psi_t\rangle$ coincide precisely with correlators in a field theory defined along the two Fermi contours. To see this, we introduce fermion fields associated to the L and R Fermi contours,

$$\hat{\psi}_{\mathrm{L}}^\dagger(k), \qquad \hat{\psi}_{\mathrm{L}}(k), \qquad \hat{\psi}_{\mathrm{R}}^\dagger(k), \qquad \hat{\psi}_{\mathrm{R}}(k), \tag{2.42}$$

for which we postulate the following two-point correlation functions,

$$\begin{aligned}\langle\hat{\psi}^\dagger_{\rm L}(k)\hat{\psi}_{\rm L}(q)\rangle &:= \frac{i\,e^{-i[\Phi_{\rm L}(k)-\Phi_{\rm L}(q)]}}{2\sin\left(\frac{k-q}{2}+i0^+\right)},\\ \langle\hat{\psi}^\dagger_{\rm R}(k)\hat{\psi}_{\rm R}(q)\rangle &:= \frac{-i\,e^{-i[\Phi_{\rm R}(k)-\Phi_{\rm R}(q)]}}{2\sin\left(\frac{k-q}{2}-i0^+\right)};\end{aligned} \tag{2.43}$$

all other two-point functions vanish. Then the fermionic creation/annihilation operators in the lattice model can be expressed in terms of these fields the following way:

	$\hat{c}^\dagger_x$
$x\in$ E	0
$x\in$ L	$\frac{e^{-i\frac{\pi}{4}}}{(2\pi)^{\frac{1}{2}}}\left\lvert\frac{dk_{\rm L,1}}{dx}\right\rvert^{\frac{1}{2}}\psi^\dagger_{\rm L}(k_{\rm L,1}(x))+\frac{e^{i\frac{\pi}{4}}}{(2\pi)^{\frac{1}{2}}}\left\lvert\frac{dk_{\rm L,2}}{dx}\right\rvert^{\frac{1}{2}}\psi^\dagger_{\rm L}(k_{\rm L,2}(x))$
$x\in$ R	$\frac{e^{i\frac{\pi}{4}}}{(2\pi)^{\frac{1}{2}}}\left\lvert\frac{dk_{\rm R,1}}{dx}\right\rvert^{\frac{1}{2}}\psi^\dagger_{\rm R}(k_{\rm R,1}(x))+\frac{e^{-i\frac{\pi}{4}}}{(2\pi)^{\frac{1}{2}}}\left\lvert\frac{dk_{\rm R,2}}{dx}\right\rvert^{\frac{1}{2}}\psi^\dagger_{\rm R}(k_{\rm R,2}(x))$
$x\in$ C	$\frac{e^{-i\frac{\pi}{4}}}{(2\pi)^{\frac{1}{2}}}\left\lvert\frac{dk_{\rm L,1}}{dx}\right\rvert^{\frac{1}{2}}\psi^\dagger_{\rm L}(k_{\rm L,1}(x))+\frac{e^{i\frac{\pi}{4}}}{(2\pi)^{\frac{1}{2}}}\left\lvert\frac{dk_{\rm L,2}}{dx}\right\rvert^{\frac{1}{2}}\psi^\dagger_{\rm L}(k_{\rm L,2}(x))$ $+\quad\frac{e^{i\frac{\pi}{4}}}{(2\pi)^{\frac{1}{2}}}\left\lvert\frac{dk_{\rm R,1}}{dx}\right\rvert^{\frac{1}{2}}\psi^\dagger_{\rm R}(k_{\rm R,1}(x))+\frac{e^{-i\frac{\pi}{4}}}{(2\pi)^{\frac{1}{2}}}\left\lvert\frac{dk_{\rm R,2}}{dx}\right\rvert^{\frac{1}{2}}\psi^\dagger_{\rm R}(k_{\rm R,2}(x))$

(2.44)

and

	$\hat{c}_x$
$x\in$ E	0
$x\in$ L	$\frac{e^{i\frac{\pi}{4}}}{(2\pi)^{\frac{1}{2}}}\left\lvert\frac{dk_{\rm L,1}}{dx}\right\rvert^{\frac{1}{2}}\psi_{\rm L}(k_{\rm L,1}(x))+\frac{e^{-i\frac{\pi}{4}}}{(2\pi)^{\frac{1}{2}}}\left\lvert\frac{dk_{\rm L,2}}{dx}\right\rvert^{\frac{1}{2}}\psi_{\rm L}(k_{\rm L,2}(x))$
$x\in$ R	$\frac{e^{-i\frac{\pi}{4}}}{(2\pi)^{\frac{1}{2}}}\left\lvert\frac{dk_{\rm R,1}}{dx}\right\rvert^{\frac{1}{2}}\psi_{\rm R}(k_{\rm R,1}(x))+\frac{e^{i\frac{\pi}{4}}}{(2\pi)^{\frac{1}{2}}}\left\lvert\frac{dk_{\rm R,2}}{dx}\right\rvert^{\frac{1}{2}}\psi_{\rm R}(k_{\rm R,2}(x))$
$x\in$ C	$\frac{e^{i\frac{\pi}{4}}}{(2\pi)^{\frac{1}{2}}}\left\lvert\frac{dk_{\rm L,1}}{dx}\right\rvert^{\frac{1}{2}}\psi_{\rm L}(k_{\rm L,1}(x))+\frac{e^{-i\frac{\pi}{4}}}{(2\pi)^{\frac{1}{2}}}\left\lvert\frac{dk_{\rm L,2}}{dx}\right\rvert^{\frac{1}{2}}\psi_{\rm L}(k_{\rm L,2}(x))$ $+\quad\frac{e^{-i\frac{\pi}{4}}}{(2\pi)^{\frac{1}{2}}}\left\lvert\frac{dk_{\rm R,1}}{dx}\right\rvert^{\frac{1}{2}}\psi_{\rm R}(k_{\rm R,1}(x))+\frac{e^{i\frac{\pi}{4}}}{(2\pi)^{\frac{1}{2}}}\left\lvert\frac{dk_{\rm R,2}}{dx}\right\rvert^{\frac{1}{2}}\psi_{\rm R}(k_{\rm R,2}(x))\,.$

(2.45)

These expressions for $\hat{c}^\dagger_x$ and $\hat{c}_x$ are constructed so that, evaluating the correlation function $\langle\psi_t|\,\hat{c}^\dagger_x\hat{c}_y\,|\psi_t\rangle$ using Eq. (2.43) automatically reproduces the results obtained above from the stationary phase approximation (as shown in the calculation (2.39)-(2.41)).

So far we have identified the fermionic two-point function at time t, $\langle\psi_t|\,\hat{c}_x^\dagger\hat{c}_y\,|\psi_t\rangle$, with correlators in a free fermion field theory. Importantly, this identification extends to all higher-point correlation functions of fermionic operators,

$$\langle\psi_t|\,\hat{c}_{x_1}^\dagger\dots\hat{c}_{x_n}^\dagger\hat{c}_{y_1}\dots\hat{c}_{y_n}\,|\psi_t\rangle\,, \tag{2.46}$$

through Wick's theorem. Therefore, all fermionic correlation functions are captured, in the asymptotic regime $t\to\infty$ with fixed $\frac{x}{t}$ and $\frac{N}{t}$, by the free fermion field theory defined by the two-point function (2.43).

Field theory of quantum fluctuations around the Fermi contours

We are interested in the OPDM, which is not easily expressible in terms of a simple fermionic correlation functions. Therefore, it is useful to bosonize the field theory. We introduce two chiral boson fields, defined along the left (L) and right (R) Fermi contours respectively,

$$\hat{\phi}_{\rm L}(k),\qquad \hat{\phi}_{\rm R}(k), \tag{2.47}$$

and postulating that these two fields have Gaussian correlation functions, with the following one- and two-point connected functions,

$$\begin{aligned}
\langle\hat{\phi}_\alpha(k)\rangle &= \Phi(k),\qquad \alpha={\rm L},{\rm R},\\
\langle\hat{\phi}_{\rm L}(k)\hat{\phi}_{\rm L}(q)\rangle_{\rm conn.} &= -\log\left(2\sin(\frac{k-q}{2}+i0^+)\right),\\
\langle\hat{\phi}_{\rm R}(k)\hat{\phi}_{\rm R}(q)\rangle_{\rm conn.} &= -\log\left(2\sin(\frac{k-q}{2}-i0^+)\right),\qquad \text{and}\\
\langle\hat{\phi}_{\rm R}(k)\hat{\phi}_{\rm L}(q)\rangle_{\rm conn.} &= 0.
\end{aligned} \tag{2.48}$$

Here Φ is the WKB phase defined in Eq. (2.37).

In terms of these chiral boson fields, the fermion fields (2.42) are given by the standard bosonization formulas

$$\begin{aligned}
\hat{\psi}_{\rm L}^\dagger(k) &= e^{i\frac{\pi}{4}}:e^{-i\hat{\phi}_{\rm L}(k)}:, \qquad \hat{\psi}_{\rm L}(k) = e^{i\frac{\pi}{4}}:e^{i\hat{\phi}_{\rm L}(k)}:,\\
\hat{\psi}_{\rm R}^\dagger(k) &= e^{-i\frac{\pi}{4}}:e^{-i\hat{\phi}_{\rm R}(k)}:, \qquad \hat{\psi}_{\rm R}(k) = e^{-i\frac{\pi}{4}}:e^{i\hat{\phi}_{\rm R}(k)}:,
\end{aligned} \tag{2.49}$$

where $:\,.\,:$ stands for normal ordering (see previous Section 1.4). The chiral bosons $\phi_{\rm R}$ and $\phi_{\rm L}$ can be interpreted as quantum fluctuations of the Fermi contours. The density operators that measure the excess of fermions near the L and R contours are given in terms of the bosonic operators $\hat{\phi}_R/\hat{\phi}_L$ as

$$\begin{aligned}
\delta\hat{\rho}_{\rm L}(k) &=:\hat{\psi}_{\rm L}^\dagger(k)\hat{\psi}_{\rm L}(k):= \partial_k\hat{\phi}_{\rm L}(k)-\partial_k\langle\hat{\phi}_{\rm L}(k)\rangle\,,\\
\delta\hat{\rho}_{\rm R}(k) &=:\hat{\psi}_{\rm R}^\dagger(k)\hat{\psi}_{\rm R}(k):= -\partial_k\hat{\phi}_{\rm R}(k)+\partial_k\langle\hat{\phi}_{\rm R}(k)\rangle\,.
\end{aligned} \tag{2.50}$$

This is the idea of the theory of 'quantum Generalized Hydrodynamics' [3, 4, 63, 123], as discussed in Section 1.5. Long wavelength quantum fluctuations of the fluid come from small fluctuations of the Fermi contour, encoded as a free chiral boson theory along that contour, with an operator $\delta\hat{\rho}_\alpha$ that measures the excess density of quasi-particles around a point on the contour. The effective theory describing those fluctuations of the Fermi contour is then similar to a Luttinger liquid (see more in Section 1.4).

The bosonic creation/annihilation operator

In order to compute the OPDM (1.24), we need to express the operators that create/annihilate a boson, $\hat{\sigma}_x^+/\hat{\sigma}_x^-$, in terms of local operators in the field theory that describe fluctuations of the contour, similarly to what is done in Ref. [63],

$$\begin{aligned}\hat{\sigma}_x^+ &= \sum_{\eta\in\mathcal{I}_x} \mathcal{C}_\eta^*(x)\hat{\mathcal{O}}_\eta^\dagger(x),\\ \hat{\sigma}_x^- &= \sum_{\eta\in\mathcal{I}_x} \mathcal{C}_\eta(x)\hat{\mathcal{O}}_\eta(x).\end{aligned} \tag{2.51}$$

Here the $\hat{\mathcal{O}}_\eta(x)$'s are operators in the free boson theory, the $\mathcal{C}(x)$'s are complex coefficients, and η is a multi-index labeling the operators (see below); η runs over a set $\mathcal{I}_x$ that depends on the number of Fermi points at position x. In principle, infinitely many field theory operators can appear in the r.h.s. of (2.51). However, in practice, these operators can be organized according to their scaling dimension, and the sum can be truncated to keep only the operators of lowest scaling dimension, which are those fixing the leading behavior of $g_1(x,y;t)$ at large distances. The operators $\mathcal{O}_\eta$ are primary operators of the following form

$$\hat{\mathcal{O}}_\eta(x) = \prod_{l=1}^{2Q} :e^{i\eta_l\hat{\phi}(k_l)}:, \tag{2.52}$$

where $2Q$ is the number of Fermi points at point x. Here we label the Fermi points at position x as follows:

- for $x\in$ L (then $2Q=2$)

$$\begin{aligned} &k_1 := k_{\mathrm{L},1}(x), && k_2 := k_{\mathrm{L},2}(x), \quad \text{and}\\ &\hat{\phi}(k_1) := \hat{\phi}_{\mathrm{L}}(k_{\mathrm{L},1}(x)), && \hat{\phi}(k_2) := \hat{\phi}_{\mathrm{L}}(k_{\mathrm{L},2}(x))\end{aligned}$$

- for $x\in$ R (then $2Q=2$)

$$\begin{aligned} &k_1 := k_{\mathrm{R},1}(x), && k_2 := k_{\mathrm{R},2}(x), \quad \text{and}\\ &\hat{\phi}(k_1) := \hat{\phi}_{\mathrm{R}}(k_{\mathrm{R},1}(x)), && \hat{\phi}(k_2) := \hat{\phi}_{\mathrm{R}}(k_{\mathrm{R},2}(x))\end{aligned}$$

- for $x\in$ C (then $2Q=4$)

$$\begin{aligned} &k_1 := k_{\mathrm{L},1}(x), && k_2 := k_{\mathrm{R},1}(x),\\ &k_3 := k_{\mathrm{R},2}(x), && k_4 := k_{\mathrm{L},2}(x), \quad \text{and}\\ &\hat{\phi}(k_1) := \hat{\phi}_{\mathrm{L}}(k_{\mathrm{L},1}(x)), && \hat{\phi}(k_2) := \hat{\phi}_{\mathrm{R}}(k_{\mathrm{R},1}(x)),\\ &\hat{\phi}(k_3) := \hat{\phi}_{\mathrm{R}}(k_{\mathrm{R},2}(x)), && \hat{\phi}(k_4) := \hat{\phi}_{\mathrm{L}}(k_{\mathrm{L},2}(x)).\end{aligned} \tag{2.53}$$

The coefficients η_l appearing in the exponentials of Eq. (2.52) can be understood as describing the displacement of the Fermi contour induced by the vertex operator $:e^{i\eta_l\hat{\phi}(k_l)}:$ in the vicinity of the point k_l. A positive value of η_l corresponds to an inward deformation, while a negative value indicates an outward deformation. The parameters η_l are half-integers, $\eta_l\in\mathbb{Z}+\frac{1}{2}$, as they represent shifts that correspond to a change in the boundary conditions of the fermions—from periodic to anti-periodic (see the next subsection for further discussion). Moreover, the bosonization formulas presented above give

$$\left[\int_{-\pi}^{\pi}(\delta\hat{\rho}_{\mathrm{L}}(k)+\delta\hat{\rho}_{\mathrm{R}}(k))dk, \hat{\mathcal{O}}(x)\right] = -\left(\sum_{l=1}^{2Q}\eta_l\right)\hat{\mathcal{O}}_\eta(x), \tag{2.54}$$

and, since all operators $\mathcal{O}_\eta(x)$ appearing in the expansion (2.51) must have charge -1 as they annihilate a particle, we must have

$$\sum_{l=1}^{2Q} \eta_l = 1. \tag{2.55}$$

In addition, the scaling dimension of the operator (2.52) is

$$\Delta_\eta = \sum_{l=1}^{2Q} \frac{\eta_l^2}{2}. \tag{2.56}$$

Looking at the sets of coefficients η_l that satisfy Eq. (2.55) and minimize Eq. (2.56), one finds the operators of minimal scaling dimension appearing in the expansion (2.51).

For 2 Fermi points ($Q = 1$) there is a single operator (2.52) of minimal scaling dimension, corresponding to

$$\eta = (\eta_1, \eta_2) = \left(+\frac{1}{2}, +\frac{1}{2}\right). \tag{2.57}$$

For 4 Fermi points ($Q = 2$), there are four operators (2.52) of minimal scaling dimension corresponding to

$$\begin{aligned} \eta = (\eta_1, \eta_2, \eta_3, \eta_4) &= \left(-\frac{1}{2}, +\frac{1}{2}, +\frac{1}{2}, +\frac{1}{2}\right), \\ \text{or} \qquad \eta &= \left(+\frac{1}{2}, -\frac{1}{2}, +\frac{1}{2}, +\frac{1}{2}\right), \\ \text{or} \qquad \eta &= \left(+\frac{1}{2}, +\frac{1}{2}, -\frac{1}{2}, +\frac{1}{2}\right), \\ \text{or} \qquad \eta &= \left(+\frac{1}{2}, +\frac{1}{2}, +\frac{1}{2}, -\frac{1}{2}\right). \end{aligned} \tag{2.58}$$

Having identified the most relevant operators appearing on the right-hand side of Eq. (2.51), we now turn to the corresponding coefficients $\mathcal{C}_\eta(x)$. These coefficients incorporate the Jacobian associated with the change of coordinates $x \mapsto k_{\alpha,a}(x)$ in the vicinity of each Fermi point (with $\alpha = \mathrm{L}, \mathrm{R}$ and $a = 1, 2$), as well as a numerical factor $B_\eta(\{k_a\})$, which depends on the configuration of Fermi points at position x,

$$\mathcal{C}_\eta(x) = B_\eta(\{k_a(x)\}_{1\le a\le 2Q}) \prod_{l=1}^{2Q} \left|\frac{\mathrm{d}k_l}{\mathrm{d}x}\right|^{1/8}. \tag{2.59}$$

In the Appendix A below, we derive the numerical factors $B_\eta(\{k_a\})$ by relating them to form factors, following Refs. [73, 81, 82, 122, 150]. The result reads

$$B_\eta(\{k_a\}_{1\le a\le 2Q}) \;=\; \frac{\left(\frac{G^2(3/2)}{\sqrt{\pi}}\right)^Q}{\sqrt{2}} \prod_{1\le a<b\le 2Q} \left|2\sin(\frac{k_b - k_a}{2})\right|^{\eta_a\eta_b}, \qquad (Q \ge 1), \tag{2.60}$$

and $B_\eta = 0$ if $Q = 0$, i.e. if there are no Fermi points at position x.

In summary, the main result of this Section is the expansion of the lattice boson creation and annihilation operators, Eq. (2.51), in terms of the corresponding field-theoretic operators. This expansion can be written as:

$$\begin{aligned} \hat{\sigma}_x^+ = \sum_{\eta\in\mathcal{I}} \frac{\left(\frac{G^2(3/2)}{\sqrt{\pi}}\right)^Q}{\sqrt{2}} \prod_{1\le a<b\le 2Q} \left|2\sin(\frac{k_b - k_a}{2})\right|^{\eta_a\eta_b} \prod_{c=1}^{2Q} \left|\frac{\mathrm{d}k_c}{\mathrm{d}x}\right|^{1/8} \prod_{l=1}^{2Q} :e^{-i\eta_l\phi(k_l)}: \\ + \text{ less relevant operators}, \end{aligned} \tag{2.61}$$

$$\hat{\sigma}_x^- = \sum_{\eta\in\mathcal{I}} \frac{\left(\frac{G^2(3/2)}{\sqrt{\pi}}\right)^Q}{\sqrt{2}} \prod_{1\le a<b\le 2Q} \left|2\sin(\frac{k_b-k_a}{2})\right|^{\eta_a\eta_b} \prod_{c=1}^{2Q} \left|\frac{\mathrm{d}k_c}{\mathrm{d}x}\right|^{1/8} \prod_{l=1}^{2Q} :e^{i\eta_l\phi(k_l)}: \\ + \text{ less relevant operators.} \tag{2.62}$$

Here $2Q = 0, 2, 4$ is the number of Fermi points at position x, and the set of indices $\mathcal{I}$ in the sum (2.51), we take

$$\begin{array}{rcll} \mathcal{I} & := & \emptyset & \text{if} \quad Q=0, \\ \mathcal{I} & := & \{(1/2,1/2)\} & \text{if} \quad Q=1, \\ \mathcal{I} & := & \{(-1/2,1/2,1/2,1/2),(1/2,-1/2,1/2,1/2), & \\ & & (1/2,1/2,-1/2,1/2),(1/2,1/2,1/2,-1/2)\} & \text{if} \quad Q=2. \end{array} \tag{2.63}$$

Thus, the sums in Eqs. (2.61)-(2.62) run over zero term (for $Q = 0$), or one term (for $Q = 1$) or four terms ($Q = 2$). Eqs. (2.61)-(2.62) are the key formulas that we use below to derive our main result for the OPDM.

2.1.4 Evaluation of The Correlation Functions

Finally, we have all the ingredients that are needed to derive our result for the equal-time OPDM (2.15)-(2.16). In particular, we have the expansion (2.61)-(2.62) of the lattice boson creation/annihilation operators in terms of the field theory operators. We see that this expansion leads to the OPDM in the form of a vector-matrix-vector product,

$$g_1(x,y;t) = \mathcal{C}^\dagger(x;t)\cdot F(x,y;t)\cdot \mathcal{C}(y;t), \tag{2.64}$$

where the vector $\mathcal{C}(x;t)$ and the matrix $F(x,y;t)$ are of small finite dimension. Specifically, the vector $\mathcal{C}(x;t)$ is either the zero vector (in that case $g_1(x,y;t) = 0$), or it is of dimension 1, or of dimension 4, depending on the position x. This is best summarized in a table:

Interval	Name	Dim. $\mathcal{C}(x;t)$	$\mathcal{C}(x;t)$
$x<-t$ or $x>N+t$	Empty (E)		0
$-t<x<\min(t,N-t)$	Left (L)	1	$\frac{G(3/2)^2}{\sqrt{\pi}}\left(\frac{1}{(2t)^{1/4}}\right)$
$N-t<x<t$ (if $t>\frac{N}{2}$)	Central (C)	4	$\frac{G(3/2)^4}{\sqrt{2}\pi}\begin{pmatrix}\frac{1}{(t^2-x^2)^{1/4}}\\ \frac{1}{(t^2-x^2)^{1/4}}\\ \frac{1}{(t^2-(N-x)^2)^{1/4}}\\ \frac{1}{(t^2-(N-x)^2)^{1/4}}\end{pmatrix}$
$\max(t,N-t)<x<N+t$	Right (R)	1	$\frac{G(3/2)^2}{\sqrt{\pi}}\left(\frac{1}{(2t)^{1/4}}\right)$
$t<x<N-t$ (if $t<\frac{N}{2}$)	Filled (F)		0 .

(2.65)

Those entries for the vector $\mathcal{C}$ are obtained by evaluating the coefficients in the expansion (2.61)-(2.62), namely

$$\mathcal{C}_\eta(x,t) = \frac{\left(\frac{G^2(3/2)}{\sqrt{\pi}}\right)^Q}{\sqrt{2}} \prod_{1\le a<b\le 2Q} \left|2\sin(\frac{k_b-k_a}{2})\right|^{\eta_a\eta_b} \prod_{c=1}^{2Q} \left|\frac{\mathrm{d}k_c}{\mathrm{d}x}\right|^{1/8}, \tag{2.66}$$

using the explicit form (2.26) of $k_a(x)$.

Similarly, the matrix $F(x,y;t)$ is either the zero matrix or it is of size 1×1, or 1×4, or 4×1 or 4×4 depending of the positions of x and y:

Dim. of $F(x,y;t)$	$x\in E$	$x\in L$	$x\in C$	$x\in R$	$x\in F$
$y\in E$					
$y\in L$		1×1	4×1	1×1	
$y\in C$		1×4	4×4	1×4	
$y\in R$		1×1	4×1	1×1	
$y\in F$					

(2.67)

and the void entries stand for the case where $F(x,y;t)$ is the zero matrix. Notice that the vector-matrix-vector product (2.64) is always well-defined. The entries of the matrix $F(x,y;t)$ are obtained by explicitly evaluating the correlation function of the field theory operators,

$$F_{\eta^x,\eta^y}(x,y;t) \;=\; \left\langle \prod_{l=1}^{2Q_x} :e^{-i\eta_l^x\hat\phi(k_l(x))}: \prod_{m=1}^{2Q_y} :e^{i\eta_m^y\hat\phi(k_m(y))}: \right\rangle \tag{2.68}$$

using Wick's theorem for the bosonic fields $\phi_{\rm R}$ and $\phi_{\rm L}$, along with its one- and two-point functions (2.48). The expression (2.68) is ambiguous because the field $\phi(k)$ is defined modulo 2π, so the exponential $e^{\frac{i}{2}\phi}$ is defined only up to a sign. This sign is of course important for our purposes, since the OPDM $g_1(x,y;t)$ is a sum of such terms, which depends on those signs. We discuss how to fix this amibiguitity in full details in Sec. 2.1.4 below.

This leads to the following entries:

$F(x,y;t)$	$x\in L$	$x\in C$	$x\in R$
$y\in L$	$M_1(x,y)$	$M_4(x,y)$	(0)
$y\in C$	$M_4^\dagger(y,x)$	$\begin{pmatrix} M_2(x,y) & \\ & M_2(N-x,N-y)\end{pmatrix}$	$M_4^\dagger(N-y,N-x)\cdot\begin{pmatrix} & & 1 & \\ & & & 1\\ 1 & & & \\ & 1 & & \end{pmatrix}$
$y\in R$	(0)	$\begin{pmatrix} & & 1 & \\ & & & 1\\ 1 & & & \\ & 1 & & \end{pmatrix}\cdot M_4(N-x,N-y)$	$M_1(N-x,N-y)$

(2.69)

where the 1×1 matrix M_1 is

$$M_1(x,y)\equiv e^{i\frac{\pi}{2}(x-y)}\frac{r(x)^{\frac14}r(y)^{\frac14}}{|x-y|^{\frac12}}\;\times\;(1)\,, \tag{2.70}$$

the 4×1 matrix M_4 is —we recall that $r(x)$, $\varphi(x)$, $D(x,y)$ are defined in Eq. (2.17)—

$$M_4(x,y)\equiv e^{i\frac{\pi}{2}(x-y)}\frac{(t/2)^{\frac14}\,r(x)^{\frac14}r(y)^{\frac14}}{r(N-x)^{\frac14}\,|x-y|^{\frac12}}\;\times\;\begin{pmatrix}0\\0\\e^{-i\varphi(N-x)}\\e^{i\varphi(N-x)}\end{pmatrix}, \tag{2.71}$$

and the 2×2 matrix M_2 is

$$\begin{aligned} M_2(x,y)\;\equiv\; & e^{-i\frac{\pi}{2}(x-y)}\frac{(t/2)^{\frac12}\,r(N-x)^{\frac14}r(N-y)^{\frac14}}{r(x)^{\frac14}r(y)^{\frac14}|x-y|^{1/2}}\times\\ & \begin{pmatrix} e^{-i\varphi(x)} & \\ & e^{i\varphi(x)}\end{pmatrix}\begin{pmatrix} D(x,y)^{-1/2} & D(x,y)^{1/2}\\ D(x,y)^{1/2} & D(x,y)^{-1/2}\end{pmatrix}\begin{pmatrix} e^{i\varphi(y)} & \\ & e^{-i\varphi(y)}\end{pmatrix}. \end{aligned} \tag{2.72}$$

The cases E/F are not present in eq. (2.69) since $g_1(x,y)$ equals to zero if one of the two points x, y lies in these intervals. Evaluating the vector-matrix-vector product (2.64) explicitly, one then arrives at our main result (2.15)-(2.16).

Conventions on fixing the phase factors

Here we discuss how we fix the phase ambiguity in the calculation of the expectation value of the product of vertex operators

$$\left\langle \prod_{l=1}^{2Q_x} :e^{-i\eta_l^x \phi(k_l(x))}: \prod_{m=1}^{2Q_y} :e^{i\eta_m^y \phi(k_m(y))}: \right\rangle, \tag{2.73}$$

which defines the matrix elements of the matrix $F(x,y;t)$. This expression involves operators on the left and right contours, but it is clear that it factorizes into two independent contributions, one from each contour. For instance, let us focus on the case when all operators are on the same contour, e.g. when $x, y \in L$. In that case we need to evaluate a four-point function

$$\left\langle :e^{-\frac{i}{2}\phi(k_{\mathrm{L},1}(x))}::e^{-\frac{i}{2}\phi(k_{\mathrm{L},2}(x))}::e^{\frac{i}{2}\phi(k_{\mathrm{L},1}(y))}::e^{\frac{i}{2}\phi(k_{\mathrm{L},2}(y))}: \right\rangle. \tag{2.74}$$

This quantity is ill-defined because the field $\phi(k)$ is only defined modulo 2π. However, the quantity $\partial_k\phi(k)$ is always well defined, it measures the fluctuations of the density of HCBs along the Fermi contours, as seen in Eq. (2.50). So we define the correlation function (2.74) as

$$\left\langle e^{-\frac{i}{2}\int_\Gamma \partial_k\phi(k)\,dk} \right\rangle, \tag{2.75}$$

properly regulated at short distance, where Γ is a union of oriented paths along the contour that go from $k_{\mathrm{L},1}(x)$ to $k_{\mathrm{L},1}(y)$ and from $k_{\mathrm{L},2}(x)$ to $k_{\mathrm{L},2}(y)$, see the figure in the top-left entry of Table 2.1. The choice of the oriented path Γ fixes the phase ambiguity in the correlation (2.74). Once the phase ambiguity has been fixed by selecting a set of oriented paths, the correlation function is evaluated using standard methods of bosonization, leading to the following expression for Eq. (2.74)

$$\begin{aligned}\left\langle e^{-\frac{i}{2}\int_\Gamma \partial_k\phi(k)\,dk} \right\rangle &= e^{-\frac{i}{2}\int_\Gamma \partial_q\Phi(q)dq} e^{-\frac{1}{8}\int_\Gamma dq\int_\Gamma dq' \left\langle \partial_q\phi(q)\partial_{q'}\phi(q')\right\rangle_{\mathrm{conn.}}} \\ &= e^{-\frac{i}{2}\int_\Gamma \partial_q\Phi(q)dq} \left| \frac{2\sin\left(\frac{k_{\mathrm{R},1}(x)-k_{\mathrm{R},2}(x)}{2}\right) 2\sin\left(\frac{k_{\mathrm{L},1}(y)-k_{\mathrm{L},2}(y)}{2}\right)}{\prod_{i,j=1,2} 2\sin\left(\frac{k_{\mathrm{L},i}(x)-k_{\mathrm{R},j}(y)}{2}\right)} \right|^{1/4}.\end{aligned} \tag{2.76}$$

More generally, in Table 2.1 we show our conventions for the choice of the oriented path Γ for all different cases. The signs $+, -$ stand for $\pm\frac{1}{2}$ in the exponent in the vertex operators associated to their given points along the contour, and the oriented path is drawn in black. We always choose our oriented paths so that they go from a '$-$' to '$+$'. We also choose our convention so that, when four points are along the same contour, the associated phase factor is one when the two points x and y coincide. In the case of two points on the same contour, the conventions are the following: the associated phase factor disappears if the point is at $N-t$ on the right contour and at t on the left contour (notice that these conventions are consistent with the symmetries of the system and the formulas shown in Eqs (2.15 - 2.17)).

The general expression that we use for the correlation function (2.68) is:

$$\left\langle e^{-\frac{i}{2}\int_\Gamma \partial_k\phi(k)\,dk}\right\rangle = e^{-\frac{i}{2}\int_\Gamma \partial_q\Phi(q)dq}\times$$
$$\frac{\prod_{\alpha=R,L}\prod_{1\le a<b\le Q_x}\left|2\sin\left(\frac{k_{\alpha,\mathrm{a}}(x)-k_{\alpha,\mathrm{b}}(x)}{2}\right)\right|^{1/4}\prod_{\beta=R,L}\prod_{1\le c<d\le Q_y}\left|2\sin\left(\frac{k_{\beta,\mathrm{c}}(y)-k_{\beta,\mathrm{d}}(y)}{2}\right)\right|^{1/4}}{\prod_{\gamma=R,L}\prod_{l=1}^{Q_x}\prod_{m=1}^{Q_y}\left|2\sin\left(\frac{k_{\gamma,\mathrm{a}}(x)-k_{\gamma,\mathrm{m}}(y)}{2}\right)\right|^{1/4}}. \quad (2.77)$$

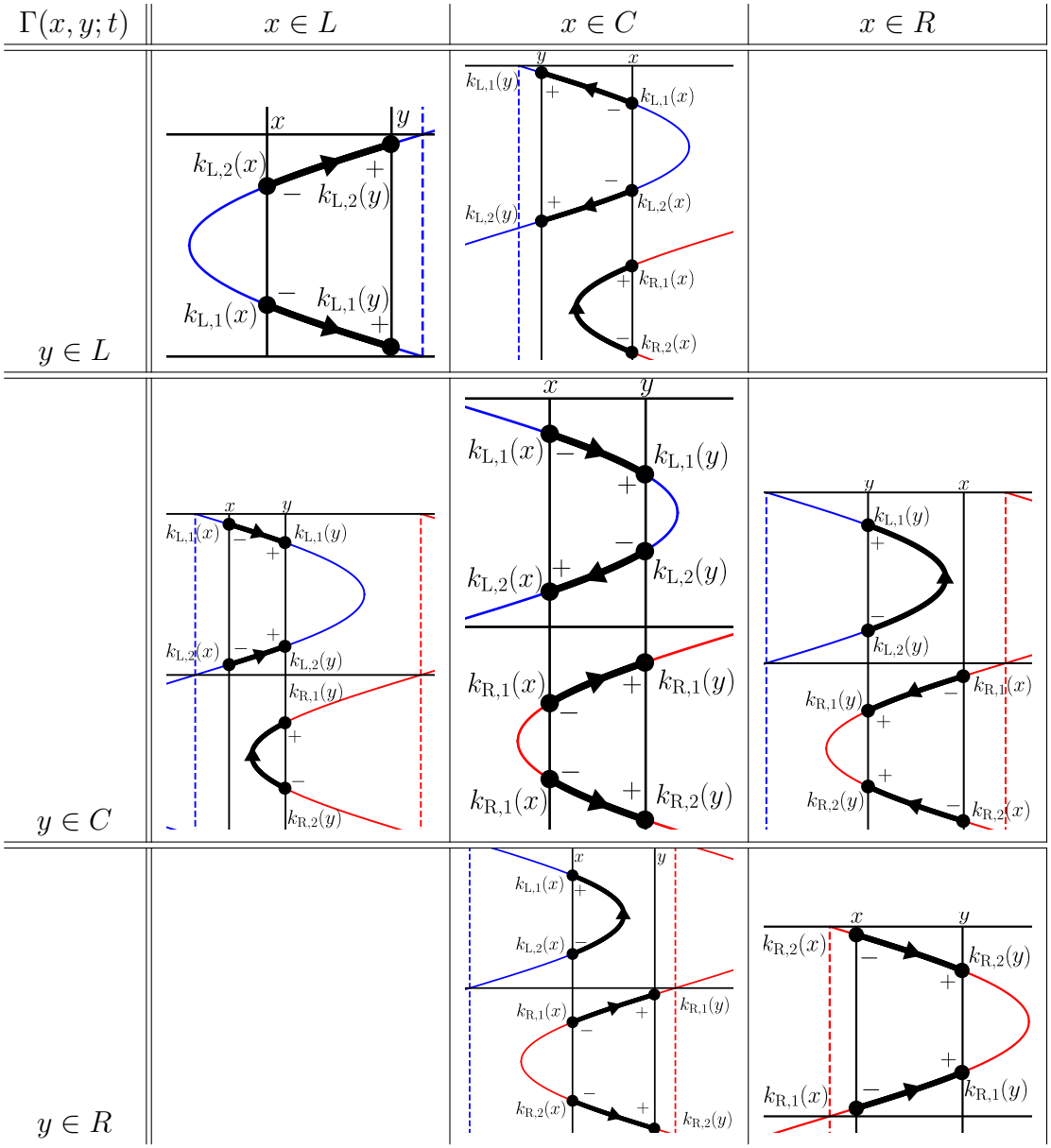


Table 2.1: Conventions for the choice of the oriented contour Γ in the various cases considered. The symbols $+$ and $-$ indicate exponents of $\pm\frac{1}{2}$ in the vertex operators associated with the corresponding points along the contour. The contour itself is shown in black, with arrows indicating its orientation. Reproduced from Ref. [130].

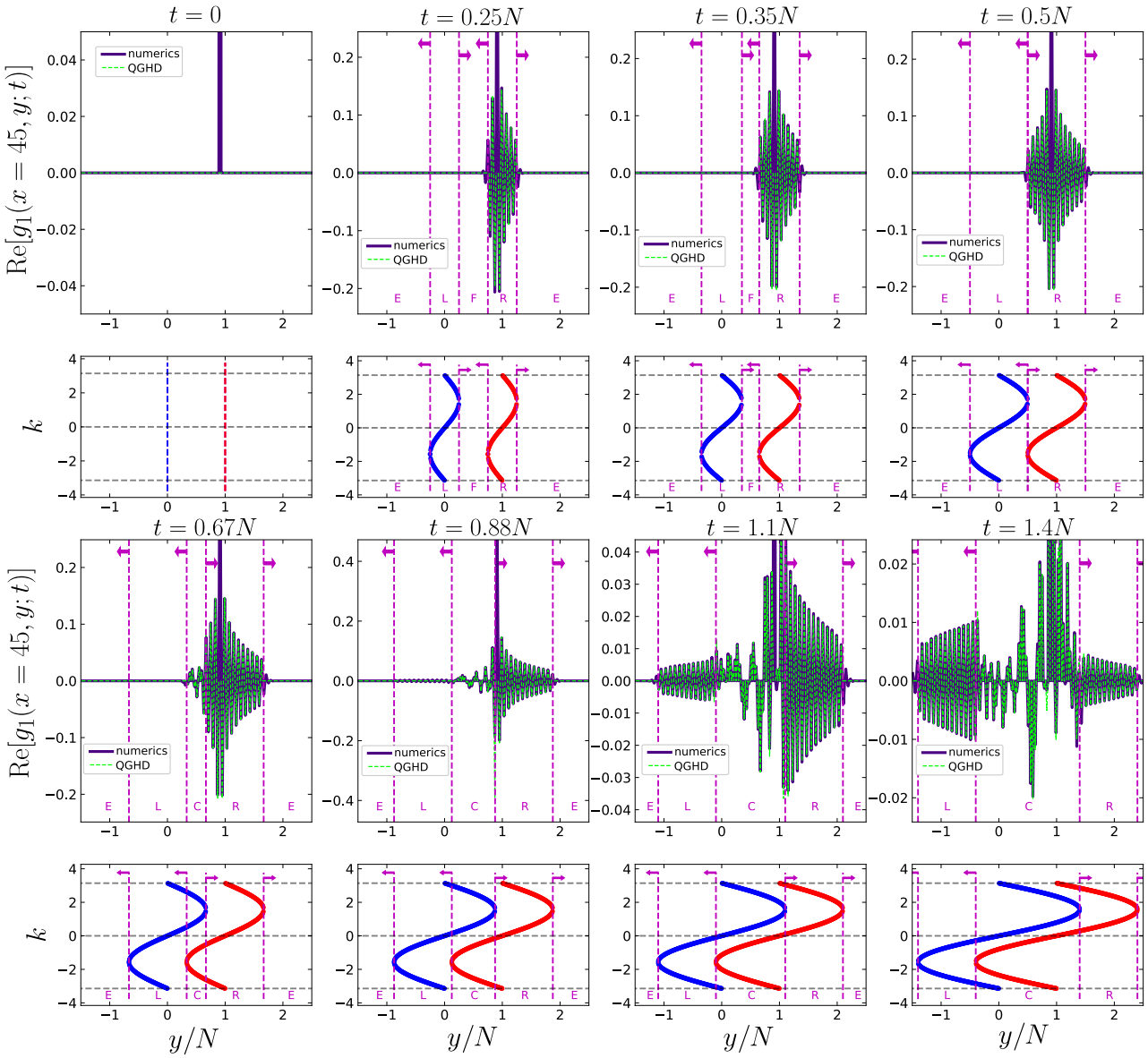


Figure 2.5: Real part of the One Particle Density Matrix ($g_1(x, y; t)$) as a function of the ratio y/N for fixed $x = 45$ and particle number $N = 50$. Each panel shows $\mathrm{Re}[g_1(x = 45, y; t)]$ together with the corresponding Fermi contours Γ (blue: left contour, red: right contour) at different times. These plots illustrate the dynamical emergence of long-range correlations and the formation of regions with split Fermi seas. Dashed purple vertical lines indicate the boundaries between different regions, labeled with purple letters according to the notation introduced in Eqs (2.14) - (2.15) and used throughout the Chapter (e.g., in Eq. (2.69)). Arrows indicate the time evolution of the region boundaries. Grey dashed horizontal lines mark the values $-\pi$, 0, and π. Analytical predictions (solid lines) are in excellent agreement with exact numerical results (dashed lines) at all times. Figure published in [130], reused with permission.

2.1.5 Quasicondensation and Off-Diagonal Long-Range Order

In this Section, we employ our exact expression for the OPDM to investigate the phenomena of quasicondensation and dynamical fermionization, which manifest at different stages of the free expansion of a hard-core boson (HCB) gas.

We begin by illustrating the time evolution of the OPDM (1.24) for a fixed particle number N

and position x, as shown in Fig. 2.5. This figure highlights the formation of spatial correlations as the HCBs expand freely, and reveals how these correlations signal the emergence of off-diagonal long-range order (ODLRO) in the OPDM. Initially, at $t = 0$, no correlations are present, since the initial state is a simple product state.

At early times $t < N/2$, nonzero correlations are confined to the 'right front' region (R) — as defined in the classification of regions given in Eq. (2.14) — which corresponds to the propagation of the front around $x = N$. Within this region, whose size grows linearly with time until $t \sim N/2$, the qualitative structure of the OPDM remains essentially unchanged. At $t = N/2$, particles emanating from the left front (located at $x = 0$) start to overlap with those from the right front, leading to the emergence of a central region (C) with qualitatively distinct, nonvanishing correlations. This region is marked by the formation of a split Fermi sea, which arises from the overlap of the light cones associated with the two distinct Fermi contours.

Notably, when particles from both domain walls begin to overlap near x, correlations also start to develop with the (L) regions, defined by $|y|/t < 1$, where particles from the right front have yet to arrive. This signals the inherently entangled character of the HCB wavefunction. The OPDM (2.15) maintains a power-law decay $g_1 \propto |x - y|^{-1/2}$ over nearly the entire evolution (whenever g_1 is nonzero), consistent with earlier numerical observations in Ref. [55].

At later times $t \gg N$, the central region (C) dominates the bulk of the system. In this regime, with $x, y \in$ C, the system effectively behaves as a homogeneous gas of length $\ell = 2t - N$, comprising two entangled particle species—each originating from one of the initial junctions. The long-range correlations now decay more rapidly, as $g_1 \sim |x - y|^{-1}$, and the bipartite entanglement entropy saturates to $S \sim \frac{1}{3}\log(N/2)$ for $t \gg N$ [67, 68].

As we discuss in detail below, the difference in the decay exponent of spatial correlations reflects two distinct physical regimes: the quasicondensate regime ($g_1 \propto |x - y|^{-1/2}$) and the dynamically fermionized regime ($g_1 \propto |x - y|^{-1}$). Our exact expression (2.15) captures both limiting behaviors as well as the crossover between them.

Figure 2.5 provides a qualitative overview of the buildup of off-diagonal long-range order. A more thorough and quantitative analysis of quasicondensation is presented in the following two subsections.

The Momentum Distribution from the OPDM

We begin by examining the time evolution of the momentum distribution

$$n(p;t) = \sum_x \sum_y ; e^{ip(x-y)} g_1(x,y;t), \tag{2.78}$$

which can be efficiently computed numerically using a fast Fourier transform of the OPDM data. The momentum distribution is normalized such that

$$\sum_p n(p;t) = 2\pi N, \quad \text{with} \quad |p| \leq \pi. \tag{2.79}$$

It is important to recall that our analytical expression for the equal-time OPDM is derived within a low-energy field-theoretic framework, and is therefore accurate only at large separations, specifically when $|x - y| \gg \max(n^{-1}(x), n^{-1}(y))$. As a result, it does not correctly capture the short-distance behavior of $g_1(x,y;t)$. To address this, a UV regularization is required before performing the Fourier transform of Eq. (2.15) to extract $n(p;t)$.

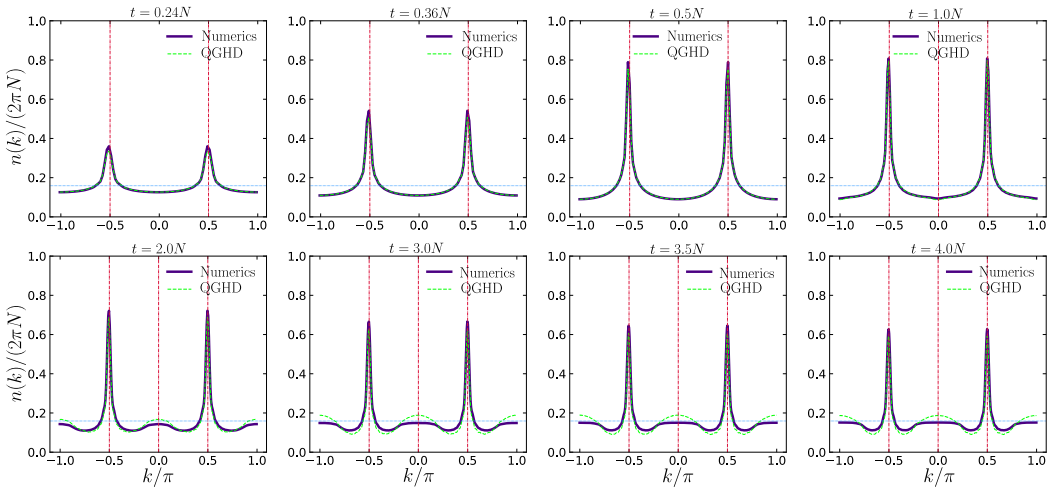


Figure 2.6: Momentum distribution function for the same setup as in Fig. 2.5. The two peaks located at $p = \pm\pi/2$ correspond to the fastest excitations and serve as a signature of quasicondensation in the HCB system. The horizontal dotted line indicates the asymptotic value of the momentum distribution in the long-time limit of free expansion, $n(p) = N$, consistent with the phenomenon of dynamical fermionization. The data, obtained by Fourier transforming the ultraviolet-regularized analytical expression for the OPDM (solid lines), show excellent agreement with exact numerical results (dashed lines) at all times. Reproduced from [130].

For times $t/N \lesssim 1$, we find that a simple and effective regularization consists of replacing the diagonal values of the OPDM with the local particle density: $g_1(x, x; t) = n(x; t)$. The corresponding time evolution of the momentum distribution is shown in Fig.2.6, for the same time slices as in Fig.2.5. This basic UV regularization yields excellent agreement with numerical results for $t/N \lesssim 1$.

At later times, $t/N \gg 1$, the agreement starts to deteriorate, and discrepancies become visible. These deviations can, in principle, be reduced by incorporating additional terms in the short-distance expansion of the OPDM, as discussed in Refs. [66, 151]. A more detailed analysis of such improved regularization techniques lies beyond the scope of this work. Nevertheless, for the time scales of interest ($t \lesssim N$), regularizing only the diagonal of $g_1(x, y; t)$ proves sufficient to match the numerics with high accuracy.

Our analytical expression (2.15) for the OPDM provides a quantitative description of the emergence of off-diagonal long-range order. In particular, over a broad time window, the OPDM exhibits a characteristic decay $g_1 \propto |x-y|^{-1/2}$ (modulo subleading corrections), a signature of quasicondensation. This is also reflected in the formation of pronounced peaks in the momentum distribution at $p = \pm\pi/2$.

At later times, when $t/N \gg 1$, the decay of the OPDM transitions to $g_1 \propto |x - y|^{-1}$, as indicated by Eq.(2.15). In this regime, the momentum distribution flattens out, approaching the value $n(p) \to N$, in accordance with the phenomenon of dynamical fermionization. Although this trend is challenging to clearly demonstrate numerically—due to both finite-size effects and the need for more refined UV treatments—the second row of Fig.2.6 already shows clear signatures of this crossover behavior at large times.

Eigenvalues of $g_1(x, y : t)$ and the evolution of the ODLRO

Having established the emergence of off-diagonal long-range order in the equal-time one-particle density matrix (OPDM), we now turn our attention to its relation with quasicondensation. This connection can be analyzed by studying the spectral properties of the OPDM, specifically its eigenvalues $\Lambda_i(t)$ and eigenvectors $\xi_i(y)$, which satisfy the equation

$$\sum_x g_1(x, y; t)\, \xi_i(y) = \Lambda_i\, \xi_i(y). \tag{2.80}$$

The functions ξ_i are known as natural orbitals, and the corresponding eigenvalues describe their occupations. Of particular interest is the largest eigenvalue, λ_0, whose scaling with the total number of particles N,

$$\Lambda_0 \sim N^{\mathcal{C}}, \tag{2.81}$$

defines an exponent $\mathcal{C}$ that characterizes the extent to which a single natural orbital is macroscopically occupied.

According to the criterion introduced by Penrose and Onsager [50], the condition $\mathcal{C} = 1$—that is, Λ_0 scaling linearly with N—is indicative of true Bose–Einstein condensation. In this case, a finite fraction of the total particle number resides in a single orbital. However, in one-dimensional systems where charge conservation is enforced, the Mermin–Wagner theorem forbids spontaneous symmetry breaking at finite temperature, implying that $\mathcal{C}$ must remain strictly less than one.

Despite this restriction, when the exponent $\mathcal{C}$ approaches one, the system is often described as being in a quasicondensate regime. This terminology has been extended in the literature to include cases where $\mathcal{C} \gtrsim 1/2$, indicating a form of partial coherence without true condensation [51–55].

In contrast, for non-interacting fermions, the Pauli exclusion principle prevents multiple occupation of any single orbital, resulting in an OPDM spectrum where the largest eigenvalue does not scale with system size ($\mathcal{C} = 0$), thereby excluding the possibility of quasicondensation.

The analytical expression we derive for the OPDM given in Eq. (2.15) indicates that off-diagonal long-range order of the form $g_1(x, y; t) \propto |x - y|^{-1/2}$ is present throughout nearly the entire time evolution. This observation motivates the introduction of a scaling ansatz for the normalized natural orbital associated with the largest eigenvalue (see also Ref. [55] for a numerical verification):

$$\xi_0(x) \sim N^{-1/2}\, \Xi_0(x/N). \tag{2.82}$$

Assuming a large particle number $N \gg 1$, one can approximate the sums over ξ_0 by integrals and estimate the dominant eigenvalue to be

$$\begin{aligned} \Lambda_0 &= \int dx \int dy\, \xi_0^*(x)\, g_1(x, y; t)\, \xi_0(y) \propto \int dx \int dy \frac{\xi_0^*(x)\xi_0(y)}{|x - y|^{1/2}} \\ &\propto \sqrt{N} \int dX \int dY \frac{\Xi_0^*(X)\Xi_0(Y)}{|X - Y|^{1/2}} \propto \sqrt{N}, \end{aligned} \tag{2.83}$$

which implies a scaling exponent $\mathcal{C} = 1/2$, consistent with earlier results in Refs. [51–55].

For large times $t/N \gg 1$ however, the exponent $\mathcal{C}$ is expected to approach zero, consistent with the phenomenon of dynamical fermionization. While reaching this asymptotic regime is computationally challenging—due to the fact that the size L of the equal-time OPDM to be diagonalized grows linearly with time—Fig. 2.7 presents results for the largest eigenvalue λ_0 as a function of N over a broad range of times, including asymptotically large values.

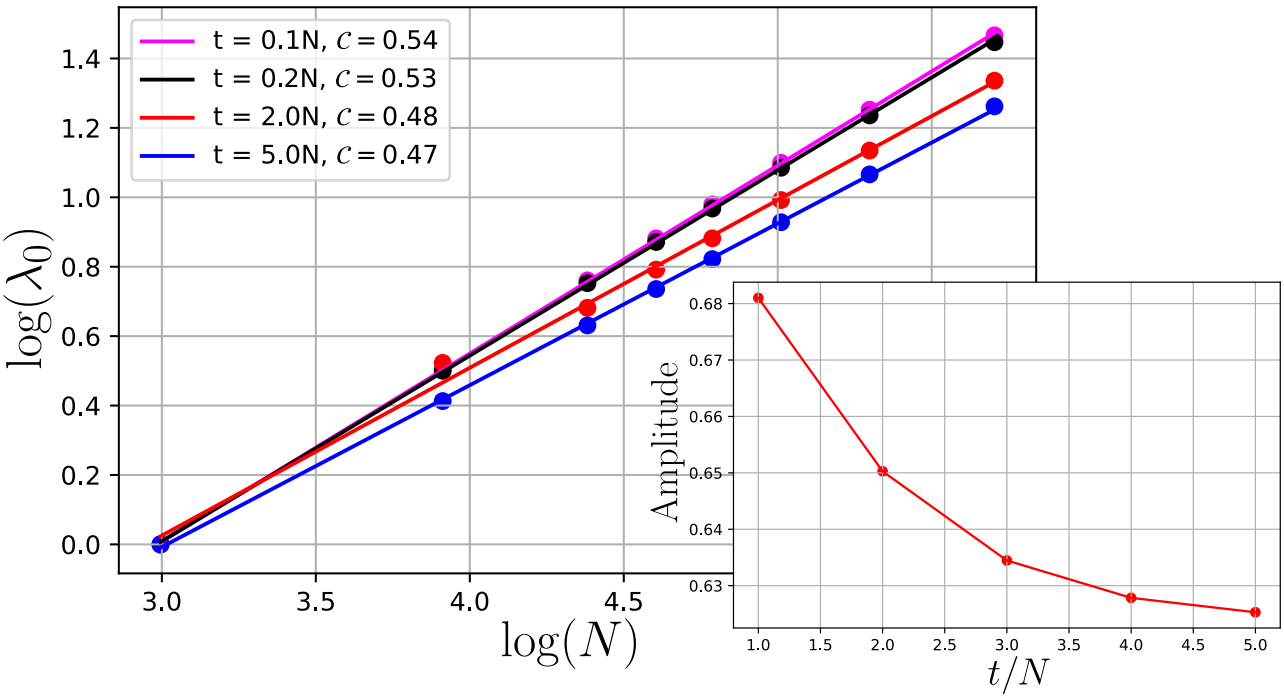


Figure 2.7: Log-log plot of the largest eigenvalue Λ_0 of the equal-time OPDM as a function of system size N, shown for various rescaled times t/N. The solid lines represent the best-fit linear functions $\log(\Lambda_0) = \mathcal{C}\log(N)$, where the exponent $\mathcal{C}$ is extracted from the slope of the data. For visual clarity, the vertical offset of the fitted lines has been set to zero. Inset: Evolution of the fitted prefactor (amplitude) as a function of time, illustrating its decay with increasing t. Figure originally published Ref. [130], reused with permission.

The data clearly indicate that the scaling exponent $\mathcal{C}$ remains close to $1/2$ even in the regime $t/N \gg 1$, where the momentum distribution already exhibits characteristics of dynamical fermionization (see Fig. 2.6). This apparent discrepancy can be resolved by observing that, although the exponent remains approximately $1/2$, the prefactor of the associated power-law scaling diminishes gradually with increasing time. This behavior is illustrated in the inset of Fig. 2.7, where a decay in the amplitude is visible.

The process of dynamical fermionization can be further understood by analyzing the full spectrum of the equal-time OPDM $g_1(x, y; t)$ and its eigenstates. For each natural orbital ξ_i, we define the quantity

$$w_i = \int_{x\in \mathrm{C}} dx\ |\xi_i(x)|^2, \tag{2.84}$$

which measures the spatial localization of the eigenstate within the central region (C). A value of w_i close to unity indicates that the orbital is predominantly localized in the central region, whereas values near zero signal localization in the region L/R. Figure 2.8 illustrates w_i for two representative times.

The plot shows that the eigenstates associated with the largest eigenvalues exhibit $w_i \simeq 0$, indicating that their support lies outside the central region. These eigenstates, localized in the outer regions (L/R), have eigenvalues scaling as $\Lambda_i \sim N^{1/2}$ and are responsible for the characteristic peaks at $p = \pm\pi/2$ in the momentum distribution (cf. Fig. 2.6). In contrast, the lower part of the OPDM spectrum is populated by a large number of eigenstates with $w_i \approx 1$, signifying localization in the bulk of the system with eigenvalues scaling as N^0. These eigenstates govern the emergent fermionic character of the system at long times. As time progresses, the outer regions supporting

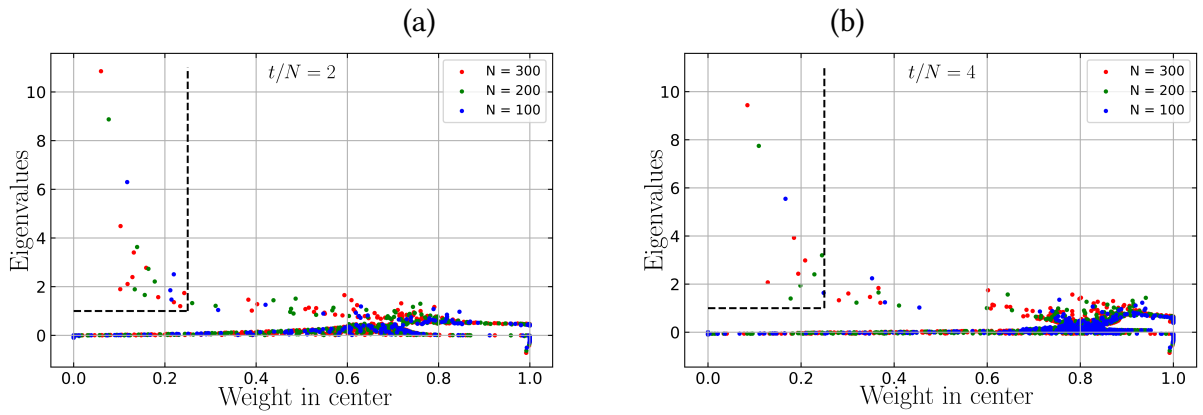


Figure 2.8: Eigenvalues of the OPDM plotted as a function of their corresponding weight within region (C) (see Eq. (2.84)) for various system sizes N at fixed values of t/N: (a) $t/N = 2$, (b) $t/N = 4$. In the thermodynamic limit, each eigenvalue exhibits a twofold degeneracy due to the exact left-right symmetry of the setup, such that each point shown represents a pair of degenerate eigenvalues. At finite system sizes left- and right-localized natural orbitals hybridize; see Ref. [55]. Dashed rectangles indicate the subset of eigenvalues satisfying $w_i \leq 0.25$, as discussed in Fig. 2.9. Figure originally published in Ref. [130], reused with permission.

the largest eigenstates move outward, effectively becoming spatially separated from the expanding central region. Simultaneously, the number of bulk-supported eigenstates increases, eventually dominating the OPDM spectrum and driving the onset of dynamical fermionization, as shown in Fig. 2.9. Notably, since the size of the L/R lobes does not scale with time while the central region expands linearly with t, and since the local particle density behaves as $n(x) \sim 1/t$ for $t/N \gg 1$ (see Ref. [68] and Eq. (2.24)), the total occupation of the outermost eigenstates decays as $1/t$, although they formally vanish only in the infinite-time limit.

Therefore, at large but finite times, the persistence of these outer eigenstates explains the effective exponent $\mathcal{C} \approx 1/2$ observed in Fig. 2.7, despite the system trending toward fermionization.

In summary, our analysis reveals the coexistence of two distinct sets of natural orbitals: one with eigenvalues scaling as $N^{1/2}$ and another as N^0. While the former dominates at earlier times, the latter gradually takes over with increasing t/N, ultimately signaling the dynamical emergence of fermionic behavior in the system.

2.1.6 Discussion

In this Section, we reported the research and results we have conducted in the context of non-equilibrium dynamics of the one-particle density matrix (OPDM) for one-dimensional hard-core bosons (HCBs) released from an initially confined domain-wall state, as illustrated in Fig. 2.1(a). Applying recent advances in quantum generalized hydrodynamics, we derived an exact analytic expression for the OPDM in the Euler scaling limit, characterized by large spatial and time scales ($x, N, t \to \infty$) at fixed ratios x/t and N/t.

This exact result provides a clear analytical description of two features of the system's evolution: dynamic quasicondensation at intermediate times and emergent fermionization at long times. Moreover, our formula also captures the crossover between these regimes. We validated the analytic predictions through a systematic comparison with exact numerical simulations across various system sizes and time scales (see, e.g., Figs. 2.2 and 2.3), finding excellent agreement throughout.

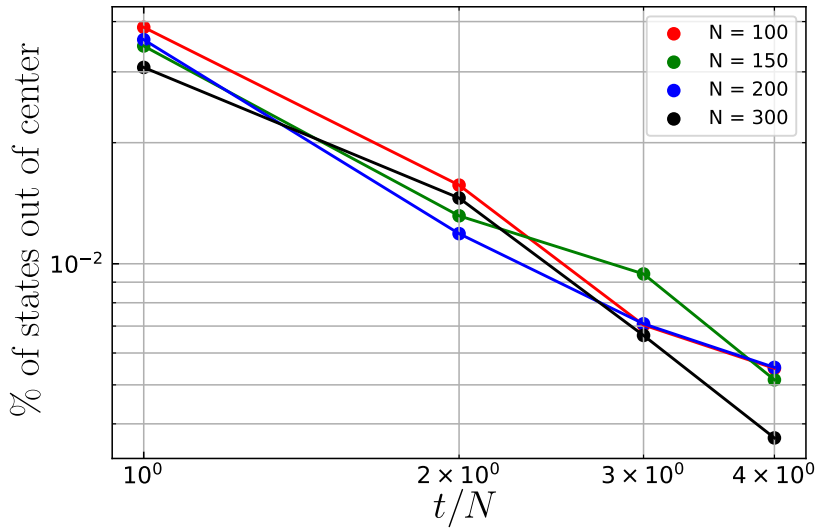


Figure 2.9: The percentage of eigenstates whose spatial weight lies predominantly outside the central region, specifically those satisfying $w_i \leq 0.25$, plotted as a function of t/N for various system sizes. The observed trend indicates a clear temporal decay of this fraction, consistent with the progressive delocalization of natural orbitals into the expanding bulk region. The eigenstates falling within this threshold are highlighted by the dashed box in Fig. 2.8. Figure originally published in Ref. [130], reused with permission.

It is worth emphasizing that Eq. (2.15) represents one of the very few known exact expressions for the equal-time OPDM of trapped hard-core bosons that is both explicit and written in terms of elementary functions. Other notable examples include dynamics in harmonic traps. [53, 114, 124, 152, 153]. While the simplicity of our final expression relies on the integrability of the model and the choice of initial state, its derivation remains technically nontrivial. The compactness and clarity of the final result, presented in Sec. 2.1.2, underscore the power of the approach.

These results and methods open a path toward the computation of the OPDM in more general out-of-equilibrium settings involving one-dimensional HCBs. As a natural extension, we are also working on obtaining correlation functions like the OPDM in systems with finite interaction strength, as we will mention later in Section 4.1. Such a generalization poses significant challenges, particularly due to the breakdown of conformal symmetry. Preliminary steps in this direction have already been undertaken for other observables in Refs. [3, 73, 122],and we expect that similar techniques can be adapted to tackle the OPDM in these more complex scenarios.

2.2 Double-Defect Interferometer for Hard-Core Bosons

Introducing a single impurity into an otherwise translationally invariant many body system can change the global behavior of the system, as it was shown by classic examples such as the Anderson orthogonality catastrophe [154] or the Kane-Fisher model [155, 156]. In the last decade, significant advancement were made in studying 1D free-fermionic systems in the presence of an impurity in the context of entanglement, e.g. [157–171]. Such works enabled the formation of a rather complete picture of free-fermions in systems with impurities in equilibrium. The out-of-equilibrium description of such systems however isn't as clear by far, due to the many different protocols and ways to drive the system out of equilibrium (see for example the works [172–182]). Recently, in the work [141] a system of free fermions was let evolve from a domain wall initial state, with the domain wall being located on a defect. The significance of this particular initial condition is its connection to several works [125, 128, 183, 184] in which such initial states were studied in the context of transport in the framework of GHD (see Section 1.3 for a brief overview).

While in the previous Section we focused on deriving analytical formulas for the equal time OPDM of hard-core bosons in the Euler limit by 'requantizing' the GHD solution following the methodology of QGHD developed in e.g.[3, 4, 73], in this Section instead we investigate the dynamics of hard-core bosons released from a domain wall initial state in the presence of two conformal defects. The observed density profile differs from the Euler-scale hydrodynamic description due to additional terms resulting from quantum interference. By analyzing boson propagators, we show that repeated scattering on the defects leads to interference patterns that cannot be captured by the hydrodynamic approach. We derive an analytic expression for the density profile during free expansion and demonstrate that a modified semi-classical scattering framework is required for the description of systems with such defects. We organize this Section as follows. Recalling the Bose-Fermi mapping between HCBs and free non-interacting fermions we detailed in the previous Section we review the results of [129] where the free expansion of a system of HCBs from a domain wall setup was investigated in the presence of a conformal defect. Using these results we derive the fermionic propagators, and we show how the dynamics have a classical interpretation that fits into the framework of the hydrodynamic picture in the Euler limit. Then we turn to the discussion of our system; we present the system with two conformal defects and the quench protocol. Next we present our results for the propagator in this setup, we show that a modified semi-classical picture can be reintroduced. Finally we show that our results for the propagators reproduce the density profile of the bosons by comparing our results to exact numerical evaluations.

2.2.1 Hard Core Bosons on a Line With a Conformal Defect

Dynamics of free fermions on a lattice with a conformal defect after a global quench were studied in relation to conformal field theory and generalized hydrodynamics in previous works [129, 169, 179], where an emerging quasi-particle picture allows the calculation of the dynamics of the bipartite entanglement. In this Section of the paper we aim to show how such a quasi particle picture emerges through the propagator of the fermions (which is a quasi particle of our model obtained through a Jordan-Wigner transform from the hard-core bosons, as discussed briefly in Eq. (2.4)). We confirm our results with comparing density profiles to the results of hydrodynamics presented in the previous works. This sets the picture for the phenomena of interference -presented in Section 2.2.2- that we observe in the presence of two conformal defects in the system.

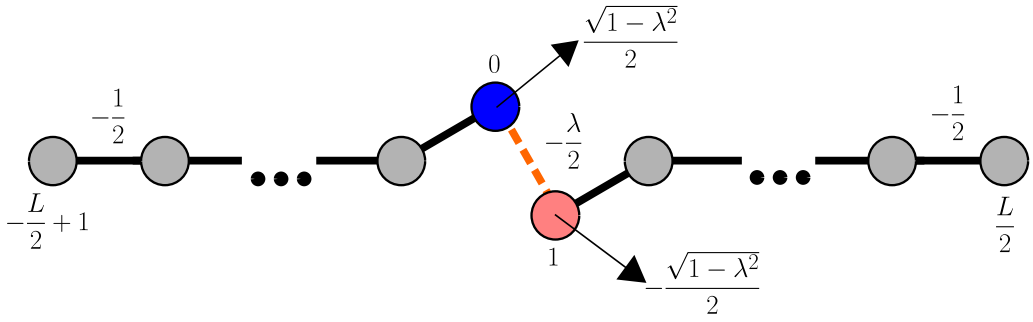


Figure 2.10: Sketch of the nearest-neighbor hopping Hamiltonian $\hat{H}_\lambda$ of Ref. [129], given by Eqs.(2.86), parameterised by the 'strength' of the impurity $\lambda \in [0,1]$. The defect is denoted with staggered sites colored blue and red to indicate the staggered nature of the on-site potential. The hopping connecting sites $0,1$ is drawn with staggered red line.

The model

We start our discussion by reviewing the case of the bosonic system with a single conformal defect. As shown in the previous Section, the Hamiltonian of hard-core bosons on a lattice can be represented by the Bose-Hubbard model (2.1), with interaction strength $U \to \infty$, resulting in the Hamiltonian (2.2), with bosonic creation/annihilation operators $\hat{b}_x^\dagger / \hat{b}_x$ that anti-commute on the same site and commute on different sites, thus representing hard-ore bosons and allowing only occupation numbers $0,1$ on a single site. Using the Jordan-Wigner transformation (2.4) the bosonic operators can be related to $\hat{c}_x^\dagger / \hat{c}_x$ fermionic creation/annihilation operators and one obtains the Hamiltonian

$$\hat{H} = \sum_{x,y\in\mathbb{Z}} h_{x,y}\hat{c}_x^\dagger \hat{c}_y \qquad h_{x,y} = -\frac{1}{2}(\delta_{x,y-1} + \delta_{x,y+1}), \tag{2.85}$$

resulting in the free fermionic Hamiltonian Eq.(2.5). I this Section we seek to investigate the dynamics and properites of a system that is modified by a defect of the form

$$h_{0,1} = h_{1,0} = -\frac{\lambda}{2} \quad h_{0,0} = -h_{1,1} = \frac{1}{2}\sqrt{1-\lambda^2}, \tag{2.86}$$

with parameter $\lambda^2 \in [0,1]$. This introduces a single weak hopping link between sites $x=0$ and $x=1$, as well as a staggered on-site potential as shown in Fig 2.10. Moreover, we also introduce a finite system size L (chosen to be even) and periodic boundary conditions (PBC) with the intent to take the thermodynamic limit later in the calculation to recover the infinite system. Thus, the Hamiltonian of the finite system can be written as

$$\hat{H}_\lambda = \sum_{i,j=-\frac{L}{2}+1}^{\frac{L}{2}} h_{i,j}\hat{c}_i^\dagger \hat{c}_j, \tag{2.87}$$

with unchanged hopping terms. The defect is located at positions $x=0,1$ given by Eq. (2.86). We also introduced the notation $\hat{H}_\lambda$ to denote a Hamiltonian with one defect of parameter λ. In order to understand the conformal nature of the defect we start by obtaining the eigenspectrum of $\hat{H}_\lambda$ defined as

$$\hat{H}_\lambda \Phi_n(x) = \varepsilon_n \Phi_n(x). \tag{2.88}$$

We start by writing the following ansatz for a one particle eigenstate $\Phi_k(x)$ of Hamiltonian $\hat{H}_\lambda$:

$$\Phi_k(x) = \begin{cases} Ae^{ikx} + Be^{-ikx}, & \text{if} \quad x \in [-\frac{L}{2}+1, 0] \\ Ce^{ikx} + De^{-ikx}, & \text{if} \quad x \in [1, \frac{L}{2}]. \end{cases} \tag{2.89}$$

The amplitudes A, B are related to amplitudes C, D through

$$\begin{pmatrix} A \\ B \end{pmatrix} = \mathbf{M}_\lambda \begin{pmatrix} C \\ D \end{pmatrix}, \tag{2.90}$$

with

$$\mathbf{M}_\lambda = \frac{1}{\lambda} \begin{pmatrix} 1 & -\sqrt{1-\lambda^2}e^{-ik} \\ -\sqrt{1-\lambda^2}e^{ik} & 1 \end{pmatrix}, \tag{2.91}$$

satisfying the conditions at the points of the defect ($x = 0, 1$). By applying periodic boundary conditions we also imply a second condition on the eigenstates

$$\Phi_n(x) = \Phi_n(x + L). \tag{2.92}$$

This condition gives a another relation between the amplitudes

$$\begin{pmatrix} C \\ D \end{pmatrix} = \mathbf{M}_L \begin{pmatrix} A \\ B \end{pmatrix}, \tag{2.93}$$

with

$$\mathbf{M}_L = \begin{pmatrix} e^{-ikL} & 0 \\ 0 & e^{ikL} \end{pmatrix}. \tag{2.94}$$

Combining the two conditions (2.90) and (2.93) we get a system of equation for amplitudes A and B in the form

$$\begin{pmatrix} A \\ B \end{pmatrix} = \mathbf{M}_\lambda \mathbf{M}_L \begin{pmatrix} A \\ B \end{pmatrix}. \tag{2.95}$$

This system of equations have a non-trivial solution only and only if the matrix $\mathbf{M}_\lambda \mathbf{M}_L$ has an eigenvector with eigenvalue one, meaning that

$$\mathbf{Det}\left[\mathbf{1} - \mathbf{M}_\lambda \mathbf{M}_L\right] = 0. \tag{2.96}$$

This results in a condition for the quasi-momenta k

$$\lambda = \cos(kL) \tag{2.97}$$

giving the quantization condition

$$k = \frac{\arccos\lambda}{L} + \frac{2\pi n}{L}, \qquad \text{for } n = 1, ..., L, \tag{2.98}$$

that can be rewritten in the form

$$e^{ikL} = \lambda + i\sqrt{1-\lambda^2}. \tag{2.99}$$

The eigenstates of the Hamiltonian $\hat{H}_\lambda$ with periodic boundary conditions are

$$\Phi_k(x) = \frac{1}{\sqrt{2L}} \begin{cases} e^{ikx} - ie^{ik(L+1)}e^{-ikx}, & \text{for} \quad x \in [1, \frac{L}{2}] \\ e^{ikL}e^{ikx} - ie^{-ik(x-1)}, & \text{for} \quad x \in [-\frac{L}{2}+1, 0] \end{cases} \tag{2.100}$$

where we replaced the numbering of eigenstates n with the quasimomenta k, related to n through the quantization condition (2.98) with the dispersion relation (unchanged compared to the clean system, with no defect)

$$\varepsilon^\lambda(k) = -\cos(k). \tag{2.101}$$

The propagator

In this system of size L, with sites $x \in \left[-\frac{L}{2}+1, \frac{L}{2}\right]$, the fermion propagator with annihilation (creation) operator $\hat{c}_x$ ($\hat{c}_x^\dagger$) is defined as

$$\hat{c}_x(t) = \sum_{y=-\frac{L}{2}+1}^{\frac{L}{2}} K_t(x,y)\hat{c}_y(0), \tag{2.102}$$

such that $\hat{c}_x(t)$ satisfies the equation

$$\frac{\mathrm{d}}{\mathrm{d}t}\hat{c}_x(t) = i\left[\hat{H}_\lambda, \hat{c}_x(t)\right]. \tag{2.103}$$

The propagator $K_t(x,y)$ can be written in terms of the eigenstates $\Phi_k(x)$ as

$$K(x,y) = \sum_k e^{it\varepsilon(k)}\Phi_k(x)\Phi_k^*(y). \tag{2.104}$$

Starting with the case $x, y \geq 1$ and substituting the eigenbasis into Eq. (2.104), we are left with the formula for the propagator

$$\begin{aligned} K(x,y) = \frac{1}{2L}\sum_k e^{-i[k(y-x)-t\varepsilon(k)]} + e^{-i[k(x-y)-t\varepsilon(k)]} + \\ \frac{1}{2L}\sum_k ie^{-i[k(L+1-x-y)-t\varepsilon(k)]} - ie^{-i[k(x+y-L-1)-t\varepsilon(k)]}. \end{aligned} \tag{2.105}$$

We evaluate this formula straightforwardly by taking the thermodynamic limit $L \to \infty$, which replaces the summation over k in Eq. (2.105) by an integral

$$\sum_k \to \int_{-\pi}^{\pi} \frac{L}{2\pi}\mathrm{d}k. \tag{2.106}$$

The dependence on the system size L in the eigenstates (2.100) in the exponents can be eliminated using the quantization condition in Eq. (2.99). After some further manipulation of the formulae, the propagator of the system in the thermodynamic limit is obtained. The calculation for the other three cases of x, y are done in the same manner. We present the result in the table:

$K_t(x,y)$	$y \leq 0$	$y \geq 1$
$x \leq 0$	$K_1(x,y,t)$	$K_2(x,y,t)$
$x \geq 1$	$K_2(x,y,t)$	$K_1(x,y,t)$

(2.107)

where

$$\begin{aligned} K_1(x,y,t) &= (-i)^{x-y}J_{x-y}(t) + \sqrt{1-\lambda^2}(-i)^{x+y-1}J_{x+y-1}(t) \quad \text{and} \\ K_2(x,y,t) &= \lambda(-i)^{x-y}J_{x-y}(t) \end{aligned} \tag{2.108}$$

with

$$J_n(t) = \frac{1}{2\pi}\int_{-\pi}^{\pi} e^{i(n(-\pi/2+k)+t\cos(k))}\mathrm{d}k \tag{2.109}$$

being nth Bessel function of the first kind.

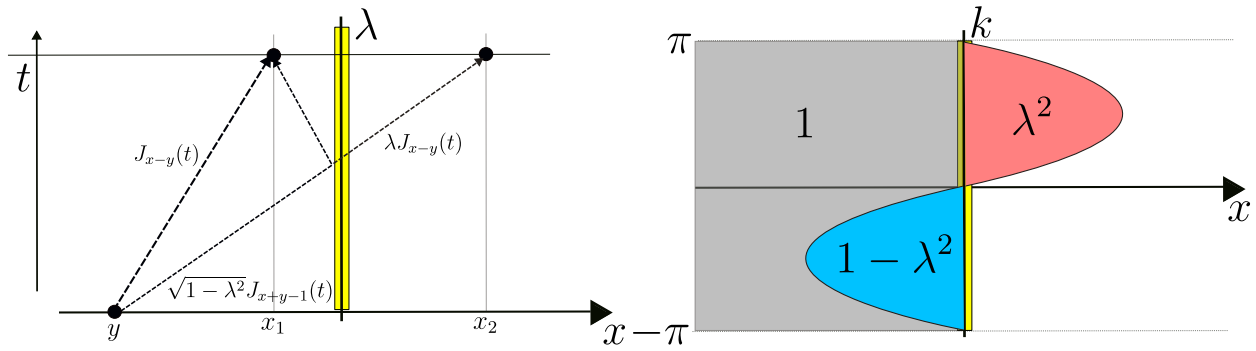


Figure 2.11: **Left**: Schematic drawing of a particle propagating from y to x_τ ($-x_\tau$) at time τ interpreted in the quasi particle picture. A particle initially at position $y < 0$ with quasimomentum k and velocity $v(k) = \sin(k)$ arriving at the defect at $x = 0$ gets reflected (transmitted) with an amplitude given by $R(\lambda)$ ($T(\lambda)$). **Right**: the emerging hydrodynamic picture. Taking a setup of a domain wall as an example discussed at Eq. (2.111) and evolving it according to the Schrödinger equation results in the quasi phase space picture analogous to the hydrodynamic description.

The semi-classical picture and the defect

The particular form of the fermion propagator presented in Eq. (2.107) allows a straightforward quasi-particle picture interpretation, that is -in the Euler limit- compatible with the aforementioned hydrodynamic description of free-fermion dynamics. A particle with quasi-momentum k initially at position y moves ballistically with velocity

$$v(k) = \frac{\mathrm{d}}{\mathrm{d}k}\varepsilon'(k) = \sin(k) \tag{2.110}$$

given by the dispersion relation of the system in Eq. (2.101), until it reaches the defect at position $x = 0$. At the defect it scatters and gets transmitted (reflected) with probability $T(\lambda) = \lambda^2$ ($R(\lambda) = 1 - \lambda^2$) after which it continues moving with $\pm v(k)$. This description is equivalent to the free fermion hydrodynamic picture discussed in Section 2.1.3 with a slight modification to account for the scattering on the defect.

Taking the system with the Hamiltonian $\hat{H}_\lambda$ prepared in the domain wall initial state [129] given by the product state

$$|\mathrm{DW}\rangle = \bigotimes_{x\leq 0} |1\rangle \bigotimes_{1\leq x} |0\rangle\,, \tag{2.111}$$

where $|0\rangle$ and $|1\rangle$ are the eigenstates of the fermionic number operator $\hat{\rho}(x) = \hat{c}_x^\dagger \hat{c}_x$ with eigenvalues $0, 1$. Then, the initial occupation function is given by

$$\nu_0(x,k) = \begin{cases} 1 & \text{if} \quad x \leq 0, \\ 0 & \text{otherwise.} \end{cases} \tag{2.112}$$

thus the domain wall is located on the defect, with the system on the left ($x \leq 0$) being filled and the right being empty. Accounting for the scattering on the defect the solution to the hydrodynamic equation is

$$\nu(x,k,t) = \begin{cases} 1 & \text{if} \quad x \leq \min[\sin(k)t, 0] \\ 1-\lambda^2 & \text{if} \quad \min[\sin(k)t, 0] < x \leq 0 \\ \lambda^2 & \text{if} \quad 0 < x \leq \max[\sin(k)t, 0] \\ 0 & \text{otherwise,} \end{cases} \tag{2.113}$$

as shown on Fig. 2.11. The particle density can now be computed following Eq. (2.24), which gives the profile presented in [129]. In the following Section we present the calculation of the density profile, starting from the propagator (2.107).

The density profile after a domain-wall quench

In [129] the density profile of a system of free spinless fermions scattering on a conformal defect of the form (2.86) -described by the Hamiltonian $\hat{H}_\lambda$- was calculated after a global quench. The system starts from an initial condition given in Eq. (2.111), and evolves according to the unitary time evolution

$$|\Psi(t)\rangle = e^{-i\hat{H}_\lambda t}\,|\mathrm{DW}\rangle\,. \tag{2.114}$$

In the Heisenberg picture the expectation value of the fermionic density can be written as

$$\rho_t(x) = \langle \mathrm{DW}|\,\hat{c}_x^\dagger(t)\hat{c}_x(t)\,|\mathrm{DW}\rangle\,, \tag{2.115}$$

where the time dependence of $\hat{c}_x^\dagger(t)/\hat{c}_x(t)$ is governed by Eq. (2.103). Using the definition of the propagator ($K_t(x,y)$) at Eq. (2.104) and the initial state $|\mathrm{DW}\rangle$ in Eq. (2.111) the formula for the fermion density can be expressed in terms of $K_t(x,y)$ as

$$\begin{aligned}\rho(x,t) &= \sum_{y\leq 0} K_t(x,y)K_t^*(x,y)\\ &= \begin{cases}\sum_{y\leq 0} J^2_{x-y}(t) + (1-\lambda^2)J^2_{x+y-1}(t), & \text{for} \quad x\leq 0\\ \sum_{y\leq 0}\lambda^2 J_{x-y}(t), & \text{for} \quad 1\leq x.\end{cases}\end{aligned} \tag{2.116}$$

Taking the hydrodynamic (Euler) limit and writing $\sum_{y\leq 0}\to\int dy$, thus replacing the sites y with a continuous coordinate, the terms in the integral can be evaluated using the saddle point approximation of $J_n(t)$

$$J_n(t) \approx \sqrt{\frac{2}{\pi\sqrt{t^2-n^2}}}\cos\left(\sqrt{t^2-n^2} - n\arccos\frac{n}{t} - \frac{\pi}{4}\right) \tag{2.117}$$

for $t\to\infty$ and $\frac{n}{t}$ fixed, giving the density profile

$$\rho(x,t) = \begin{cases}1 - \frac{\lambda^2}{\pi}\arccos\left(\frac{-x}{t}\right), & \text{for} - t\leq x\\ 1, & \text{otherwise}\end{cases} \tag{2.118}$$

for $x\leq 0$ and

$$\rho(x,t) = \frac{\lambda^2}{\pi}\arccos\left(\frac{x}{t}\right) \tag{2.119}$$

for $1\leq x$, which is in perfect agreement with the results obtained through the hydrodynamic picture, presented in [129].

2.2.2 The Case of Two Conformal Defects

Introducing a second conformal defect at a distance $N << L$ from the first one changes the dynamics in a non-trivial way, due to interference between reflected particles, leading to an emergence of quantum interference visible at the level of the density profile, resulting in significant deviations from the hydrodynamic picture. As we discuss in this Section, a quasi-particle interpretation can be restored by taking into account such interference terms. We conclude this Section by looking at the evolution of the density profile after a quench from the domain wall initial state defined in Eq. (2.111) and compare our findings to free fermion numerics.

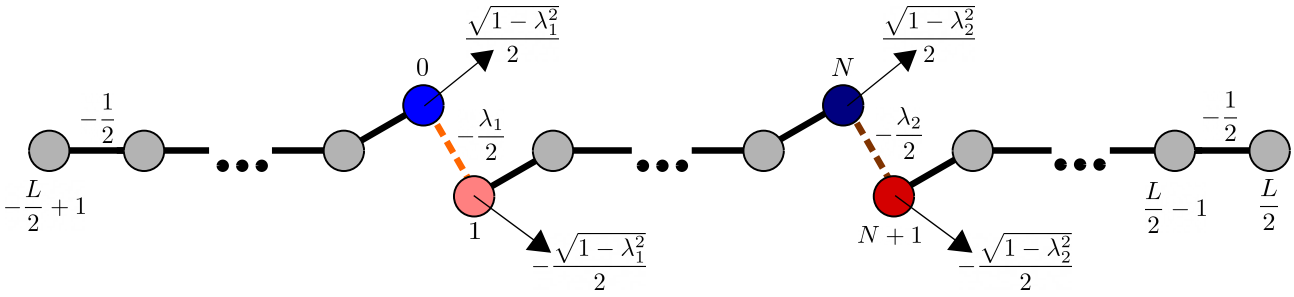


Figure 2.12: Sketch of the nearest-neighbor hopping Hamiltonian $\hat{H}_{\lambda_1,\lambda_2}$ given by Eqs.(2.120), parameterized by the 'strength' of the impurity $\lambda_1, \lambda_2 \in [0,1]$ located at sites $0, 1$ and $N, N+1$ respectively. The defects are denoted with staggered sites colored blue and red to indicate the staggered nature of the on-site potential, and with different shades to indicate that $\lambda_1 \neq \lambda_2$ generally. The hopping connecting sites $0, 1$ and $N, N+1$ are drawn with staggered red lines.

Model with two defects of strength λ_1, λ_2

The Hamiltonian of the system is given by adding a second conformal defect in position $x = N, N+1$ to Eq. (2.87), keeping in mind the periodic boundary conditions. At the defects the hopping terms are given by

$$\begin{aligned} h_{0,1} = h_{1,0} &= -\frac{\lambda_1}{2} \qquad \text{and} \quad h_{N,N+1} = h_{N+1,N} = -\frac{\lambda_2}{2}, \quad \text{with} \\ h_{0,0} = -h_{1,1} &= \frac{1}{2}\sqrt{1-\lambda_1^2} \qquad \text{and} \quad h_{N,N} = -h_{N+1,N+1} = \frac{1}{2}\sqrt{1-\lambda_2^2}, \end{aligned} \tag{2.120}$$

staggered onsite potentials, where parameters $\lambda_1, \lambda_2 \in [0,1]$. We shall refer to the hamiltonian with two conformal defects given in Eq. (2.120) as $\hat{H}_{\lambda_1,\lambda_2}$. In order to obtain the popagator and the density profile, we proceed as in the case of one defect: by solving the eigenvalue problem of the Hamiltonian $\hat{H}^{\lambda_1,\lambda_2}$ first.

Similarly to the case with one defect, we start by writing the eigenstates $\Psi_k(x)$ of $\hat{H}_{\lambda_1,\lambda_2}$ defined as

$$\hat{H}_{\lambda_1,\lambda_2}\Psi_k(x) = \varepsilon(k)\Psi_k(x), \tag{2.121}$$

in the ansatz

$$\Psi_k(x) = \frac{1}{\sqrt{V}} \begin{cases} Ae^{ikx} + Be^{-ik(x-1)} & \text{for } x \in [-L/2+1, 0] \\ Ce^{ikx} + De^{-ik(x-1)} & \text{for } x \in [0, N+1] \\ e^{ikx} + Fe^{-ik(x-1)} & \text{for } x \in [N+1, L/2] \end{cases}. \tag{2.122}$$

The relation between the amplitudes can be derived by writing the conditions $\Psi_k(x)$ has to satisfy at the defects, and the conditions arising from the periodic boundary condition. The resulting system of equations is

$$\begin{pmatrix} 1 \\ F \end{pmatrix} = \begin{bmatrix} e^{-ikL} & 0 \\ 0 & e^{ikL} \end{bmatrix} \begin{pmatrix} A \\ B \end{pmatrix} = M_L \begin{pmatrix} A \\ B \end{pmatrix}, \tag{2.123a}$$

coming from the periodic boundary condition of $\Psi_k(x) = \Psi_k(x+L)$,

$$\begin{pmatrix} A \\ B \end{pmatrix} = \frac{1}{\lambda_1} \begin{bmatrix} 1 & -\sqrt{1-\lambda_1^2} \\ -\sqrt{1-\lambda_1^2} & 1 \end{bmatrix} \begin{pmatrix} C \\ D \end{pmatrix} = M_{\lambda_1} \begin{pmatrix} C \\ D \end{pmatrix} \tag{2.123b}$$

coming from the defect located at $x = 0, 1$ and

$$\begin{pmatrix} C \\ D \end{pmatrix} = \frac{1}{\lambda_2} \begin{bmatrix} 1 & -\sqrt{1-\lambda_2^2}e^{-i2Nk} \\ -\sqrt{1-\lambda_2^2}e^{i2Nk} & 1 \end{bmatrix} \begin{pmatrix} 1 \\ F \end{pmatrix} = M_{\lambda_2} \begin{pmatrix} 1 \\ F \end{pmatrix}, \tag{2.123c}$$

from the defect located at $x = N, N+1$. This system of equations have a solution if, and only if

$$\mathrm{Det}\left[\mathbf{1} - M_L M_{\lambda_1} M_{\lambda_2}\right] = 0, \tag{2.124}$$

which provides us with the quantization condition in the form

$$\lambda_1\lambda_2 = \cos(kL) + \sqrt{1-\lambda_1^2}\sqrt{1-\lambda_2^2}\cos(kL - 2kN), \tag{2.125}$$

which gives the quasimomenta k

$$k_\pm = \frac{-i\log z_\pm}{L} + \frac{2\pi n}{L}, \qquad \text{with} \quad n = 0, 1, ..., L/2-1, \tag{2.126}$$

where we define $z_\pm$ as

$$z_\pm = e^{ik_\pm L} = \frac{\lambda_1\lambda_2 \pm i\sqrt{2-\lambda_1^2-\lambda_2^2+2\sqrt{1-\lambda_1^2}\sqrt{1-\lambda_2^2}\cos(2kN)}}{1+\sqrt{1-\lambda_1^2}\sqrt{1-\lambda_2^2}e^{-2ik_\pm N}}. \tag{2.127}$$

The amplitudes then can be written as

$$\begin{gathered} F_\pm = \frac{\frac{\lambda_2}{\lambda_1}\sqrt{1-\lambda_1^2}z_\pm + \sqrt{1-\lambda_2^2}w_N^\pm}{1-\frac{\lambda_2}{\lambda_1 z_\pm}} \\ D_\pm = \frac{\frac{\lambda_2}{\lambda_1}\sqrt{1-\lambda_1^2}z_\pm + \sqrt{1-\lambda_2^2}w_N^\pm}{\lambda_1 z_\pm - \lambda_2} + \frac{\sqrt{1-\lambda_1^2}z_\pm}{\lambda_1} \\ C_\pm = \lambda_1 z_\pm + \sqrt{1-\lambda_1^2}D_\pm \\ A_\pm = z_\pm \\ B_\pm = \frac{F_\pm}{z_\pm}; \end{gathered} \tag{2.128}$$

with normalization factor

$$V = 2L + 2N(|C_\pm|^2 - 1); \tag{2.129}$$

here we also introduced

$$w_N^\pm = e^{2iNk_\pm} \tag{2.130}$$

for the sake of simplicity. The form of the dispersion relation is unaffected by the defect and is still given by

$$\varepsilon(k_\pm) = -\cos(k_\pm). \tag{2.131}$$

Access to the dispersion relation and the corresponding eigenstates allows the calculation of the propagator analogously to the case with one defect, as we now proceed to do.

The propagator $K_t(x, y)$

We present our findings for the fermion propagator $K_t(x, y)$ in the system with two conformal defects and show an example of it's derivation. We introduce the notation L, C, R referring to the Left ($x, y \in \left[\frac{-L}{2}+1, 0\right]$), Center ($x, y \in [0, N]$) and Right ($x, y \in \left[N+1, \frac{L}{2}\right]$) part of the system respectively. The results for the propagator defined in (2.104) are given in the table:

	$y \in L$	$y \in C$	$y \in R$
$x \in L$	$K_{LL}^{\lambda_1\lambda_2}(x, y, t)$	$[K_{CL}^{\lambda_1\lambda_2}(y, x, -t)]^*$	$[K_{RL}^{\lambda_2\lambda_1}(N+1-x, N+1-y, t)]^*$
$x \in C$	$K_{CL}^{\lambda_1\lambda_2}(x, y, t)$	$K_{CC}^{\lambda_1\lambda_2}(x, y, t)$	$-[K_{CL}^{\lambda_2\lambda_1}(N+1-x, N+1-y, t)]^*$
$x \in R$	$K_{RL}^{\lambda_1\lambda_2}(x, y, t)$	$K_{CL}^{\lambda_2\lambda_1}(N+1-y, N+1-x, -t)$	$[K_{LL}^{\lambda_2\lambda_1}(N+1-x, N+1-y, t)]^*$

(2.132)

Here we defined the functions

$$K_{LL}^{\lambda_1\lambda_2}(x,y,t) = (-i)^{x-y}J_{x-y}(t) - \sqrt{1-\lambda_1^2}(-i)^{x+y-1}J_{x+y-1}(t) + \lambda_1^2\sum_{n=0}^{\infty}(-1)^{n+1}(1-\lambda_1^2)^{\frac{n}{2}}(1-\lambda_2^2)^{\frac{n+1}{2}}(-i)^{x+y-1-2N(n+1)}J_{x+y-1-2N(n+1)}(t), \tag{2.133a}$$

$$K_{CL}^{\lambda_1\lambda_2}(x,y,t) = \lambda_1\sum_{n=0}^{\infty}(-1)^{n}(1-\lambda_1^2)^{\frac{n}{2}}(1-\lambda_2^2)^{\frac{n}{2}}(-i)^{x-y+2Nn}J_{x-y+2Nn}(t) + \lambda_1\sum_{n=0}^{\infty}(-1)^{n+1}(1-\lambda_1^2)^{\frac{n}{2}}(1-\lambda_2^2)^{\frac{n+1}{2}}(-i)^{x+y-1-2N(n+1)}J_{x+y-1-2N(n+1)}(t), \tag{2.133b}$$

$$K_{RL}^{\lambda_1\lambda_2}(x,y,t) = \lambda_1\lambda_2\sum_{n=0}^{\infty}(-1)^{n}(1-\lambda_1^2)^{\frac{n}{2}}(1-\lambda_2^2)^{\frac{n}{2}}(-i)^{x-y+2Nn}J_{x-y+2Nn}(t) \tag{2.133c}$$

and

$$\begin{aligned}K_{CC}^{\lambda_1\lambda_2}(x,y,t) = \sum_{n=0}^{\infty}(1-\lambda_1^2)^{\frac{n}{2}}(1-\lambda_2^2)^{\frac{n}{2}}(-1)^{n}[&(-i)^{x-y+2Nn}J_{x-y+2Nn}(t)\\ &+(-i)^{x-y-2Nn}J_{x-y-2Nn}(t) + \sqrt{1-\lambda_1^2}(-i)^{x+y-1+2Nn}J_{x+y-1+2Nn}(t)\\ &-\sqrt{1-\lambda_2^2}(-i)^{x+y-1+2N(n+1)}J_{x+y-1+2N(n+1)}(t)] - (-i)^{x-y}J_{x-y}(t).\end{aligned} \tag{2.133d}$$

In the following we show how to obtain the formula for the propagator $K_{RL}^{\lambda_1\lambda_2}(x,y,t)$. The derivation of the other cases above follow the same steps. Writing the propagator according to the definition gives

$$\begin{aligned}K_{RL}^{\lambda_1\lambda_2}(x,y,t) &= \frac{1}{V}\sum_{\alpha=+,-}\sum_{k_\alpha}e^{i\varepsilon(k)t}\phi_{k_\alpha}(x)\phi_{k_\alpha}^*(y) =\\ &\sum_{\alpha=+,-}\sum_{k_\alpha}e^{i\varepsilon(k)t}\left(\frac{1}{z_\alpha}e^{ik_\alpha(x-y)} + z_\alpha e^{ik_\alpha(y-x)} + \frac{F_\alpha}{z_\alpha}e^{-ik_\alpha(x+y-1)} + z_\alpha F_\alpha^* e^{ik_\alpha(x+y-1)}\right),\end{aligned} \tag{2.134}$$

using the formula for the propagator given in terms of the eigenstates of $H^{\lambda_1\lambda_2}$. Here we also used the fact that the amplitude F_α given in (2.128) is a phase, thus $F_\alpha F_\alpha^* = 1$. Now using the quantization condition for the quasimomenta in (2.127) we can complete the sum over α with the following assumption: the expression of the propagator only contains dependences on the quasimomenta k_α through the exponents. Taking the thermodynamic limit $L\to\infty$ while keeping N constant, the correction term $\propto \frac{\log z_\pm}{L}$ in the quasimomenta $k_\pm$ only gives a non-negligible contribution in the exponent if it is $\propto k_\pm L$, in which case it can be evaluated using the formula for $z_\pm$ in Eq (2.127). In all other cases

$$k_\pm \approx \frac{2\pi n}{L} + \mathcal{O}(L^{-1}), \quad \text{with} \quad 0,1,...,L/2-1. \tag{2.135}$$

Now the summation over $\alpha = +,-$ in Eq. (2.134) can be completed, giving

$$\begin{aligned}\sum_\alpha z_\alpha &= \frac{2\lambda_1\lambda_2}{1+\sqrt{1-\lambda_1^2}\sqrt{1-\lambda_2^2}[w_N^\pm]^*}\\ &= 2\lambda_1\lambda_2\sum_{n=0}^{\infty}(-1)^n(1-\lambda_1^2)^{\frac{n}{2}}(1-\lambda_2^2)^{\frac{n}{2}}\left[\frac{1}{w_N^\pm}\right]^n\end{aligned} \tag{2.136a}$$

and

$$\sum_{\alpha} \frac{F_\alpha}{z_\alpha} = 0. \tag{2.136b}$$

This means that there are no contributions to the propagator coming from the third and fourth terms in (2.134). Replacing the sum in the thermodynamic limit as $\sum_k \to \int \frac{L}{2\pi} \mathrm{d}k$, the first and second term can be evaluated using Eq. (2.130) and by transforming the second term as $q = -k$, giving the integral:

$$\int_{-\pi}^{\pi} \frac{\mathrm{d}k}{2\pi} e^{ik(x-y+2Nn)-i\cos(k)t} = J_{x-y+2Nn}(t)(-i)^{x-y+2Nn}, \tag{2.137}$$

inside the summation over n, resulting in Eq. (2.133c). This calculation gives a clear recipe for obtaining the rest of the propagators above: using the formula (2.104) one obtains the propagator in terms of the amplitudes (2.128), where one can evaluate the summation over the two different species by pairing the quasimomenta that correspond to the same quantum number n. The resulting amplitudes can always be written as geometric series. Taking the thermodynamic limit then as discussed above, the integral over the quasimomenta k can be evaluated resulting in the propagators as sums of Bessel functions. This form of the propagator allows a semiclassical interpretation.

Semiclassical Picture

As shown in Table (2.132) and Eqs. (2.133), the propagator of a particle $K^{\lambda_1\lambda_2}(x, y, t)$ is given by a sum of Bessel functions of the first kind. Deriving a semiclassical picture for the particle dynamics can be done by carefully examining the terms present in the propagators.

Taking for example the case of $x, y \in [-\frac{L}{2} + 1, 0]$, the propagator is given by $K_{LL}^{\lambda_1\lambda_2}(x, y, t)$ in Eq. (2.133), we see three different terms describing different 'classical' paths. The first term being $\propto J_{x-y}(t)$ representing a propagation from point y to x without being affected by either of the defects, with an additional phase given by the length of the propagation. It is important to note that the length here includes a sign as both $x, y \leq 0$. The second term is $\propto J_{x+y-1}(t)$, with $x+y-1$ being the length of the classical path of the particle from y to x with a reflection at position 1. This term has the same phase coming from the classical path as well as an additional sign coming from the fact that the reflection causes the particle to go in the opposite direction than before. The amplitude $\sqrt{1-\lambda_1^2}$ can be understood classically as the probability that the particle got reflected at the defect. Looking at the last term given by an infinite sum of terms of the form

$$\lambda_1^2(-1)^{n+1}(1-\lambda_1^2)^{\frac{n}{2}}(1-\lambda_2^2)^{\frac{n+1}{2}}(-i)^{x+y-1-2N(n+1)}J_{x+y-1-2N(n+1)}(t), \tag{2.138}$$

using the arguments for the previous two terms it can be concluded that it describes a 'classical' path of a particle from position y reaching the first defect (with parameter λ_1) scattering on it, then getting transmitted, giving a factor λ_1 in the amplitude. After that the particle 'bounces' (gets reflected multiple times by both defects) in the central region n times giving the factors $(1-\lambda_1^2)^{\frac{n}{2}}(1-\lambda_2^2)^{\frac{n}{2}}$ in the amplitude from the multiple reflections, finally getting reflected on the second defect and transmitted on the first one, hence the remaining factor $\lambda_1\sqrt{1-\lambda_2^2}$. The phases, like in the previous cases are given by the (signed) distance 'travelled' by the particle (giving the factor $(-i)^{x+y-1-2N(n+1)}$) during time evolution from $t = 0$. as well as the number of times the particle changed to the opposite direction as it's initial propagation direction (giving the factor $(-1)^{n+1}$)). The classical paths emerging from this semiclassical interpretation are shown on Fig. 2.13 for the examples of $K_{LL}^{\lambda_1\lambda_2}(x, y, t)$, $K_{CL}^{\lambda_1\lambda_2}(x, y, t)$ and $K_{RL}^{\lambda_1\lambda_2}(x, y, t)$ respectively.

We show how the propagators can be used to obtain corrections to the naive hydrodynamic picture for a density profile of fermion being released from a domain wall initial state and let freely expand.

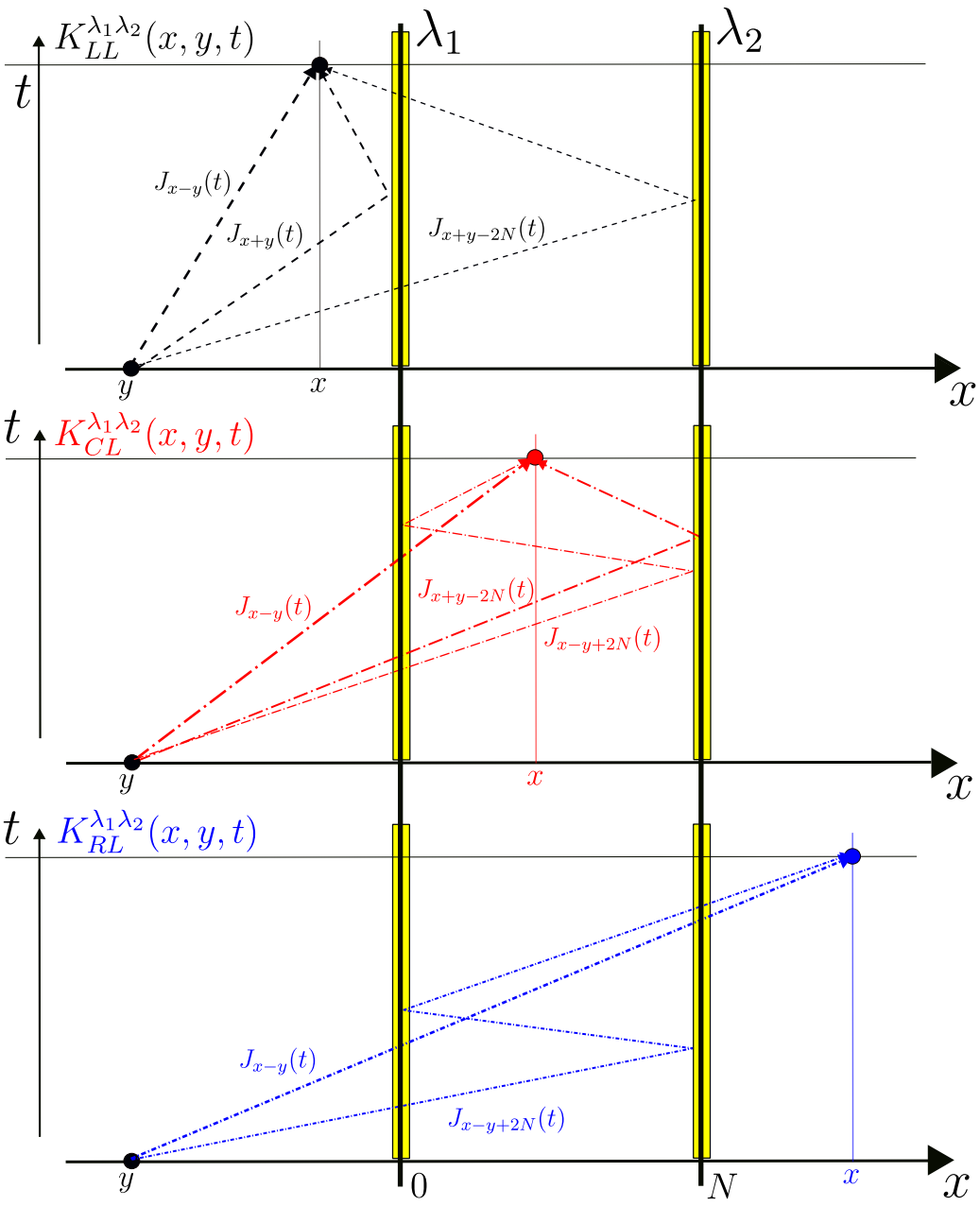


Figure 2.13: Schematic drawing of the semiclassical picture of the propagators for different positions of x ($x \in L, C, R$ respectively) and $y \in L$, with time being the vertical axis and coordinate the horizontal, with defect strengths of $\lambda_1, \lambda_2 \in [0, 1]$ at $x = 0, N$ respectively.

2.2.3 The Propagator and the Density

At $t = 0$ the system is prepared in the product state given in Eq. (2.111). This corresponds to filling the left side of the system up to and including $x = 0$, where the first defect - with parameter λ_1 - is located. At $t > 0$ the system is let evolve with the Hamiltonian (2.120) (2.87) containing the two defects. Similarly to the case of the density profile for the system with one defect (2.116) the density profile is given by

$$\rho(x,t) = \sum_{y\leq 0} K_t(x,y)K_t^*(x,y). \tag{2.139}$$

Using the formulas derived for the propagator in Table (2.132) and Eqs. (2.133) the density profile for the free expansion is given by:
For $x \leq 0$:

$$\begin{aligned}\rho(x,t) = &\sum_{y\leq 0} J_{x-y}(t)^2 + (1-\lambda_1^2)J_{x+y-1}(t)^2 \\ &+ 2\lambda_1^2 \sum_{n=0}^{\infty} (-1)^{N(n+1)+n}(1-\lambda_1^2)^{\frac{n+1}{2}}(1-\lambda_2^2)^{\frac{n+1}{2}} \\ &\quad \times J_{x+y-1}(t)J_{x+y-1-2N(n+1)}(t) \\ &+ \lambda_1^4 \sum_{n,m=0}^{\infty} (-1)^{(N+1)(n+m)}(1-\lambda_1^2)^{\frac{n+m}{2}}(1-\lambda_2^2)^{\frac{n+m}{2}+1} \\ &\quad \times J_{x+y-1-2N(n+1)}(t)J_{x+y-1-2N(m+1)}(t),\end{aligned} \tag{2.140a}$$

for $1 \leq x \leq N$:

$$\begin{aligned}\rho(x,t) = \lambda_1^2 \sum_{y\leq 0} \sum_{n,m=0}^{\infty} &(-1)^{(N+1)(n+m)}(1-\lambda_1^2)^{\frac{n+m}{2}}(1-\lambda_2^2)^{\frac{n+m}{2}}(J_{x-y+2Nn}(t)J_{x-y+2Nm}(t) \\ &+ (1-\lambda_2^2)J_{x+y-1-2N(n+1)}(t)J_{x+y-1-2N(m+1)}(t))\end{aligned} \tag{2.140b}$$

and for $N < x$:

$$\begin{aligned}\rho(x,t) = \lambda_1^2\lambda_2^2 \sum_{y\leq 0} \sum_{n,m=0}^{\infty} &(1-\lambda_1^2)^{\frac{n+m}{2}}(1-\lambda_2^2)^{\frac{n+m}{2}}(-1)^{(N+1)(n+m)} \\ &\times J_{x-y+2Nn}(t)J_{x-y+2Nm}(t).\end{aligned} \tag{2.140c}$$

The hydrodynamic limit can be obtained by taking $x, t, L \to \infty$ with ratios x/t and L/t fixed. Assuming coarse grained continuous coordinate (as usual in hydrodynamic descriptions) the sum over lattice sites can be approximated as an integral over the new coarse grained coordinate:

$$\sum_{y<0} \to \int_{-\infty}^{0} \mathrm{d}y.$$

This allows us to evaluate the diagonal terms (i.e $n = m$) in Eqs. (2.140) -using the saddle point approximation of the Bessel functions given in (2.117)- to obtain the density profile in the hydrodynamic limit. The result is given by:

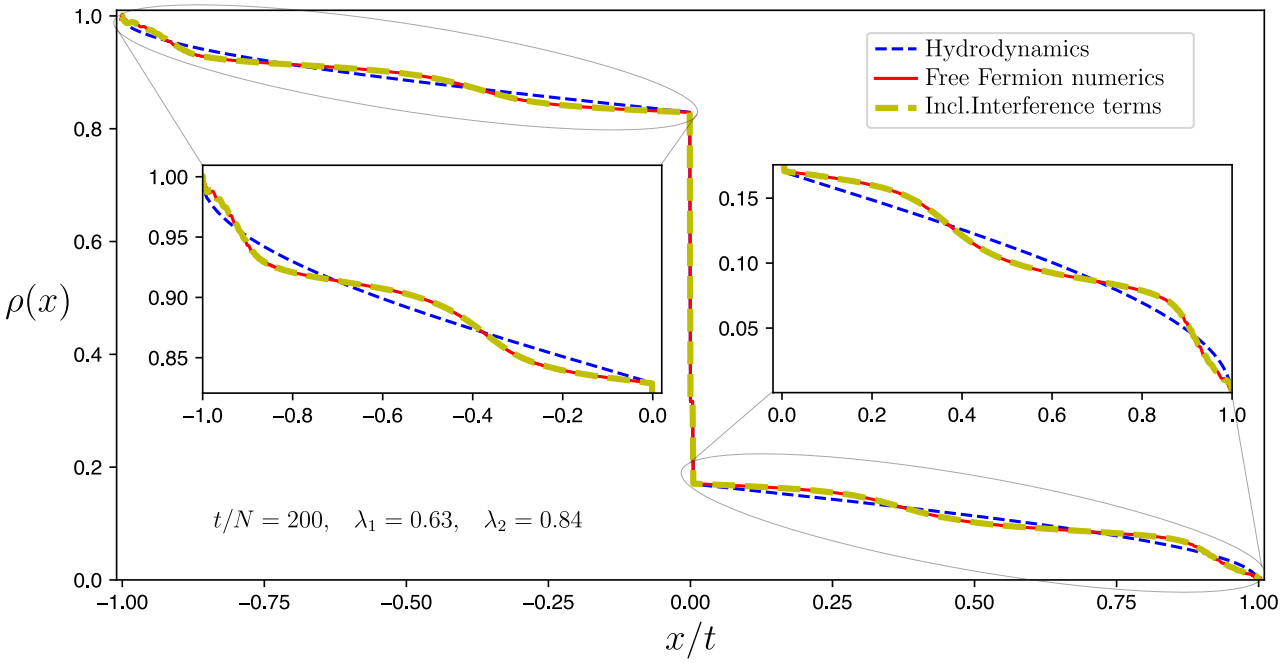


Figure 2.14: Density profile of the free expansion from the domain wall initial state in Eq. (2.111), for a time $t \gg N$, and defect strengths $\lambda_1 = 0.63, \lambda_2 = 0.84$, comparing the formula for the density (green staggered) to free fermion numerics (red solid) and the hydrodynamic profile (blue staggered). The insets show the region to the left and right of the defects where the corrections to the hydrodynamic picture are the most significant.

1. For $x \leq 0$:

$$\begin{aligned}\rho(x,t) = 1 - \frac{\lambda_1^2}{\pi}\arccos\left(\frac{-x}{t}\right) \quad &+ \frac{\lambda_1^4}{\pi}\sum_{n=0}^{\lfloor\frac{t+x}{2N}\rfloor}(1-\lambda_1^2)^n(1-\lambda_2^2)^{n+1}\arccos\left(\frac{2nN-x}{t}\right) \\ &+ 2\lambda_1^2\sum_{n=0}^{\infty}(-1)^{N(n+1)+n}\sqrt{1-\lambda_1^2}^{n+1}\sqrt{1-\lambda_2^2}^{n+1} \\ &\times J_{x+y-1}(t)J_{x+y-1-2N(n+1)}(t) \\ &+ 2\lambda_1^4\sum_{n<m}^{\infty}(-1)^{(N+1)(n+m)}\sqrt{1-\lambda_1^2}^{n+m}\sqrt{1-\lambda_2^2}^{n+m+2} \\ &\times J_{x+y-1-2N(n+1)}(t)J_{x+y-1-2N(m+1)}(t). \end{aligned} \tag{2.141a}$$

2. For $1 \leq x \leq N$:

$$\begin{aligned}\rho_t(x) = &\frac{\lambda_1^2}{\pi}\sum_{n=0}^{\lfloor\frac{t-x}{2N}\rfloor}(1-\lambda_1^2)^n(1-\lambda_2^2)^n\arccos\left(\frac{x+2nN}{t}\right) \\ &+ \frac{\lambda_1^2}{\pi}\sum_{n=0}^{\lfloor\frac{t+x}{2N}\rfloor}(1-\lambda_1^2)^n(1-\lambda_2^2)^{n+1}\arccos\left(\frac{2(n+1)N-x}{t}\right) \\ &+ 2\lambda_1^2\sum_{y\leq 0}\sum_{n<m}(-1)^{(N+1)(n+m)}\sqrt{1-\lambda_1^2}^{n+m}\sqrt{1-\lambda_2^2}^{n+m} \\ &\times \left[J_{x-y+2Nn}(t)J_{x-y+2Nm}(t) + (1-\lambda_2^2)J_{x+y-1-2N(n+1)}(t)J_{x+y-1-2N(m+1)}(t)\right]. \end{aligned} \tag{2.141b}$$

3. For $N < x$:

$$\rho_t(x) = \frac{\lambda_1^2\lambda_2^2}{\pi}\sum_{n=0}^{\lfloor\frac{t-x}{2N}\rfloor}(1-\lambda_1^2)^n(1-\lambda_2^2)^n\arccos\left(\frac{x+2nN}{t}\right) + 2\lambda_1^2\lambda_2^2\sum_{y\leq 0}\sum_{n<m}(-1)^{(N+1)(n+m)}\sqrt{1-\lambda_1^2}^{n+m}\sqrt{1-\lambda_2^2}^{n+m} \times J_{x-y+2Nn}(t)J_{x-y+2Nm}(t). \tag{2.141c}$$

The agreement with results for the density profile of free fermion numerical calculations is very good as seen in Fig. 2.14. It is also important to note that keeping only the terms diagonal in n in the formulas (2.133) leads to the result obtained by the hydrodynamic picture, meaning that the off-diagonal terms contain the corrections coming from the interference phenomenon that can be understood through the 'semiclassical' interpretation we discuss in Section 2.2.2.

2.2.4 Discussion

In this part of the thesis, we presented the results of our investigation of the dynamics of hard-core bosons released from a domain wall initial state in the presence of two conformal defects, where the Euler-scale dynamics differ significantly from the predictions of the standard hydrodynamic description. This discrepancy arises due to quantum interference effects coming from repeated scattering on the defects. Due to the classical nature of the hydrodynamic equations (see more in Section 1.3) such effects are not captured in the GHD framework. The interference can be qualitatively understood through the analysis of the boson propagators. We derived and demonstrated that a 'semi-classical' approach can be restored by refining the naive scattering picture that was previously successful for systems with a single conformal defect [129]. This methodology straightforwardly generalizes to the presence of an arbitrary number of such defects. To validate our findings, we derived an analytic expression for the boson density profile during free expansion both for intermediate times and for the Euler limit, and benchmark it against exact numerics, finding perfect agreement. This work is a natural extension of [129], where the time evolution of the entanglement entropy was studied in a domain wall melting across one conformal defect. The results presented in this Section raise intriguing questions, such as how to systematically incorporate interference corrections into the hydrodynamic framework and how to extend this approach to capture more complex observables, such as bipartite entanglement or equal time correlation functions such as the previously discussed OPDM.

Chapter 3

Correlations of Trapped Bose Gases at Finite Temperature

One of the most ubiquitous quantities in studying Bose-Einstein condensates and cold atoms is the momentum distribution, that can be measured in 'time-of-flight' experiments (see Section 1.2.2). This quantity has been used extensively since the early days of BEC to describe and characterize a wide range of phenomena in many different quantum systems. In the context of 1D quantum gases, some of the examples are -but not limited to- the observation of dynamical fermionization, benchmarking Generalized Hydrodynamics and characterizing dipolar interactions. The momentum distribution is defined as the Fourier transform of the One Particle Density Matrix (OPDM)

$$f(\mathbf{p}) = \int d\mathbf{x} \int d\mathbf{y}\ e^{-i\mathbf{p}(\mathbf{x}-\mathbf{y})} g_1(\mathbf{x},\mathbf{y}), \tag{3.1}$$

with $g_1(\mathbf{x},\mathbf{y})$ denoting the OPDM, that -we remind- is defined as

$$g_1(\mathbf{x},\mathbf{y}) = \langle \hat{\Psi}^\dagger(\mathbf{x})\hat{\Psi}(\mathbf{y})\rangle, \tag{3.2}$$

with $\hat{\Psi}^\dagger(\mathbf{x})$ and $\hat{\Psi}(\mathbf{x})$ bosonic creation and annihilation operators. During our calculation in this chapter we set $\hbar = 1$ as we have done throughout this thesis so far; we reintroduce it when we make comparisons between numerical and analytical results.

Deriving formulas for the OPDM or obtaining results numerically are generally known to be difficult, making evaluation of the momentum distribution also a challenge, especially for correlated out-of-equilibrium gases. Analytical results for bosonic gases are generally restricted to 1D, where direct calculations are restricted to the TG (or HCB) limit where the system maps to free Fermions (see Sections 1.2.5 or 2.1). As for numerical methods, obtaining the momentum distribution is done by quantum Monte-Carlo simulation, and in integrable cases, form factor resummation methods, or Matrix Product State techniques such as DMRG.

In this Chapter of the thesis we introduce a numerical method for obtaining momentum distributions and one-particle correlations in one-dimensional Bose-gases confined in smoothly varying trapping potentials for finite interaction strengths and temperatures. In our description we combine long range asymptotics (similar to Luttinger liquid theory) and known asymptotic results for short-distances. We then compare results obtained from this framework to numerics and experiments.

We organize the Chapter as follows. We start by recalling existing results for short range and long range asymptotics for the OPDM of the trapped Lieb-Liniger gas, relying on the notations

and definitions introduced in Chapter 1. We then turn to the study of the trapped Lieb-Liniger gas following techniques of the 'inhomogeneous Luttinger liquid' [73] (or Section 1.4), where we derive analytical formulas for the OPDM at finite temperature in the TG- and the weakly-interacting regime. We then proceed with detailing the numerical method used for evaluating the OPDM for arbitrary interaction strengths at finite temperatures, generalizing the results of [74]. We proceed with benchmarking our results with quantum Monte Carlo, and compare it to recent experimental results. We finish this Chapter with a discussion and possible extensions. The results and figures presented in this Chapter were published in our work [185].

3.1 Asymptotics of the OPDM

In this chapter we focus on the Lieb-Liniger gas with repulsive interaction. We recall the Hamiltonian

$$\hat{H}_0 = \frac{1}{2}\int_0^L dx\ \hat{\Psi}^\dagger(x)\left[-\partial_x^2 + c\hat{\Psi}^\dagger(x)\hat{\Psi}(x)\right]\hat{\Psi}(x). \tag{3.3}$$

with interaction strength c. The Lieb-Liniger gas can be solved with the Bethe-Ansatz that gives an exact description of the spectrum of the model, as reviewed in Section 1.2.3. In the thermodynamic limit the solution is given by the Thermodynamic Bethe Ansatz. Even though one gains access to the complete spectrum of the system through these methods, evaluating correlation functions proves extremely difficult in most cases. The existing methods require sophisticated numerical algorithms, see e.g. [80, 186] (the exact results for finite interaction strengths on Fig. 3.1 were obtained in [186]).

Long-distance asymptotics

Another way of obtaining correlation functions is through effective theories. Indeed, there exist well-known results for the OPDM of 1D bosonic gases. In homogeneous (translationally invariant) cases, the long-distance asymptotics of the $g_1(x,y)$ in the ground state are predicted by Luttinger liquid theory and are written in the general form

$$\frac{g_1(x,y)}{n} \underset{|x-y|\gg d(n)}{\simeq} \sum_{m\geq 0} \frac{B_m 2\cos(2mk_F|x-y|)}{(n|x-y|)^{2m^2K+\frac{1}{2K}}}, \tag{3.4}$$

with n being the atomic density, k_F being the Fermi wavevector, and K is the Luttinger parameter, which decodes the interaction between the bosons in the microscopic theory. The parameter $d(n)$ is the characteristic length scale of the microscopic problem, generally taken to be the maximum between the interparticle distance n^{-1} and the healing length $\xi_{\text{heal}} \propto 1/\sqrt{n}$. Each term in the sum is weighed by a dimensionless amplitude B_m that is dependent of the microscopic details of the model and are related to Umklapp scattering processes, their values are determined by field form factors in the thermodynamic limit, as we describe in Appendix B (the $m = 0$ is the same form factor we compute in the previous Chapter, when evaluating the OPDM of HCBs in Section 2.1). The Luttinger liquid theory also allows for thermal fluctuations to be incorporated in the description. By incorporating the effect of a temperature T into the Luttinger liquid Eq. (3.4) becomes

$$\frac{g_1(x,0)}{n} \approx \frac{B_0 n^{-\frac{1}{2K}}}{\left[\xi_T \sinh\left(\frac{|x|}{\xi_T}\right)\right]^{\frac{1}{2K}}}, \tag{3.5}$$

by truncating the sum at leading order $m = 0$. This expression remains valid for translationally invariant systems in the regime $\xi_T \ll d(n) \ll |x|$, where $\xi_T = \pi T/v$ with sound velocity v (1.115)

denotes the thermal length (setting the Boltzmann constant $k_B = 1$). Such calculations are discussed in the work [5] in more detail, and in the explanation later on in this Chapter.

Short-distance asymptotics

The long-distance asymptotics obtained by Luttinger liquid formalism display an ultraviolet divergence in the limit of short distances i.e. $|x-y| \to 0$. This feature of the description is not present in the microscopic theory and is an artifact of the effective field theory. Thus the OPDM obtained in equations (3.5) and (3.4) has to be renormalized when calculating quantities such as the momentum distribution. However, there exists an asymptotic description of $g_1(x,y)$ in the short-distance limit, that was derived in the works [66, 187, 188]. In its most general form it is given by the equation

$$\frac{g_1(x,y)}{n} \underset{|x-y|\ll d(n)}{\simeq} 1 + \sum_{q>1} C_q (n|x-y|)^q, \tag{3.6}$$

however, in this work we only keep the terms up to order $q = 4$. The coefficients C_q expressed in terms of thermodynamic Bethe Ansatz quantities are

$$C_2(\gamma) = -\frac{\epsilon_2(\gamma) - \gamma\epsilon_2'(\gamma)}{2}, \tag{3.7}$$

$$C_3(\gamma) = \frac{\gamma^2\epsilon_2'(\gamma)}{12}, \tag{3.8}$$

and

$$C_4(\gamma) = \frac{18\epsilon_2^2 - 9\epsilon_4 - 2\epsilon_2(2+3\epsilon_2')\gamma + \gamma[2\epsilon_4' + \epsilon_2'\gamma(2+\gamma)]}{24}. \tag{3.9}$$

Here we defined the functions

$$\epsilon_{2k}(\gamma) = \frac{\int_{-1}^{1} du\; g(u,\alpha_\gamma) u^{2k}}{\left[\int_{-1}^{1} du\; g(u,\alpha_\gamma)\right]^{2k+1}}. \tag{3.10}$$

Strictly speaking, Eq. (3.6) applies to the ground state of the Lieb-Liniger model. However, while low but finite temperatures modify the long-distance behavior of the one-body density matrix (OPDM), changing it from algebraic to exponential decay [see Eqs. (3.4) and (3.5)], they only have a minor impact on the short-distance regime. The applicability of Eq. (3.6) to finite-temperature systems was confirmed through comparisons with quantum Monte Carlo results in Refs. [189, 190]. In Fig 3.1 we show the One-Particle Density Matrix of a translationally invariant Lieb-Liniger gas in its ground state at different values of the effective interaction strength γ defined in Eq. (1.72). We obtained our results by combining long- and short- distance asymptotics in Equations (3.4) and (3.6) respectively. For the remaining parts of this Chapter we assume that $V(x) = V(-x)$, so that in the ground state the gas is confined in $x \in [-R, R]$, with R being the radius of the atomic cloud. The generalization of the results obtained and discussed in the following sections is straightforward.

3.2 Trapped bosons at finite temperature

In the previous section we introduced a scheme of combining existing short- and long-range asymptotic results for the OPDM of translationally invariant Bose gases. Experimentally, however (as we briefly discuss in Section 1.2.2) 1D ultra cold gases are realized - either by optical lattices [5, 14]

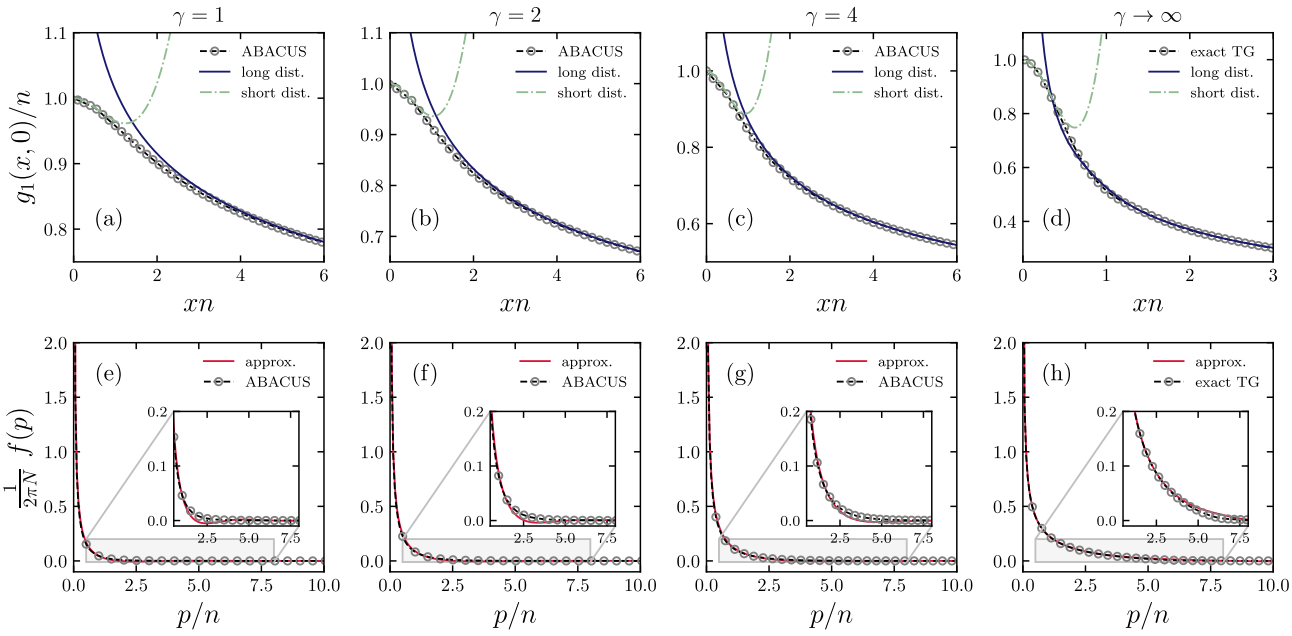


Figure 3.1: **Top row:** Results for $g_1(x, 0)$ (symbols) obtained from ABACUS from Ref. [186] at finite interaction strength and the exact result from the Bose-Fermi mapping in the infinite repulsion limit are compared with the leading-order asymptotic expression (solid line, corresponding to $m = 0$ in Eq. (3.4)) and with the short-distance expansion up to order $q = 4$ (dot-dashed line, see Eq. (3.6)). **Bottom row:** The corresponding normalized momentum distribution $f(p)$, derived from the exact $g_1(x, 0)$ (dashed line), is compared with the result obtained by interpolating between the two asymptotic approximations for $g_1(x, 0)$ (solid line). Insets highlight the behavior of $f(p)$ at intermediate momenta. Figure published in [185], reused with permission.

or atom chips [25]- in the presence of a confining potential $V(x)$, modifying the translationally invariant Hamiltonian as

$$\hat{H} = \hat{H}_0 + \int_0^L dx\, V(x)\hat{\Psi}^\dagger(x)\hat{\Psi}(x). \tag{3.11}$$

Although due to the confining potential translational invariance and thus the Bethe Ansatz solvability of the system is broken, the Local Density Approximation (LDA) can still be applied treating $V(x)$ as a local chemical potential $\mu - V(x)$, as done for example in the works [5, 14]. We discussed this description in more detail in Section 1.3.2. Implementing the LDA description in this way results in a position-dependent Fermi surface, on top of which low energy fluctuations can be implemented following ideas from Luttinger liquid theory. This description results in the theory of inhomogeneous Luttinger liquids with Hamiltonian

$$\hat{H}_{\text{inh}} = \int_0^L \frac{dx\; v_{\text{LDA}}(x)}{2\pi} \left(K(x) \left[\partial_x \hat{\theta}(x)\right]^2 + \frac{\left[\partial_x \hat{\phi}(x)\right]^2}{K(x)} \right), \tag{3.12}$$

as we discussed in Section 1.4.2. The parameter $K(x) = [1^{\text{dr}}(\lambda_F(x)]^2$ is the local Luttinger parameter and $v_{\text{LDA}} = \pi n_{\text{LDA}}(x)/K(x)$ is the local sound velocity. The long- distance asymptotics are then obtained by using Wick's theorem, as the Hamiltonian (3.12) is quadratic in the fields. The resulting formula for the OPDM is

$$g_1(x,y) = e^{G_{\theta\theta}(x,y)} \prod_{z=x,y} \frac{\sqrt{B_0(z)} n_{\text{LDA}}(z)^{\frac{2K(z)-1}{4K(z)}}}{[\mathcal{T} v_{\text{LDA}}(z)]^{\frac{1}{4K(z)}}} e^{-\frac{1}{2}G_{\theta\theta}(z)}, \tag{3.13}$$

up to order $m = 0$ of the expansion, for $|x-y| \gg \max[d_{\text{LDA}}(x), d_{\text{LDA}}(y)]$. Here, $B_0(x) = B_0(c/n_{\text{LDA}}(x))$ is the local nonuniversal amplitude, and $G_{\theta\theta}(x)$ and $G_{\theta\theta}(x,y)$ are the Green's functions of the phase fluctuating field $\hat{\theta}(x)$, as we discussed in Section 1.4.4 of this thesis.

As mentioned, Equation (3.13) gives access to the long-distance asymptotics of $g_1(x,y)$ through the Green's functions $G_{\theta\theta}(x)$ and $G_{\theta\theta}(x,y)$. However, there are generally no analytic results for the Green's functions. We present a numerical method for their construction in the following sections of this chapter for finite interaction strengths and temperature, also presenting analytical results for the weakly and the strongly interacting limits further down in this section. It is also important to note that analogously to the translationally invariant case, in the limit of $x \to y$ Eq. (3.13) diverges. In order to avoid such divergences, the short-distance asymptotics (3.6) can be generalized for trapped systems. The short-distance expansion for $|x-y| \ll \min[d_{\text{LDA}}(x), d_{\text{LDA}}(y)]$ becomes

$$\begin{aligned} g_1(x,y) = n_{\text{LDA}}(\zeta) \big(1 + C_2(\zeta) \left[n_{\text{LDA}}(\zeta)|x-y|\right]^2 \\ + C_3(\zeta) \left[n_{\text{LDA}}(\zeta)|x-y|\right]^3 + C_4(\zeta) \left[n_{\text{LDA}}(\zeta)|x-y|\right]^4 \big), \end{aligned} \tag{3.14}$$

with $\zeta = (x+y)/2$ and the coefficients $C_q(x) \equiv C_q(c/n_{\text{LDA}}(x))$ obtained as simple LDA extensions of the results discussed in Section 3.1.

3.2.1 Weakly Interacting Bosons in a Harmonic trap, at Finite Temperature

In the limit of weak repulsive interactions $c \to 0$ and large density $n(x) \to \infty$ such that $cn(x)$ is kept constant, analytical results can be derived for the OPDM in a harmonic trap $V(x) = \frac{1}{2}\omega^2 x^2$ [76].

Using the equation of state, $\mu = cn$ [75], and applying the LDA we obtain the following result for the local density

$$n_{\rm LDA}(x) = \frac{\omega^2 R^2}{2c}\left(1 - \frac{x^2}{R^2}\right), \tag{3.15}$$

where $R = \sqrt{2\mu}/\omega$. Equivalently, R can be related to the number of particles through

$$N = \frac{2\omega^2 R^3}{6c}. \tag{3.16}$$

For this interaction strength, Bogoliubov theory predicts a divergent Luttinger parameter [49]

$$K(x) \overset{\gamma\to 0^+}{\simeq} \frac{\pi}{\sqrt{\gamma(x)}} = \pi\sqrt{\frac{n_{\rm LDA}(x)}{c}}, \tag{3.17}$$

while the sound velocity is

$$v_{\rm LDA}(x) \overset{\gamma\to 0^+}{\simeq} \sqrt{c\, n_{\rm LDA}(x)}. \tag{3.18}$$

In the special case where the confining potential is a harmonic potential, the Luttinger liquid Hamiltonian (3.12) can be diagonalized by introducing the bosonic mode expansion [76–78]

$$\hat\theta(x) = i\omega\sqrt{\frac{c}{2}}\sum_{p>0}\frac{\alpha_p(x/R)}{\sqrt{\varepsilon_p}}(\hat a_p^\dagger - \hat a_p), \tag{3.19}$$

$$\hat\phi(x) = \frac{\pi\omega}{\sqrt{2c}}\sum_{p>0}\frac{\beta_p(x/R)}{\sqrt{\varepsilon_p}}(\hat a_p^\dagger + \hat a_p), \tag{3.20}$$

where the bosonic creation and annihilation operators $\hat a_p^\dagger/\hat a_p$ have commutation relations

$$[\hat a_p, \hat a_q^\dagger] = \delta_{p,q}, \quad [\hat a_p, \hat a_q] = 0, \tag{3.21}$$

and the phonon dispersion in the trap is

$$\varepsilon_p = \omega\sqrt{\frac{p(p+1)}{2}}. \tag{3.22}$$

The amplitudes $\alpha_p(u)$ and $\beta_p(u)$ defined in Eqs. (3.19) and (3.20) have analytical expressions in terms of the Legendre polynomials $\mathcal{L}_p(u)$ [76–78]

$$\alpha_p(u) = \sqrt{p+\frac{1}{2}}\mathcal{L}_p(u), \tag{3.23}$$

$$\beta_p(u) = -\sqrt{\frac{p+1/2}{2p(p+1)}}(1-u^2)\mathcal{L}_p'(u), \tag{3.24}$$

and satisfy the differential equation

$$\begin{pmatrix} 0 & \partial_u \\ -\frac{1-u^2}{2}\partial_u & 0 \end{pmatrix}\begin{pmatrix} \alpha_p \\ \beta_p \end{pmatrix} = \sqrt{\frac{p(p+1)}{2}}\begin{pmatrix} \alpha_p \\ \beta_p \end{pmatrix}, \tag{3.25}$$

with a normalization

$$\int_{-1}^{1} du\, \alpha_p(u)\alpha_q(u) = \int_{-1}^{1} du\, \frac{2\beta_p(u)\beta_q(u)}{1-u^2} = \delta_{p,q}. \tag{3.26}$$

Then, the Luttinger liquid Hamiltonian (3.12) can be diagonalized by Eqs. (3.19) and (3.20), and reads

$$\hat{H}_{\text{inh}} = \sum_{p>0} \varepsilon_p \, \hat{a}_p^\dagger \hat{a}_p, \tag{3.27}$$

up to a constant. The two-point correlation functions of fields $\hat{\phi}(x)$ and $\hat{\theta}(x)$ in the ground state in harmonic traps can be expressed in terms of amplitudes $\alpha_p(u)$ and $\beta_p(u)$ to be of the form

$$\langle \hat{\theta}(x)\hat{\theta}(y)\rangle = \frac{c\omega^2}{2} \sum_{p>0} \frac{\alpha_p(x)\alpha_p(y)}{\varepsilon_p} \tag{3.28a}$$

$$\langle \hat{\phi}(x)\hat{\phi}(y)\rangle = \frac{\pi^2\omega^2}{2c} \sum_{p>0} \frac{\beta_p(x)\beta_p(y)}{\varepsilon_p}, \tag{3.28b}$$

$$\langle \hat{\phi}(x)\hat{\theta}(y)\rangle = i\frac{\pi\omega^2}{2} \sum_{p>0} \frac{\beta_p(x)\alpha_p(y)}{\varepsilon_p}. \tag{3.28c}$$

We note that the sums entering in Eqs. (3.28a)–(3.28c) converge fast in p. The result for finite temperature can be obtained straightforwardy by generalizing the formulas above, by accounting for a Bose-Einstein weight $n_{\text{BE}}(\varepsilon) = 1/(1 - e^{-\varepsilon/T})$ of the bosonic modes. Thus, the finite-temperature form of Eqs. (3.28a) and (3.28b) is given by

$$\langle \hat{\theta}(x)\hat{\theta}(y)\rangle = \frac{c\omega^2}{2} \sum_{p>0} \frac{\alpha_p(x)\alpha_p(y)}{\varepsilon_p}[1 + 2n_{\text{BE}}(\varepsilon_p)]; \tag{3.29}$$

$$\langle \hat{\phi}(x)\hat{\phi}(y)\rangle = \frac{\pi^2\omega^2}{2c} \sum_{p>0} \frac{\beta_p(x)\beta_p(y)}{\varepsilon_p}[1 + 2n_{\text{BE}}(\varepsilon_p)], \tag{3.30}$$

while $\langle \hat{\phi}(x)\theta(y)\rangle$ in Eq. (3.28c) remains unchanged.

Using Eqn. (3.29) and the known result for the nonuniversal amplitude $B_0 \simeq 1$ for $\gamma \to 0^+$ [73], one can obtain an analytical formula for the asymptotic long-distance behavior of the OPDM (3.11) in the weakly interacting regime in the presence of harmonic trapping potential. The result is

$$g_1(x,x') = \exp\left(\frac{c\omega^2}{2} \sum_{p>0} \alpha_p(x)\alpha_p(x') \frac{[1 + 2n_{\text{BE}}(\varepsilon_p)]}{\varepsilon_p}\right)$$
$$\times \prod_{z=x,x'} \frac{n_{\text{LDA}}(z)^{\frac{2K(z)-1}{4K(z)}}}{\exp\left(\frac{c\omega^2}{4} \sum_{p>0} \alpha_p^2(z) \frac{[1+2n_{\text{BE}}(\varepsilon_p)]}{\varepsilon_p}\right)}. \tag{3.31}$$

Fig. 3.2 displays the results derived by evaluating Eq. (3.31) at the center of the trap at different values of temperature. The same results can be obtained from Eq. (3.13) by inserting $G_{\theta\theta}(x,y)$ given in Eq. (3.29)(upon using the change of coordinates we detail in Equation (1.123)).

3.2.2 Hard-Core Bosons in a Trap, at Finite Temperature

In the hard core limit (also known as the Tonks-Girardeau limit) $\gamma \to \infty$ analytical results can be obtained for the OPDM of a trapped Lieb-Liniger gas. The reason for that is that the Luttinger parameter $K(\gamma \to \infty) \to 1$ takes a constant value in space regardless of the trapping potential

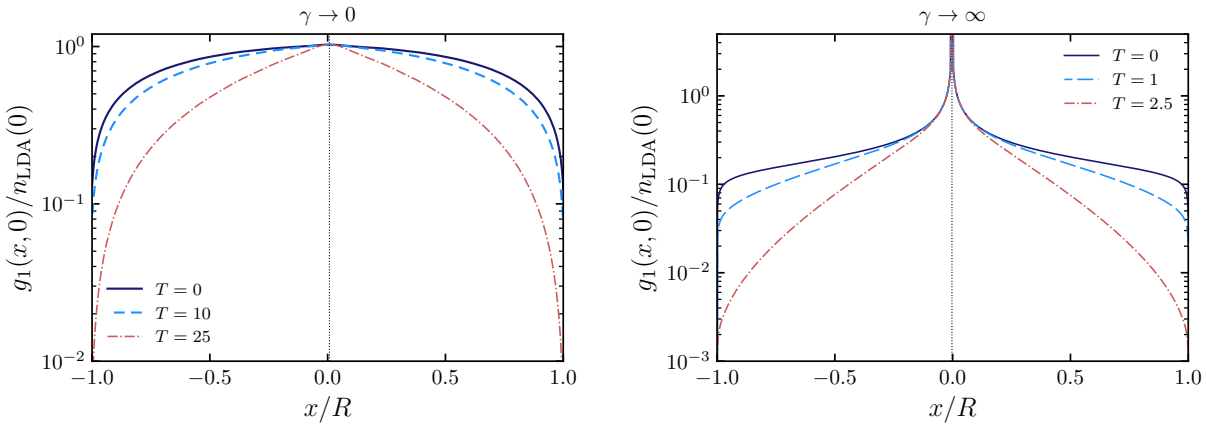


Figure 3.2: **Left**: Long-distance asymptotics of $g_1(x, x')$ for bosons in the weakly interacting regime ($\gamma \to 0$) confined in a harmonic trap $V(x) = \frac{1}{2}\omega x^2$, obtained from Eq. (3.31), with frequency $\omega = 1$ and particle number $N = 20$. We plot $g_1(x, x')$ vs x/R (R is the radius of atom cloud) for $x' = 0$ and for different temperatures. The temperatures are to be compared with the energy scale $\mathcal{T}^{-1} \simeq 0.47$ of the inhomogeneous Luttinger liquid. **Right**: Long-distance asymptotics of $g_1(x, x')$ for hard-core bosons ($\gamma \to \infty$) confined in a harmonic trap $V(x) = \frac{1}{2}\omega x^2 - \mu$, obtained from Eq. (3.13) and (3.35), with trap frequency $\omega = 1$ and particle number $N = 20$. The plot shows $g_1(x, x')$ vs x/R (where $R = \sqrt{2\mu/\omega}$ is the radius of the cloud) for $x' = 0$ and for different temperatures. The energy scale of the inhomogeneous Luttinger liquid is $\mathcal{T}^{-1} \simeq 0.2$. Figure published in [185], reused with permission.

$V(x)$. Analytical formulas for zero-temperature were derived previously in the works [63, 85, 122], so in this section we focus on the case of a finite temperature regime. The constant value of Luttinger parameter K simplifies the problem by allowing us to reduce the inhomogeneous Luttinger liquid Hamiltonian to the one of compact free boson. The resulting theory is a conformal field theory with action [48, 49, 97]

$$\mathcal{S} = \frac{1}{2\pi} \int_0^{\beta/\mathcal{T}} d\tau \int_0^1 ds \left(\nabla\hat{\phi}\right)^2, \tag{3.32}$$

with inverse temperature $\beta = \frac{1}{T}$, $\nabla = (\partial_s, \partial_\tau)$ gradient in 2D Euclidean spacetime, τ is the dimensionless (i.e., rescaled by $1/\mathcal{T}$) imaginary time, and the field $\hat{\phi}$ is periodic in the direction of τ:

$$\phi(x, \tau + \beta/\mathcal{T}) = \phi(x, \tau). \tag{3.33}$$

The spatial coordinate x has been replaced with the stretched coordinate [73, 85, 122]

$$s(x) = \mathcal{T}^{-1} \int_{-R}^{x} \frac{dx'}{v_{\rm LDA}(x')}, \tag{3.34}$$

we introduced earlier in Eqn. (1.123), with R denoting the radius of the gas cloud. The field $\hat{\phi}$ has Dirichlet boundary conditions at points $\phi(0, \tau) = \phi(1, \tau)$. Thus the action in Eq. (3.32) describes free Gaussian bosons on a cylinder of width 1 and circumference $\beta/\mathcal{T}$. The finite-temperature Green's function of the phase fields reads

$$G_{\theta\theta}(x, y) = -\frac{1}{2} \log \left| \frac{\vartheta_1\left(\frac{s(x)-s(y)}{2} \,\middle|\, \frac{i\beta}{2\mathcal{T}}\right) \vartheta_1\left(\frac{s(x)+s(y)}{2} \,\middle|\, \frac{i\beta}{2\mathcal{T}}\right)}{\left[\partial_z \vartheta_1\left(0 \,\middle|\, \frac{i\beta}{2\mathcal{T}}\right)\right]^2} \right| \tag{3.35}$$

with

$$\vartheta_1(z|\tau) = -i \sum_{r\in\mathbb{Z}+\frac{1}{2}} (-1)^{r-\frac{1}{2}} e^{2\pi r i z} e^{2\pi \frac{r^2}{2} i\tau} \tag{3.36}$$

being the Jacobi theta function. Now the regularized Green's function can be obtained to be of the form

$$\begin{aligned} G_{\theta\theta}(x) &= \lim_{x'\to x}\left[G_{\theta\theta}(x,x') + \frac{1}{4}\log|s(x)-s(x')|^2\right] \\ &= -\frac{1}{2}\log\left|\frac{\frac{\pi}{2}\vartheta_1\big(s(x)\,\big|\,\frac{i\beta}{2\mathcal{T}}\big)}{\partial_z\vartheta_1\big(0\,\big|\,\frac{i\beta}{2\mathcal{T}}\big)}\right|. \end{aligned} \tag{3.37}$$

We detail the calculation of these correlation functions in Appendix 1.4.7. Here we continue with the evaluation of the OPDM, which is now accessible using the Green's functions (3.37) and (3.35), as well as the form factor

$$B_0(\infty) = \mathrm{G}(3/2)^4/\sqrt{2\pi} \simeq 0.5214, \tag{3.38}$$

where $\mathrm{G}(\cdot)$ is the Barnes G-function [51, 53, 138, 191] (or Appendix A). The analytic formula for the One Particle Density Matrix takes the form

$$\begin{aligned} g_1(x,y) = \frac{B_0(\infty)}{\sqrt{2\mathcal{T}}}\times \\ \frac{\left|\partial_z\vartheta_1\big(0\,\big|\,\frac{i\beta}{2\mathcal{T}}\big)\right|^{\frac{1}{2}}\left|\vartheta_1\big(s(x)\,\big|\,\frac{i\beta}{2\mathcal{T}}\big)\right|^{\frac{1}{4}}\left|\vartheta_1\big(s(y)\,\big|\,\frac{i\beta}{2\mathcal{T}}\big)\right|^{\frac{1}{4}}}{\left|\vartheta_1\Big(\frac{s(x)-s(y)}{2}\,\Big|\,\frac{i\beta}{2\mathcal{T}}\Big)\right|^{\frac{1}{2}}\left|\vartheta_1\Big(\frac{s(x)+s(y)}{2}\,\Big|\,\frac{i\beta}{2\mathcal{T}}\Big)\right|^{\frac{1}{2}}}. \end{aligned} \tag{3.39}$$

This result is plotted in the right panel of Fig. 3.2 for the case of a harmonic trapping potential. In the limit of zero temperature $\beta\to\infty$ the formula (3.39) reduces to the formula derived in the works [53, 85].

3.3 Finite Temperature Green's Function of the Inhomogeneous Luttinger Liquid

In the previous section we derived analytical results in the cases of weak ($\gamma\to 0$) and strong ($\gamma\to\infty$) interaction limits. In this section we present an efficient numerical method for obtaining the Green's function of the fields $\hat\theta$ and $\hat\phi$ of an inhomogeneous Luttinger Liquid (3.12), that is valid for finite temperatures and arbitrary values of the contact interaction. These results are motivated by and are a generalization of the method used in Bastianello, Dubail, and Stéphan [74], where a similar numerical method is described for the zero-temperature Green's functions (see also Ref. [122]). We follow this algorithm and extend it for finite temperature.

We start with the Hamiltonian (3.12), which we express in terms of the stretched coordinate $s(x)$ defined in (3.34)

$$\hat H_{\text{inh}} = \frac{1}{2\pi\mathcal{T}}\int_0^1 ds\left(\pi^2 K(s)\hat\Pi^2(s) + \frac{\left[\partial_s\hat\phi(s)\right]^2}{K(s)}\right), \tag{3.40}$$

with sound velocity $v_{\text{LDA}}(x) = \pi n_{\text{LDA}}(x)/K(x)$, and we also define the canonical conjugate momentum $\hat\Pi(s) = \partial_s\hat\theta(s)/\pi$ such that

$$[\hat\Pi(s),\hat\phi(s)] = -i\delta(s-s'). \tag{3.41}$$

We then discretize the Hamiltonian as follows:

$$\hat{H}_{\text{inh}} = \frac{\pi}{2M\mathcal{T}} \sum_{j=1}^{M} K_j \hat{\Pi}_j^2 + \frac{M}{\pi\mathcal{T}} \sum_{j=1}^{M+1} \frac{(\hat{\phi}_j - \hat{\phi}_{j-1})^2}{K_j + K_{j-1}}, \tag{3.42}$$

where $M \gg 1$ is the number of sampling points in the unit interval, and $K_j \equiv K(s_j)$ is the discretized Luttinger parameter. The fields $\hat{\phi}$ and $\hat{\Pi}$ of the Luttinger liquid are replaced with their discretized version $\hat{\Pi}_j$, $\hat{\phi}_j$ satisfying the discretized commutation relations $[\hat{\Pi}_j, \hat{\phi}_{j'}] = -i\delta_{j,j'}$. We impose open boundary conditions, so that $\hat{\phi}_0 = \hat{\phi}_{M+1} = 0$ and $K_0 = K_{M+1} = 1$. The discretized Hamiltonian of the inhomogeneous Luttinger liquid (3.42) can be written in a matrix form:

$$\hat{H}_{\text{inh}} = \hat{\mathbf{\Phi}}^{\mathrm{T}}\, h\, \hat{\mathbf{\Phi}}, \tag{3.43}$$

where the vector $\hat{\mathbf{\Phi}}^{\mathrm{T}}$ is defined as

$$\mathbf{\Phi}^{\mathrm{T}} = \left(\hat{\phi}_1, \ldots, \hat{\phi}_M, \hat{\Pi}_1, \ldots, \hat{\Pi}_M\right), \tag{3.44}$$

and h is a $2M \times 2M$ matrix with elements

$$h_{i,j} = \frac{M}{\pi\mathcal{T}} \left[\frac{\delta_{i,j} - \delta_{i,j+1} - \delta_{i+1,j}}{K_j + K_{j-1}} + \frac{\delta_{i,j}}{K_{j+1} + K_j}\right]; \tag{3.45}$$

$$h_{i+M,j+M} = \frac{\pi}{2M\mathcal{T}} \delta_{i,j} K_j, \tag{3.46}$$

for $i, j = 1, \ldots, M$. We introduce bosonic modes

$$\hat{b}_j^{\pm} = \frac{\hat{\phi}_j \pm i\hat{\Pi}_j}{\sqrt{2}}, \tag{3.47}$$

satisfying commutation relations $[\hat{b}_j^{+}, \hat{b}_{j'}^{-}] = \delta_{j,j'}$ and commuting otherwise, that we collect in the $2M$-vector we change the operator basis

$$\hat{\boldsymbol{b}}^{\dagger} \equiv \left(\hat{b}_1^{-}, \ldots, \hat{b}_M^{-}, \hat{b}_1^{+}, \ldots, \hat{b}_M^{+}\right) = \hat{\mathbf{\Phi}}^{\mathrm{T}} W^{\dagger} \tag{3.48}$$

where the matrix W of shape $2M \times 2M$ has elements

$$\begin{aligned} &W_{j,j} \equiv W_{j,j+M} = 1/\sqrt{2}, \\ &W_{j+M,j} = i/\sqrt{2}, \quad W_{j+M,j+M} = -i/\sqrt{2}, \end{aligned} \tag{3.49}$$

for $j = 1, \ldots, M$, with all other terms being 0. In this new basis of bosonic modes the Hamiltonian (3.42) can be written in the quadratic form

$$\hat{H}_{\text{inh}} = \hat{\boldsymbol{b}}^{\dagger} \left(W^{\dagger}\, h\, W\right) \hat{\boldsymbol{b}}. \tag{3.50}$$

This Hamiltonian can be diagonalized by a unitary transformation U. Introducing the new operator basis $\hat{\boldsymbol{\eta}} = U\hat{\boldsymbol{b}}$, we obtain

$$\hat{H}_{\text{inh}} = \hat{\boldsymbol{\eta}}^{\dagger} U \left(W^{\dagger}\, h\, W\right) U^{\dagger} \hat{\boldsymbol{\eta}} = \sum_{j=1}^{M} \varepsilon_j (\hat{\eta}_j^{\dagger} \hat{\eta}_j + \hat{\eta}_j \hat{\eta}_j^{\dagger}), \tag{3.51}$$

with

$$\hat{\boldsymbol{\eta}}^{\dagger} = (\hat{\eta}_1^{\dagger}, \ldots, \hat{\eta}_M^{\dagger}, \hat{\eta}_1, \ldots, \hat{\eta}_M) \tag{3.52}$$

with eigenvalues $\varepsilon_j \equiv \varepsilon_{j+M}$ for $j = 1, \ldots, M$. This can be seen from the fact that the unitary transform U has a symplectic structure, as it has to preserve the commutation relations of operators $\hat{b}_j^{\pm}$, as explained in [74]. For convenience, we introduce the matrix

$$\tilde{h} = \begin{pmatrix} \mathrm{Id} & 0 \\ 0 & -\mathrm{Id} \end{pmatrix} \left(W^{\dagger}\, h\, W \right), \tag{3.53}$$

with Id being the $M \times M$ identity matrix, and project on the negative eigenvalue spectrum of $\tilde{h}$ such that the degeneracy of the spectrum is removed.

Denoting now γ_j as the eigenvectors, and $\omega_j < 0$ as the eigenvalues of the matrix $\tilde{h}$ restricted to the negative energy subspace, the two-point correlation matrix takes the form

$$\langle \hat{b}_i^{+} \hat{b}_j^{-} \rangle = \gamma_i^{\dagger}\, [\mathcal{P}_T(\omega)]_{ij}\, \gamma_j, \tag{3.54}$$

with $\mathcal{P}_T(\omega)$ being a $M \times M$ diagonal matrix that projects onto the target state over which the expectation value is computed. In a thermal state its weights are given by Bose-Einstein distribution of the bosonic modes

$$[\mathcal{P}_T(\omega)]_{i,j} = \frac{\delta_{i,j}}{1 - e^{-\omega_j/T}}. \tag{3.55}$$

The formula given in (3.54) fixes the correlation function up to a normalization factor for the eigenvectors γ_j. To fix it, we introduce a (Hermitian) matrix

$$O_{ij} = \gamma_i^{\dagger} \begin{pmatrix} \mathrm{Id} & 0 \\ 0 & -\mathrm{Id} \end{pmatrix} \gamma_i \tag{3.56}$$

with eigenvectors u_j. Then, the normalized eigenvectors are [74, 122]

$$v_j = \frac{u_j}{\sqrt{u_j^{\dagger} \begin{pmatrix} -\mathrm{Id} & 0 \\ 0 & \mathrm{Id} \end{pmatrix} u_j}}, \quad j = 1, \ldots, M. \tag{3.57}$$

The final step is to get back the correlation matrix in the original operator basis $\hat{\mathbf{\Phi}}$. In order to do so we consider the $2M \times 2M$ canonical transformation implemented by the matrix

$$\Omega = \left(\begin{array}{ccc|ccc} v_1^{\dagger}(M+1) & \ldots & v_1^{\dagger}(2M) & & & \\ \vdots & \vdots & \vdots & & & \\ v_M^{\dagger}(M+1) & \ldots & v_M^{\dagger}(2M) & & & \\ v_1^{\dagger}(1) & \ldots & v_1^{\dagger}(M) & v_1 & \ldots & v_M \\ \vdots & \vdots & \vdots & & & \\ v_M^{\dagger}(1) & \ldots & v_M^{\dagger}(M) & & & \end{array} \right), \tag{3.58}$$

so that

$$\Omega^{\dagger}\, h\, \Omega = \begin{pmatrix} \varepsilon_1 & & & & & \\ & \ddots & & & & \\ & & \varepsilon_M & & & \\ & & & \varepsilon_1 & & \\ & & & & \ddots & \\ & & & & & \varepsilon_M \end{pmatrix}. \tag{3.59}$$

In the original field basis of the Luttinger Liquid (3.44) the correlation matrix is

$$\langle \hat{\mathbf{\Phi}}^{\mathrm{T}} \hat{\mathbf{\Phi}} \rangle = W\, \Omega \begin{pmatrix} \mathrm{Id} + \mathcal{P}_T(2\varepsilon) & \\ & \mathcal{P}_T(2\varepsilon) \end{pmatrix} \Omega^{\dagger}\, W^{\dagger}, \tag{3.60}$$

where the factor 2 follows our choice of normalization. This correlation matrix now contains the discretized Green's functions the following way:

$$\langle \hat{\mathbf{\Phi}}^{\mathrm{T}} \hat{\mathbf{\Phi}} \rangle = \begin{pmatrix} \left[\langle \hat{\phi}_i \hat{\phi}_j \rangle\right]_{i,j=1}^{M} & \left[\langle \hat{\phi}_i \hat{\Pi}_j \rangle\right]_{i,j=1}^{M} \\ \left[\langle \hat{\Pi}_i \hat{\phi}_j \rangle\right]_{i,j=1}^{M} & \left[\langle \hat{\Pi}_i \hat{\Pi}_j \rangle\right]_{i,j=1}^{M} \end{pmatrix}. \tag{3.61}$$

In order to obtain the Green's functions in terms of the field $\hat{\theta}$ we perform the numerical integration

$$\mathcal{C} = A\, \langle \hat{\mathbf{\Phi}}^{\mathrm{T}} \hat{\mathbf{\Phi}} \rangle\, A^{\mathrm{T}}, \tag{3.62}$$

with the matrix

$$A = \left(\begin{array}{c|cccccc} \mathrm{Id} & & & & & & \\ \hline & 1 & & & & & \\ & \frac{\pi}{M} & 1 & & & & \\ & \frac{\pi}{M} & \frac{\pi}{M} & 1 & & & \\ & \vdots & & \ddots & \ddots & & \\ & \frac{\pi}{M} & \cdots & & \frac{\pi}{M} & 1 \end{array}\right), \tag{3.63}$$

arriving at the Green's functions for density and phase fluctuating fields $\hat{\phi}$ and $\hat{\theta}$ in position $x_j \equiv x(s_j)$,

$$\mathcal{C} = \begin{pmatrix} [G_{\phi\phi}(x_i, x_j)]_{i,j=1}^{M} & [G_{\phi\theta}(x_i, x_j)]_{i,j=1}^{M} \\ [G_{\theta\phi}(x_i, x_j)]_{i,j=1}^{M} & [G_{\theta\theta}(x_i, x_j)]_{i,j=1}^{M} \end{pmatrix}. \tag{3.64}$$

To calculate regularized Green's functions we remove the ultraviolet divergences appearing in the correlation functions in coinciding points. Starting with $G_{\theta\theta}(x, x')$:

$$G_{\theta\theta}(x_j) = G_{\theta\theta}(x_{j+1}, x_{j-1}) + \frac{K_j}{4} \log\left(\frac{2}{2+M}\right)^2 \tag{3.65}$$

for $j \neq 1, M$, and at the boundaries

$$G_{\theta\theta}(x_1) = G_{\theta\theta}(x_1, x_2) + \frac{K_2}{4} \log\left(\frac{1}{2+M}\right)^2, \tag{3.66}$$

$$G_{\theta\theta}(x_M) = G_{\theta\theta}(x_M, x_{M-1}) + \frac{K_{M+1}}{4} \log\left(\frac{1}{2+M}\right)^2. \tag{3.67}$$

The other Green's function, namely, $G_{\phi\phi}$ can be regularized the same way.

In order to calculate the OPDM for a trapped Lieb-Liniger gas at finite temperature at any strength of the contact potential, the Green's function (3.64) and it's regularized version (3.65)–(3.67) can be used as a numerical input for the formula (3.13).

In Fig. 3.3 we compare the numerical Green's functions with the analytical results available in the limiting cases $\gamma \to 0$ and $\gamma \to \infty$, respectively. One can see that there is an excellent agreement for the temperatures shown. In the following section, we benchmark the validity of our approach for finite interaction strengths and different temperatures against quantum Monte Carlo simulations.

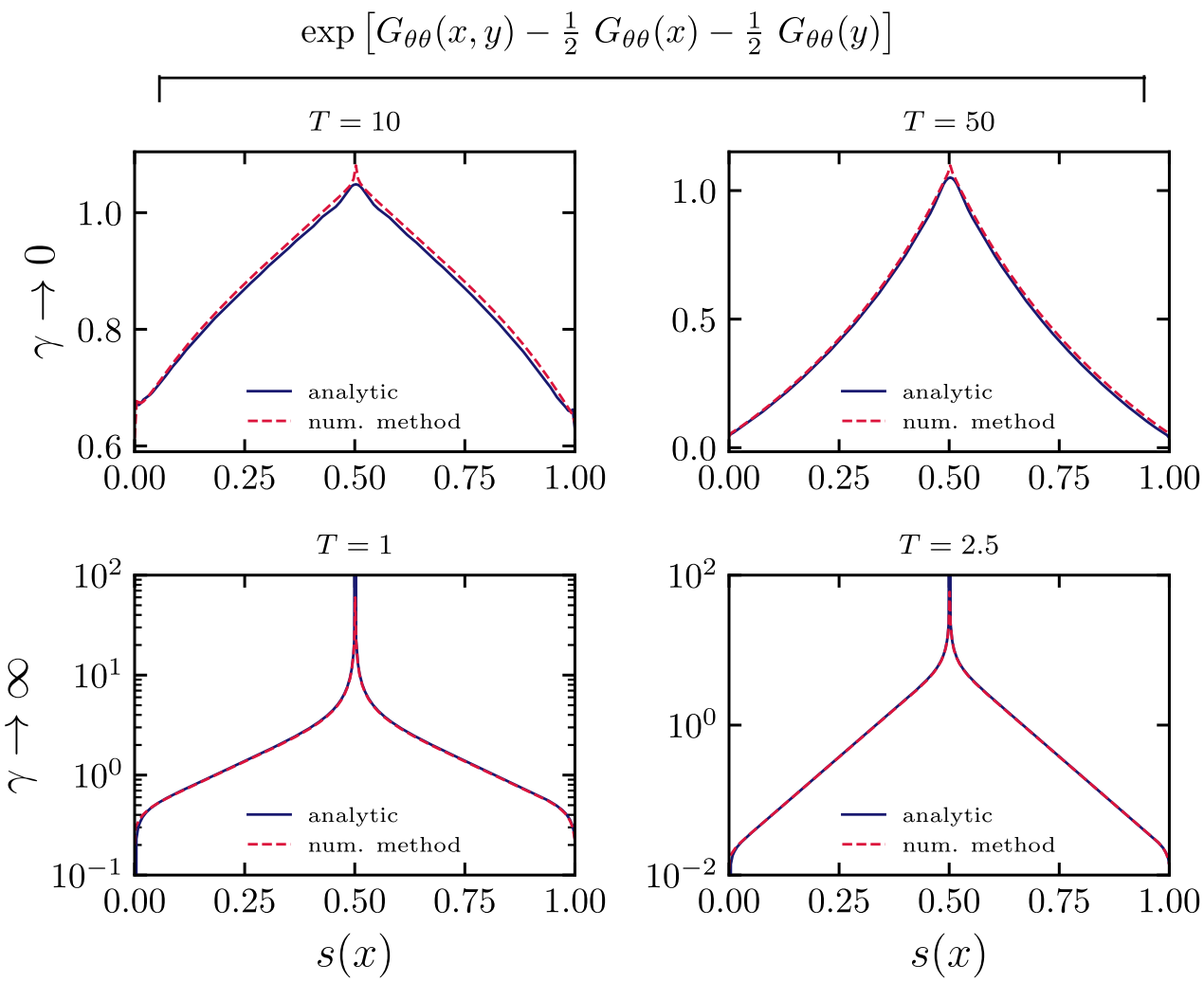


Figure 3.3: Plots showing results for $\exp[G_{\theta\theta}(x,y) - \frac{1}{2}G_{\theta\theta}(x) - \frac{1}{2}G_{\theta\theta}(y)]$ -entering in the formula for $g_1(x,y)$ in Eq. (3.13)- for $s(y) = 0.5$ obtained numerically following the method of 3.3(dashed lines) and analytically (solid lines) in the limits $\gamma \to 0$ and $\gamma \to \infty$. The values of temperatures for which we obtain results are to be compared to the energy scale $\mathcal{T}^{-1}$ of the inhomogeneous Luttinger Liquid shown in Fig. 3.2. Figure published in [185], reused with permission.

3.4 OPDM and momentum distribution of trapped bosons at finite temperature

In the following we restore the physical values of fundamental constants $\hbar$, k_b and use the parameters of recent experimental results to test our calculations. We consider a gas of ^{162}Dy atoms confined in a harmonic trap with a frequency $\omega = 2\pi \times 36.4$ Hz [192].

Starting with the hard-core limit ($\gamma \to \infty$), we show comparisons between our analytical approach (discussed in Section 3.2.2) and numerical results from low-density lattice hard-core boson calculations [193]. These lattice calculations have been instrumental in describing experimental observations, both in and out of equilibrium [192, 194]. Moving to the soft-core case ($\gamma \sim \mathcal{O}(1)$), we then compare our numerical method (presented in Section 3.3) against quantum Monte Carlo simulations. To simplify our discussion in this section, we'll refer to the methods from Sections 3.2.2 and 3.3 collectively as "*our approach*", distinguishing them from the "*exact results*" derived from unbiased numerical calculations.

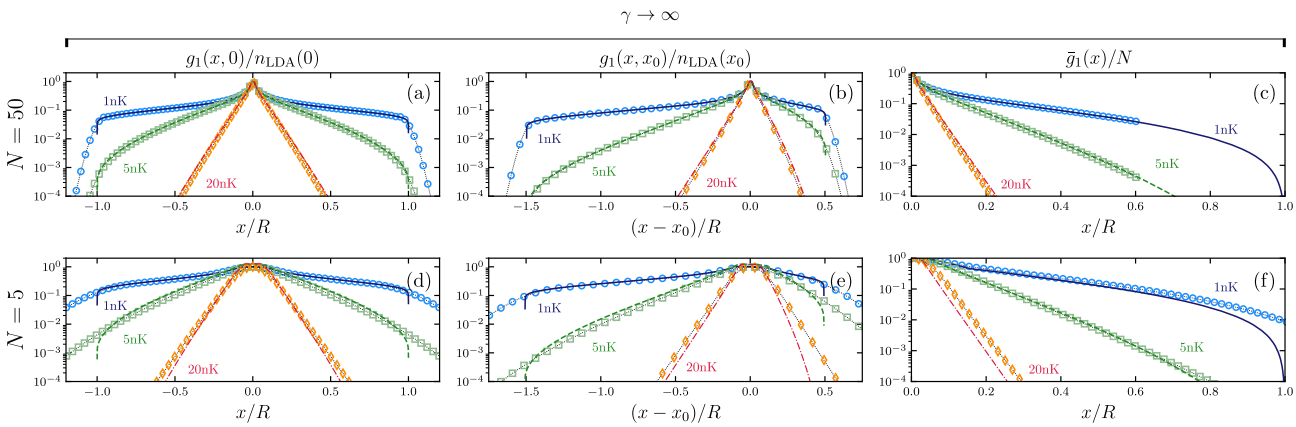


Figure 3.4: OPDM of a gas containing ^{162}Dy atoms in a harmonic trapping potential, in the hard-core (or TG) limit. The frequency of the trapping potential is 36.4Hz. results for g_1 are shown for different values of x_0: (a) and (d) in the middle of the trap: (b) and (e) for $x_0 = R/2$. We also show results for the average g_1 [see Eq. (3.68)] in panels (c) and (f). In the top row ((a),(b) and (c)) the particle number is $N = 50$, while for the bottom row ((d),(e) and (f)) $N = 5$. In each plot symbols connected with thin solid lines are results obtained by numerical lattice calculations, that we call '*exact results*' in the main text, while thick lines are used for the minimum value between the long-distance asymptotics given by Eq. (3.39) and the the short-distance expansion in Eq. (3.14)., which we refer to as the result of '*our approach*'. Results are shown for temperatures $T = 1, 5, 20nK$. Figure published in [185], reused with permission.

3.4.1 Hard-Core Bosons

We report the One-Particle Density Matrix (OPDM) results for the hard-core limit ($\gamma \to \infty$) in Fig. 3.4. "*Our approach*" utilizes the regularized OPDM, which is the minimum value between the long-distance asymptotic given by Eq. (3.39) and the short-distance expansion from Eq. (3.14).

Figures 3.4(a) through 3.4(c) illustrate these results for $N = 50$ hard-core bosons across three temperatures ($T = 1$, 5, and 20 nK). Specific trap positions include the center ($x_0 = 0$) in Fig. 3.4(a) and $x_0 = R/2$ in Fig. 3.4(b). The average, $\bar{g}_1(x)$, calculated using

$$\bar{g}_1(x) \equiv \frac{1}{R}\int dx_0\, g_1(x_0, x_0 - x), \tag{3.68}$$

is shown in Fig. 3.4(c). At lower temperatures ($T = 1$ and 5 nK), the agreement between *our approach* (continuous lines) and the *exact results* (symbols) is excellent. This agreement, predictably, gets worse as temperature rises, with differences becoming visible at $T = 20$ nK despite remaining small.

The strong agreement between *our approach* and the *exact results* for $N = 50$ in Figs. 3.4(a)–3.4(c) is notable, considering that our method is theoretically justified only for systems with a significantly larger number of particles ($N \gg 1$). Experimental setups with ultracold gases in 2D optical lattices ([32, 33, 192, 194–197]) commonly involve arrays with thousands of 1D gases, each possessing a different atom count, typically being maximal at the array's center. For example, recent experiments with ^{162}Dy atoms [192, 194] featured central 1D gases with around 40 atoms. Thus, the excellent performance demonstrated in Figs. 3.4(a)–3.4(c) validates *our approach* for describing the OPDM of 1D gases containing around 50 atoms under conditions relevant to experiments.

In Figures 3.4(d)–3.4(f) we illustrate the effect of decreasing the number of particles, showing results for $N = 5$. Despite this small particle number, *our approach* still gives a good approximation

to the *exact results*, especially for positions at the trap center [Fig. 3.4(d)] and $x_0 = R/2$ [Fig. 3.4(e)]. However, the deviations are more pronounced for the average $\bar{g}_1(x)$ [Fig. 3.4(f)], largely because finite-size effects cause the *exact results* to show a greater cloud size, as it is visible by looking at the increase in the support of the correlations from the top ($N = 50$) to the bottom ($N = 5$) panels in the *exact results*.

In Fig. 3.5, we display our results for the momentum distribution in the hard-core limit ($\gamma \to \infty$). Following *Our approach* we obtain these by computing the Fourier transform of the regularized OPDM. For $N = 50$ (shown on Fig. 3.5(a)), the differences between *our approach* and the *exact results* are small and difficult to see. For small particle number $N = 5$ (see Fig. 3.5(b)) however, these differences, while still small, become more visible. We estimate the differences between the result of *our approach* and the *exact results* in Appendix C.

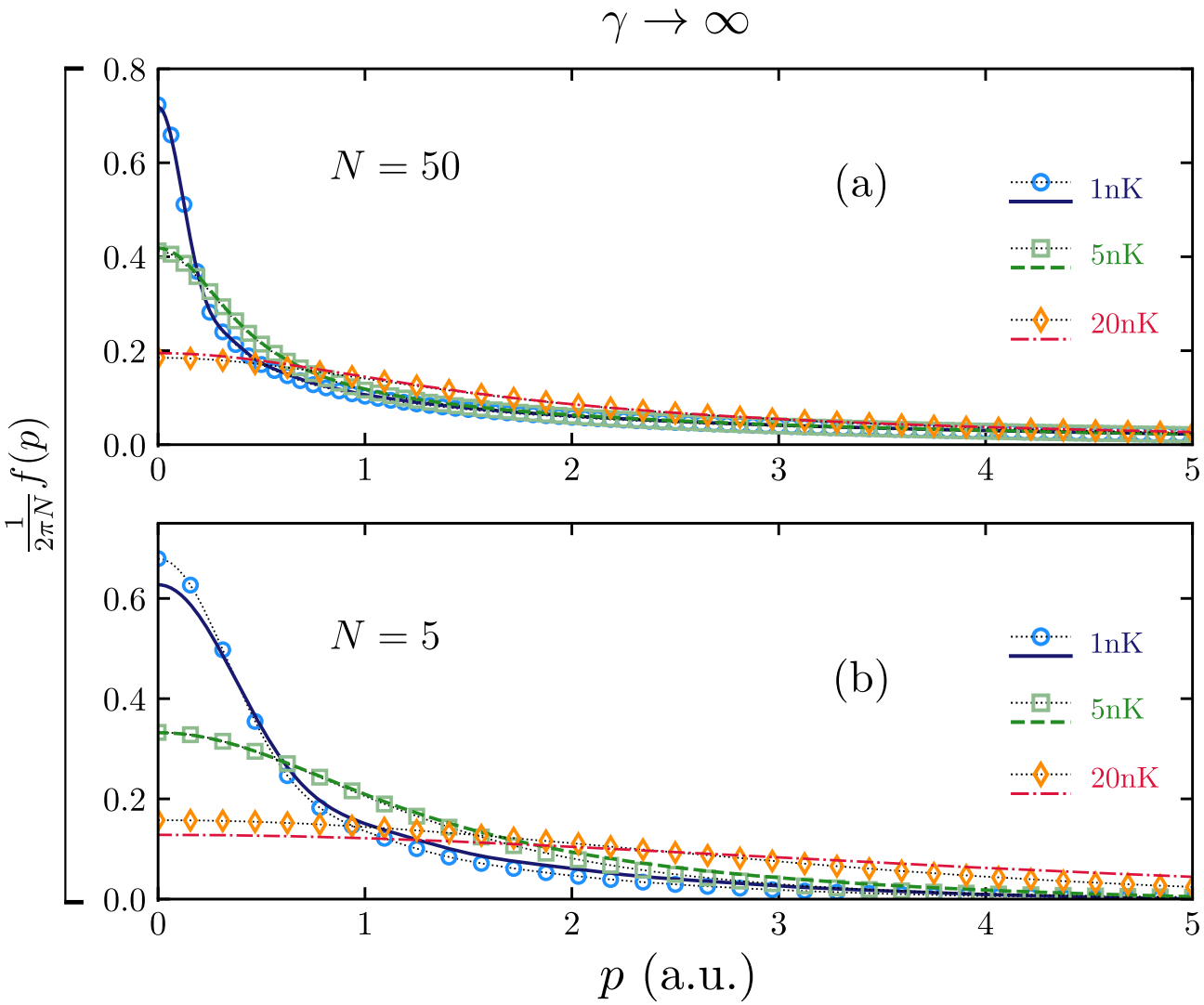


Figure 3.5: The momentum distribution, computed through Fourier transforming the OPDM (Fig. 3.4). Panel (a) shows the results for $N = 50$ and (b) for $N = 5$. Figure published in [185], reused with permission.

In Fig. 3.6 we compare results from experimental measurement of the momentum distribution and results coming from the *exact approach*, as reported in Fig. 3(a) of Li et al. [192] to the results computed following *our approach* detailed in this chapter. Although about 33% of the tubes of gases in the experiment contain 5 of less particles we see good agreement, with the average temperature being approximately $T = 10nK$. Even though Eq. (3.14) was originally derived for the ground state

of the gas, it stays valid at particle numbers and temperatures relevant to experimental realizations.

The averaged momentum distribution we present in Fig. 3.6 is computed as

$$\langle f(p)\rangle_{\text{tubes}} = \frac{1}{\mathcal{N}} \sum_{N} w_N f_{[N,T_N]}(p), \tag{3.69}$$

with w_N being the number of tubes containing N atoms, and $f_{[N,T_N]}(p)$ is the momentum distribution for a fixed number of atoms N at fixed temperature T_N. We normalize the distribution with a factor $\mathcal{N}$ so that

$$\int \langle f(p)\rangle_{\text{tubes}} dp = 1. \tag{3.70}$$

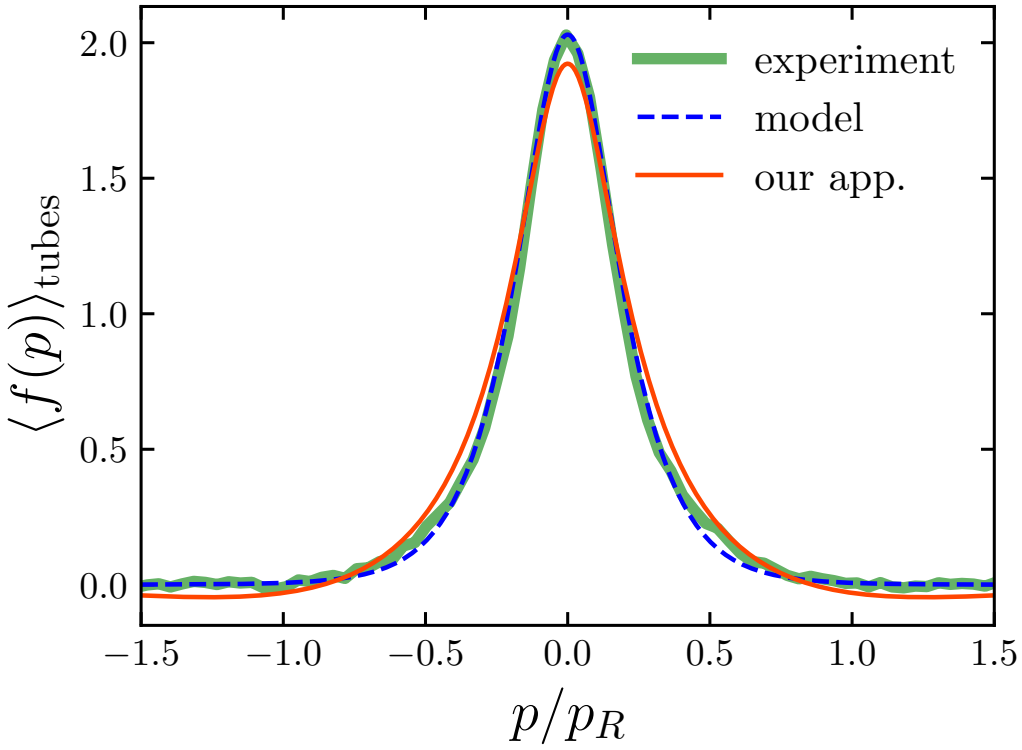


Figure 3.6: Momentum distribution averaged over an array of tubes containing 1D dysprosium gas in the hard-core regime considered in Li et al. [192], with contact interaction strength $c = 263\,\mu\text{m}^{-1}$ and trap frequency $\omega = 36.4$ Hz. We compare the experimental results and results of the *exact approach* presented in Fig. 3(a) of Ref. [192] with the results coming from *our approach*. The values for the momentum are rescaled by the recoil momentum $p_R = 2\pi/741$ nm (for more information about the experimental setup see Ref. [192]). Figure published in [185], reused with permission.

3.4.2 Soft-Core Bosons

We now turn to the discussion of our results in the case of interaction strengths $\gamma \sim \mathcal{O}(1)$. We show the results for the average OPDM and (see Eq. (3.68)) the momentum distribution in Figures 3.7 and 3.8 respectively. We display the results for particle number $N = 50$ in the main panel and show the results for $N = 5$ in the insets. The difference between *our approach* and the *exact results* seems to behave similarly in the case of increasing temperature and in the case of decreasing the number

of particles for all values of interaction strengths. We find that the difference increases slowly as contact interactions decreases. This is expected since the impact of finite temperatures increases with weaker interactions.

Finally we compare our results obtained using *our approach* with experimental results for the momentum distribution at the interaction strength $c = 8.5\,\mu\text{m}^{-1}$ (with an estimated average value of $\gamma = 6.7$, according to Li et al. [192]) and their modeling based on the *exact approach* which were reported in Fig. 3(b) of Ref. [192]. The agreement is good, similar to the hard-core gas, even though approximately $\approx 13\%$ of the tubes averaged over contain 5 or fewer particles and that the average temperature of the gases is ≈ 17 nK.

3.5 Discussion

In this chapter, we introduced a numerical method for obtaining the one particle density matrix and the momentum distribution of trapped one-dimensional Bose gases at finite temperatures for arbitrary (repulsive) strengths of the contact interaction (see Section 3.4). Our methodology is motivated by and is built on previous results obtained for the long-distance asymptotics of the OPDM using inhomogeneous Luttinger liquid theory [49, 73, 74, 85, 122, 143], as well as existing results for the short-distance expansions for the Bose gas [66, 187, 188]. In the limits of weak and infinite interaction strengths, we discussed and derived analytical results for the long-distance asymptotics of the OPDM (the weak interaction limit derived previously in Refs. [76, 77]), where we considered harmonic trapping potential for weak cases and arbitrary potential for the hard-core (infinite) limit. In the cases of finite interaction strengths and temperature values, the Green's functions entering the formula for the long-distance asymptotics of OPDM need to be computed numerically. In section 3.4 we explained in detail our numerical method for obtaining these correlation functions. Using these methods, we then obtained the OPDM for different values of interaction strengths, temperatures, and particle numbers, by using equations Eq. (3.13) for the long-distance and Eq. (3.14) for the short-distance behaviors.

To check the validity of our method we benchmarked our results against exact numerical calculations in the hard-core limit and quantum Monte-Carlo simulations for finite repulsive interaction strengths. We also demonstrated that our framework gives a reliable description of recent experimental observations. This agreement is particularly noteworthy given the small number of particles in many of the one-dimensional clouds of gases studied, as well as the relatively high temperatures involved. These results are encouraging, especially considering that our approach is computationally efficient: the calculations can be performed within minutes on a laptop, whereas quantum Monte Carlo simulations typically demand hundreds of CPU hours and access to high-performance computing clusters.

Another advantage our method offers compared to quantum Monte-Carlo is that it is not limited to describing equilibrium situations. We plan to continue developing this method by determining how accurately it captures the evolution of the momentum distribution in quantum quench scenarios similar to the ones studied in the works [32, 192]. Computing the momentum distribution with currently existing theoretical methods is only possible in the limit of strong interactions, where exact solutions are available [63], and numerical calculations have already been benchmarked against experimental data, showing good agreement [33, 194].

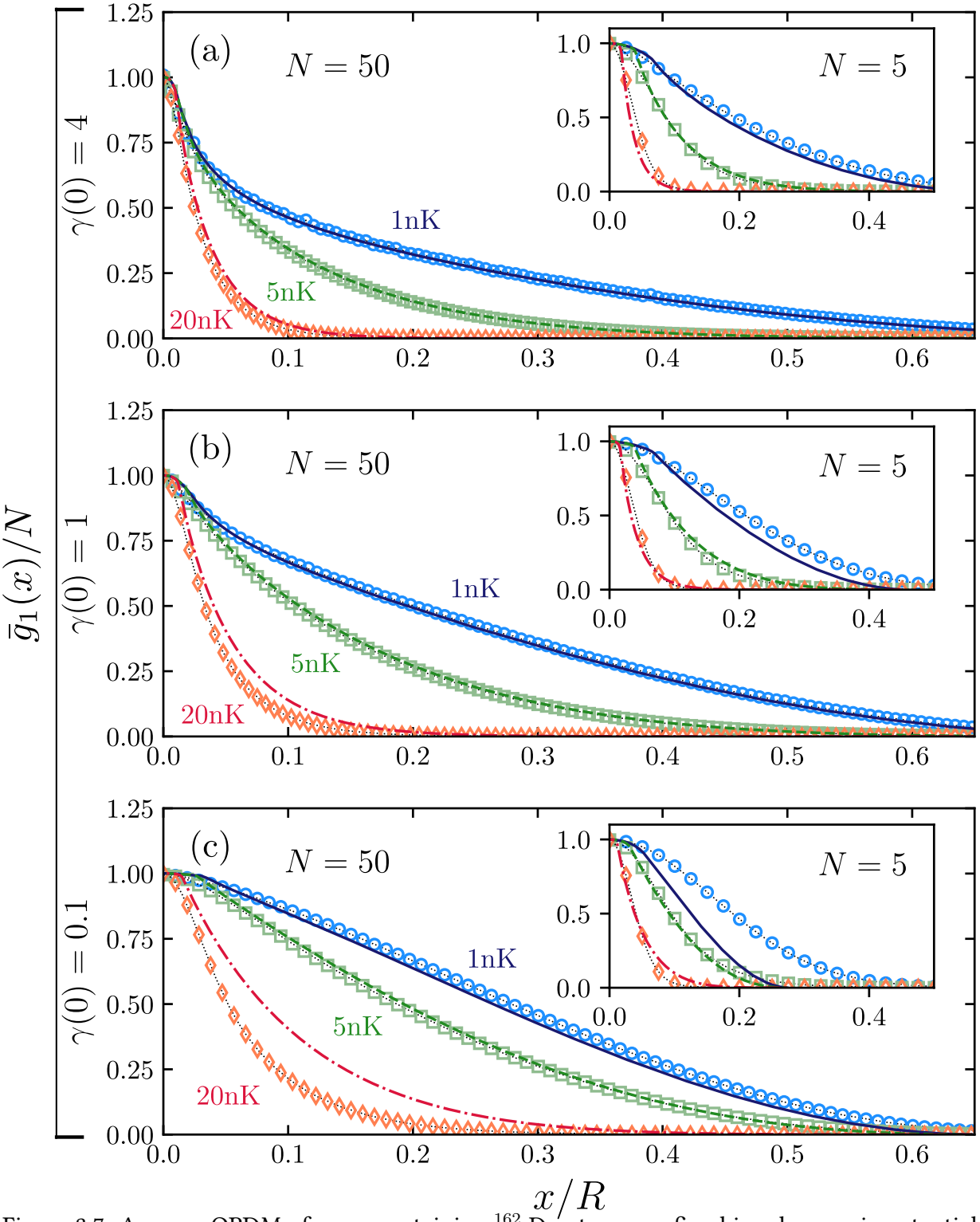


Figure 3.7: Average OPDM of a gas containing ^{162}Dy atoms confined in a harmonic potential trap with frequency 36.4 Hz. The results are plotted for different values of contact interaction, with a) $\gamma(0) = 4$, (b) 1, and (c) 0.1. The main panels display the results for the particle number $N = 50$, while the insets for $N = 5$. Numerical results obtained using quantum Monte Carlo simulations are shown with symbols connected by thin solid lines (in the main text we refer to them as *exact results*). The results of *our approach* of taking the minimum between the result from numerical method detailed in Sec. 3.3 (long-distance asymptotics) and the result from Eq. (3.14) (short-distance expansion) are plotted with thick solid lines. We show results for temperatures $T = 1,\ 5,\ 20$ nK. Figure published in [185], reused with permission.

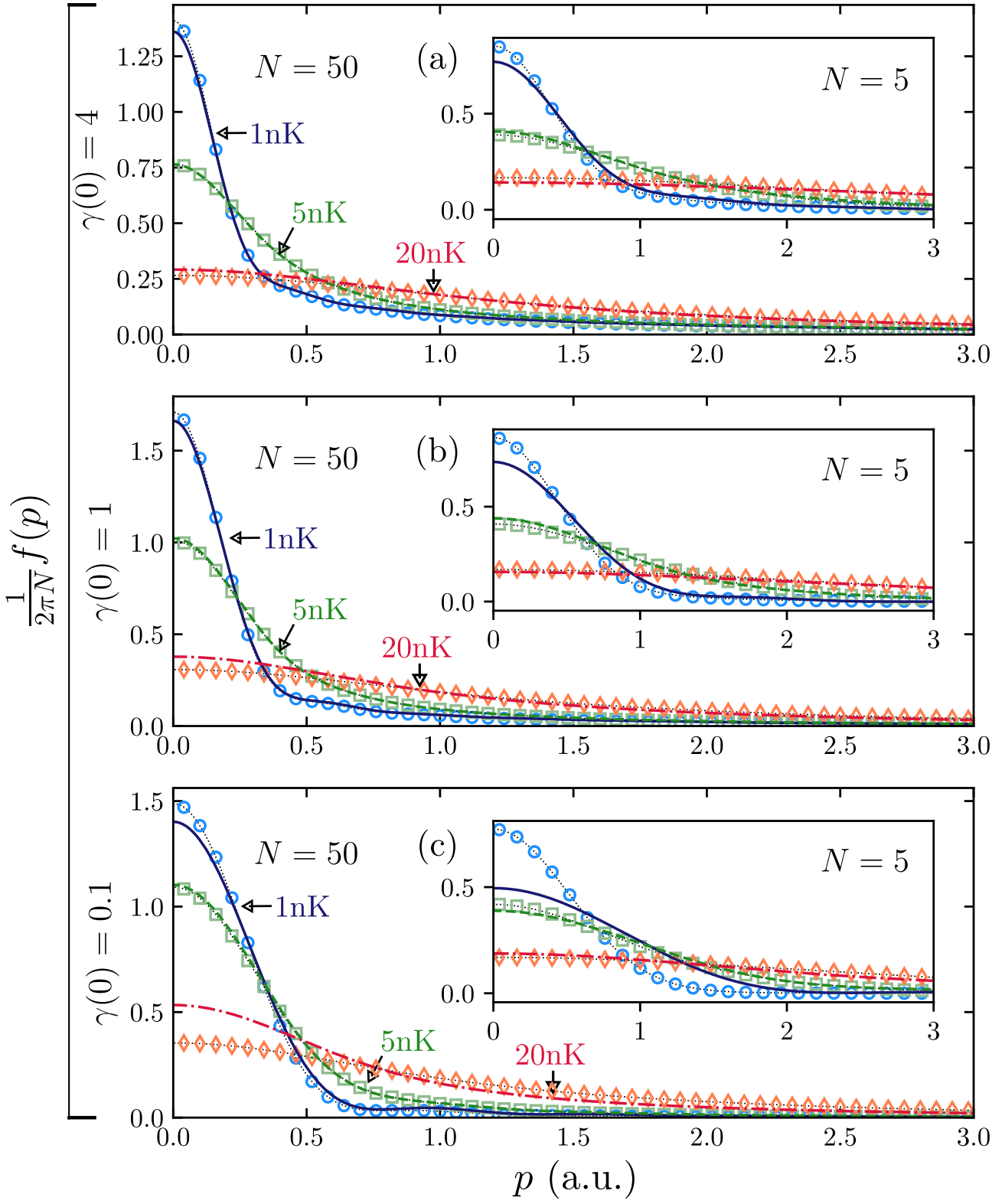


Figure 3.8: The momentum distribution, computed through Fourier transforming the OPDM in Fig. 3.7. Figure published in [185], reused with permission.

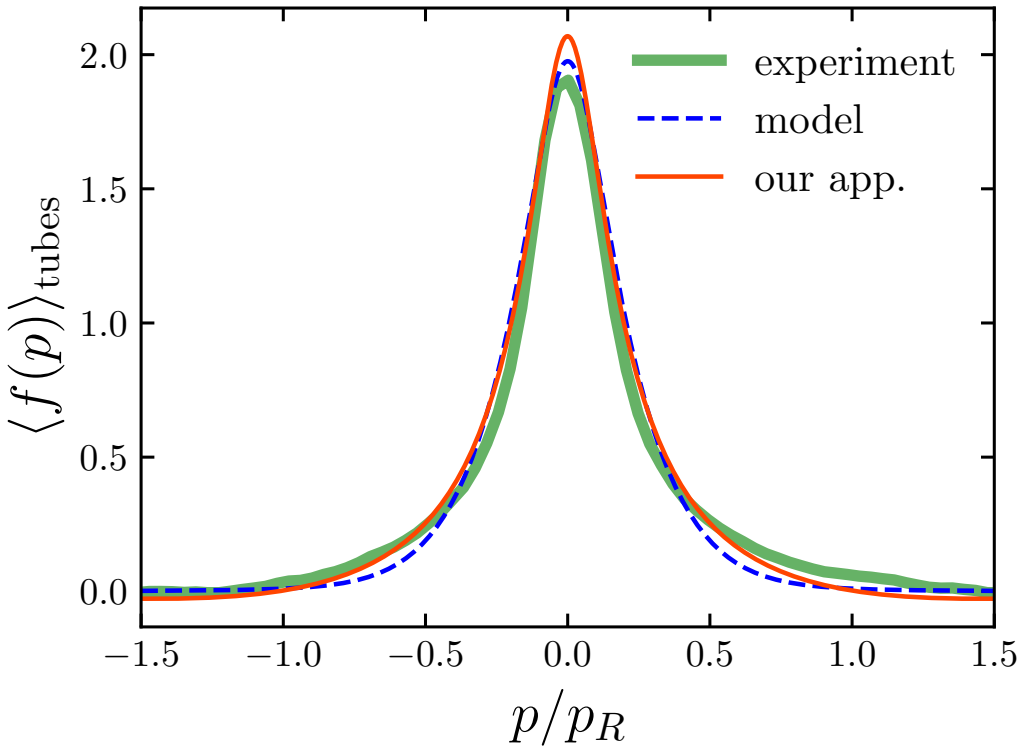


Figure 3.9: Momentum distribution averaged over an array of tubes containing 1D dysprosium gas in the soft-core regime with contact interaction strength $c = 8.5\,\mu\text{m}^{-1}$ and trap frequency $\omega = 36.4$ Hz. We compare the experimental results and results of the *exact approach* presented in Fig. 3(b) of Ref. [192] with the results coming from *our approach*. Figure published in [185], reused with permission.

Chapter 4

Some Preliminary Results

In this part we would like to briefly showcase some preliminary works very closely related to - and building on - the problems and results presented earlier. We start with a short discussion on a project closely related to our results in Chapter 2, where we aim to calculate correlation functions of a Lieb-Liniger gas out-of-equilibrium after a global quench at arbitrary repulsive interaction strength. Then we give a quick motivation for a project on deriving correlation functions for an attractive Lieb-Liniger gas at finite temperature, a natural continuation of the results obtained in Chapter 3.

4.1 Quantum Newton's Cradle of Bose gas

As we have emphasized in this thesis, the out-of-equilibrium behavior of low-dimensional (integrable) quantum systems on large temporal and spatial scales is well described by the theory of Generalized Hydrodynamics constructed in 2016 [1, 2]. The theory gives a semi-classical description of Euler scale dynamics (see Section 1.3) using the continuity equations of conserved quantities emerging from the Bethe Ansatz solution of the system; which remains valid with good approximation in the presence of slowly varying trapping/chemical potentials [62] following the argument of Separation of Scales that allow a Local Density Approximation, leading each mesoscopic fluid cell to be locally relaxed to a state given by quantities of a local Thermodynamic Bethe Ansatz.

To calculate equal-time correlation functions, one must go beyond this semiclassical description and 'requantize' the hydrodynamic theory. In the limit of zero-entropy (see Section 1.3.3), this can be achieved using the framework of Quantum Generalized Hydrodynamics (QGHD) [3, 4, 63, 130] (or through similar approaches [198]). This description incorporates concepts from bosonization and Luttinger liquid theory [48] in order to describe small fluctuations around the zero-entropy state [3, 4] (also see Section 1.5 for a brief overview). For Bose gases in the limit of large contact interaction strength (TG and HCB limits) such descriptions were applied effectively to obtain equal time correlations such as the OPDM [63, 130].

In this section, we present a work-in-progress project that aims to obtain equal time correlations of a Lieb-Liniger gas with finite interaction strength, in the context of a quench protocol inspired by the quantum Newton's Cradle experiment realized in 2006 reported in the work by Kinoshita, Wenger, and Weiss [104]. We begin by reviewing the initial state and quench setup. We then outline our method for computing correlation functions at $t = 0$ and describe the strategy for propagating them in time. We conclude with a summary of our current progress and a brief discussion of the project's future outlook.

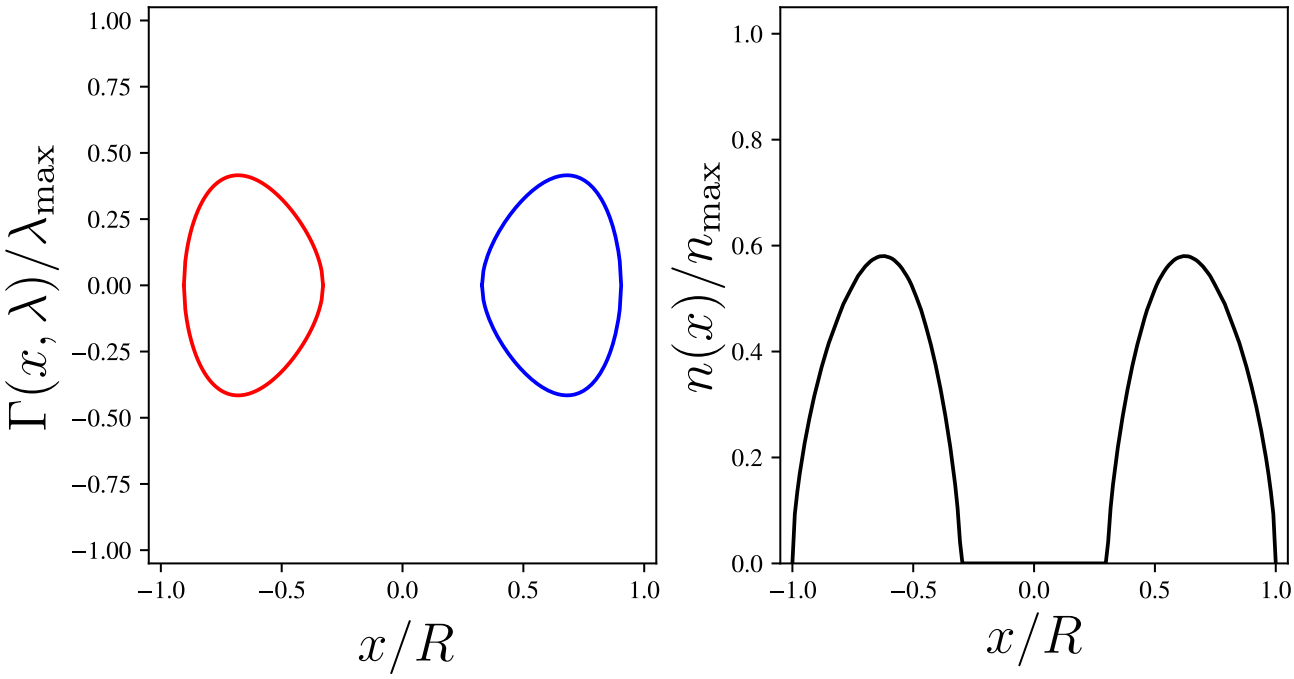


Figure 4.1: Initial state of the two gas clouds in the trapping potential (4.2) before the quench at $t < 0$, for contact interaction $c = 5$, and particle number $N = 20$ (10 for each separate cloud).**Left:** The Fermi contour Γ_t of the two gas clouds (solid red anf blue lines); **Right:** The particle density of the cloud in the initial state.

4.1.1 GHD of trapped Bose gas

We are interested in the dynamics of a Bose gas with contact interaction. We recall that such a system of bosons is described by the Lieb-Liniger Hamiltonian written in Eq. (1.20):

$$\hat{H}_0 = \frac{1}{2}\int_0^L dx\ \hat{\Psi}^\dagger(x)\left[-\partial_x^2 + c\hat{\Psi}^\dagger(x)\hat{\Psi}(x)\right]\hat{\Psi}(x), \tag{4.1}$$

with interaction strength $c > 0$ and $\hat{\Psi}^\dagger(x)/\hat{\Psi}(x)$ bosonic creation/annihilation operators with commutation relations (1.17).

The system is prepared in the LDA groundstate of a double well potential defined as

$$V_0(x) = ax^4 - \frac{1}{2}\omega^2 x^2 + \bar{V}_0 - \mu, \tag{4.2}$$

with μ chemical potential and parameters $a, \bar{V}_0$. As usual in this thesis, we choose $\hbar = 1$, and we also set the mass of the particles to $m = 1$. The chemical potential is fixed in such a way that the particles are in two separated clouds, each containing N particles. For more details on the LDA groundstate of the Lieb-Liniger model in the presence of an arbitrary trapping potential and fixing the chemical potential for given particle number N see Section 1.3.2.

4.1.2 The quench and dynamics

At $t = 0$ we quench to a harmonic potential

$$V(x) = -\frac{1}{2}\omega^2 x^2, \tag{4.3}$$

and look at the time evolution of the system at the Euler scale. Since the system was initialized in a zero-entropy state it stays in a zero entropy state throughout the time evolution, that is given by zero-entropy GHD (see more in Section 1.3.3). Thus parameterizing the Fermi-contour Γ_t as $\Gamma_t = \{(x_t(s), \lambda_t(s)); s \in (0, 2\pi]\}$ the GHD equation is

$$\frac{\mathrm{d}}{\mathrm{d}t}\begin{pmatrix} x_t(s) \\ \lambda_t(s) \end{pmatrix} = \begin{pmatrix} v^{eff}(\lambda_t(s)) \\ -\partial_x V(x_t(s)), \end{pmatrix} \tag{4.4}$$

as in (1.97). Numerical simulation of this equation is straightforward by discretizing the contour, such that every point x_i in space has Fermi points $\{\lambda_j^+(x_i), \lambda_j^-(x_i)\}_{j=1}^q$, where q is the number of split Fermi seas at point x_i, and we introduced the subscript $\pm$ to denote the lower and upper Fermi rapidities. An example of the density profile resulting from such a numerical simulation is shown on Fig. 4.2.

4.1.3 Quantum GHD approach

As we mentioned earlier, our aim in this work is to obtain equal time correlation functions (such as the OPDM) of the gas at a finite interaction strength c as it was done in [3]. The difficulty lies in the fact that, opposite to the case of infinite interaction strengths (TG gas or HCBs) investigated in [63] (or in our work [130] in Section 2.1) where the equations describing the evolution of the small density fluctuations (1.178) decouple, in the case of finite interactions the equations remain complicated. Here we propose a method to effectively time evolve the small density fluctuations and obtain their correlation functions at later times.

The recipe for obtaining equal time correlation functions follows the main idea of QGHD introduced in [3, 4, 63] (or see Section 1.5 for a short introduction) and is as follows. Correlation functions in the ground state can be calculated by bosonization arguments, where small fluctuations around the Fermi sea can be described by an inhomogeneous Luttinger Liquid [48], as reviewed in Section 1.4. The fields $\hat{\phi}(x)$ and $\hat{\theta}(x)$ of the Luttinger liquid can be directly related to the density fluctuations around the ground state. Writing the density profile of the gas in the LDA ground state it is characterized by the upper and lower Fermi rapidities $\lambda^+(x)$,$\lambda^-(x)$:

$$n(x) = \int_{\lambda_-(x)}^{\lambda_+(x)} d\lambda \left(\frac{1}{2\pi}\right)^{\mathrm{dr}} (\lambda, x), \tag{4.5}$$

with the superscript $.^{\mathrm{dr}}$ denoting the dressing operation defined in (1.55). Introducing small fluctuations of the Fermi rapidities $\lambda_\pm(x) \to \lambda_\pm(x) + \delta\lambda_\pm(x)$ for the upper and lower Fermi rapidities respectively, we obtain the excess density $\delta\rho(x)$ in point x as

$$\delta\rho(x) \approx (\delta\lambda_+(x) - \delta\lambda_-(x)) \left(\frac{1}{2\pi}\right)^{dr} (\lambda_+(x)). \tag{4.6}$$

Promoting the density fluctuations to be operators $\delta\rho(x) \to \delta\hat{\rho}(x)$ (and subsequently $\delta\lambda_\pm(x) \to \delta\hat{\lambda}_\pm(x)$) following the prescriptions of QGHD allows us to relate the operators of the Luttinger liquid theory to the density fluctuations, according to (1.104):

$$\delta\hat{\rho}(x) \simeq \frac{1}{2\pi}\partial_x\hat{\phi}(x). \tag{4.7}$$

Using the symmetric nature of the ground LDA ground state around the zero rapidity $\lambda_+(x) = -\lambda_-(x)$, the full momentum of the state has to disappear. This results in an additional relation

$$\delta\lambda_+(x) + \delta\lambda_-(x) = 2\partial_x\hat{\theta}(x), \tag{4.8}$$

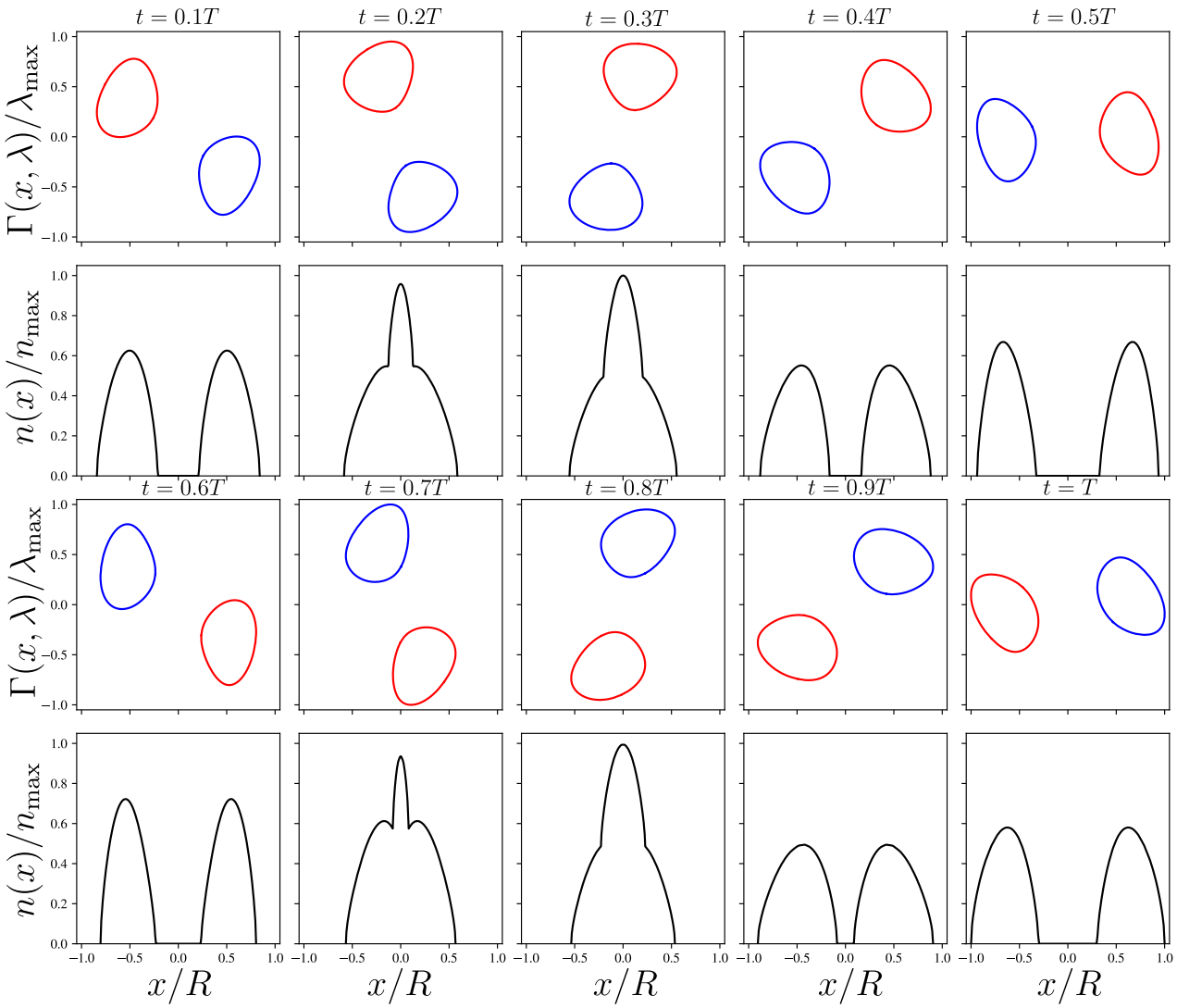


Figure 4.2: Evolution of the Fermi contour $\Gamma(x, \lambda)$ (red and blue line, for each separate gas cloud) from the initial state shown in Fig. 4.1; normalized by the maximal value of Fermi rapidity $\lambda_{\max}$ during the time evolution. The corresponding particle density is plotted below with black solid lines, normalized by the maximal value of density $n_{\max}$ during time evolution. The parameter R normalizing the coordinate is the distance between the edge of the system and $x = 0$ before the quench, and $T = \frac{2\pi}{\omega}$ is the 'classical' period time corresponding to the harmonic trap with frequency ω, and $\gamma_{\min} = \frac{c}{n_{\max}} \simeq 1.46$.

between the fluctuations of the Fermi contour and the operator $\hat{\theta}(x)$ of the Luttinger liquid. This correspondence allows one to obtain groundstate correlation functions of the Bose gas, following the well established formalism of Luttinger liquids [48], giving access to correlation functions such as:

$$\langle \delta\hat{\rho}(x)\delta\hat{\rho}(y)\rangle_0, \tag{4.9}$$

where we introduced the subscript 0 to denote $t = 0$.

4.1.4 Green's function of time evolution

In the infinite interaction limit $c \to \infty$ the time evolution equation obeyed by the small density fluctuations decouple from each other, thus simplifying Equation (1.178), as it was argued in [4] and [63]. In the case of finite interactions we propose a numerical algorithm for obtaining the Green's function for Equation (1.178) in the limit of linear response theory.

Let us discretize the initial contour $\Gamma_0(s)$ to $\Gamma_0(s_i)$ such that

$$\Gamma_0(s_i) = \{(x_0(s_i), \lambda_0(s_i); i = 1, ..., N; s \in (0, 2\pi]\}. \tag{4.10}$$

The discretized contour time evolved using zero-entropy GHD is given as $\Gamma_t(s_i)$ with $t = 1, ..., N$ at time $t > 0$. Let us introduce a contour which we call the perturbed contour $\Gamma_0^j(s_i)$, where we have modified the Fermi rapidity $\lambda_0(s_j) \to \lambda_0(s_j) + \varepsilon$. This corresponds to a small excess density around $x_0(s_j)$ that is

$$\delta\rho_0(s_j) \simeq \Delta_\varepsilon \cdot \left(\frac{1}{2\pi}\right)^{\mathrm{dr}} (\lambda_0(s_j), x_0(s_j)). \tag{4.11}$$

The quantity Δ_ε is the (signed) excess area (positive if $\mathrm{sign}(\varepsilon) = \mathrm{sign}(\lambda_0(s_j))$ and negative otherwise) around the parameter s_j on the contour $\Gamma_0^j(s_i)$. This allows us to define the function $\Delta_\varepsilon(\Gamma_0^j(s_i), \Gamma_0(s_i))$, which calculates this excess area in every point s_i of the discretized contour shown on Fig. 4.3 , and the matrix

$$\mathbf{M}_\varepsilon^0 = \begin{pmatrix} \Delta_\varepsilon(\Gamma_0^1(s_i), \Gamma_0(s_i)) \\ \cdots \\ \Delta_\varepsilon(\Gamma_0^j(s_i), \Gamma_0(s_i)) \\ \cdots \\ \Delta_\varepsilon(\Gamma_0^N(s_i), \Gamma_0(s_i)) \end{pmatrix}. \tag{4.12}$$

Under the zero entropy GHD time evolved perturbed/clean contours are given by $\Gamma_t^j(s_i)/\Gamma_t(s_i)$ respectively. Here we define another matrix

$$\mathbf{M}_\varepsilon^t = \begin{pmatrix} \Delta_\varepsilon(\Gamma_t^1(s_i), \Gamma_t(s_i)) \\ \cdots \\ \Delta_\varepsilon(\Gamma_t^j(s_i), \Gamma_t(s_i)) \\ \cdots \\ \Delta_\varepsilon(\Gamma_t^N(s_i), \Gamma_t(s_i)) \end{pmatrix}, \tag{4.13}$$

which is related to $\mathbf{M}_\varepsilon^0$ defined in (4.12) through

$$\mathbf{M}_\varepsilon^t = \mathbf{G}_\varepsilon(t)\mathbf{M}_\varepsilon^0, \tag{4.14}$$

where

$$\lim_{\varepsilon\to 0} \mathbf{G}_\varepsilon(t) \tag{4.15}$$

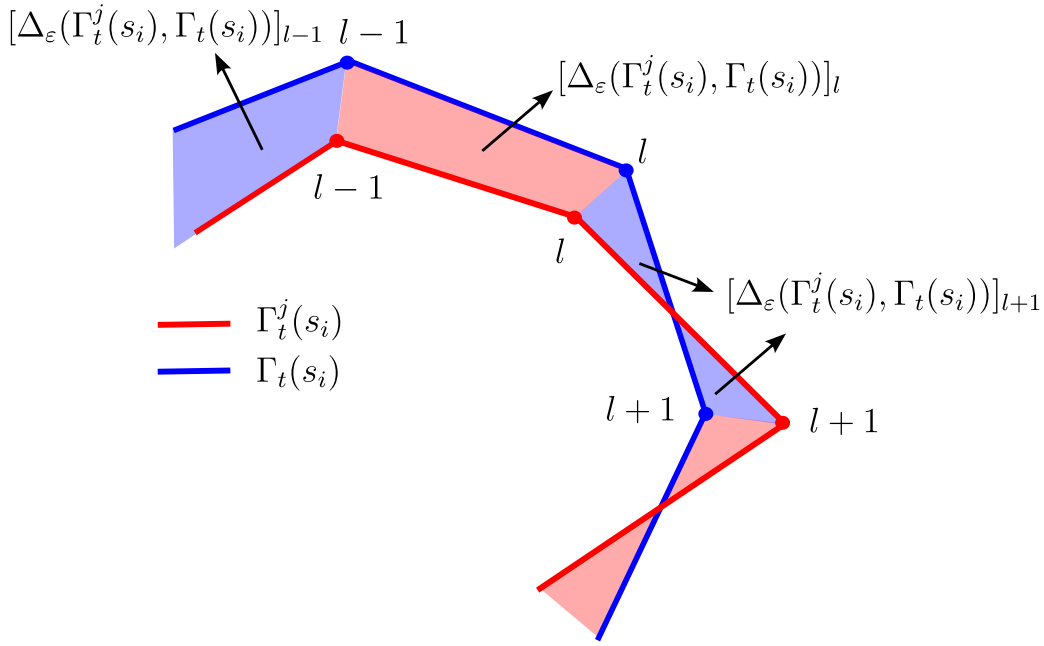


Figure 4.3: Sketch of a possible definition of the quantity $\Delta_\varepsilon(\Gamma_0^j(s_i),\Gamma_0(s_i))$ denoting the excess area between the discretized Fermi contours $\Gamma_t^j(s_i)$ and $\Gamma_t(s_i)$ at every point l. The contours are denoted with solid red and blue lines respectively, while the excess areas between the contours in points $l-1, l$ and $l+1$ are colored with alternating blue and red colors for clarity.

is the discretized Green's function of the evolution of the density fluctuations (1.178) such that

$$\delta\rho_t(s_i) = G_{i,j}(t)\delta\rho_0(s_j), \tag{4.16}$$

allowing the evaluation of correlation functions at time t by

$$\langle\delta\rho_t(s_i)\delta\rho_t(s_j)\rangle = G_{i,l}(t)\langle\delta\rho_0(s_l)\delta\rho_0(s_k)\rangle G_{k,j}(t) \tag{4.17}$$

One of the non-trivial complications of this method comes from the definition of the function $\Delta_\varepsilon(\Gamma(s_i),\Gamma'(s_i))$. The 'differences' between contours are promoted to operators $\delta\rho_t(s_i) \to \delta\hat{\rho}_t(s_i)$ which are then related to bosonic fields $\hat{\phi}(s_i)$ and $\hat{\theta}(s_i)$ from Luttinger liquid theory, thus prescribing non-trivial commutation relations.

4.2 Correlations of the trapped sTG gas at finite temperature

In Chapter 3 we reported a general recipe for constructing correlation functions (namely the one particle density matrix) of a Lieb-Liniger gas for arbitrary trapping potentials temperatures and repulsive interaction strength. We are aiming to extend this framework to the attractive regime of the interaction. This regime in the strong interaction limit $\gamma \ll -1$ is known as the super Tonks-Girardeau limit, and can be experimentally realized by tuning the interaction strength using magnetic fields, as we mentioned in Section 1.2.6. Our aim, similarly to what we discussed in Chapter 3, is to directly compare our results for the OPDM to experimental results.

4.2.1 Density profile at zero temperature

In Fig. 4.4 we show results for the density profile of a Lieb-Liniger gas at different interaction strength, at zero temperature, following [73]. Notice that as we cross to the attractive regime the

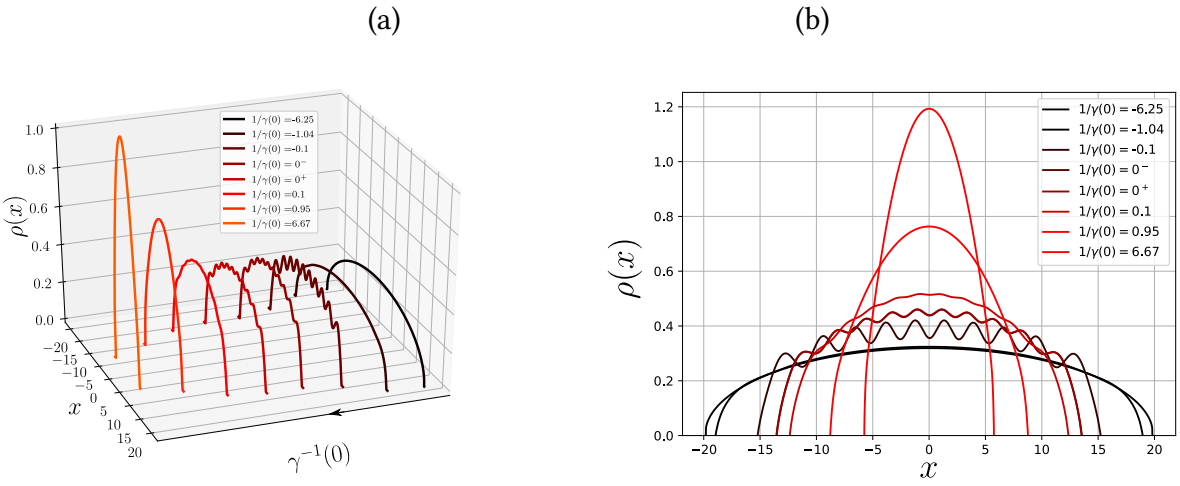


Figure 4.4: Density profiles as a function of the inverse dimensionless interaction strength $1/\gamma$ and spatial coordinates on a 3D plot (a), and the density profiles plotted on a 2D plot as a function of spatial coordinates (b)

oscillations will become more pronounced.

4.2.2 OPDM at finite temperature

In Fig. 4.5 we present some of our results for the long-distance asymptotics of the OPDM in the attractive regime of Lieb-Liniger gas in a harmonic trap, where we compare it to results in the repulsive regime at similar absolute values of dimensionless interaction strength γ. In the near future we aim to compute the momentum distribution and compare these quantities to recent experimental results following the methods outlined in Chapter 3. Obtaining these quantities in the attractive regime of the Lieb-Liniger gas would be a powerful tool, as to the best of our knowledge there is no other theoretical framework that gives access to these quantities.

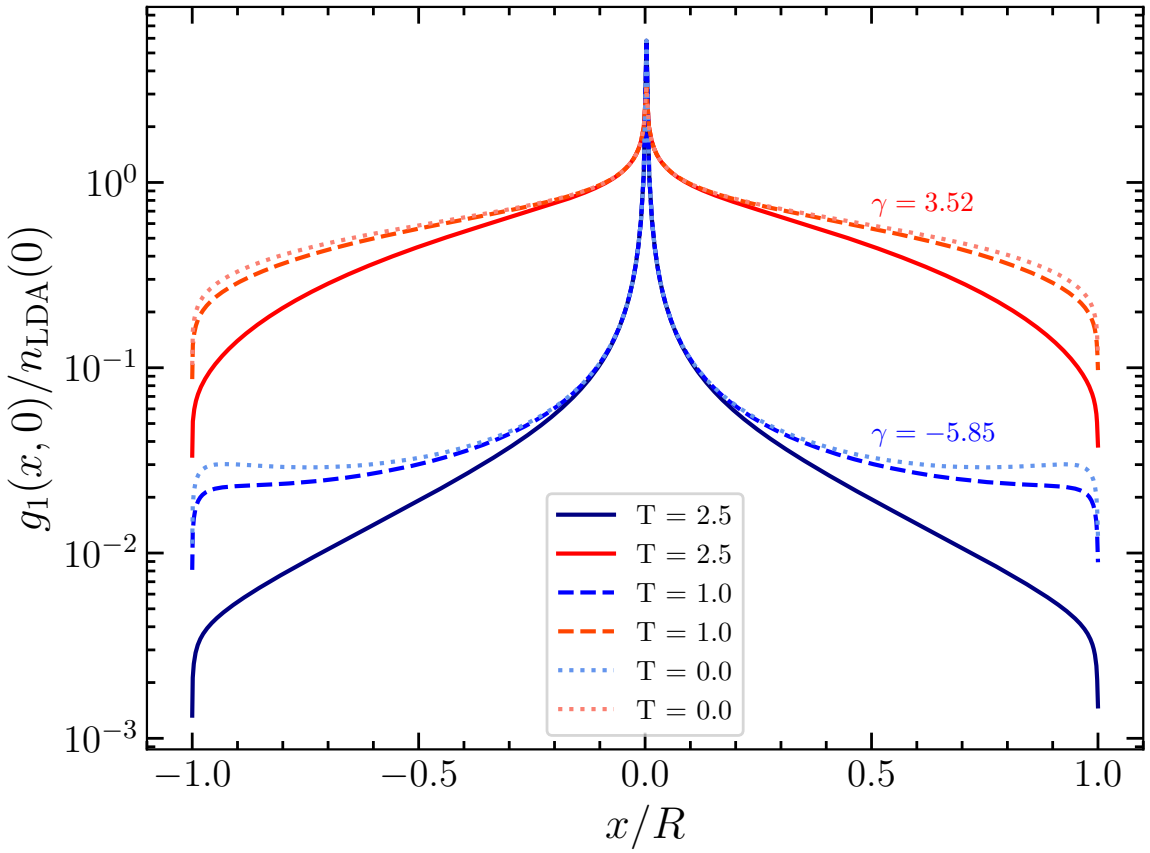


Figure 4.5: Comparison of the long-distance asymptotics of $g_1(x, x')$ for bosons in the attractive regime ($\gamma < 0$) to the repulsive regime ($\gamma > 0$) at similar absolute values of dimensionless interaction strength γ, confined in a harmonic trap $V(x) = \frac{1}{2}\omega x^2$ with frequency $\omega = 1$ and particle number $N = 10$. We plot $g_1(x, x')$ vs x/R (R is the radius of atom cloud) for $x' = 0$ and for different temperatures $T = 0, 1.0$ and 2.5. The temperatures are to be compared with the energy scale $\mathcal{T}^{-1} \simeq 0.17$ and 0.22 of the inhomogeneous Luttinger liquid for the repulsive and attractive cases respectively.

Chapter 5

Conclusion

Throughout this thesis we have studied correlations in 1D Bose gases in- and out-of equilibrium focusing on systems where integrability is broken by the presence of a trapping potential. We have reviewed that in such cases the Local Density Approximation (LDA) provides an approximate description of the ground state of the system. During our work we have also used extensively that the Euler scale out-of equilibrium dynamics of systems that in the translationally invariant case are exactly solvable through the framework of the Bethe Ansatz are described by the theory of Generalized Hydrodynamics (GHD). By applying the theory of Quantum Generalized Hydrodynamics and taking elements from bosonization and Tomonaga-Luttinger liquid theory we obtained one-body correlations and momentum distributions during out-of equilibrium time evolution.

The works presented in **Chapter 2** focus on the dynamics and correlations in hard-core bosons. We present our published work [130], where we derived an exact analytic expression for the OPDM in the Euler scaling limit by applying recent advances in quantum generalized hydrodynamics. We also found that this exact result provided a clear analytical description of two features of the system's evolution: dynamic quasicondensation at intermediate times and emergent fermionization at long times. Moreover, our formula also captured the crossover between these regimes. We validated the analytic predictions through a systematic comparison with exact numerical simulations across various system sizes and time scales, finding excellent agreement throughout. These results and methods open a path toward the computation of the OPDM in more general out-of-equilibrium settings involving one-dimensional HCBs. As a natural extension, we are also working on obtaining correlation functions like the OPDM in systems with finite interaction strength, (as we briefly sketch in Section 4.1). We also presented the results of our investigation of the dynamics of hard-core bosons released from a domain wall initial state in the presence of two conformal defects. Using exact numerical calculations we found that the Euler-scale dynamics differ significantly from the predictions of the standard hydrodynamic description. This discrepancy arises due to quantum interference effects coming from repeated scattering on said defects. We showed that the interference can be qualitatively understood through the analysis of the boson propagators, which we derived and demonstrated that a 'semi-classical' approach can be restored by refining the naive scattering picture. The methodology straightforwardly generalizes to the presence of an arbitrary number of such defects. The results presented here raise very intriguing questions, such as how interference corrections can be incorporated into the already existing hydrodynamic framework used to describe the dynamics of such systems. Furthermore, the computation of correlation functions and quantities such as bipartite entanglement remain a challenge.

In **Chapter 3** we discuss our results on computing one-particle correlation functions in trapped Bose gases at finite temperatures and arbitrary (repulsive) interaction strengths. In the limits of

weak interaction strength in a harmonic trap and strong interaction for arbitrary trapping potential we derived analytical results. In the case of arbitrary interactions we introduced a numerical method for obtaining the OPDM and the momentum distribution, valid for finite temperatures. We benchmarked our results against exact numerics (quantum Monte-Carlo) and recent experimental results, demonstrating that our framework gives a reliable description of recent experimental observations. These results are encouraging, especially considering that our approach is computationally efficient compared to other existing theoretical methods such as the quantum Monte Carlo. The methods described here also very exciting as -compared to quantum Monte-Carlo- they are not limited to equilibrium scenarios. We are working on extending this framework to describe correlations in out-of equilibrium setups as well as in the attractive regime (sTG) of the Lieb-Liniger gas. The results of this chapter have been published in our work [185].

Chapter 4 provides an outlook to the results reported in Chapters 2 and 3. In it, we talk about the natural continuation of our work. Namely, extending our description of the dynamics of correlation functions in a bosonic gas to finite repulsive interaction strengths through the framework of quantum generalized hydrodynamics, as well as extending our description of the correlation of trapped Bose gases at finite temperatures to the attracive interaction regime.

The results and methods discussed in this thesis further our understanding of equal time correlations of Bethe Ansatz integrable systems out-of-equilibrium, and the effect of finite temperature on these quantities. We used and further developed already existing methodologies and frameworks allowing their application to more complex systems and dynamics. Some of our goals include the extension of the finite temperature description to the attractive Bose gas commonly referred to as the super Tonks-Girardeau gas, where - to the best of our knowledge - no other theoretical tool exists that enables the calculation of correlation functions in- or out- of equilibrium.

We are also interested in further developing the theory of quantum Generalized Hydrodynamics by applying them to compute correlations and entanglement in Lieb-Liniger gases with arbitrary interaction strengths (attractive or repulsive), as well as other, more complicated Bethe-integrable systems, such as Heisenberg spin chains.

Appendix A

The numerical factor $B_\eta(\{k_a\})$ for Hard core bosons in a free expansion

A.1 The numerical factor $B_\eta(\{k_a\})$

Here we explain how to derive Eq. (2.60). The numerical coefficients $B_\eta(\{k_a\})$ can be extracted from the thermodynamic limit of the finite-size form factors of the operator $\hat{\sigma}^-_x$, as explained in detail in Refs. [73, 81, 82, 122, 150] (and briefly mentioned in Section 1.4.4):

$$B_\eta(\{k_a\}_{1\le a\le 2Q}) = \lim_{L\to\infty} \left(\frac{L}{2\pi}\right)^{\Delta_\eta} \left|\langle\{q_i^\eta\}_{i=1}^{N-1}| \,\hat{\sigma}^-_x\, |\{p_j\}_{j=1}^N\rangle\right|, \tag{A.1}$$

for carefully chosen eigenstates $\left|\{p_j\}_{j=1}^N\right\rangle$ and $\left|\{q_i^\eta\}_{i=1}^{N-1}\right\rangle$ of the Hamiltonian (2.3) for L spins with periodic boundary conditions. For convenience, in this section we label the sites of the chain by integers $x = 0, \dots, L-1$ (as opposed half-integers in the rest of the paper). This convention can affect the phase of the matrix element $\langle\{q_i^\eta\}_{i=1}^{N-1}| \,\hat{\sigma}^-_x\, |\{p_j\}_{j=1}^N\rangle$, but since we are interested only in its modulus in Eq. (A.1), this does not change the result, and it simplifies the formulas below. Here the eigenstates are normalized, $\langle\{p_j\}\rangle\,\{p_j\} = \langle\{q_i^\eta\}\rangle\,\{q_i^\eta\} = 1$.

All the eigenstates $|\{p_j\}\rangle$ are easily constructed using the fermionic form of the Hamiltonian (2.5): they are obtained by creating fermions with rapidities p_a over the vacuum $|0\rangle$,

$$\left|\{p_j\}_{j=1}^N\right\rangle \;:=\; \hat{c}^\dagger(p_1)\dots\hat{c}^\dagger(p_N)\,|0\rangle\,, \tag{A.2}$$

where $\hat{c}^\dagger(p) = \frac{1}{\sqrt{L}}\sum_{x=0}^{L-1} e^{ipx}\hat{c}^\dagger_x$; notice that $\hat{c}^\dagger(p)$ has normalization $1/\sqrt{L}$ due to the finite size. Crucially, the set of allowed momenta depends on the parity of the number of bosons N,

$$\begin{array}{ll} N \text{ even}: & p\in\{-\frac{2\pi}{L}\frac{L-1}{2}, -\frac{2\pi}{L}\frac{L-3}{2}, \dots, \frac{2\pi}{L}\frac{L-3}{2}, \frac{2\pi}{L}\frac{L-1}{2}\} \\ N \text{ odd}: & p\in\{-\frac{2\pi}{L}\frac{L}{2}, -\frac{2\pi}{L}\frac{L-2}{2}, \dots, \frac{2\pi}{L}\frac{L-4}{2}, \frac{2\pi}{L}\frac{L-2}{2}\}, \end{array} \tag{A.3}$$

where we are assuming that the number of sites L is even. This is a well-known consequence of the Jordan-Wigner transformation from the boson Hamiltonian (2.3) to the free fermion one (2.5) for finite length L. While the bosons always obey periodic boundary conditions (b.c.), the fermions have anti-periodic b.c. if N is even, and periodic b.c. if N is odd.

Now, let us assume that N is odd. In formula (A.1), a specific choice is made for the eigenstate $\left|\{p_j\}_{j=1}^N\right\rangle$ which depends on the set of Fermi momenta $\{k_a\}_{1\le a\le 2Q}$ in the l.h.s of (A.1). This eigenstate is a finite-size realization of a 'split Fermi sea' or 'Moses state' [199], defined by the following

set of rapidities:

$$\{p_j\}_{j=1}^{N} := ([k_1,k_2]\cup[k_3,k_4]\cup\cdots\cup[k_{2Q-1},k_{2Q}])\cap \\ \cap\{-\frac{2\pi}{L}\frac{L}{2},-\frac{2\pi}{L}\frac{L-2}{2},\ldots,\frac{2\pi}{L}\frac{L-4}{2},\frac{2\pi}{L}\frac{L-2}{2}\}. \tag{A.4}$$

Here we are simply assuming that this is consistent with N being odd, and, for convenience, we define the number of fermions in each component of the split Fermi sea, $N_1, N_2, \ldots, N_Q$, such that

$$\begin{aligned} p_1,\ldots,p_{N_1} &\in [k_1,k_2],\\ p_{N_1+1},\ldots,p_{N_2} &\in [k_3,k_4],\\ &\cdots\\ p_{N_{Q-1}+1},\ldots,p_{N_Q} &\in [k_{2Q-1},k_{2Q}]. \end{aligned}$$

The other eigenstate in Eq. (A.1), $\left|\{q_i^\eta\}_{i=1}^{N-1}\right\rangle$, must contain $N-1$ particles, and this is an even number (because N is assumed to be odd). Therefore its rapidities must live in the other set in Eq. (A.3). A minimal way of constructing such an eigenstate starting from the set $\{p_j\}_{j=1}^{N}$ is to select a sequence $\eta=(\eta_a)_{1\le a\le 2Q}$ such that

$$\eta_a=\pm\frac{1}{2},\qquad \sum_{a=1}^{2Q}\eta_a=1, \tag{A.5}$$

and choose its set of rapidities as

$$\{q_i^\eta\}_{i=1}^{N-1} := \left\{k_1+\frac{2\pi\eta_1}{L},k_1+\frac{2\pi\eta_1}{L}+\frac{2\pi}{L},\ldots,k_2-\frac{2\pi\eta_2}{L}\right\}\cup \\ \cup\left\{k_3+\frac{2\pi\eta_3}{L},\ldots,k_4-\frac{2\pi\eta_4}{L}\right\}\cup\cdots\cup\left\{k_{2Q-1}+\frac{2\pi\eta_{2Q-1}}{L},\ldots,k_{2Q}-\frac{2\pi\eta_{2Q}}{L}\right\}. \tag{A.6}$$

The idea is that the eigenstate $|\{q_i\}_{i=1}^{N-1}\rangle$ obtained from this 'minimal' modification of the rapidities in the eigenstate $|\{p_j\}_{j=1}^{N-1}\rangle$ corresponds precisely to the lowest possible excitations around the split Fermi sea $\{k_a\}_{1\le a\le 2Q}$ in the thermodynamic limit $L\to\infty$. Formulas (A.5)-(A.6) define the eigenstates entering in Eq. (A.1).

Now let us turn to the matrix element $\langle\{q_i^\eta\}_{i=1}^{N-1}|\,\hat\sigma_x^-\,|\{p_j\}_{j=1}^{N}\rangle$ in Eq. (A.1). The absolute value of that matrix element is independent of x because both eigenstates are eigenvectors of the lattice translation operator. Therefore we can choose x to be on the leftmost site of the chain ($x=0$ in our conventions) so that, under the Jordan-Wigner transformation, one simply has $\hat\sigma_0^-=\hat c_0$. Then the matrix element can be expressed as

$$\langle\{q_a^\eta\}_{a=1}^{N-1}|\,\hat\sigma_{1/2}^-\,|\{p_b\}_{b=1}^{N}\rangle=\langle 0|\,\hat c(q_{N-1}^\eta)\ldots\hat c(q_1^\eta)\hat c_{1/2}\hat c^\dagger(p_1)\ldots\hat c^\dagger(p_N)\,|0\rangle\,. \tag{A.7}$$

Then the key step in the calculation is to observe that, for rapidities p and q belonging to the two different sets (A.3), the fermion annihilation operators are related through

$$\hat c(p)=\frac{1}{L}\sum_q\frac{2}{2i\sin\left(\frac{p-q}{2}\right)}\hat c(q). \tag{A.8}$$

Then we use $\hat c_0=\frac{1}{\sqrt{L}}\sum_p\hat c_p$, and we apply Wick's theorem to express the matrix element (A.7) as a

determinant,

$$\langle\{q_a^\eta\}_{a=1}^{N-1}|\,\hat{\sigma}^-_{1/2}\,|\{p_b\}_{b=1}^{N}\rangle = \begin{vmatrix} \frac{1}{\sqrt{L}} & \frac{2}{2Li\sin\left(\frac{p_1-q_1^\eta}{2}\right)} & \cdots & \frac{2}{2Li\sin\left(\frac{p_1-q_{N-1}^\eta}{2}\right)} \\ \frac{1}{\sqrt{L}} & \frac{2}{2Li\sin\left(\frac{p_2-q_1^\eta}{2}\right)} & \cdots & \frac{2}{2Li\sin\left(\frac{p_2-q_{N-1}^\eta}{2}\right)} \\ \vdots & \vdots & \ddots & \vdots \\ \frac{1}{\sqrt{L}} & \frac{2}{2Li\sin\left(\frac{p_N-q_1^\eta}{2}\right)} & \cdots & \frac{2}{2Li\sin\left(\frac{p_N-q_{N-1}^\eta}{2}\right)} \end{vmatrix}. \tag{A.9}$$

The latter $N\times N$ determinant can be turned into a Cauchy determinant by adding a rapidity q_0^η to the set $\{q_i^\eta\}_{i=1}^{N-1}$, which one then sends to infinity as follows:

$$\lim_{q_0^\eta\to i\infty}\frac{\sqrt{L}}{2}e^{-iq_0^\eta/2}\begin{vmatrix} \frac{2}{2Li\sin\left(\frac{p_1-q_0^\eta}{2}\right)} & \frac{2}{2Li\sin\left(\frac{p_1-q_1^\eta}{2}\right)} & \cdots & \frac{2}{2Li\sin\left(\frac{p_1-q_{N-1}^\eta}{2}\right)} \\ \frac{2}{2Li\sin\left(\frac{p_2-q_0^\eta}{2}\right)} & \frac{2}{2Li\sin\left(\frac{p_2-q_1^\eta}{2}\right)} & \cdots & \frac{2}{2Li\sin\left(\frac{p_2-q_{N-1}^\eta}{2}\right)} \\ \vdots & \vdots & \ddots & \vdots \\ \frac{2}{2Li\sin\left(\frac{p_N-q_0^\eta}{2}\right)} & \frac{2}{2Li\sin\left(\frac{p_N-q_1^\eta}{2}\right)} & \cdots & \frac{2}{2Li\sin\left(\frac{p_N-q_{N-1}^\eta}{2}\right)} \end{vmatrix}. \tag{A.10}$$

Our matrix element is then

$$\begin{aligned}\langle\{q_a^\eta\}_{a=1}^{N-1}|\,\hat{\Psi}(0)\,|\{p_b\}_{b=1}^{N}\rangle &= \frac{\sqrt{L}}{2}\lim_{q\to i\infty}e^{-iq/2}\det\left(\left[\frac{2}{2Li\sin\left(\frac{p_a-q_b^\eta}{2}\right)}\right]_{1\le a\le N,0\le b\le N-1}\right) \\ &= \frac{\sqrt{L}}{2}\lim_{q\to i\infty}e^{-iq/2}\frac{2^N}{L^N}\frac{\prod_{1\le a<b\le N}2i\sin\left(\frac{p_a-p_b}{2}\right)\prod_{1\le c<d\le N}2i\sin\left(\frac{q_a^\eta-q_b^\eta}{2}\right)}{\prod_{1\le i\le N}\prod_{1\le j\le N}2i\sin\left(\frac{p_i-q_j^\eta}{2}\right)},\end{aligned} \tag{A.11}$$

leading to the final result for the modulus of the matrix element:

$$\left|\langle\{q_i^\eta\}_{i=1}^{N-1}|\,\hat{\Psi}(0)\,|\{p_j\}_{j=1}^{N}\rangle\right| = \frac{2^{N-1}}{L^{N-\frac{1}{2}}}\frac{\prod_{1\le a<b\le N}\left|2\sin\left(\frac{p_a-p_b}{2}\right)\right|\prod_{1\le c<d\le N-1}\left|2\sin\left(\frac{q_c^\eta-q_d^\eta}{2}\right)\right|}{\prod_{i=1}^{N}\prod_{j=1}^{N-1}\left|2\sin\left(\frac{p_i-q_j^\eta}{2}\right)\right|}. \tag{A.12}$$

We then arrive at the following expression for the numerical factor $B_\eta(\{k_a\})$,

$$B_\eta(\{k_a\}_{1\le a\le 2Q}) = \lim_{L\to\infty}\left(\frac{L}{2\pi}\right)^{\frac{Q}{4}}\frac{2^{N-1}}{L^{N-\frac{1}{2}}}\frac{\prod_{1\le a<b\le N}\left|2\sin\left(\frac{p_a-p_b}{2}\right)\right|\prod_{1\le c<d\le N-1}\left|2\sin\left(\frac{q_c^\eta-q_d^\eta}{2}\right)\right|}{\prod_{i=1}^{N}\prod_{j=1}^{N-1}\left|2\sin\left(\frac{p_i-q_j^\eta}{2}\right)\right|}. \tag{A.13}$$

It is this formula which we use to arrive at the final expression (2.60) for the numerical factors. To evaluate the limit, we rely on the asymptotic formula (A.15) presented in detail in A.2. This asymptotic formula directly leads to our final result (2.60).

A.2 Two conjectures about asymptotic limits of products used

In the previous Section text we use the asymptotic formula Eq. (A.15) to compute the numerical factors $B_\eta(\{k_a\})$, see paragraph A. Here we explain where the asymptotic formulas (A.14) and (A.15)

come from. We have not been able to prove these two formulas beyond the special case $Q = 1$, but we have performed extensive numerical checks, and we provide a physical intuition based on electrostatics that strongly supports them.

A.2.1 Conjecture 1.

Let $K_1 < K_2 < \cdots < K_{2Q}$ be integers, and $\eta_j = \pm\frac{1}{2}$ for $j = 1, \ldots, 2Q$. Let us consider the set of integers

$$\mathcal{I} := \mathbb{Z} \cap ([K_1, K_2] \cup [K_3, K_4] \cup \cdots \cup [K_{2Q-1}, K_{2Q}])$$

and the set of half-integers

$$\mathcal{J} := (\mathbb{Z} + \frac{1}{2}) \cap ([K_1 + \eta_1, K_2 - \eta_2] \cup [K_3 + \eta_3, K_4 - \eta_4] \cup \cdots \cup [K_{2Q-1} + \eta_{2Q-1}, K_{2Q} - \eta_{2Q}]).$$

The cardinals of these two sets are $|\mathcal{I}| = \sum_{j=1}^{2Q}(K_{2j} - K_{2j-1} + 1)$ and $|\mathcal{J}| = \sum_{j=1}^{2Q}(K_{2j} - K_{2j-1} + 1 - \eta_{2j} - \eta_{2j-1})$.

Then we have the following asymptotic formula when all the K_j's are large:

$$\frac{\prod_{a<b\in\mathcal{I}} |b-a| \prod_{c<d\in\mathcal{J}} |d-c|}{\prod_{i\in\mathcal{I}, j\in\mathcal{J}} |i-j|} \simeq \left(\frac{G(3/2)}{\pi^{1/4}}\right)^{2Q} \sqrt{\pi}^{|\mathcal{I}|+|\mathcal{J}|} \prod_{1\le a<b\le 2Q} |K_b - K_a|^{\eta_a \eta_b}. \tag{A.14}$$

Here the notation '$\simeq$' means that the ratio of the l.h.s and the r.h.s goes to one in the limit $|K_1|, |K_2|, \ldots, |K_{2Q}| \to \infty$, keeping the ratios K_2/K_1, K_3/K_1 etc. fixed.

A.2.2 Conjecture 2.

Let $K_1 < K_2 < \cdots < K_{2Q} < L$ be integers, and $\eta_j = \pm\frac{1}{2}$ for $j = 1, \ldots, 2Q$. Let $\mathcal{I}$ and $\mathcal{J}$ be defined exactly as in Conjecture 1.

Then we have the following asymptotic formula when all the K_j's and L are large:

$$\begin{aligned}&\frac{\prod_{a<b\in\mathcal{I}} |\frac{L}{\pi}\sin\frac{\pi(b-a)}{L}| \prod_{c<d\in\mathcal{J}} |\frac{L}{\pi}\sin\frac{\pi(d-c)}{L}|}{\prod_{i\in\mathcal{I}, j\in\mathcal{J}} |\frac{L}{\pi}\sin\frac{\pi(j-i)}{L}|} \\ &\simeq \left(\frac{G(3/2)}{\pi^{1/4}}\right)^{2Q} \sqrt{\pi}^{|\mathcal{I}|+|\mathcal{J}|} \prod_{1\le a<b\le 2Q} \left|\frac{L}{\pi}\sin\frac{\pi(K_b - K_a)}{L}\right|^{\eta_a\eta_b}.\end{aligned} \tag{A.15}$$

A.2.3 Physical argument supporting the two conjectures.

Let us start with the first conjecture. The product is equal to the 2D Coulomb energy of a set of charges placed along a line:

$$\frac{\prod_{a<b\in\mathcal{I}} |b-a| \prod_{c<d\in\mathcal{J}} |d-c|}{\prod_{i\in\mathcal{I}, j\in\mathcal{J}} |i-j|} = \exp(-E) \tag{A.16}$$

where

$$\begin{aligned}E &= -\sum_{a<b\in\mathcal{I}} \log|a-b| - \sum_{c<d\in\mathcal{I}} \log|c-d| + \sum_{i\in\mathcal{I}, j\in\mathcal{J}} \log|i-j| \\ &= \frac{1}{2} dx\, dy\, (\rho_{\mathcal{I}}(x) - \rho_{\mathcal{J}}(x))(\rho_{\mathcal{I}}(y) - \rho_{\mathcal{J}}(y))(-\log|x-y|),\end{aligned}$$

with $\rho_{\mathcal{I}}(x) := \sum_{i\in\mathcal{I}} \delta(x-i)$ and $\rho_{\mathcal{J}}(x) := \sum_{j\in\mathcal{J}} \delta(x-j)$. The integral needs to be properly regulated when $x = y$, hence the notation ''. Now, the point is that in the limit of large K_j's, we may view $\rho_{\mathcal{I}}(x)$ and $\rho_{\mathcal{J}}(x)$ as continuous densities of charges. Inside all intervals $[K_j, K_{j+1}]$ these continuous densities are the same, except at the boundary points where they differ by $\pm\eta_j$. Namely, we have

$$\rho_{\mathcal{I}}(x) - \rho_{\mathcal{J}}(x) \simeq \sum_{j=1}^{2Q} \eta_j \delta(x - K_j). \tag{A.17}$$

In other words, at large scale the system of 'positive' charges in $\mathcal{I}$ and 'negative' charges in $\mathcal{J}$ looks neutral, except at the boundary points K_j where there is a 'residual' charge η_j. Thus, the Coulomb energy of the full set of charges is dominated by the Coulomb energy of those residual charges. Moreover, because of the short-distance regularisation of the integral when $x = y$, we expect to have a first subleading contribution to the Coulomb energy proportional to the length of the intervals, then a second subleading correction of order $O(1)$ associated with each boundary point, and then corrections that go to zero in the limit of large K_j's. In summary, in that limit we expect to have

$$E = \sum_{1\le i<j\le 2Q} -\eta_i\eta_j \log|K_i - K_j| + D_0 \frac{|\mathcal{I}| + |\mathcal{J}|}{2} + \sum_{j=1}^{2Q} D_{\eta_j} + o(1) \tag{A.18}$$

where D_0, $D_{1/2}$ and $D_{-1/2}$ are three unknown constants, and $o(1)$ are subleading terms that go to zero. Here we choose to write the total length of the intervals as $(|\mathcal{I}| + |\mathcal{J}|)/2$, but one could write it differently, for instance simply as $|\mathcal{I}|$, or as $|\mathcal{J}|$. These different choices would lead to differences of terms of order $O(1)$ that can be absorbed in a redefinition of the constants $D_{1/2}$ and $D_{-1/2}$.

This physical argument then leads to the conclusion that the product should behave as

$$\frac{\prod_{a<b\in\mathcal{I}} |b-a| \prod_{c<d\in\mathcal{J}} |d-c|}{\prod_{i\in\mathcal{I},j\in\mathcal{J}} |i-j|} \simeq \prod_{1\le i<j\le 2Q} |K_i - K_j|^{\eta_i\eta_j} \, (e^{-D_0/2})^{|\mathcal{I}|+|\mathcal{J}|} \prod_{j=1}^{2Q} e^{-D_{\eta_j}}. \tag{A.19}$$

The constants D_0, $D_{1/2}$ and $D_{-1/2}$ still need to be fixed. But, importantly, these constants are independent of the K_j's and η_j's.

Now let us turn to the second conjecture. The product is still equal to the 2D electrostatic energy of a distribution of charges in the plane, but this time along a circle of diameter L/π,

$$\frac{\prod_{a<b\in\mathcal{I}} |\frac{L}{\pi}\sin\frac{\pi(b-a)}{L}| \prod_{c<d\in\mathcal{J}} |\frac{L}{\pi}\sin\frac{\pi(d-c)}{L}|}{\prod_{i\in\mathcal{I},j\in\mathcal{J}} |\frac{L}{\pi}\sin\frac{\pi(j-i)}{L}|} = e^{-E'} \tag{A.20}$$

with

$$E' = -\sum_{a<b\in\mathcal{I}} \log|z_a - z_b| - \sum_{c<d\in\mathcal{J}} \log|z_c - z_d| + \sum_{i\in\mathcal{I},j\in\mathcal{J}} \log|z_i - z_j|, \tag{A.21}$$

where we use the following notation,

$$z_n = \frac{L}{2\pi} e^{i\frac{2\pi}{L}n} \in \mathbb{C}. \tag{A.22}$$

Then, by the same argument as above, in the limit of large K_j's and L, keeping all ratios of length fixed, we expect the Coulomb energy to be dominated by the residual charges at the endpoints of the support of the charge distribution. We also expect to have a subleading extensive term proportional to the total length $(|\mathcal{I}| + |\mathcal{J}|)/2$ and a term of order $O(1)$ for each endpoint. The latter two terms should involve the same constants D_0, $D_{1/2}$, $D_{-1/2}$ as in conjecture 1, because they are local

contribution, insensitive to the global geometry of the distribution of the charges. In conclusion, we expect

$$E' = \sum_{1\leq i<j\leq 2Q} -\eta_i\eta_j \log|z_{K_i} - z_{K_j}| + D_0\frac{|\mathcal{I}| + |\mathcal{J}|}{2} + \sum_{j=1}^{2Q} D_{\eta_j} + o(1) \tag{A.23}$$

and thus

$$\begin{aligned}&\frac{\prod_{a<b\in\mathcal{I}}|\frac{L}{\pi}\sin\frac{\pi(b-a)}{L}|\prod_{c<d\in\mathcal{J}}|\frac{L}{\pi}\sin\frac{\pi(d-c)}{L}|}{\prod_{i\in\mathcal{I},j\in\mathcal{J}}|\frac{L}{\pi}\sin\frac{\pi(j-i)}{L}|}\\ &\simeq \prod_{1\leq i,j\leq 2Q}\left|\frac{L}{\pi}\sin\frac{\pi(K_i-K_j)}{L}\right|^{\eta_i\eta_j}(e^{-D_0/2})^{|\mathcal{I}|+|\mathcal{J}|}\prod_{j=1}^{2Q}e^{-D_{\eta_j}}\end{aligned} \tag{A.24}$$

with the same constants D_0, $D_{1/2}$ and $D_{-1/2}$ as above.

A.2.4 Fixing the constants D_0, $D_{1/2}$, $D_{-1/2}$.

It turns out that the case of a single interval, i.e. $Q = 1$, is easier, and we can do the calculation exactly. This allows to identify the constants D_0, $D_{1/2}$, $D_{-1/2}$. We focus first on the case

$$\mathcal{I} = \{1,\dots,N\} \quad \text{and} \quad \mathcal{J} = \{1+1/2,\dots,N-1/2\}, \tag{A.25}$$

corresponding to $\eta_1 = \eta_2 = 1/2$. In that special case, one finds the following exact formula for any N:

$$\frac{\prod_{a<b\in\mathcal{I}}|b-a|\prod_{c<d\in\mathcal{J}}|d-c|}{\prod_{i\in\mathcal{I},j\in\mathcal{J}}|i-j|} = \pi^{N-1}G(3/2)^2\frac{G(N)G(N+1)}{G(N+1/2)^2}. \tag{A.26}$$

Here $G(.)$ is the Barnes G-function. Using the asymptotics of the Barnes G-function, one finds

$$\frac{G(N)G(N+1)}{G(N+1/2)^2} = N^{1/4} + O(N^{-3/4}) \tag{A.27}$$

for large N. Then comparing Eq. (A.26) to Eq. (A.19), using $(|\mathcal{I}|+|\mathcal{J}|)/2 = N-1/2$, one finds that $e^{-D_0} = \pi$ and $e^{-D_{1/2}} = \frac{G(3/2)}{\pi^{1/4}}$. To fix the constant $D_{-1/2}$, we focus on the case

$$\mathcal{I} = \{1,\dots,N\} \quad \text{and} \quad \mathcal{J} = \{1+1/2,\dots,N+1/2\}, \tag{A.28}$$

corresponding to $\eta_1 = 1/2$ and $\eta_2 = -1/2$. In that case we have the exact formula for any N:

$$\frac{\prod_{a<b\in\mathcal{I}}|b-a|\prod_{c<d\in\mathcal{J}}|d-c|}{\prod_{i\in\mathcal{I},j\in\mathcal{J}}|i-j|} = \pi^{N-1/2}G(3/2)^2\frac{\Gamma(N)}{\Gamma(N+1/2)}\frac{G(N)G(N+1)}{G(N+1/2)^2}. \tag{A.29}$$

The asymptotics of the Gamma function gives $\Gamma(N)/\Gamma(N+1/2) = N^{-1/2} + O(N^{-3/2})$. Then, comparing this with Eq. (A.19), and using $(|\mathcal{I}|+|\mathcal{J}|)/2 = N$, we find that $e^{-D_{-1/2}} = \frac{G(3/2)}{\pi^{1/4}}$, which is the same value as for the constant $e^{-D_{1/2}}$. This then leads to the two conjectures (A.14) and (A.15) above.

Appendix B

Calculation of the nonuniversal amplitudes $B_m(\gamma)$ in Chapter 3

In this Appendix we briefly summarize the method we used to obtain the non-universal amplitudes B_m appearing in the long-distance asymptotic expansion of the OPDM in Chapter 3. The calculation is detailed in the works [73, 81, 82, 122] The computation follows the methods outlined in Section 1.4.4 of Chapter 1. We exploit the operator state correspondence between operators of the effective field theory and the low-energy excited states of the underlying microscopic model. The amplitude B_m for a system of N bosons on a ring of size L is written as [73, 122]

$$\sqrt{B_m} = \lim_{N,L\to\infty} \left(\frac{L}{2\pi}\right)^{\Delta}_{m} \frac{\left|\langle \{J_j^{(m)}\}_{j=1}^{N-1} | \, \hat{\Psi}(0) \, | \{I_i\}_{i=1}^{N} \rangle\right|}{\sqrt{\langle \{J_j^{(m)}\}_{j=1}^{N-1} \rangle} \sqrt{\langle \{I_i\}_{i=1}^{N} \rangle}}. \tag{B.1}$$

The matrix elements can be obtained by using the determinant formula of Ref. [79]. The state $|\{I_i\}_{i=1}^{N}\rangle$ is the ground state of the gas that is fully specified by a set of Bethe integers as discussed in detail in section 1.2.3:

$$I_i = -\frac{N+1}{2} + i, \qquad i = 1, \ldots, N. \tag{B.2}$$

The state $|\{J_j^{(m)}\}_{j=1}^{N-1}\rangle$ is an excited state (low energy) characterized by the Bethe integers

$$J_j^{(m)} = -\frac{N}{2} + j + m, \qquad j = 1, \ldots, N-1. \tag{B.3}$$

As we discuss in section 1.4.4 and in the previous Appendix the nonuniversal field amplitude (B.1) is obtained by taking the thermodynamic limit $N, L \to \infty$ while keeping the density $n = N/L$ constant along with the interaction strength c, (at fixed γ). As we recall, in practice this is done by choosing fixed values of N and L and extrapolating to the thermodynamic limit with a polynomial fit in $1/N$. The result of this method is plotted in Fig. B.1 for the leading term $m = 0$. Notice that this result is directly related to the $B(\gamma)$ through

$$\sqrt{B_0(\gamma)} = B(\gamma), \tag{B.4}$$

plotted in Figure 1.6 of section 1.4.4.

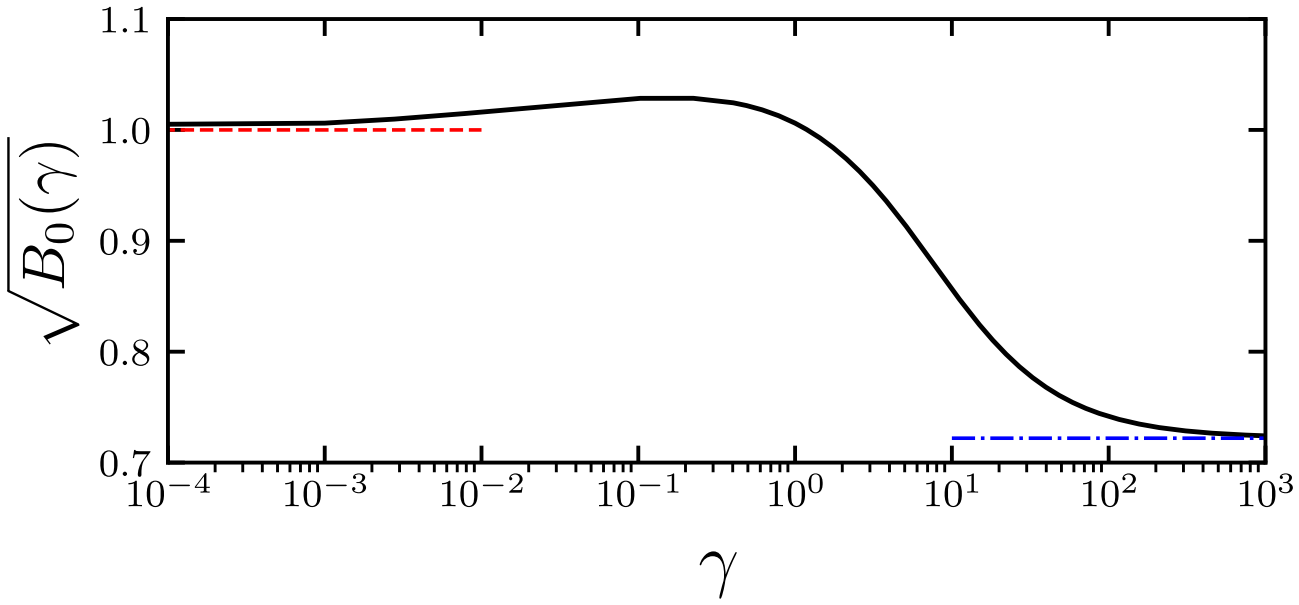


Figure B.1: The field amplitude $\sqrt{B_0(\gamma)}$ appearing in the leading order term of the long distance asymptotic of the OPDM as a function of the dimensionless interaction strength γ, with the limits $B_0(\gamma \to 1) \to 1$ [73] (dashed line) and $B_0(\infty) \simeq 0.5213$ [137] (dotted-dashed line). Originally published in [185], reused with permission.

Appendix C

Estimating the Error of the Momentum Distribution Obtained by *our approach* in Chapter 3

To compare the result of the momentum distribution computed using *our approach* to the *exact results* we proceed as follows. We define the quantity integrated difference as

$$\Delta(p_{\max}) = \frac{\int_{-p_{\max}}^{p_{\max}} dp\, |f_{\text{exact}}(p) - f_{\text{appr.}}(p)|}{\int_{-p_{\max}}^{p_{\max}} dp\, f_{\text{exact}}(p)} \tag{C.1}$$

where $f_{\text{appr.}}(p)$ is obtained by *our approach* and $f_{\text{exact}}(p)$ are the *exact results*. The results we find are reported in Table **??** for the hard-core and in Table **??** for the soft-core case.

For hard-core bosons, in the case of $N = 50$ we see that the differences Δ are smaller than the differences between the experimental and the model results reported in Li et al. [192]. For the small particle number $N = 5$, for smaller temperatures $T = 1, 5$ nK the Δ values are a bit larger, while for $T = 20$ nK it is more significant compared to the results in Li et al. [192].

Δ for hard-core bosons			
T (nK)	1	5	20
$N = 50$	0.033	0.033	0.039
$N = 5$	0.138	0.102	0.253

Table C.1: The integrated difference defined in Eq. (C.1) in the case of the hard-core limit, for different particle numbers and temperatures. We set the cutoff to be $p_{\max} = 8$.

In the case of the soft-core bosons, the values for the difference Δ defined in (C.1) are quantitatively similar to those we obtained in the hard-core limit. As expected the value of Δ increases as the particle number and the interaction strength (measured in the middle of the gas cloud: $\gamma(x = 0)$) decreases.

Δ for soft-core bosons						
T (nK)	1		5		20	
N	50	5	50	5	50	5
$\gamma(0) = 4$	0.032	0.137	0.021	0.084	0.050	0.219
$\gamma(0) = 1$	0.043	0.180	0.022	0.087	0.130	0.159
$\gamma(0) = 0.1$	0.087	0.443	0.029	0.079	0.287	0.138

Table C.2: The integrated difference defined in Eq. (C.1) in the case of soft-core bosons, for different particle numbers, temperatures and interaction strengths (measured in the center of the gas cloud). We set the cutoff to be $p_{\max} = 8$.

Bibliography

[1] Olalla A Castro-Alvaredo, Benjamin Doyon, and Takato Yoshimura. "Emergent hydrodynamics in integrable quantum systems out of equilibrium". In: *Phys. Rev. X* 6 (2016), p. 041065.

[2] Bruno Bertini et al. "Transport in Out-of-Equilibrium X X Z Chains: Exact Profiles of Charges and Currents". In: *Phys. Rev. Lett.* 117 (2016), p. 207201.

[3] Paola Ruggiero et al. "Quantum generalized hydrodynamics". In: *Phys. Rev. Lett.* 124 (2020), p. 140603.

[4] Paola Ruggiero et al. "Quantum generalized hydrodynamics of the Tonks–Girardeau gas: density fluctuations and entanglement entropy". In: *Journal of Physics A: Mathematical and Theoretical* 55 (2021), p. 024003.

[5] MA Cazalilla et al. "One dimensional bosons: From condensed matter systems to ultracold gases". In: *Rev. Mod. Phys.* 83 (2011), p. 1405.

[6] Marcos Rigol and Alejandro Muramatsu. "Universal properties of hard-core bosons confined on one-dimensional lattices". In: *Physical Review A* 70 (2004), p. 031603.

[7] MD Girardeau and EM Wright. "Breakdown of time-dependent mean-field theory for a one-dimensional condensate of impenetrable bosons". In: *Phys. Rev. Lett.* 84 (2000), p. 5239.

[8] Patrizia Vignolo and Anna Minguzzi. "Universal contact for a Tonks-Girardeau gas at finite temperature". In: *Phys. Rev. Lett.* 110 (2013), p. 020403.

[9] Enej Ilievski et al. "Quasilocal charges in integrable lattice systems". In: *Journal of Statistical Mechanics: Theory and Experiment* 2016 (2016), p. 064008. DOI: 10.1088/1742-5468/2016/06/064008.

[10] Marcos Rigol et al. "Relaxation in a completely integrable many-body quantum system: An ab initio study of the dynamics of the highly excited states of 1d lattice hard-core bosons". In: *Physical review letters* 98 (2007), p. 050405. DOI: 10.1103/PhysRevLett.98.050405.

[11] Isabelle Bouchoule and Jérôme Dubail. "Generalized hydrodynamics in the one-dimensional Bose gas: theory and experiments". In: *Journal of Statistical Mechanics: Theory and Experiment* 2022 (2022), p. 014003. ISSN: 1742-5468. DOI: 10.1088/1742-5468/ac3659.

[12] Isabelle Bouchoule, N. J. van Druten, and Christoph I Westbrook. "Atom chips and one-dimensional Bose gases". In: *Atom chips*. Ed. by J. Reichel and V. Vuletic. Wiley-VCH Verlag GmbH, 2011, p. 331.

[13] Marvin Girardeau. "Relationship between systems of impenetrable bosons and fermions in one dimension". In: *J. Math. Phys.* 1 (1960), pp. 516–523.

[14] Immanuel Bloch, Jean Dalibard, and Wilhelm Zwerger. "Many-body physics with ultracold gases". In: *Rev. Mod. Phys.* 80 (2008), pp. 885–964. DOI: 10.1103/RevModPhys.80.885.

[15] M. Olshanii. "Atomic Scattering in the Presence of an External Confinement and a Gas of Impenetrable Bosons". In: *Phys. Rev. Lett.* 81 (1998), pp. 938–941. DOI: 10.1103/PhysRevLett.81.938.

[16] Henning Moritz et al. "Confinement Induced Molecules in a 1D Fermi Gas". In: *Physical Review Letters* 94 (2005). ISSN: 1079-7114. DOI: 10.1103/physrevlett.94.210401.

[17] A. Görlitz et al. "Realization of Bose-Einstein Condensates in Lower Dimensions". In: *Phys. Rev. Lett.* 87 (2001), p. 130402. DOI: 10.1103/PhysRevLett.87.130402.

[18] S. Dettmer et al. "Observation of Phase Fluctuations in Elongated Bose-Einstein Condensates". In: *Phys. Rev. Lett.* 87 (2001), p. 160406. DOI: 10.1103/PhysRevLett.87.160406.

[19] Markus Greiner et al. "Exploring Phase Coherence in a 2D Lattice of Bose-Einstein Condensates". In: *Phys. Rev. Lett.* 87 (2001), p. 160405. DOI: 10.1103/PhysRevLett.87.160405.

[20] Henning Moritz et al. "Exciting Collective Oscillations in a Trapped 1D Gas". In: *Phys. Rev. Lett.* 91 (2003), p. 250402. DOI: 10.1103/PhysRevLett.91.250402.

[21] B. Laburthe Tolra et al. "Observation of Reduced Three-Body Recombination in a Correlated 1D Degenerate Bose Gas". In: *Phys. Rev. Lett.* 92 (2004), p. 190401. DOI: 10.1103/PhysRevLett.92.190401.

[22] N. Fabbri et al. "Momentum-resolved study of an array of one-dimensional strongly phase-fluctuating Bose gases". In: *Phys. Rev. A* 83 (2011), p. 031604. DOI: 10.1103/PhysRevA.83.031604.

[23] Elmar Haller et al. "Realization of an Excited, Strongly Correlated Quantum Gas Phase". In: *Science* 325 (2009), pp. 1224–1227. ISSN: 1095-9203. DOI: 10.1126/science.1175850.

[24] Toshiya Kinoshita, Trevor Wenger, and David S. Weiss. "Local Pair Correlations in One-Dimensional Bose Gases". In: *Phys. Rev. Lett.* 95 (2005), p. 190406. DOI: 10.1103/PhysRevLett.95.190406.

[25] Ron Folman et al. "Controlling Cold Atoms using Nanofabricated Surfaces: Atom Chips". In: *Phys. Rev. Lett.* 84 (2000), pp. 4749–4752. DOI: 10.1103/PhysRevLett.84.4749.

[26] A. H. van Amerongen et al. "Yang-Yang Thermodynamics on an Atom Chip". In: *Phys. Rev. Lett.* 100 (2008), p. 090402. DOI: 10.1103/PhysRevLett.100.090402.

[27] Isabelle Bouchoule and Max Schemmer. "Asymptotic temperature of a lossy condensate". In: *SciPost Physics* 8 (2020). ISSN: 2542-4653. DOI: 10.21468/scipostphys.8.4.060.

[28] Isabelle Bouchoule, Max Schemmer, and Carsten Henkel. "Cooling phonon modes of a Bose condensate with uniform few body losses". In: *SciPost Physics* 5 (2018). DOI: 10.21468/scipostphys.5.5.043.

[29] I. Bouchoule et al. "Finite-temperature hydrodynamics for one-dimensional Bose gases: Breathing-mode oscillations as a case study". In: *Phys. Rev. A* 94 (2016), p. 051602. DOI: 10.1103/PhysRevA.94.051602.

[30] Chen-Ning Yang and C. P. Yang. "Thermodynamics of one-dimensional system of bosons with repulsive delta function interaction". In: *J. Math. Phys.* 10 (1969), pp. 1115–1122. DOI: 10.1063/1.1664947.

[31] Nicole Fabbri et al. "Momentum-resolved study of an array of one-dimensional strongly phase-fluctuating Bose gases". In: *Phys. Rev. A* 83 (2011), p. 031604.

[32] Neel Malvania et al. "Generalized hydrodynamics in strongly interacting 1D Bose gases". In: *Science* 373 (2021), pp. 1129–1133. ISSN: 1095-9203. DOI: 10.1126/science.abf0147.

[33] Joshua M. Wilson et al. "Observation of dynamical fermionization". In: *Science* 367 (2020), pp. 1461–1464. DOI: 10.1126/science.aaz0242.

[34] Elliott H. Lieb. "Exact Analysis of an Interacting Bose Gas. II. The Excitation Spectrum". In: *Phys. Rev.* 130 (1963), pp. 1616–1624. DOI: 10.1103/PhysRev.130.1616.

[35] Elliott H. Lieb and Werner Liniger. "Exact Analysis of an Interacting Bose Gas. I. The General Solution and the Ground State". In: *Phys. Rev.* 130 (1963), pp. 1605–1616. DOI: 10.1103/PhysRev.130.1605.

[36] M. Girardeau. "Relationship between Systems of Impenetrable Bosons and Fermions in One Dimension". In: *J. Math. Phys.* 1 (1960), p. 516. DOI: 10.1063/1.1703687.

[37] M. A. Cazalilla. "Differences between the Tonks regimes in the continuum and on the lattice". In: *Phys. Rev. A* 70 (2004), p. 041604. DOI: 10.1103/PhysRevA.70.041604.

[38] P. Jordan and E. Wigner. "Über das Paulische Äquivalenzverbot". In: *Zeitschrift für Physik* 47 (1928). DOI: 110.1007/BF01331938.

[39] Tim Keller, Thomás Fogarty, and Thomas Busch. "Self-Pinning Transition of a Tonks-Girardeau Gas in a Bose-Einstein Condensate". In: *Phys. Rev. Lett.* 128 (2022), p. 053401. DOI: 10.1103/PhysRevLett.128.053401.

[40] Shu Chen et al. "Realization of effective super Tonks-Girardeau gases via strongly attractive one-dimensional Fermi gases". In: *Phys. Rev. A* 81 (2010), p. 031608. DOI: 10.1103/PhysRevA.81.031608.

[41] Liming Guan and Shu Chen. "Super-Tonks-Girardeau Gas of Spin-1/2 Interacting Fermions". In: *Phys. Rev. Lett.* 105 (2010), p. 175301. DOI: 10.1103/PhysRevLett.105.175301.

[42] Yu Chen and Xiaoling Cui. "Ultrastable Super-Tonks-Girardeau Gases under Weak Dipolar Interactions". In: *Phys. Rev. Lett.* 131 (2023), p. 203002. DOI: 10.1103/PhysRevLett.131.203002.

[43] M T Batchelor et al. "Evidence for the super Tonks–Girardeau gas". In: *Journal of Statistical Mechanics: Theory and Experiment* 2005 (2005), pp. L10001–L10001. ISSN: 1742-5468. DOI: 10.1088/1742-5468/2005/10/l10001.

[44] Miłosz Panfil, Jacopo De Nardis, and Jean-Sébastien Caux. "Metastable Criticality and the Super Tonks-Girardeau Gas". In: *Physical Review Letters* 110 (2013). ISSN: 1079-7114. DOI: 10.1103/physrevlett.110.125302.

[45] Maciej Marciniak et al. "Super-Tonks-Girardeau quench in the extended Bose-Hubbard model". In: *Phys. Rev. A* 108 (2023), p. 043304. DOI: 10.1103/PhysRevA.108.043304.

[46] KB Efetov and AI Larkin. "Correlation functions in one-dimensional systems with a strong interaction". In: *Sov. Phys. JETP* 42 (1976), p. 11.

[47] FDM Haldane. "'Luttinger liquid theory'of one-dimensional quantum fluids. I. Properties of the Luttinger model and their extension to the general 1D interacting spinless Fermi gas". In: *Journal of Physics C: Solid State Physics* 14 (1981), p. 2585.

[48] Thierry Giamarchi. *Quantum physics in one dimension*. Vol. 121. Clarendon press, 2003.

[49] MA Cazalilla. "Bosonizing one-dimensional cold atomic gases". In: *J. Phys. B: Atomic, Molecular and Optical Physics* 37 (2004), S1.

[50] Oliver Penrose and Lars Onsager. "Bose-Einstein Condensation and Liquid Helium". In: *Phys. Rev.* 104 (1956), pp. 576–584. DOI: 10.1103/PhysRev.104.576.

[51] Andrew Lenard. "Momentum distribution in the ground state of the one-dimensional system of impenetrable bosons". In: *J. Math. Phys.* 5 (1964), pp. 930–943.

[52] V I Yukalov and M D Girardeau. "Fermi-Bose mapping for one-dimensional Bose gases". In: *Laser Physics Letters* 2 (2005), p. 375. DOI: 10.1002/lapl.200510011.

[53] PJ Forrester et al. "Finite one-dimensional impenetrable Bose systems: Occupation xnumbers". In: *Phys. Rev. A* 67 (2003), p. 043607.

[54] Andrea Colcelli et al. "Universal off-diagonal long-range-order behavior for a trapped Tonks-Girardeau gas". In: *Phys. Rev. A* 98 (2018), p. 063633.

[55] Marcos Rigol and Alejandro Muramatsu. "Emergence of Quasicondensates of Hard-Core Bosons at Finite Momentum". In: *Physical Review Letters* 93 (2004). ISSN: 1079-7114. DOI: 10.1103/physrevlett.93.230404.

[56] Robert Pezer and Hrvoje Buljan. "Momentum distribution dynamics of a Tonks-Girardeau gas: Bragg reflections of a quantum many-body wave packet". In: *Phys. Rev. Lett.* 98 (2007), p. 240403.

[57] C. J. Bolech et al. "Long-Time Behavior of the Momentum Distribution During the Sudden Expansion of a Spin-Imbalanced Fermi Gas in One Dimension". In: *Phys. Rev. Lett.* 109 (2012), p. 110602. DOI: 10.1103/PhysRevLett.109.110602.

[58] Dario Jukić, Bruno Klajn, and Hrvoje Buljan. "Momentum distribution of a freely expanding Lieb-Liniger gas". In: *Phys. Rev. A* 79 (2009), p. 033612.

[59] Benjamin Doyon. "Lecture notes on generalised hydrodynamics". In: *SciPost Phys. Lecture Notes* (2020), p. 018.

[60] Fabian H.L. Essler. "A short introduction to Generalized Hydrodynamics". In: *Physica A: Statistical Mechanics and its Applications* 631 (2023), p. 127572. ISSN: 0378-4371. DOI: 10.1016/j.physa.2022.127572.

[61] Jérôme Dubail. "A more efficient way to describe interacting quantum particles in 1d". In: *Physics 9* 153 (2016).

[62] Benjamin Doyon and Takato Yoshimura. "A note on generalized hydrodynamics: inhomogeneous fields and other concepts". In: *SciPost Physics* 2 (2017), p. 014.

[63] S. Scopa et al. "One-particle density matrix and momentum distribution of the out-of-equilibrium one-dimensional Tonks-Girardeau gas: Analytical results at large N". In: *Physical Review A* 108 (2023). ISSN: 2469-9934. DOI: 10.1103/physreva.108.013324.

[64] Benjamin Doyon et al. "Large-Scale Description of Interacting One-Dimensional Bose Gases: Generalized Hydrodynamics Supersedes Conventional Hydrodynamics". In: *Physical Review Letters* 119 (2017). ISSN: 1079-7114. DOI: 10.1103/physrevlett.119.195301.

[65] D. Karevski. "Scaling behaviour of the relaxation in quantum chains". In: *The European Physical Journal B - Condensed Matter* 27 (2002), pp. 147–152. ISSN: 1434-6036. DOI: 10.1140/epjb/e20020139.

[66] Maxim Olshanii and Vanja Dunjko. "Short-distance correlation properties of the Lieb-Liniger system and momentum distributions of trapped one-dimensional atomic gases". In: *Phys. Rev. Lett.* 91 (2003), p. 090401.

[67] Viktor Eisler. "Entanglement spreading after local and extended excitations in a free-fermion chain". In: *Journal of Physics A: Mathematical and Theoretical* 54 (2021), p. 424002. DOI: 10.1088/1751-8121/ac21e4.

[68] Stefano Scopa, Pasquale Calabrese, and Jerome Dubail. "Exact hydrodynamic solution of a double domain wall melting in the spin-1/2 XXZ model". In: *SciPost Phys.* 12 (2022), p. 207.

[69] Bess Fang et al. "Momentum-space correlations of a one-dimensional Bose gas". In: *Phys. Rev. Lett.* 116 (2016), p. 050402.

[70] Maximilian Schemmer et al. "Generalized hydrodynamics on an atom chip". In: *Phys. Rev. Lett.* 122 (2019), p. 090601.

[71] Isabelle Bouchoule and Jérôme Dubail. "Generalized hydrodynamics in the one-dimensional Bose gas: theory and experiments". In: *J. Stat. Mech.* 2022 (2022), p. 014003.

[72] H. P. Büchler, G. Blatter, and W. Zwerger. "Commensurate-Incommensurate Transition of Cold Atoms in an Optical Lattice". In: *Physical Review Letters* 90 (2003). ISSN: 1079-7114. DOI: 10.1103/physrevlett.90.130401.

[73] Yannis Brun and Jerome Dubail. "The Inhomogeneous Gaussian Free Field, with application to ground state correlations of trapped 1d Bose gases". In: *SciPost Phys* 4 (2018), p. 037.

[74] Alvise Bastianello, Jérôme Dubail, and Jean-Marie Stéphan. "Entanglement entropies of inhomogeneous Luttinger liquids". In: *Journal of Physics A: Mathematical and Theoretical* 53 (2020), p. 155001. ISSN: 1751-8121. DOI: 10.1088/1751-8121/ab7580.

[75] Lev Pitaevskii and Sandro Stringari. *Bose-Einstein Condensation and Superfluidity*. Oxford University Press, 2016. ISBN: 9780198758884. DOI: 10.1093/acprof:oso/9780198758884.001.0001.

[76] R Citro et al. "Luttinger hydrodynamics of confined one-dimensional Bose gases with dipolar interactions". In: *New Journal of Physics* 10 (2008), p. 045011. ISSN: 1367-2630. DOI: 10.1088/1367-2630/10/4/045011.

[77] D. S. Petrov, D. M. Gangardt, and G. V. Shlyapnikov. "Low-dimensional trapped gases". In: *Journal de Physique IV (Proceedings)* 116 (2004), pp. 5–44. ISSN: 1155-4339. DOI: 10.1051/jp4:2004116001.

[78] Marek Gluza, Per Moosavi, and Spyros Sotiriadis. "Breaking of Huygens–Fresnel principle in inhomogeneous Tomonaga–Luttinger liquids". In: *Journal of Physics A: Mathematical and Theoretical* 55 (2022), p. 054002. ISSN: 1751-8121. DOI: 10.1088/1751-8121/ac39cc.

[79] N.A. Slavnov. "Calculation of scalar products of wave functions and form factors in the framework of the algebraic Bethe ansatz". In: *Theoretical and Mathematical Physics (English Translation)* 79 (1989), pp. 502–508. ISSN: 0040-5779.

[80] Jean-Sébastien Caux. "Correlation functions of integrable models: A description of the ABACUS algorithm". In: *J. Math. Physics* 50 (2009), p. 095214.

[81] Aditya Shashi et al. "Nonuniversal prefactors in the correlation functions of one-dimensional quantum liquids". In: *Phys. Rev. B* 84 (2011), p. 045408.

[82] Aditya Shashi et al. "Exact prefactors in static and dynamic correlation functions of one-dimensional quantum integrable models: Applications to the Calogero-Sutherland, Lieb-Liniger, and X X Z models". In: *Phys. Rev. B* 85 (2012), p. 155136.

[83] N Kitanine et al. "A form factor approach to the asymptotic behavior of correlation functions in critical models". In: *Journal of Statistical Mechanics: Theory and Experiment* 2011 (2011), P12010. DOI: 10.1088/1742-5468/2011/12/P12010.

[84] N Kitanine et al. "Form factor approach to dynamical correlation functions in critical models". In: *Journal of Statistical Mechanics: Theory and Experiment* 2012 (2012), P09001. DOI: 10.1088/1742-5468/2012/09/P09001.

[85] Yannis Brun and Jerome Dubail. "One-particle density matrix of trapped one-dimensional impenetrable bosons from conformal invariance". In: *SciPost Phys.* 2 (2017), p. 012.

[86] Nikita Slavnov. "Nonequal-time current correlation function in a one-dimensional Bose gas". In: *Theoretical and Mathematical Physics - THEOR MATH PHYS-ENGL TR* 82 (1990), pp. 273–282. DOI: 10.1007/BF01029221.

[87] T. Kojima, V. E. Korepin, and N. A. Slavnov. "Determinant Representation for Dynamical Correlation Functions of the Quantum Nonlinear Schrödinger Equation". In: *Communications in Mathematical Physics* 188 (1997), pp. 657–689. ISSN: 1432-0916. DOI: 10.1007/s002200050182.

[88] Alexander M. Polyakov. "Conformal symmetry of critical fluctuations". In: *JETP Lett.* 12 (1970), pp. 381–383.

[89] A. A. Belavin, Alexander M. Polyakov, and A. B. Zamolodchikov. "Infinite Conformal Symmetry in Two-Dimensional Quantum Field Theory". In: *Nucl. Phys. B* 241 (1984). Ed. by I. M. Khalatnikov and V. P. Mineev, pp. 333–380. DOI: 10.1016/0550-3213(84)90052-X.

[90] V. S. Dotsenko and V. A. Fateev. "Conformal Algebra and Multipoint Correlation Functions in Two-Dimensional Statistical Models". In: *Nucl. Phys. B* 240 (1984). Ed. by I. M. Khalatnikov and V. P. Mineev, p. 312. DOI: 10.1016/0550-3213(84)90269-4.

[91] J L Cardy. "Conformal invariance and universality in finite-size scaling". In: *Journal of Physics A: Mathematical and General* 17 (1984), p. L385. DOI: 10.1088/0305-4470/17/7/003.

[92] John Cardy. *Conformal Field Theory and Statistical Mechanics*. 2008. arXiv: 0807.3472 [cond-mat.stat-mech].

[93] Paul Ginsparg. *Applied Conformal Field Theory*. 1988. arXiv: hep-th/9108028 [hep-th].

[94] P. Francesco, P. Mathieu, and D. Senechal. *Conformal Field Theory*. Graduate Texts in Contemporary Physics. Springer New York, 2012. ISBN: 9781461222569.

[95] Hermann Weyl. "Zur Gravitationstheorie". In: *Annalen der Physik* 359 (1917), pp. 117–145. DOI: 10.1002/andp.19173591804.

[96] Alexei M Tsvelik. *Quantum field theory in condensed matter physics*. Cambridge university press, 2007.

[97] P. Di Francesco, P. Mathieu, and D. Senechal. *Conformal Field Theory*. Graduate Texts in Contemporary Physics. New York: Springer-Verlag, 1997. ISBN: 978-0-387-94785-3, 978-1-4612-7475-9. DOI: 10.1007/978-1-4612-2256-9.

[98] L Landau. "Theory of the Superfluidity of Helium II". In: *Physical Review* 60 (1941), p. 356.

[99] N. N. Bogolyubov. "On the theory of superfluidity". In: *J. Phys. (USSR)* 11 (1947), pp. 23–32.

[100] Christophe Mora and Yvan Castin. "Extension of Bogoliubov theory to quasicondensates". In: *Phys. Rev. A* 67 (2003), p. 053615.

[101] P. B. Wiegmann. "Hydrodynamics of Euler incompressible fluid and the fractional quantum Hall effect". In: *Phys. Rev. B* 88 (2013), p. 241305. DOI: 10.1103/PhysRevB.88.241305.

[102] Paul Wiegmann and Alexander G. Abanov. "Anomalous Hydrodynamics of Two-Dimensional Vortex Fluids". In: *Phys. Rev. Lett.* 113 (2014), p. 034501. DOI: 10.1103/PhysRevLett.113.034501.

[103] P. Wiegmann. *Quantization of Hydrodynamics: Rotating Superfluid and Gravitational Anomaly*. 2019. arXiv: 1906.03788 [cond-mat.str-el].

[104] Toshiya Kinoshita, Trevor Wenger, and David S. Weiss. "A quantum Newton's cradle". In: *Nature* 440 (2006), pp. 900–903. DOI: 10.1038/nature04693.

[105] Jerome Dubail. "LARGE-SCALE DESCRIPTIONS OF THE 1D BOSE GAS & OTHER SELECTED TOPICS IN LOW-DIMENSIONAL QUANTUM MANY-BODY PHYSICS". Habilitation à diriger des recherches. Université de Lorraine, 2022.

[106] Tod M. Wright et al. "Nonequilibrium Dynamics of One-Dimensional Hard-Core Anyons Following a Quench: Complete Relaxation of One-Body Observables". In: *Phys. Rev. Lett.* 113 (2014), p. 050601. DOI: 10.1103/PhysRevLett.113.050601.

[107] Marcos Rigol, Alejandro Muramatsu, and Maxim Olshanii. "Hard-core bosons on optical superlattices: Dynamics and relaxation in the superfluid and insulating regimes". In: *Phys. Rev. A* 74 (2006), p. 053616. DOI: 10.1103/PhysRevA.74.053616.

[108] Lev Vidmar and Marcos Rigol. "Generalized Gibbs ensemble in integrable lattice models". In: *Journal of Statistical Mechanics: Theory and Experiment* 2016 (2016), p. 064007. DOI: 10.1088/1742-5468/2016/06/064007.

[109] Lev Vidmar, Deepak Iyer, and Marcos Rigol. "Emergent Eigenstate Solution to Quantum Dynamics Far from Equilibrium". In: *Phys. Rev. X* 7 (2017), p. 021012. DOI: 10.1103/PhysRevX.7.021012.

[110] Lev Vidmar, Wei Xu, and Marcos Rigol. "Emergent eigenstate solution and emergent Gibbs ensemble for expansion dynamics in optical lattices". In: *Phys. Rev. A* 96 (2017), p. 013608. DOI: 10.1103/PhysRevA.96.013608.

[111] Yicheng Zhang, Lev Vidmar, and Marcos Rigol. "Quantum dynamics of impenetrable $\mathrm{SU}(N)$ fermions in one-dimensional lattices". In: *Phys. Rev. A* 99 (2019), p. 063605. DOI: 10.1103/PhysRevA.99.063605.

[112] Yicheng Zhang, Lev Vidmar, and Marcos Rigol. "Emergent eigenstate solution for generalized thermalization". In: *Phys. Rev. A* 104 (2021), p. L031303. DOI: 10.1103/PhysRevA.104.L031303.

[113] Bill Sutherland. "Exact Coherent States of a One-Dimensional Quantum Fluid in a Time-Dependent Trapping Potential". In: *Phys. Rev. Lett.* 80 (1998), pp. 3678–3681. DOI: 10.1103/PhysRevLett.80.3678.

[114] A. Minguzzi and D. M. Gangardt. "Exact Coherent States of a Harmonically Confined Tonks-Girardeau Gas". In: *Phys. Rev. Lett.* 94 (2005), p. 240404. DOI: 10.1103/PhysRevLett.94.240404.

[115] A. S. Campbell, D. M. Gangardt, and K. V. Kheruntsyan. "Sudden Expansion of a One-Dimensional Bose Gas from Power-Law Traps". In: *Phys. Rev. Lett.* 114 (2015), p. 125302. DOI: 10.1103/PhysRevLett.114.125302.

[116] Zhongtao Mei et al. "Unveiling hidden structure of many-body wave functions of integrable systems via sudden-expansion experiments". In: *Phys. Rev. A* 93 (2016), 021607(R). DOI: 10.1103/PhysRevA.93.021607.

[117] T. Kinoshita, T. Wenger, and D. S. Weiss. "Observation of a One-Dimensional Tonks-Girardeau Gas". In: *Science* 305 (2004), p. 1125. DOI: 10.1126/science.1100700.

[118] B. Paredes et al. "Tonks-Girardeau gas of ultracold atoms in an optical lattice". In: *Nature (London)* 429 (2004), p. 277. DOI: 10.1038/nature02530.

[119] J. P. Ronzheimer et al. "Expansion dynamics of interacting bosons in homogeneous lattices in one and two dimensions". In: *Phys. Rev. Lett.* 110 (2013), p. 205301. DOI: 10.1103/PhysRevLett.110.205301.

[120] L. Vidmar et al. "Dynamical Quasicondensation of Hard-Core Bosons at Finite Momenta". In: *Phys. Rev. Lett.* 115 (2015), p. 175301. DOI: 10.1103/PhysRevLett.115.175301.

[121] Jacopo De Nardis and Miłosz Panfil. "Edge Singularities and Quasilong-Range Order in Nonequilibrium Steady States". In: *Phys. Rev. Lett.* 120 (2018), p. 217206. DOI: 10.1103/PhysRevLett.120.217206.

[122] Stefano Scopa, Lorenzo Piroli, and Pasquale Calabrese. "One-particle density matrix of a trapped Lieb–Liniger anyonic gas". In: *J. Stat. Mech.* 2020 (2020), p. 093103.

[123] Stefano Scopa et al. "Exact entanglement growth of a one-dimensional hard-core quantum gas during a free expansion". In: *J. Phys. A: Math. Theor.* 54 (2021), p. 404002.

[124] Paola Ruggiero, Yannis Brun, and Jérome Dubail. "Conformal field theory on top of a breathing one-dimensional gas of hard core bosons". In: *SciPost Phys.* 6 (2019), p. 51.

[125] Mario Collura et al. "Domain wall melting in the spin-$\frac{1}{2}$ XXZ spin chain: Emergent Luttinger liquid with a fractal quasiparticle charge". In: *Phys. Rev. B* 102 (2020), p. 180409. DOI: 10.1103/PhysRevB.102.180409.

[126] Filiberto Ares, Stefano Scopa, and Sascha Wald. "Entanglement dynamics of a hard-core quantum gas during a Joule expansion". In: *Journal of Physics A: Mathematical and Theoretical* 55 (2022), p. 375301.

[127] Federico Rottoli, Stefano Scopa, and Pasquale Calabrese. "Entanglement Hamiltonian during a domain wall melting in the free Fermi chain". In: *Journal of Statistical Mechanics: Theory and Experiment* 2022 (2022), p. 063103. ISSN: 1742-5468. DOI: 10.1088/1742-5468/ac72a1.

[128] Stefano Scopa and Dragi Karevski. "Scaling of fronts and entanglement spreading during a domain wall melting". In: *The European Physical Journal Special Topics* 232 (2023), pp. 1763–1781. ISSN: 1951-6401. DOI: 10.1140/epjs/s11734-023-00845-1.

[129] Luca Capizzi et al. "Domain wall melting across a defect". In: *Europhysics Letters* 141 (2023), p. 31002. ISSN: 1286-4854. DOI: 10.1209/0295-5075/acb50a.

[130] A Takács et al. "Quasicondensation and off-diagonal long-range order of hard-core bosons during a free expansion". In: *Journal of Physics A: Mathematical and Theoretical* 57 (2024), p. 495003. DOI: 10.1088/1751-8121/ad7fa8.

[131] Nicolas Allegra et al. "Inhomogeneous field theory inside the arctic circle". In: *Journal of Statistical Mechanics: Theory and Experiment* 2016 (2016), p. 053108.

[132] T. Antal et al. "Transport in the XX chain at zero temperature: Emergence of flat magnetization profiles". In: *Phys. Rev. E* 59 (1999), pp. 4912–4918. DOI: 10.1103/PhysRevE.59.4912.

[133] T. Antal, P. L. Krapivsky, and A. Rákos. "Logarithmic current fluctuations in nonequilibrium quantum spin chains". In: *Phys. Rev. E* 78 (2008), p. 061115. DOI: 10.1103/PhysRevE.78.061115.

[134] Thierry Platini and Dragi Karevski. "Relaxation in the XX quantum chain". In: *Journal of Physics A: Mathematical and Theoretical* 40 (2007), p. 1711. DOI: 10.1088/1751-8113/40/8/002.

[135] Fabrice Gerbier et al. "Momentum distribution and correlation function of quasicondensates in elongated traps". In: *Phys. Rev. A* 67 (2003), p. 051602.

[136] C. A. Regal et al. "Momentum Distribution of a Fermi Gas of Atoms in the BCS-BEC Crossover". In: *Phys. Rev. Lett.* 95 (2005), p. 250404. DOI: 10.1103/PhysRevLett.95.250404.

[137] Hemant G Vaidya and CA Tracy. "One particle reduced density matrix of impenetrable bosons in one dimension at zero temperature". In: *J. Math. Phys.* 20 (1979), pp. 2291–2312.

[138] Andrew Lenard. "Some remarks on large Toeplitz determinants". In: *Pac. J. Math.* 42 (1972), pp. 137–145.

[139] Mario Collura, Andrea De Luca, and Jacopo Viti. "Analytic solution of the domain-wall nonequilibrium stationary state". In: *Physical Review B* 97 (2018). ISSN: 2469-9969. DOI: 10.1103/physrevb.97.081111.

[140] Jad C. Halimeh et al. "Domain-wall melting in ultracold-boson systems with hole and spin-flip defects". In: *Phys. Rev. A* 89 (2014), p. 063603. DOI: 10.1103/PhysRevA.89.063603.

[141] Luca Capizzi et al. "Domain wall melting across a defect". In: *Europhysics Letters* 141 (2023), p. 31002. DOI: 10.1209/0295-5075/acb50a.

[142] Matthias Gruber and Viktor Eisler. "Magnetization and entanglement after a geometric quench in the XXZ chain". In: *Phys. Rev. B* 99 (2019), p. 174403. DOI: 10.1103/PhysRevB.99.174403.

[143] Jérôme Dubail et al. “Conformal field theory for inhomogeneous one-dimensional quantum systems: the example of non-interacting Fermi gases”. In: *SciPost Phys.* 2 (2017), p. 002.

[144] Maurizio Fagotti. “Higher-order generalized hydrodynamics in one dimension: The noninteracting test”. In: *Physical Review B* 96 (2017), p. 220302.

[145] Maurizio Fagotti. “Locally quasi-stationary states in noninteracting spin chains”. In: *SciPost Phys.* 8 (2020), p. 048.

[146] Saverio Bocini. “Connected correlations in partitioning protocols: A case study and beyond”. In: *SciPost Phys.* 15 (2023), p. 027. DOI: 10.21468/SciPostPhys.15.1.027.

[147] Benjamin Doyon et al. “Large-scale description of interacting one-dimensional Bose gases: generalized hydrodynamics supersedes conventional hydrodynamics”. In: *Phys. Rev. Lett.* 119 (2017), p. 195301.

[148] Margarida Hinarejos, A Pérez, and Mari-Carmen Bañuls. “Wigner function for a particle in an infinite lattice”. In: *New Journal of Physics* 14 (2012), p. 103009.

[149] Pierre Wendenbaum, Mario Collura, and Dragi Karevski. “Hydrodynamic description of hard-core bosons on a Galileo ramp”. In: *Phys. Rev. A* 87 (2013), p. 023624. DOI: 10.1103/PhysRevA.87.023624.

[150] R Bondesan et al. “Chiral SU (2) k currents as local operators in vertex models and spin chains”. In: *Journal of Physics A: Mathematical and Theoretical* 48 (2015), p. 065205.

[151] Isabelle Bouchoule and Jérôme Dubail. “Breakdown of Tan’s relation in lossy one-dimensional Bose gases”. In: *Phys. Rev. Lett.* 126 (2021), p. 160603.

[152] Mario Collura, Spyros Sotiriadis, and Pasquale Calabrese. “Equilibration of a Tonks-Girardeau gas following a trap release”. In: *Physical Review Letters* 110 (2013), p. 245301.

[153] Mario Collura, Spyros Sotiriadis, and Pasquale Calabrese. “Quench dynamics of a Tonks–Girardeau gas released from a harmonic trap”. In: *Journal of Statistical Mechanics: Theory and Experiment* 2013 (2013), P09025.

[154] P. W. Anderson. “Infrared Catastrophe in Fermi Gases with Local Scattering Potentials”. In: *Phys. Rev. Lett.* 18 (1967), pp. 1049–1051. DOI: 10.1103/PhysRevLett.18.1049.

[155] C. L. Kane and Matthew P. A. Fisher. “Transport in a one-channel Luttinger liquid”. In: *Phys. Rev. Lett.* 68 (1992), pp. 1220–1223. DOI: 10.1103/PhysRevLett.68.1220.

[156] C. L. Kane and Matthew P. A. Fisher. “Transmission through barriers and resonant tunneling in an interacting one-dimensional electron gas”. In: *Phys. Rev. B* 46 (1992), pp. 15233–15262. DOI: 10.1103/PhysRevB.46.15233.

[157] Ingo Peschel. “Entanglement entropy with interface defects”. In: *Journal of Physics A: Mathematical and General* 38 (2005), p. 4327. DOI: 10.1088/0305-4470/38/20/002.

[158] Michael Gutperle and John D. Miller. “Entanglement entropy at CFT junctions”. In: *Phys. Rev. D* 95 (2017), p. 106008. DOI: 10.1103/PhysRevD.95.106008.

[159] Luca Capizzi, Sara Murciano, and Pasquale Calabrese. “Rényi entropy and negativity for massless Dirac fermions at conformal interfaces and junctions”. In: *Journal of High Energy Physics* 2022 (2022). ISSN: 1029-8479. DOI: 10.1007/jhep08(2022)171.

[160] Luca Capizzi, Sara Murciano, and Pasquale Calabrese. "Rényi entropy and negativity for massless complex boson at conformal interfaces and junctions". In: *Journal of High Energy Physics* 2022 (2022). ISSN: 1029-8479. DOI: 10.1007/jhep11(2022)105.

[161] Mihail Mintchev and Erik Tonni. "Modular Hamiltonians for the massless Dirac field in the presence of a defect". In: *Journal of High Energy Physics* 2021 (2021). ISSN: 1029-8479. DOI: 10.1007/jhep03(2021)205.

[162] Jorrit Kruthoff, Raghu Mahajan, and Chitraang Murdia. "Free fermion entanglement with a semitransparent interface: the effect of graybody factors on entanglement islands". In: *SciPost Phys.* 11 (2021), p. 063. DOI: 10.21468/SciPostPhys.11.3.063.

[163] David Rogerson, Frank Pollmann, and Ananda Roy. "Entanglement entropy and negativity in the Ising model with defects". In: *Journal of High Energy Physics* 2022 (2022). ISSN: 1029-8479. DOI: 10.1007/jhep06(2022)165.

[164] Ananda Roy and Hubert Saleur. "Entanglement Entropy in the Ising Model with Topological Defects". In: *Phys. Rev. Lett.* 128 (2022), p. 090603. DOI: 10.1103/PhysRevLett.128.090603.

[165] Israel Klich and Leonid Levitov. "Quantum Noise as an Entanglement Meter". In: *Phys. Rev. Lett.* 102 (2009), p. 100502. DOI: 10.1103/PhysRevLett.102.100502.

[166] Kazuhiro Sakai and Yuji Satoh. "Entanglement through conformal interfaces". In: *Journal of High Energy Physics* 2008 (2008), p. 001. DOI: 10.1088/1126-6708/2008/12/001.

[167] V. Eisler and I. Peschel. "Entanglement in fermionic chains with interface defects". In: *Annalen der Physik* 522 (2010), pp. 679–690. DOI: https://doi.org/10.1002/andp.201000055. eprint: https://onlinelibrary.wiley.com/doi/pdf/10.1002/andp.201000055.

[168] Pasquale Calabrese, Mihail Mintchev, and Ettore Vicari. "Entanglement entropy of quantum wire junctions". In: *Journal of Physics A: Mathematical and Theoretical* 45 (2012), p. 105206. DOI: 10.1088/1751-8113/45/10/105206.

[169] Ingo Peschel and Viktor Eisler. "Exact results for the entanglement across defects in critical chains". In: *Journal of Physics A: Mathematical and Theoretical* 45 (2012), p. 155301. DOI: 10.1088/1751-8113/45/15/155301.

[170] Pasquale Calabrese, Mihail Mintchev, and Ettore Vicari. "Exact relations between particle fluctuations and entanglement in Fermi gases". In: *Europhysics Letters* 98 (2012), p. 20003. DOI: 10.1209/0295-5075/98/20003.

[171] Enrico M. Brehm and Ilka Brunner. "Entanglement entropy through conformal interfaces in the 2D Ising model". In: (2015). arXiv: 1505.02647 [hep-th].

[172] Viktor Eisler and Ingo Peschel. "On entanglement evolution across defects in critical chains". In: *Europhysics Letters* 99 (2012), p. 20001. DOI: 10.1209/0295-5075/99/20001.

[173] H. Francis Song et al. "Entanglement entropy from charge statistics: Exact relations for non-interacting many-body systems". In: *Phys. Rev. B* 83 (2011), p. 161408. DOI: 10.1103/PhysRevB.83.161408.

[174] Ferenc Iglói, Zsolt Szatmári, and Yu-Cheng Lin. "Entanglement entropy with localized and extended interface defects". In: *Phys. Rev. B* 80 (2009), p. 024405. DOI: 10.1103/PhysRevB.80.024405.

[175] Mario Collura and Pasquale Calabrese. "Entanglement evolution across defects in critical anisotropic Heisenberg chains". In: *Journal of Physics A: Mathematical and Theoretical* 46 (2013), p. 175001. DOI: 10.1088/1751-8113/46/17/175001.

[176] Matthias Gruber and Viktor Eisler. "Time evolution of entanglement negativity across a defect". In: *Journal of Physics A: Mathematical and Theoretical* 53 (2020), p. 205301. ISSN: 1751-8121. DOI: 10.1088/1751-8121/ab831c.

[177] Paola Ruggiero et al. "Electrostatic solution of massless quenches in Luttinger liquids". In: *SciPost Phys.* 13 (2022), p. 111. DOI: 10.21468/SciPostPhys.13.5.111.

[178] Viktor Eisler and Ingo Peschel. "Evolution of entanglement after a local quench". In: *Journal of Statistical Mechanics: Theory and Experiment* 2007 (2007), P06005. DOI: 10.1088/1742-5468/2007/06/P06005.

[179] Luca Capizzi and Viktor Eisler. "Entanglement evolution after a global quench across a conformal defect". In: *SciPost Phys.* 14 (2023), p. 070. DOI: 10.21468/SciPostPhys.14.4.070.

[180] Oleksandr Gamayun, Oleg Lychkovskiy, and Jean-Sébastien Caux. "Fredholm determinants, full counting statistics and Loschmidt echo for domain wall profiles in one-dimensional free fermionic chains". In: *SciPost Phys.* 8 (2020), p. 036. DOI: 10.21468/SciPostPhys.8.3.036.

[181] Oleksandr Gamayun et al. "Nonequilibrium phase transition in transport through a driven quantum point contact". In: *Phys. Rev. B* 103 (2021), p. L041405. DOI: 10.1103/PhysRevB.103.L041405.

[182] Andrea De Luca and Alvise Bastianello. "Entanglement front generated by an impurity traveling in an isolated many-body quantum system". In: *Phys. Rev. B* 101 (2020), p. 085139. DOI: 10.1103/PhysRevB.101.085139.

[183] Mario Collura, Andrea De Luca, and Jacopo Viti. "Analytic solution of the domain-wall nonequilibrium stationary state". In: *Phys. Rev. B* 97 (2018), p. 081111. DOI: 10.1103/PhysRevB.97.081111.

[184] Marko Ljubotina, Spyros Sotiriadis, and Tomaz Prosen. "Non-equilibrium quantum transport in presence of a defect: the non-interacting case". In: *SciPost Physics* 6 (2019). DOI: 10.21468/scipostphys.6.1.004.

[185] Attila Takács et al. "One-body correlations and momentum distributions of trapped one-dimensional Bose gases at finite temperature". In: *Phys. Rev. A* 111 (2025), p. 033317. DOI: 10.1103/PhysRevA.111.033317.

[186] Jean-Sébastien Caux, Pasquale Calabrese, and Nikita A Slavnov. "One-particle dynamical correlations in the one-dimensional Bose gas". In: *J. Stat. Mech.* 2007 (2007), P01008.

[187] D M Gangardt. "Universal correlations of trapped one-dimensional impenetrable bosons". In: *J. Phys. A: Math. Gen.* 37 (2004), pp. 9335–9356.

[188] Maxim Olshanii et al. "Connection between nonlocal one-body and local three-body correlations of the Lieb-Liniger model". In: *Physical Review A* 96 (2017). ISSN: 2469-9934. DOI: 10.1103/physreva.96.033624.

[189] Giulia De Rosi et al. “Correlation properties of a one-dimensional repulsive Bose gas at finite temperature”. In: *New J. Phys.* 25 (2023), p. 043002. ISSN: 1367-2630. DOI: 10.1088/1367-2630/acc6e6.

[190] Giulia De Rosi et al. “Thermal fading of the $1/k^4$ tail of the momentum distribution induced by the hole anomaly”. In: *Phys. Rev. A* 109 (2024), p. L031302. DOI: 10.1103/PhysRevA.109.L031302.

[191] Harold Widom. “Toeplitz determinants with singular generating functions”. In: *Am. J. Math.* 95 (1973), pp. 333–383.

[192] Kuan-Yu Li et al. “Rapidity and momentum distributions of one-dimensional dipolar quantum gases”. In: *Phys. Rev. A* 107 (2023), p. L061302. DOI: 10.1103/PhysRevA.107.L061302.

[193] M. Rigol. “Finite-temperature properties of hard-core bosons confined on one-dimensional optical lattices”. In: *Phys. Rev. A* 72 (2005), p. 063607. DOI: 10.1103/PhysRevA.72.063607.

[194] Kangning Yang et al. “Phantom energy in the nonlinear response of a quantum many-body scar state”. In: *Science* 385 (2024), pp. 1063–1067. DOI: 10.1126/science.adk8978.

[195] Yanliang Guo et al. “Observation of the 2D–1D crossover in strongly interacting ultracold bosons”. In: *Nat. Phys.* 20 (2023), pp. 934–938. DOI: 10.1038/s41567-024-02459-3.

[196] Yuan Le et al. “Observation of hydrodynamization and local prethermalization in 1D Bose gases”. In: *Nature* 618 (2023), pp. 494–499. ISSN: 1476-4687. DOI: 10.1038/s41586-023-05979-9.

[197] Yanliang Guo et al. “Anomalous cooling of bosons by dimensional reduction”. In: *Sci. Adv.* 10 (2024), eadk6870. DOI: 10.1126/sciadv.adk6870.

[198] Andrew Urilyon et al. *Quantum fluctuating theory for one-dimensional shock waves.* 2024. arXiv: 2403.08875 [cond-mat.stat-mech].

[199] Sebastiaan Eliëns. “On quantum seas”. PhD thesis. Ph. D. thesis, 2017.

Université de Lorraine

École doctorale C2MP

Laboratoire de Physique et Chimie Théoriques (LPCT)

Résumé détaillé de la Thèse

Corrélations dans les gaz quantiques uni-dimensionnels

Par Attila Takács

Thèse de doctorat de Physique

Dirigée par Jérôme Dubail

Et par Pasquale Calabrese (en cas de co-direction et non de co-encadrement)

Devant un jury composé de :

Benoit Estienne, Prof. HDR	Sorbonne Université	Rapporteur
Paola Ruggiero, Lecturer	King's College London, Royaume-Uni	Rapportrice
Sara Murciano, DR	Université Paris-Saclay	Examinatrice
Christophe Chatelain, HDR	Université de Lorraine	Examinateur
Jérôme Dubail, HDR	Université de Strasbourg	Directeur de thèse
Pasquale Calabrese, Full Professor	SISSA, Italie	Co-directeur de thèse

Ces dernières années, l'étude des systèmes quantiques unidimensionnels (1D) est devenue un domaine d'une richesse remarquable pour la physique tant théorique qu'expérimentale. Grâce aux récentes avancées dans les expériences d'atomes froids, il est désormais possible de réaliser et de manipuler des gaz quantiques isolés, confinés dans des géométries effectivement unidimensionnelles, avec un contrôle élevé sur les interactions, la température et les potentiels de piégeage. Ces progrès technologiques ont permis aux expérimentateurs d'accéder directement à des régimes où les descriptions thermodynamiques conventionnelles cessent d'être valides, et où les effets des statistiques quantiques, des interactions et des contraintes dimensionnelles deviennent dominants. En particulier, nous nous concentrerons sur un type spécifique de systèmes bosoniques de basse dimension appartenant au groupe des systèmes intégrables. Bien que la définition exacte de l'intégrabilité dans le contexte des systèmes quantiques fasse l'objet d'un vif débat, lorsque nous parlons de système intégrable, nous nous référons à des systèmes dont le spectre peut être résolu de manière exacte en utilisant la technique de l'Ansatz de Bethe.

Le travail présenté dans cette thèse porte sur la description des propriétés de corrélation des gaz atomiques froids confinés en une dimension, en mettant un accent particulier sur la dynamique hors d'équilibre ainsi que sur le comportement à l'équilibre à température finie. L'objectif de ce travail est de comprendre comment des grandeurs telles que la force d'interaction et la température influencent les quantités observables, comme les distributions d'impulsion et les matrices de densité à une particule, lesquelles encodent des informations fondamentales sur la cohérence, la condensation et l'évolution dynamique dans ces systèmes quantiques de basse dimension.

La thèse est organisée en trois chapitres principaux : le chapitre 1 présente le contexte général et les outils théoriques utilisés dans ce travail, tout en fournissant également un base nécessaire. Plus précisément, notre objectif est ici de servir de prologue et de doter le lecteur des connaissances requises pour comprendre et apprécier pleinement les résultats qui suivent. Le chapitre 2 est consacré aux bosons à cœur dur — une limite du modèle de Lieb-Liniger où la forte répulsion conduit à une fermionisation effective. Nous étudions ce système dans des configurations hors d'équilibre, en nous concentrant particulièrement sur les corrélations à temps égal, la fermionisation dynamique, la quasi-condensation et l'effet des défauts dans le système. Dans le chapitre 3, nous étudions les propriétés d'équilibre à température finie d'un gaz de Lieb-Liniger piégé.

Dans le **chapitre 1**, nous présentons les diverses méthodes et théories établies utilisées dans le domaine des atomes froids de basse dimension afin de préparer le terrain pour nos résultats, et nous définissons également certaines grandeurs, méthodes et concepts importants. Nous commençons par une brève revue de la thermalisation des systèmes quantiques, en nous concentrant sur les systèmes avec des charges conservées pour introduire la section suivante. Nous abordons ensuite la discussion sur les gaz de Bose en 1 dimension, en particulier le gaz de Lieb-Liniger, en discutant de leurs propriétés fondamentales et en présentant certaines des avancées expérimentales dans l'observation et la mesure de tels systèmes, lesquelles constituent une très forte motivation pour les résultats que nous présentons par la suite. Nous passons en revue la diagonalisation exacte de son hamiltonien par l'Ansatz de Bethe et son extension à la limite thermodynamique. Nous mettons en évidence quelques limites importantes et intéressantes de la force d'interaction, à savoir la limite de répulsion infiniment forte, appelée gaz de Tonk-Girardeau (TG), et le cas attractif, désigné sous le nom de gaz de super Tonk-Girardeau (sTG). La section suivante est consacrée à la revue de la théorie de l'hydrodynamique généralisée, un cadre théorique présenté en 2016 par Castro-Alvaredo et al. [1] et Bertini et al. [2], qui fournit une description de l'hydrodynamique

à l'échelle d'Euler pour les systèmes quantiques intégrables. Nous nous concentrons tout particulièrement sur la description de l'évolution des états dits à entropie nulle, que nous utilisons abondamment par la suite dans ce travail. Nous concluons ce chapitre par une discussion sur la théorie des liquides de Tomonaga-Luttinger, dans le contexte de son utilisation pour obtenir les fonctions de corrélation de l'état fondamental des systèmes d'atomes froids de basse dimension, et par une introduction à l'hydrodynamique généralisée quantique [3, 4].

Le **chapitre 2** est axé sur le comportement hors d'équilibre d'une classe particulièrement intéressante de systèmes quantiques à N corps, constitués de bosons avec de fortes interactions répulsives, communément appelés bosons à cœur dur (HCB). À une dimension spatiale, de tels systèmes peuvent être mis en correspondance avec des fermions sans spin et sans interaction via les transformations de Jordan-Wigner [5]. Cette correspondance permet le développement de techniques numériques efficaces pour explorer leur dynamique hors d'équilibre. Malgré cette simplification, l'obtention de résultats analytiques pour les grandeurs hors d'équilibre reste une tâche ardue. En conséquence, une grande partie des progrès dans ce domaine s'est appuyée sur des approches numériques [6–8]. Dans ce travail, nous présentons au contraire des expressions analytiques pour les fonctions de corrélation hors d'équilibre, en nous basant sur le cadre de l'hydrodynamique généralisée quantique (QGHD).

L'une des caractéristiques les plus fascinantes des bosons à cœur dur (HCB) unidimensionnels (1D) est que, malgré leur mise en correspondance avec des fermions sans spin et sans interaction, leur dynamique hors d'équilibre peut présenter un comportement fondamentalement différent. Un exemple de cette différence réside dans l'évolution de la distribution d'impulsion : tandis que les systèmes fermioniques invariants par translation ne présentent aucune évolution temporelle avec des conditions aux limites périodiques ou affichent des oscillations persistantes avec des conditions aux limites ouvertes [106], la distribution d'impulsion des HCB 1D relaxe vers une valeur stationnaire [10, 107], qui est bien décrite par l'Ensemble de Gibbs Généralisé (GGE)[108]. De plus, à l'équilibre, les HCB 1D sont connus pour présenter une quasi-condensation [6], un phénomène qui n'est pas limité à l'état fondamental. Dans les régimes loin de l'équilibre, des caractéristiques rappelant la quasi-condensation — en particulier, des pics d'impulsion à des valeurs finies — peuvent également émerger [55].

Un éclairage théorique sur ce comportement a été fourni par le cadre de la solution des états propres émergents pour la dynamique quantique [109]. Dans cette approche, il est avancé que pour une classe appropriée d'états initiaux hors d'équilibre, le système évolue à travers une séquence d'états propres instantanés d'un hamiltonien local effectif. Cette description émergente reste valide sur des échelles de temps qui croissent linéairement avec le nombre de particules [109–112].

Un protocole particulièrement adapté pour observer la quasi-condensation dans les HCB consiste à initialiser le système dans un état produit de type mur de domaine, où les régions de sites entièrement occupés et de sites vides sont nettement séparées. De telles configurations peuvent être réalisées expérimentalement en préparant les HCB dans une région centrale flanquée de sites vides, par exemple, en utilisant un potentiel de type boîte. L'intégrabilité du modèle HCB 1D assure que la mémoire de l'état initial persiste bien au-delà des échelles de temps auxquelles les signatures de quasi-condensation deviennent visibles. Pendant l'expansion à partir d'un piège en boîte, la distribution d'impulsion évolue et finit par s'approcher de celle des fermions sans spin et sans interaction, reflétant la mise en correspondance sous-jacente. Ce processus, connu sous le nom de fermionisation dynamique,

a également été observé dans d'autres modèles intégrables [57, 113–116].

Ce qui rend les HCB particulièrement attractifs d'un point de vue pratique est leur accessibilité expérimentale. Des réalisations existent à la fois dans des systèmes continus [117] et dans des montages de réseaux optiques [118, 119], permettant l'observation expérimentale directe de la quasi-condensation [120] et de la fermionisation dynamique [33]. Ces développements soulignent l'importance théorique de la construction de cadres analytiques capables de capturer toute la dynamique hors d'équilibre de tels systèmes.

À l'équilibre, les éclairages théoriques sur la quasi-condensation proviennent en grande partie des analyses de la matrice de densité à une particule (OPDM), dont la transformée de Fourier donne la distribution d'impulsion. Dans les systèmes homogènes, la théorie des liquides de Luttinger prédit une décroissance en loi de puissance de l'OPDM, indiquant un ordre à longue portée hors-diagonale. Ceci peut être interprété comme une forme de quasi-condensation à travers le comportement d'échelle de la plus grande valeur propre de l'OPDM, conformément au critère de Penrose-Onsager [50], ou via l'émergence de pics dans la distribution d'impulsion [6, 56]. De telles analyses ont d'abord été étendues aux états fondamentaux de HCB piégés harmoniquement [53], puis généralisées à des configurations inhomogènes arbitraires en utilisant des extensions de la théorie des liquides de Luttinger [54, 73, 85, 121, 122].

Ce n'est que récemment qu'il est devenu possible d'obtenir des expressions entièrement analytiques pour l'OPDM à temps égal dans des potentiels génériques hors d'équilibre [63], grâce au développement d'un nouveau cadre d'hydrodynamique quantique (QHD). L'idée centrale est conceptuellement simple : les fonctions de corrélation à grande échelle peuvent être approximées analytiquement en construisant une théorie des liquides de Luttinger spatialement variable par-dessus le profil hydrodynamique classique du système HCB en évolution à température nulle [3, 4, 123, 124]. Cette approche a produit une variété de résultats analytiques, en particulier pour la dynamique de l'intrication, et sa validité a été corroborée dans des scénarios de fusion de murs de domaine [68, 123, 125–129].

Dans la première partie de ce chapitre, nous nous concentrons sur le calcul de l'OPDM à temps égal pour des HCB 1D initialement confinés dans un potentiel de type boîte. En nous appuyant sur les récentes avancées analytiques, nous dérivons des expressions exactes pour l'OPDM dans cette configuration hors d'équilibre. Ces résultats nous permettent de revisiter l'émergence de la quasi-condensation et d'analyser le développement des corrélations hors-diagonales dans la dynamique loin de l'équilibre des bosons à cœur dur. Cette section est organisée comme suit. Nous discutons d'abord de la configuration des bosons à cœur dur (HCB) et de sa mise en correspondance avec celle des fermions libres sans spin ; nous spécifions ensuite l'état initial de type mur de domaine et le protocole de trempe que nous avons étudié. Nous continuons en présentant le résultat principal pour l'OPDM à temps égal des HCB pendant l'expansion libre. La discussion qui suit contient une dérivation détaillée du résultat principal. Celle-ci consiste en la révision de l'hydrodynamique classique des fermions libres, sa re-quantification avec des arguments de bosonisation (voir la section 2.1.3), et plusieurs détails non triviaux sur la dérivation de l'OPDM. Nous nous tournons ensuite vers les applications de nos résultats. En particulier, nous démontrons l'émergence de la quasi-condensation et le phénomène connu sous le nom de fermionisation dynamique à différents stades de l'évolution. Ceci est réalisé en analysant le comportement de la plus grande valeur propre de l'OPDM, en utilisant le critère de Penrose-Onsager, et en examinant l'évolution temporelle de la distribution d'impulsion obtenue à partir de nos calculs. Cette section est basée sur notre article [130], où les résultats présentés ici ont été publiés pour la première fois.

De plus, nous explorons un système particulier de bosons à cœur dur hors d'équilibre en présence de défauts dits conformes. L'hamiltonien du système est donné par l'ajout de deux défauts conformes dans un système initialement invariant par translation de bosons à cœur dur sur réseau.

L'introduction d'une seule impureté dans un système à N corps autrement invariant par translation peut modifier le comportement global du système, comme l'ont montré des exemples classiques tels que la catastrophe d'orthogonalité d'Anderson [154] ou le modèle de Kane-Fisher [155, 156]. Au cours de la dernière décennie, des progrès significatifs ont été réalisés dans l'étude des systèmes de fermions libres 1D en présence d'impuretés dans le contexte de l'intrication, par ex. [157–171]. Ces travaux ont permis de former une image assez complète des fermions libres dans des systèmes avec impuretés à l'équilibre. La description hors d'équilibre de tels systèmes est cependant loin d'être aussi claire, en raison des nombreux protocoles et manières différentes de mettre le système hors d'équilibre (voir par exemple les travaux [172–182]). Récemment, dans le travail [141], un système de fermions libres a été laissé évoluer à partir d'un état initial de type mur de domaine, le mur de domaine étant situé sur un défaut. L'importance de cette condition initiale particulière réside dans sa connexion avec plusieurs travaux [125, 128, 183, 184] dans lesquels de tels états initiaux ont été étudiés dans le contexte du transport dans le cadre de la GHD (voir la section 1.3 pour un bref aperçu).

Tandis que dans la première partie du chapitre 2, nous nous concentrons sur l'obtention de formules analytiques pour l'OPDM à temps égal des bosons à cœur dur à la limite d'Euler en « re-quantifiant » la solution GHD en suivant la méthodologie de la QGHD développée par ex. dans [3, 4, 73], dans la seconde partie, nous étudions au contraire la dynamique de bosons à cœur dur libérés d'un état initial de type mur de domaine en présence de deux défauts conformes. Le profil de densité observé diffère de la description hydrodynamique à l'échelle d'Euler en raison de termes additionnels résultant de l'interférence quantique. En analysant les propagateurs de bosons, nous montrons que la diffusion répétée sur les défauts conduit à des figures d'interférence qui ne peuvent pas être capturées par l'approche hydrodynamique. Nous dérivons une expression analytique pour le profil de densité pendant l'expansion libre et démontrons qu'un cadre de diffusion semi-classique modifié est requis pour la description des systèmes avec de tels défauts. Nous organisons cette section comme suit. En rappelant la mise en correspondance Bose-Fermi entre les HCB et les fermions libres sans interaction que nous avons détaillée dans la section précédente, nous passons en revue les résultats de [129] où l'expansion libre d'un système de HCB à partir d'une configuration de mur de domaine a été étudiée en présence d'un défaut conforme. En utilisant ces résultats, nous dérivons les propagateurs fermioniques, et nous montrons comment la dynamique a une interprétation classique qui s'inscrit dans le cadre de l'image hydrodynamique à la limite d'Euler. Nous passons ensuite à la discussion de notre système ; nous présentons le système avec deux défauts conformes et le protocole de trempe. Ensuite, nous présentons nos résultats pour le propagateur dans cette configuration, et nous montrons qu'une image semi-classique modifiée peut être réintroduite. Finalement, nous montrons que nos résultats pour les propagateurs reproduisent le profil de densité des bosons en comparant nos résultats à des évaluations numériques exactes.

Dans le **chapitre 3**, nous présentons une méthode pour calculer les corrélations à un corps et la distribution d'impulsion des gaz de Bose unidimensionnels dans des potentiels de piégeage lisses, pour des forces d'interaction et des températures finies. Cette méthode consiste à combiner des développements connus à courte distance de la matrice de densité à une particule avec un comportement à longue distance du gaz, que nous calculons de

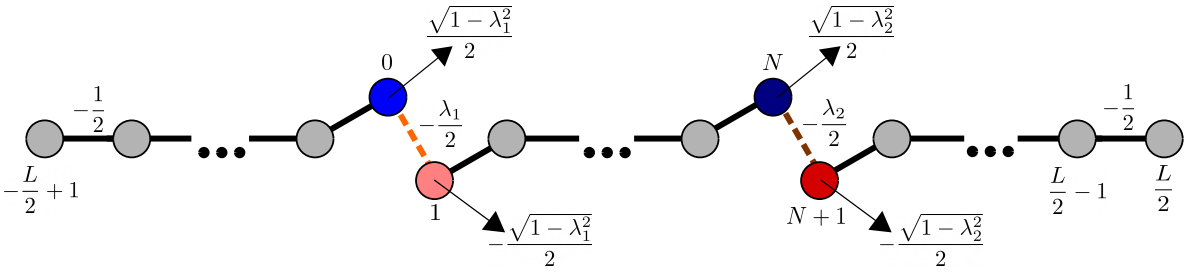


Figure C.1: Schéma de l'hamiltonien de sauts aux plus proches voisins que nous étudions dans la seconde partie du chapitre 2, incluant les défauts conformes paramétrés par la « force » de l'impureté $\lambda_1, \lambda_2 \in [0, 1]$, situés respectivement sur les sites $0, 1$ et $N, N+1$. Les défauts sont indiqués par des sites décalés colorés en bleu et rouge pour marquer la nature décalée du potentiel sur site, et avec des teintes différentes pour indiquer que $\lambda_1 \neq \lambda_2$ en général. Les sauts connectant les sites $0, 1$ et $N, N+1$ sont dessinés avec des lignes rouges en quinconce.

manière similaire au cadre de la théorie des liquides de Luttinger. Dans le cas du régime de quasi-condensat (faible force d'interaction répulsive) et dans la limite de Tonks-Girardeau (forte interaction), nous dérivons des résultats analytiques pour les fonctions de corrélation. Nous fournissons également une procédure générale pour obtenir les corrélations à un corps à n'importe quelle force d'interaction, ainsi qu'une explication détaillée de la méthode numérique utilisée pour calculer les fonctions de Green dont nous avons besoin comme données d'entrée pour notre théorie. Finalement, nous évaluons la validité de notre méthode en la comparant à des calculs numériques exacts et à des résultats expérimentaux récents.

L'une des grandeurs les plus omniprésentes dans l'étude des condensats de Bose-Einstein et des atomes froids est la distribution d'impulsion, qui peut être mesurée dans des expériences de « temps de vol » (voir la section 1.2.2). Cette grandeur a été largement utilisée depuis les débuts de la BEC pour décrire et caractériser un large éventail de phénomènes dans de nombreux systèmes quantiques différents. Dans le contexte des gaz quantiques 1D, quelques exemples incluent, sans s'y limiter, l'observation de la fermionisation dynamique, l'étalonnage de l'hydrodynamique généralisée et la caractérisation des interactions dipolaires. La distribution d'impulsion est définie comme la transformée de Fourier de l'OPDM

$$f(\mathbf{p}) = \int d\mathbf{x} \int d\mathbf{y}\; e^{i\mathbf{p}(\mathbf{x}-\mathbf{y})} g_1(\mathbf{x}, \mathbf{y}), \tag{C.2}$$

où $g_1(\mathbf{x}, \mathbf{y})$ désigne l'OPDM, qui est définie comme

$$g_1(\mathbf{x}, \mathbf{y}) = \langle \hat{\Psi}^\dagger(\mathbf{x}) \hat{\Psi}(\mathbf{y}) \rangle, \tag{C.3}$$

où $\hat{\Psi}^\dagger(\mathbf{x})$ et $\hat{\Psi}(\mathbf{y})$ sont les opérateurs bosoniques de création et d'annihilation. Au cours de notre calcul dans ce chapitre, nous posons $\hbar = 1$, comme nous l'avons fait jusqu'à présent dans cette thèse ; nous le réintroduisons lorsque nous faisons des comparaisons entre les résultats numériques et analytiques.

L'obtention de formules pour l'OPDM ou de résultats numériques est généralement reconnue comme difficile, ce qui fait de l'évaluation de la distribution d'impulsion également un défi, en particulier pour les gaz corrélés hors d'équilibre. Les résultats analytiques pour les gaz bosoniques sont généralement limités à la 1D, où les calculs directs sont restreints

à la limite TG (ou HCB) dans laquelle le système peut être mis en correspondance avec des fermions libres (voir les sections 1.2.5 ou 2.1). Quant aux méthodes numériques, l'obtention de la distribution d'impulsion se fait par simulation Monte-Carlo quantique, et dans les cas intégrables, par des méthodes de resommation des facteurs de forme, ou par des techniques d'états produits de matrices telles que le DMRG.

Dans ce chapitre de la thèse, nous introduisons une méthode numérique pour obtenir les distributions d'impulsion et les corrélations à une particule dans des gaz de Bose unidimensionnels confinés dans des potentiels de piégeage variant de manière lisse, pour des forces d'interaction et des températures finies. Dans notre description, nous combinons des résultats asymptotiques à longue portée (similaires à la théorie des liquides de Luttinger) et des résultats asymptotiques connus à courte distance. Nous comparons ensuite les résultats obtenus à partir de ce cadre avec des simulations numériques et des expériences.

Nous organisons le chapitre comme suit. Nous commençons par rappeler les résultats existants pour les asymptotiques à courte et longue portée de l'OPDM du gaz de Lieb-Liniger piégé, en nous appuyant sur les notations et définitions introduites au chapitre 1. Nous nous tournons ensuite vers l'étude du gaz de Lieb-Liniger piégé en suivant les techniques du « liquide de Luttinger inhomogène » [73] (ou section 1.4), où nous dérivons des formules analytiques pour l'OPDM à température finie dans le régime TG et le régime faiblement interactif. Nous procédons ensuite en détaillant la méthode numérique utilisée pour évaluer l'OPDM pour des forces d'interaction arbitraires à des températures finies, généralisant les résultats de [74]. Nous continuons en comparant nos résultats avec des simulations Monte-Carlo quantiques, et les comparons à des résultats expérimentaux récents. Nous terminons ce chapitre par une discussion et des extensions possibles. Les résultats et figures présentés dans ce chapitre ont été publiés dans notre travail [185].

Avec ces résultats, nous visons à contribuer à la compréhension plus large des systèmes quantiques de basse dimension en comblant le fossé entre les solutions exactes, les descriptions hydrodynamiques effectives et les observables expérimentalement pertinentes. Nous discutons brièvement et motivons les projets en cours qui s'appuient sur les résultats que nous rapportons dans ce travail dans le **chapitre 4**. La thèse est en partie basée sur les articles publiés listés ci-dessus ainsi que sur certains travaux en cours de publication.